




University of Stavanger

FACULTY OF SCIENCE AND TECHNOLOGY

Master's Thesis

Study program/specialization: Petroleum Engineering/ Drilling Technology	Spring semester, 2023 Open
Author: Kyleen Weber	 (Signature of author)
Program coordinator: Supervisor(s): Mesfin Belayneh	
Title of bachelor's thesis: New Eco-Friendly Drilling Fluids Synthesis and Characterization: Experimental and Simulation Studies	
Credits: 30	
Keywords: Chia Mandarin KCL Based drilling fluid Bentonite Based Drilling Fluid TiN Nanoparticles Viscosity Sagging Viscoelasticity Lubricity	Number of pages: 142 + Supplemental material/other: 42 Date/year 12/06/2023 Stavanger

Abstract

Drilling fluids are an essential part of a safe and successful drilling operation. They offer several key functions such as transporting cuttings to the surface and controlling wellbore pressure. When designing a new drilling fluid, it is important to consider its cost, performance and environmental impact. The drilling fluid must be designed according to the expected wellbore conditions such as the well's design and anticipated formation pressure, temperature and chemistry.

The focus of this thesis is to study the effects of chia, mandarin peel powder and TiN nanoparticles. On the properties of water-based drilling fluids. Two different water-based drilling fluid systems are utilized in this study, one that uses bentonite as a base and one that uses potassium chloride. The reference fluids are based on a flat rheology system formulated in a previous study. The fluids containing the ecological additives were characterized in terms of rheological, viscoelastic and filtration properties. They were then further tested in hydraulic simulations to evaluate their effects on the drilling fluid's pump pressure and equivalent circulating density. Finally, nanoparticles were added to further enhance their drilling capabilities which were evaluated using Torque and Drag simulations.

It was found that in the bentonite-based drilling fluid, the optimum weight concentration is 0.4 wt% Chia and 0.4 wt% MPP and KCl the optimum concentration is 0.57wt% Chia and 0.2wt% MPP. Results showed these formulations to be thermally stable, increased viscosity, reduced friction, and reduced filtrate loss. These concentrations could also replace up to a third of Pac and PolyPac for the Bentonite-based drilling fluid or a third of Xanthan Gum for the KCl-based drilling fluid.

Acknowledgement

The completion of this study could not have been possible without the expertise of my supervisor, Mesfin Belayneh. His guidance and advice throughout the entire process has helped me to a very great extent to accomplish this task. The dedication of his time to answering my many questions and emails showed his deep care for all his students and was truly inspiring.

I would also like to thank my cats, Jessie and James, for being with me throughout the entirety of the endless hours spent writing this thesis.

Contents

List of Figures	viii
List of Tables	xiv
List of Abbreviations	xvi
1 Introduction.....	1
1.1 Background	1
1.2 Problem Formulation	2
1.3 Objective	3
1.4 Research Methods	3
2 Theory	5
2.1 Drilling Fluid	5
2.1.1 Drilling Fluid Properties.....	5
2.1.2 Drilling Fluid Types	7
2.2 Rheology	9
2.2.1 Rheological Properties	9
2.2.2 Shear Stress and Shear Rate	10
2.3 Rheological Models.....	12
2.3.1 Newtonian Fluids	13
2.3.2 Non-Newtonian Fluids	14
2.4 Viscoelasticity.....	20
2.4.1 Oscillatory Tests	21
2.4.2 Methods for Measuring Viscoelasticity	21
2.4.3 Static Sag Test	29
2.5 Hydraulics Model	30
2.5.1 Equivalent Circulating Density	32
2.5.2 Pump Pressure	32
2.6 Tribology and Friction	35
2.6.1 Coefficient of Friction and the Coulomb Model	35
2.6.2 Industrial Application of Friction and Lubrication	37
2.7 Torque and Drag Modelling	38

3	Literature Study	39
3.1	Eco Friendly Based Drilling Fluid	39
3.2	Nanotechnology	40
3.3	Nanoparticle Based Drilling Fluids	41
4	Experimental Work	43
4.1	Description of Drilling Fluid Additives	43
4.1.1	Bentonite.....	43
4.1.2	Soda Ash.....	44
4.1.3	Barite.....	45
4.1.4	Polymer Additives	45
4.1.5	Titanium Nitride Nanoparticle	47
4.1.6	Mandarin Peel Powder	48
4.1.7	Chia	48
4.1.8	Potassium Chloride (KCl).....	49
4.1.9	Xanthan	49
4.2	Experimental Equipment	50
4.2.1	Hamilton Beach Mixer.....	50
4.2.2	OFITE Viscometer and Rheology Measurements.....	50
4.2.3	Anton Paar Rheometer	51
4.2.4	pH-Meter.....	52
4.2.5	API Static Filter Press and Fluid Loss Measurement Procedure	52
4.2.6	Tribometer and Frictional Measurement	53
4.2.7	Haver EML 200 Digital Sieve Shaker.....	54
4.3	Drilling Fluid Formulation	55
4.3.1	Bentonite Based Drilling Fluid Formulation	55
4.3.2	Potassium Based Mud with Polypac and Pac.....	57
4.3.3	KCl Based Mud with Xanthan Gum	58
5	Results	60
5.1	Characterization of Chia in Bentonite-Based Water-based Mud	60
5.1.2	Effect of Amount of Chia on Sag Factor	63
5.1.3	Effect of Chia Preparation on Rheology.....	65
5.1.4	Effect of Chia Preparation on Sag Factor	67

5.2	Characterization of Chia in Potassium Chloride based Drilling Mud	68
5.2.1	Chia Characterization in Pac/Polypac	68
5.2.2	Effect of Chia on Potassium Chloride-based Mud with Xanthan Gum	71
5.3	The Addition of Mandarin Peel Powder.....	79
5.3.1	Rheology	79
5.3.2	Effect of Mandarin on Sag Factor	82
5.4	Filtrate Loss	84
5.5	Ecological Replacement of Polymers for Filtrate Loss	86
5.6	Amplitude Sweep Tests.....	87
5.7	Ecological Replacement of Polymers for Filtrate Loss	89
5.8	Effect of Chia, Mandarin, and TiN nanoparticles on lubricity of KCl Drilling Fluid.....	93
6	Hydraulics Simulations and Rheology Modelling.....	95
6.1	Hydraulic Performance Simulation	95
6.1.1	Simulation Set-Up	95
6.1.2	Chia in Bentonite.....	96
6.1.3	ECD and Pump Pressure with MPP in Bentonite	99
6.1.4	Chia and Mandarin in KCl-based drilling fluid.....	102
6.2	Rheological Modeling.....	105
6.2.1	Best-Fit Rheological Model for Bentonite.....	106
6.2.2	Temperature Effects on Rheological Parameters in Bentonite	108
6.2.3	Best-Fit Rheological Model for KCl.....	111
6.2.1	Temperature Effects on Rheological Parameters in Bentonite	113
6.3	Torque and Drag Simulation	115
6.3.1	Simulation Assumptions and Setup	116
6.3.2	Effect of Chia, Mandarin, and TiN nanoparticles on Torque and Drag.....	116
7	Summary and Discussion	120
7.1	Drilling Fluid Characterization.....	120
7.1.1	The Bentonite-based Drilling Fluid.....	120
7.1.2	The KCl-Based Drilling Fluid	123
7.1.3	Chia and Mandarin Peel Powder as a Replacement for other additives	126
7.2	Performance Evaluation.....	129
7.2.1	Hydraulics.....	129
7.2.2	Rheology Modeling	130

7.2.3	Torque and Drag Simulation	130
7.3	Limitations and Uncertainties	130
8	Conclusion	133
9	References	135
10	Appendices	144
10.1	Torque	144
10.1.1	Drag in Straight Inclined/Horizontal Section.....	145
10.1.2	Torque	150
10.1.3	Torsional and Tensile Limits.....	152
10.2	Rheology Data	155
10.2.1	Effect of Chia and Mandarin on Bentonite-based drilling fluid	155
10.2.2	Effect of Chia and Mandarin on rheology data.....	160
10.3	Sag Factor Data	165
10.4	Results from Hydraulics Simulations.....	169
10.4.1	Annular Pressure Loss	169
10.4.2	Pump Pressures.....	173
10.4.3	ECD.....	178

List of Figures

Figure 1.1: Summary of the Research Method used	4
Figure 2.1: A material's structure in a solid state (left) and in a fluid state (right).....	10
Figure 2.2: Two plate model illustrating shear stress and shear rate of a fluid	11
Figure 2.3: Graph showing the linear relationship between shear rate and shear stress of a Newtonian Fluid.....	13
Figure 2.4:Graph showing the relationship between shear stress and shear rate of a Bingham Plastic Fluid versus a Newtonian Fluid	14
Figure 2.5 Graph showing the relationship between shear stress and shear rate of the Power Law Model	16
Figure 2.6: Graph showing shear stress and shear rate relationship of the Herschel-Bulkley Model.....	18
Figure 2.7:Graph showing an example of the Robertson-Stiff Model on a log-log scale	20
Figure 2.8: Two-Plate Model for an oscillatory test showing ideally elastic behavior in the shear stress and shear strain sine curves.....	21
Figure 2.9: Amplitude Sweep example with 5 steps of increased shear strain and amplitudes (Anton Paar GmbH, n.d-a).....	22
Figure 2.10: Shear strain and resulting shear stress as two sinusoidal functions, offset by phase shift angle (Anton, Paar GmbH, n.d.-b).....	25
Figure 2.11: Example of results from two amplitude sweep tests showing a gel-like or solid sample (left) or a fluid sample (right).....	26
Figure 2.12: Example of an amplitude sweep test where the loss modulus reaches its maximum after exceeding the LVE range (Anton Paar GmbH, n.d.-a)	27
Figure 2.13: Example of an amplitude sweep test where functions of storage and loss modulus are plotted in terms of shear stress (Anton Paar GmbH, n.d.-a)	28
Figure 2.14: Drilling fluids in cup for static sag	29
Figure 2.15: Typical drilling fluid circulation system (Guo and Liu, 2011)	33
Figure 2.16: Frictional pressure losses in circulating system (Zeynalov, 2018)	34
Figure 2.17: Static and kinetic behavior as a function of time	36
Figure 4.1:Illustration of the basic structure of montmorillonite (Skjeggstad, 1989	44
Figure 4.2: TiN Nanoparticles.....	47
Figure 4.3: Hamilton Beach Mixer blending drilling mud	50
Figure 4.4:Ofite Viscometer	51

Figure 4.5: Anton Paar Rheometer	51
Figure 4.6:pH-meter conducting a pH measurement.....	52
Figure 4.7: API Static Filter Press	53
Figure 4.8: CSM tribometer instrument used for friction tests	54
Figure 4.9: Siever shaker shaking mandarin peel powder	55
Figure 5.1: Plastic Viscosity vs Chia Amount in Bentonite	61
Figure 5.2: Yield Strength vs Amount of Chia in Bentonite	62
Figure 5.3: YS/PV vs Chia Amount.....	63
Figure 5.4: Sag Factor vs Amount of Chia in Bentonite Systems	64
Figure 5.5: Pictures of the sample from left; reference, reference +1g chia, reference +2g chia.....	64
Figure 5.6: Plastic Viscosity vs Chia Preparation in Bentonite	65
Figure 5.7: Yield Stress vs Chia Preparation in Bentonite	66
Figure 5.8: YS/PV vs Chia Preparation.....	67
Figure 5.9: Chia Preparation vs Sag Factor in Bentonite.....	68
Figure 5.10: Plastic Viscosity vs Chia Preparation in KCl-Pac/Polypac System	69
Figure 5.11: Yield Strength vs Chia Preparation in KCl-Pac/Polypac System	70
Figure 5.12: Sag Factor vs Cooking Preparations in KCl-Pac/Polypac System	71
Figure 5.13: Picture of two samples containing 2g uncooked chia, the left containing Pac and PolyPac and the right containing Xanthan Gum	71
Figure 5.14: Plastic Viscosity vs Chia Preparation in KCl-Xanthan Gum System.....	72
Figure 5.15: Yield Stress vs Chia Preparation in KCl-Xanthan Gum System.....	73
Figure 5.16: Low Shear Yield Stress vs Chia Preparation in KCl-Xanthan Gum System	73
Figure 5.17: YS/PV vs Chia Preparation in KCl-Xanthan Gum System.....	74
Figure 5.18: Effect of Chia Preparation on Sag Factor in KCl-based system with Xanthan Gum.....	75
Figure 5.19: Picture containing the samples from left; KCl+2.14g XG, KCl+1.5g XG + 1g Chia, KCl+1.5g XG +2g Chia.....	76
Figure 5.20: Plastic Viscosity vs Amount of Chia in KCl-Xanthan Gum System.....	77
Figure 5.21: Yield Stress vs Amount of Chia in KCl-Xanthan Gum system.....	77
Figure 5.22: YS/PV vs Amount of Chia in KCl-Xanthan Gum system.....	78
Figure 5.23: Sag Factor vs Amount of Chia in KCl-Xanthan Gum system.....	79
Figure 5.24: Yield Stress vs Amount of Mandarin in Bentonite-based fluid	80
Figure 5.25: Yield Stress vs Mandarin Addition in KCl-Based Fluid.....	80

Figure 5.26: YS/PV vs Amount of Mandarin in Bentonite 81

Figure 5.27: YS/PV vs Addition of Mandarin in KCl-based fluid 81

Figure 5.28: Effect of Mandarin on Sag Factor in Bentonite 82

Figure 5.29: Effect of Mandarin on Sag Factor in KCl 83

Figure 5.30: Photo of the samples from left to right; Ref, Ref+1.5g MPP, and Ref+2g MPP..... 83

Figure 5.31: Filtrate Loss vs Amount of Chia in Bentonite..... 84

Figure 5.32: Filtrate Loss vs Amount of Mandarin in Bentonite 85

Figure 5.33: Filtrate Loss vs Amount of Chia and Mandarin Peel Powder in KCl..... 85

Figure 5.34: Shear Stress vs Damping Angle in Bentonite 87

Figure 5.35: Shear Stress vs Damping Angle vs Amount of Chia in KCl..... 88

Figure 5.36: Shear Stress vs Damping Angle vs Amount of Mandarin..... 89

Figure 5.37: Yield Stress with Reduced Pac/PolyPac 91

Figure 5.38: Plastic Viscosity with Reduced Pac/Polypac 91

Figure 5.39: Yield stress with Reduced Xanthan Gum 92

Figure 5.40: Plastic Viscosity with Reduced Xanthan Gum 92

Figure 5.41: Ground Chia for lubricity test Figure 5.42: Photo of the resulting oil from the
ground chia 94

Figure 5.43: Averaged Results from Lubricity Tests..... 94

Figure 6.1: Well setup for the hydraulics performance simulation 96

Figure 6.2: ECD at various Temperatures vs Amount of Chia in Bentonite-based Drilling fluid..... 98

Figure 6.3: Pump Pressure vs Flow rate for Ref+2g Chia 98

Figure 6.4: ECD vs Amount of Mandarin added at various temperatures in Bentonite 100

Figure 6.5: Pump Pressure vs amounts of MPP at various temperatures in Bentonite 101

Figure 6.6: ECD vs Amount of Chia in KCl..... 104

Figure 6.7: Pump Pressure at various flow rates in KCl 104

Figure 6.8: Pump Pressure results for Ref+3g Chia+1g MPP 105

Figure 6.9: % Deviation between model prediction and actual values 107

Figure 6.10: Percent deviations of model predictions from actual measurements 112

Figure 6.11: Estimated well data applied to the simulated well 116

Figure 6.12: Coefficient of Friction for samples used in simulation 116

Figure 6.13: Torque Simulations 117

Figure 6.14: Drag Simulations 118

Figure 7.1: Bingham Yield Stress of best bentonite-based fluids at 50°C and 80°C 121

Figure 7.2: Plastic Viscosity and Chia additions at 20°C, 50°C, and 80°C..... 121

Figure 7.3: Yield Stress vs Chia Preparation at 20°C, 50°C, and 80°C 122

Figure 7.4: Yield Stress vs Mandarin Concentration at at 50°C, and 80°C..... 122

Figure 7.5: Yield Strength vs Chia Preparation 124

Figure 7.6: Yield Stress vs Chia Concentrations in KCl-based fluid 125

Figure 7.7: Yield Stress and the addition of MPP..... 125

Figure 7.8: Yield Stress with Reduced Pac and PolyPac..... 127

Figure 7.9: Yield Stress with Reduced Xanthan Gum..... 128

Figure 10.1: Typical simulation well trajectory..... 144

Figure 10.2: Force balance example for a pipe being pulled along a straight surface (Aadnoy et al., 2010)
..... 146

Figure 10.3: Example of a build-up bend section force free body diagram (Aadnoy, 2006) 148

Figure 10.4: Helical Buckling Illustrations 153

Figure 10.5: Viscometer data at 20°C of bentonite reference fluid and chia 155

Figure 10.6:Viscometer Data at 50°C of bentonite reference fluid and chia..... 156

Figure 10.7:Viscometer Data at 80°C of bentonite reference fluid and chia..... 156

Figure 10.8:Viscometer data at 20°C of bentonite reference fluid and chia preparation 157

Figure 10.9:Viscometer data at 50°C of bentonite reference fluid and chia preparation 157

Figure 10.10:Viscometer data at 80°C of bentonite reference fluid and chia preparation..... 158

Figure 10.11:Viscometer data at 20°C of bentonite reference fluid and MPP..... 158

Figure 10.12:Viscometer data at 50°C of bentonite reference fluid and MPP 159

Figure 10.13:Viscometer data at 80°C of bentonite reference fluid and MPP 159

Figure 10.14: Viscometer data for reduced Pac and PolyPac in Bentonite 160

Figure 10.15:Viscometer data at 20°C of KCl and Pac/Polypac reference fluid and chia preparation 160

Figure 10.16:Viscometer data at 50°C of KCl and Pac/Polypac reference fluid and chia preparation 161

Figure 10.17:Viscometer data at 80°C of KCl and Pac/Polypac reference fluid and chia preparation 161

Figure 10.18:Viscometer data at 20°C of KCl and Xanthan Gum reference fluid and chia preparation... 162

Figure 10.19:Viscometer data at 50°C of KCl and Xanthan Gum reference fluid and chia preparation... 162

Figure 10.20:Viscometer data at 50°C of KCl and Xanthan Gum reference fluid and chia preparation... 163

Figure 10.21:Viscometer data at 20°C of KCl and Xanthan Gum reference fluid and chia and MPP 163

Figure 10.22:Viscometer data at 50°C of KCl and Xanthan Gum reference fluid and chia and MPP 164

Figure 10.23:Viscometer data at 80°C of KCl and Xanthan Gum reference fluid and chia and MPP 164

Figure 10.24: Viscometer data of reduced Xanthan Gum at Various Temperatures 165

Figure 10.25:Annular Pressure Loss of chia in bentonite at 20°C..... 169

Figure 10.26:Annular Pressure Loss of chia in bentonite at 50°C..... 169

Figure 10.27:Annular Pressure Loss of chia in bentonite at 80°C..... 170

Figure 10.28:Annular Pressure Loss of MPP in bentonite at 20°C..... 170

Figure 10.29:Annular Pressure Loss of MPP in bentonite at 50°C..... 171

Figure 10.30:Annular Pressure Loss of MPP in bentonite at 80°C..... 171

Figure 10.31:Annular Pressure Loss of chia in KCl at 20°C..... 172

Figure 10.32:Annular Pressure Loss of chia in KCl at 50°C..... 172

Figure 10.33:Annular Pressure Loss of chia in KCl at 80°C..... 173

Figure 10.34:Pump Pressure of chia in bentonite at 20°C 173

Figure 10.35:Pump Pressure of chia in bentonite at 50°C 174

Figure 10.36:Pump Pressure of chia in bentonite at 80°C 174

Figure 10.37:Pump Pressure of MPP in Bentonite at 20°C 175

Figure 10.38:Pump Pressure of MPP in Bentonite at 50°C 175

Figure 10.39:Pump Pressure of MPP in Bentonite at 80°C 176

Figure 10.40:Pump Pressure of Chia and MPP in KCl at 20°C..... 176

Figure 10.41:Pump Pressure of Chia and MPP in KCl at 50°C..... 177

Figure 10.42:Pump Pressure of Chia and MPP in KCl at 80°C..... 177

Figure 10.43:ECD of Chia in Bentonite at 20°C 178

Figure 10.44:ECD of Chia in Bentonite at 50°C 178

Figure 10.45:ECD of Chia in Bentonite at 80°C 179

Figure 10.46:ECD of MPP in Bentonite at 20°C..... 179

Figure 10.47: ECD of MPP in Bentonite at 50°C..... 180

Figure 10.48: ECD of MPP in Bentonite at 80°C..... 180

Figure 10.49: ECD of Chia and MPP in KCl at 20°C..... 181

Figure 10.50: ECD of Chia and MPP in KCl at 50°C..... 181

Figure 10.51: ECD of Chia and MPP in KCl at 80°C..... 182

Figure 10.52: Percent Difference in ECD of chia in bentonite at 20°C..... 182

Figure 10.53:Percent Difference in ECD of chia in bentonite at 50°C..... 183

Figure 10.54:Percent Difference in ECD of chia in bentonite at 80°C..... 183

Figure 10.55:Percent Difference in ECD of MPP in bentonite at 20°C..... 184
Figure 10.56:Percent Difference in ECD of MPP in bentonite at 50°C..... 184
Figure 10.57:Percent Difference in ECD of MPP in bentonite at 80°C..... 185
Figure 10.58:Percent Difference in ECD of Chia and MPP in KCl at 20°C..... 185
Figure 10.59:Percent Difference in ECD of Chia and MPP in KCl at 50°C..... 186
Figure 10.60:Percent Difference in ECD of Chia and MPP in KCl at 80°C..... 186

List of Tables

Table 2.1: The relationship between material behavior, phase shift angle, and storage-and-loss modulus	28
Table 2.2: Summary of equations and parameters used in the Unified Hydraulics Model (Robertson and Stiff, 1976).....	32
Table 4.1: Chemical Composition of Bentonite (Kutlic et al., 2012)	43
Table 4.2: Chemical Content of a Mandarin Peel (Czech et al., 2020).....	48
Table 4.3: Composition of Chia Seeds (Jin et al)	49
Table 4.4: Content of the bentonite reference fluid.....	56
Table 4.5: Mixing procedure of the bentonite reference fluid	56
Table 4.6: Amount of chia in each bentonite based sample	57
Table 4.7: Content of Potassium mud reference fluid made with PolyPac and Pac.....	57
Table 4.8: Mixing Procedure of Potassium Chloride based fluid	58
Table 4.9: Chia content of the samples made with Potassium Chloride and Polypac and Pac	58
Table 4.10: Content of Potassium Chloride reference fluid with Xanthan Gum	58
Table 4.11: Mixing Procedures of Potassium Chloride and Xanthan Gum Reference Fluid	59
Table 4.12: Amount of chia per sample in Potassium Chloride and Xanthan Gum fluids	59
Table 5.1: Effect of Reduction of Pac and Polypac in Bentonite.....	86
Table 5.2: Effect of Reduction of Xanthan Gum in KCl	87
Table 5.3: Flow Point and Yield Point vs Amount of Chia in Bentonite	88
Table 5.4: Flow Point and Yield Point vs Amount of Chia in KCl	88
Table 5.5:Flow Point vs Yield Point vs Amount of Mandarin	89
Table 5.6: Effect of Reduction of Pac and Polypac in Bentonite.....	90
Table 5.7: Effect of Reduction of Xanthan Gum in KCl	90
Table 5.8: Flow and Yield Point for reduced Pac and Polypac.....	93
Table 5.9: Flow and Yield Point for reduced Xanthan Gum	93
Table 5.10: Formulation of KCl with TiN nanoparticles	93
Table 6.1:Summary of Chia in Bentonite viscometer dial readings applied in hydraulics simulation.....	96
Table 6.2: Summary of Chia in Bentonite viscometer dial readings applied in hydraulics simulation (cont.)	97
Table 6.3: Summary of Mandarin in Bentonite viscometer dial readings applied in hydraulics simulation	99

Table 6.4: Summary of MPP in Bentonite viscometer dial readings applied in hydraulics simulation (Cont.)	99
Table 6.5: Summary of Chia and MPP in KCl viscometer dial readings applied in hydraulics simulation	102
Table 6.6: Summary of Chia and MPP in KCl viscometer dial readings applied in hydraulics simulation (cont.).....	102
Table 6.7: Viscometer Dial Readings for Ref+2g Chia+2g MPP.....	106
Table 6.8:Model parameters at 20°C.....	107
Table 6.9:Model parameters at 50°C.....	107
Table 6.10:Model parameters at 80°C.....	108
Table 6.11: Summary of all rheological parameters for Ref+2g chia+2g MPP	110
Table 6.12:Viscometer Dial Readings for Ref+3g Chia+1g MPP.....	111
Table 6.13:Model parameters at 20°C.....	112
Table 6.14:Model parameters at 50°C.....	112
Table 6.15:Model parameters at 80°C.....	113
Table 6.16: Summary of all rheological parameters in KCl	115
Table 7.1: Chia and Mandarin Effect on Filtrate Loss in Bentonite-based fluid	123
Table 7.2: Chia and Mandarin Effect on Filtrate Loss in KCl-based fluid	126
Table 7.3: Filtrate Loss and reduced Pac and PolyPac	127
Table 7.4: Flow Point and Yield Point with Reduced Pac and PolyPac	127
Table 7.5: Filtrate Loss and Reduced Xanthan Gum	128
Table 7.6: Flow Point and Yield Point with reduced Xanthan Gum	129
Table 9.1: Static Weight of the Drill String.....	145
Table 9.2: Forces in Straight Incline or Horizontal Section	147
Table 9.3: Forces in the Build Up sections of the string.....	149
Table 9.4: Torque in the Straight Section	151
Table 9.5: Top Sag Factor Data for Chia in Bentonite	165
Table 9.6:Bottom Sag Factor Data for Chia in Bentonite.....	166
Table 9.7: Top and Bottom Sag Factor Data for MPP in Bentonite	166
Table 9.8: KCl with Pac and Polypac top and bottom sag factor data.....	167
Table 9.9: Top Sag Factor data for KCl with Xanthan Gum, Chia and MPP.....	167
Table 9.10:Bottom Sag Factor data for KCl with Xanthan Gum, Chia and MPP	168

List of Abbreviations

BHA	Bottom Hole Assembly
DP	Drill Pipe
EC	Electrical Conductivity
EDS	Energy Dispersive Spectroscopy
ERD	Extended Reach Drilling
HPHT	High Pressure High Temperature
KOP	Kick-Off Point
LVE	Linear Viscoelastic
MPP	Mandarin Peel Powder
NP	Nanoparticle
OBM	Oil Based Mud
PV	Plastic Viscosity
ROP	Rate of Penetration
SBM	Synthetic-based Mud
TC	Thermal Conductivity
TOB	Torque-on-bit
WBM	Water Based-Mud
YP	Yield Point
POOH	Pull Out Of Hole
RIH	Run Into Hole

1 Introduction

This thesis will present a formulation and characterization of a new eco-friendly drilling fluid that is modified with chia seeds, mandarin peel powder and nanoparticles. The drilling fluids are formulated, tested, and characterized by their rheological properties at t 22°C, 50°C, and 80°C. In this study, the characterizations that are being measured through experimental approaches include viscoelasticity, pH, sag factor, filtrate loss, and coefficient of friction. The drilling fluids' performance in simulation pump pressure, ECD, torque, and drag are also calculated through simulated approaches. The effect of chia seeds and mandarin peel powder will be evaluated based on the experimental and simulation results.

1.1 Background

Drilling fluids are one of the most vital and fundamental components of the drilling and well-construction process. The main functions of drilling fluid are to maintain wellbore stability, cool and lubricate drill bits, transport cuttings, seal permeable formations, control subsurface pressure, prevent well control issues, and reduce formation damage. There are three main types of drilling fluids, water-based muds, oil-based muds, and gaseous drilling fluid, in this study, only water-based muds are studied. There are many factors to take into consideration when designing a drilling fluid for a well drilling operation, of which the main ones are technical performance, cost, and environmental impact (Watts and Bagherpour, 2015). With the rise in fewer conventional wells, the need for more specialized drilling fluids is increasing. For example, with deep-water, arctic, and extended-reach reservoirs, drilling fluids must be suitable for high-temperature and high-pressure conditions (Alshubbar et al., 2017, Smith et al., 2018).

Generally, oil-based drilling fluid is used for high-pressure-high-temperature (HPHT) drilling operations. This is due to the properties of water-based drilling fluids changing significantly under high pressure. Whereas oil-based drilling fluids are superior for offering higher penetration rates, enhanced shale stability, reduced downhole fluid losses, and lubricity leading to reduced torque and drag on the drill string and drill bit. The main drawbacks of oil-based drilling fluid are the high costs and environmental concerns associated with the chemicals used

in oil-based drilling fluid. Many of the commonly used additives in drilling fluid are considered environmentally hazardous due to them being non-degradable. Therefore, use of water-based drilling fluid has increased in the petroleum industry as well as research into developing additives and recipes that increase its performance.

One of the main ingredients in water-based drilling fluids is bentonite, which is a clay that is remarkable for its characteristics that include gelling abilities, filtration control, and viscosity. Bentonite alone does not produce a high enough density water-based drilling fluid to control formation pressure, thus additives that increase the density must be added to achieve the required density to control the formation pressure. Many of the commonly used additives are environmentally hazardous materials because they are categorized as non-degradable (Al-Hameedi et al., 2019a, Amanullash, 2007, Zheng et al., 2020). It is necessary to reduce the environmental impact of drilling operations, therefore discovering new eco-friendly additives that can replace the currently used environmentally hazardous additives has become imperative.

Several studies have been conducted that have investigated the implementation of food waste materials alongside nanoparticles as additives in water-based drilling fluids. Some of the food-waste materials and plant-based materials that have been tested include grass clippings, palm leaves, xanthan gum, chia and mandarin peels. Many ecological additives have shown improvements in filtration properties as well as other rheological parameters. Chia seeds have been studied extensively for their gelling abilities but have not been studied as an additive in the drilling fluid. In summary, the use of mandarin peel powder and chia seeds as additives in water-based drilling fluid will be studied.

1.2 Problem Formulation

With the growing demand of the petroleum industry to be more environmentally conscious, water-based drilling fluids have grown in use over oil-based drilling fluids as they are a more environmentally sustainable and cost-efficient fluid. However, when it comes to fluid properties such as temperature stability, rheological performance, fluid loss, and reduced frictional resistance; oil-based drilling fluids are superior to water-based drilling fluids. One of the biggest problems is that WBM tends to be more affected by high temperatures than OBM therefore it is

important to formulate WBM that is thermally stable. It has become necessary to improve water-based drilling fluid with additives that are environmentally friendly and cost-effective. In this thesis the following issues are addressed:

- Performance of chia seed suspensions on water-based drilling fluid
- Performance of mandarin peel powder on water-based drilling fluid
- Performance of titanium nitride nanoparticle suspensions on the best chia-based water-based drilling fluid.

1.3 Objective

This thesis aims to investigate the issues addressed in the problem formulation through experimental and simulation studies. The main objectives are as follows:

- Literature study on the theories used to characterize drilling fluid and to simulate the drilling fluid performance
- Investigate the effect of different concentrations of chia seeds on water-based drilling fluid
- Evaluate the combination of mandarin peel powder and chia seeds on water-based drilling fluid
- Evaluate the application of chia seed, mandarin peel powder and titanium nitride with respect to cost and environmental issues.
- TiN nanoparticles effects on thermally stable water-based drilling fluid

1.4 Research Methods

In this study, the approach used to achieve these objectives is divided into three main categories: literature study, experimental work, and drilling fluid performance simulation study. Figure 1.1 illustrates the scope and process of the work. The literature study will involve covering the theory behind the functions of drilling fluid and properties such as rheology, torque and drag, friction, electrical and thermal conductivity, and hydraulics. Additionally, descriptions of the chemicals and equipment used in the study will be presented. Next, the experimental work section covers the formulation and characterization of drilling fluids with the addition of chia seeds, mandarin

peel powder, and titanium nitride. The final section, the simulation study, will present the hydraulic performance simulation of the drilling fluid enhanced with chia seeds and mandarin peel powder. The torque and drag simulation will simulate the best fluid formulations enhanced with titanium nitride.

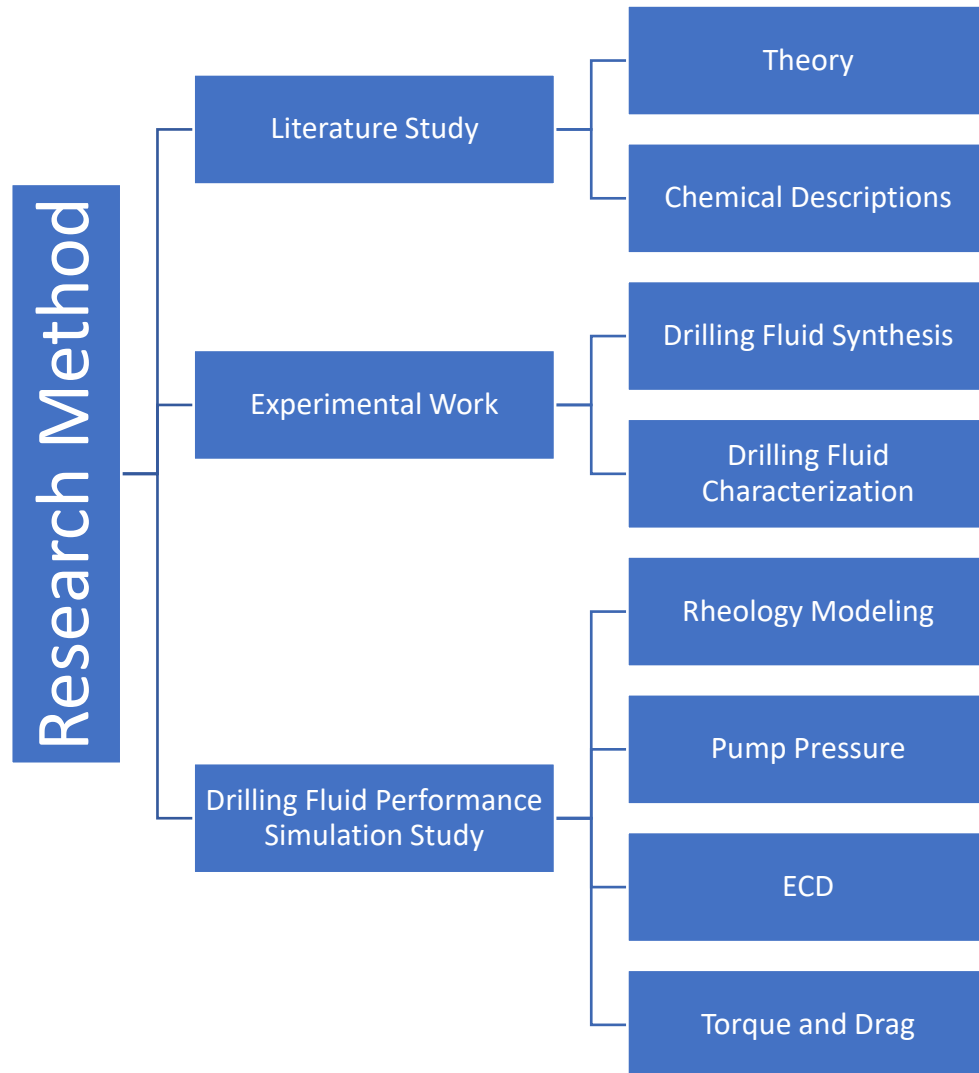


Figure 1.1: Summary of the Research Method used

2 Theory

The foundations of the experimental and simulation research used in this study are presented in this chapter. Drilling fluid theory, including its rheological, viscoelastic, and friction properties will be necessary for the characterization procedure, whereas the simulation study will call for an understanding of hydraulics and torque and drag.

2.1 Drilling Fluid

Drilling fluid is any fluid that is circulated in the borehole during a drilling operation. Drilling fluids and drilling mud is considered synonymous (Schlumberger Limited, n.d.-c), except for gaseous drilling fluid which uses a variety of gasses and may or may not contain bentonite. Generally, drilling fluids that contain bentonite and are water or oil-based are referred to as drilling mud. Drilling fluids serve a variety of purposes and a few of their quintessential functions are as follows (Williamson et al., 2013):

- Cuttings removal
- Formation pressure control
- Lubricating and cooling the drill bit
- Wellbore stability

Drilling fluids account for approximately ten percent of the total cost of the drilling operation, with additives being some of the most expensive components (Lake and Mitchell, 2006). One way to reduce the cost is to investigate more cost-efficient alternatives that do not compromise the drilling fluid properties. A well-designed and maintained drilling fluid is critical to the drilling operation as a poorly designed or maintained mud can lead to lost circulation, a destabilized wellbore, or decreased rates of penetration. Factors such as the geology, pressure, and temperature of the wellbore must be considered when designing a drilling fluid.

2.1.1 Drilling Fluid Properties

The properties of the drilling fluid are critical to the drilling operation and factors such as wellbore condition and maintenance must be considered. This section will the importance of the physical and chemical properties including mud weight, fluid loss, pH, electrical conductivity, and thermal

conductivity. Another important property is viscosity, but that is covered under the rheological property section.

2.1.1.1 Mud Weight

The main property that dictates the amount of hydrostatic pressure produced by the drilling mud is the mud weight. Hydrostatic pressure is critical in drilling operations as it prevents the collapse of the open hole or casing as well as preventing formation fluids from flowing into the wellbore. Mud weight, also known as mud density, is defined as the mass per unit volume of drilling fluid. The main consideration in designing a mud weight is that it lies within the safe operation window for the well, meaning that the wellbore pressure with the mud lies between the pore and fracture pressure of the well. A wellbore pressure below the pore pressure will cause formation fluid to enter the well and a wellbore pressure above the fracture pressure will lead to the drilling fluid fracturing the formation (Schlumberger Limited, n.d.-h).

2.1.1.2 Fluid Loss

Fluid loss, also known as filtrate loss, refers to the leakage of the drilling fluid into the formation, which can lead to a buildup of solid material that is referred to as filter cake (Schlumberger Limited, n.d.-e). Filter cake forms as solid particles in the drilling fluid accumulates on the wall of the wellbore and form a solid matter. The filter cake can lead to issues such as stuck pipe, higher torque and drag, and reduced production if it forms on the producing zones of the wellbore, but it is also desirable to have a certain degree of filter cake building up to isolate the formation from the drilling fluids. Therefore, drilling fluids are studied to predict the filter cake properties such as cake thickness, toughness, slickness, and permeability (Strand, 1998). For example, the thickness of the filter cake is related to the number of solid particles in the drilling fluid as well as the amount of fluid loss. The factors that lead to fluid loss are the formation's permeability and porosity, the drilling fluid's ability to form a dense filter cake, and the difference in the pressure of the wellbore and formation. It is therefore necessary to control the fluid loss and consequentially minimize the thickness and permeability of the filter cake. One way to control filter loss is by using additives. Currently, the industry uses clays, dispersants, and polymers as fluid loss additives.

2.1.1.3 *pH*

pH is the measure of how acidic or basic a substance is on a scale of 0 to 14, with 0 being more acidic and 14 being more basic. A fluid with a pH of 7 is considered neutral. pH more specifically refers to the concentration of hydrogen ions in a solution. Drilling fluid is commonly a very complex mixture of basic elements such as water and bentonite and more complex chemical additives. To ensure that this mixture functions as designed, the pH must be within a certain range. One study found that the optimal range for water-based mud is 8.0 to 10.5 (McCoremick, 2015). A drilling fluid that is too acidic can lead to the drilling fluid being corrosive to the equipment within the well and can cause pollution in the surrounding environment. Also, changes in the pH of the drilling fluid can cause drastic changes in the rheological properties. Therefore, it is necessary to monitor the pH of the drilling fluid and adjust the pH with additives such as soda ash, sodium hydroxide, potassium hydroxide, or calcium hydroxide.

2.1.2 *Drilling Fluid Types*

When planning and designing a drilling operation, the choice in which type of drilling fluid to use is vital and can impact the entire operation. There is no drilling fluid that works in all well types, therefore it is crucial to choose the optimal one. The major factors to consider are the cost and environmental impact. Other factors that will be considered is if the well is a high-temperature and high-pressure well, loss zones, type of shales encountered, and the well trajectory. Safety issues must also not be overlooked as the drilling fluid's mud weight must be able to control the well and the surge and swab pressures must not be excessive. The main types of drilling fluids are water-based mud, oil-based mud, and gaseous drilling fluids (Lake and Mitchell, 2006, Schlumberger Limited, n.d.-q). Each of these have their own advantages and disadvantages.

2.1.2.1 *Water-Based Mud*

About 80% of drilling operations use water-based mud, making it the most used drilling fluid. This could be due to being less expensive compared to oil-based and gaseous drilling fluids. The water used as a base in the water-based mud can be fresh water, seawater, brine, saturated brine, or a formate brine (Lake and Mitchell, 2006, Schlumberger Limited, n.d.-q). The choice of what kind of water to use relies on anticipated well conditions as well as the characteristics of the interval of the well being drilled. Water-based mud can be classified into two different categories:

dispersed or non-dispersed. Non-dispersed muds are muds where the clay is treated through dilution, encapsulation or flocculation to prevent the clay from hydrating. Dispersed drilling muds are treated with chemical dispersants that deflocculate the clay particles to allow better control over the rheology. Non-dispersed muds are typically used for drilling at the surface.

2.1.2.2 Oil-Based Mud

Oil-based muds were introduced in the 1960s and are an emulsion of oil and water. The oil typically used in oil-based mud is diesel, kerosene, fuel oil, crude oil, or mineral oil. For the water phase, typically freshwater is used or a solution of sodium or calcium chloride. The structure of the oil-based mud is maintained using emulsifiers, wetting agents and gellants. If the emulsion is not stable, it could separate into two distinct layers. Oil-based muds were created to address issues such as formation clays that react to water, high downhole temperatures, contaminants, stuck pipe, and high torque and drag (Elkatatny, 2018, Lake and Mitchell, 2006). Oil-based mud are the preferred drilling fluid in complex wells such as high-pressure high-temperature wells and horizontal and direction wells. The main disadvantage of oil-based mud is their high cost and their environmental impact.

2.1.2.3 Gaseous Drilling Fluid

Gaseous drilling fluid is the term for when systems of compressed air, mist, foam, or gas are used as a drilling fluid. When using gaseous drilling fluid, a technique called underbalanced drilling must be used where the hydrostatic head of the drilling fluid is lower than the formation pressure of the wellbore. There are a few reasons that gaseous drilling fluid is used, and one is that it is considerably cheaper than using water-based mud or oil-based mud. Another reason is to maximize hydrocarbon recovery, this is because when using air there is no contamination of the wellbore with solids or mud filtrate. Gaseous drilling fluid use also leads to there being no need for well cleanup once the well is drilled. Another advantage is that gaseous drilling fluids can lead to higher ROP and it allows any produced fluids to be analyzed immediately to determine where the producing zone is.

2.2 Rheology

Rheology is the study of the flow and deformation of a material and how materials flow related to shear rate, time, temperature, and pressure (Chilingarian and Vorabutr, 1983). Rheology is important to the oil industry as every step in the process to produce oil and gas involves fluid flow. This study focuses on fluid used while drilling, but the rheology of the produced fluids as well as fluids used during completion and workover operations are also critical to successfully produce the well. Two of the rheological properties that are considered most significant are flow rate and flow pressure. These properties affect the drilling fluid's ability to transport cuttings and the drilling fluid's circulation pressure (Devereux, 2012, Lake and Mitchell, 2006, Schlumberger limited, n.d.-I).

2.2.1 Rheological Properties

Rheological properties include viscosity, gel strength and yield point. The oil industry is most concerned about viscosity, which is the fluid's resistance to flow. This is because the entire point of the oil industry is to transport fluids from deep in the earth to the surface and is important to drilling fluids as they are circulated through the well. These three properties are explained in the following subsections.

2.2.1.1 Viscosity

There are two types of viscosity: apparent viscosity and plastic viscosity. Apparent viscosity is the relation between shear stress and shear rate of a fluid. For this study, we will be focusing on plastic viscosity as we are studying drilling fluid. Plastic viscosity is the resistance to the flow of a fluid in bores. The resistance is caused by the friction between solids and liquids within the drilling fluid. Plastic viscosity is measured in centipoise (cP) and is determined by the fluid's viscosity and particle content (Kolle and Mesel, 1998, Strand, 1998).

2.2.1.2 Gel Strength

The amount of gelling that will happen when circulation stalls is determined by the gel strength, which is a measurement of the inter-particle forces in a drilling fluid. Gel strength is measured in pounds per 100 square feet (lb/100ft²). It is usually measured using a viscometer. Gel strength is an important factor in drilling fluid as it relates to the drilling fluid's ability to efficiently transport

cuttings made during drilling up to the surface (Schlumberger Limited, n.d.-p, Strand, 1998). The drilling fluid jellifying during static conditions provides it the ability to support the drill string when not actively drilling.

2.2.1.3 Yield Point

The yield point refers to the amount of shear stress required to make the material flow or yield. More specifically, it indicates how much shear stress must be applied for shear stress to become the dominant force that leads to the particle structure of the fluid to flow (Anton Paar GmbH, n.d.-b, Strand, 1998). In solids this would be the amount of shear stress that transform the solid into a fluid state. When it comes to drilling fluids, yield point is used to evaluate the fluid's ability to lift cuttings out of the annulus. A high yield point would indicate that the drilling fluid is better at carrying cuttings than a drilling fluid with a similar density but lower yield point. Yield point can be increased in drilling fluids by adding a flocculant or by adding more dispersed clay and it can be decreased by adding a deflocculant.

Figure 2.1 illustrates the change in particle structure as a material's structure is broken down by shear stress and begins to flow.

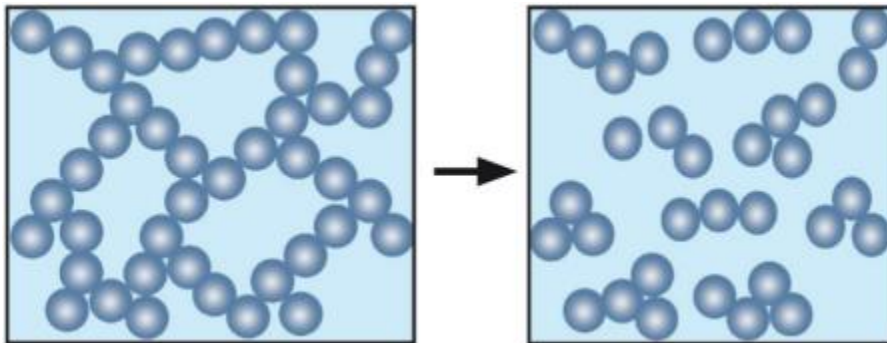


Figure 2.1: A material's structure in a solid state (left) and in a fluid state (right)

2.2.2 Shear Stress and Shear Rate

Shearing refers to the occurrence of shear stress and shear rate wherein a material deforms due to forces applied to the material (Chilingarian and Vorabutr, 1983). It is usually modeled in physics as two plates where one plate is stationary, and the other plate moves parallel to the stationary

plate as shown in figure 2.2. Shear stress and shear rate are further elaborated in the following subsections.

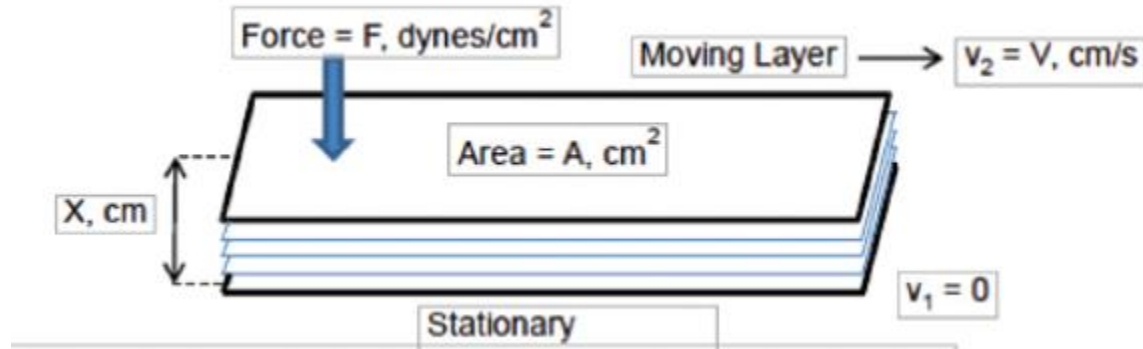


Figure 2.2: Two plate model illustrating shear stress and shear rate of a fluid

2.2.2.1 Shear Stress

Shear stress is the force required to maintain a constant flow of a fluid. In the petroleum industry it is defined as the force required to maintain a constant rate of flow. For drilling fluids, the force is provided by the pump pressure. The resistance to flow is caused by the frictional resistance between the layers of displaced fluid within the fluid. The units are in Pascals (Pa) and is a measurement of the applied shear force divided by the surface area exposed to the shear force. Shear Stress can be expressed mathematically as follows (Chilingarian and Vorabutr, 1983, Kollé and Mesel, 1998, Schlumberger Limited, n.d.-n):

$$\tau = \frac{F}{A}$$

(2.1)

Where:

- τ = Shear stress [Pa]
- F = Applied force [N]
- A = Surface area exposed to shear [m^2]

2.2.2.2 Shear Rate

Shear rate is the rate of change of velocity. This occurs when one layer of fluid passes over an adjacent. It is commonly measured as a velocity gradient across the diameter of fluid channels such as pipes or annuli or similar shapes. In the petroleum industry it is expressed as the ratio of the fluid velocity and the distance from the pipe wall. This means that the shear rate increases the closer the fluid is to the pipe wall, as shown in equation 2.2 (Chilingarian and Vorabutr, 1983, Schlumberger Limited, n.d.-m):

$$\dot{\gamma} = \frac{dv}{dr} \tag{2.2}$$

Where:

- $\dot{\gamma}$ = Shear rate [1/s]
- dv = Fluid velocity [m/s]
- dr = Distance from pipe wall [m]

In a pipe, the fluid at the center of the pipe tends to have the highest velocity whereas with shear rate where it has a lower value than fluid at the walls of the pipe (Skjeggestad, 1989). The geometrical structure of the pipe as well as the fluid's viscous properties affect the magnitude of the shear rate (Chilingarian and Vorabutr, 1983).

2.3 Rheological Models

Rheological Models attempt to describe the behavior of a fluid's rheology such as the relationship between shear rate and viscosity. Many have been developed to try to describe the behavior of drilling fluids, but most are not accurate when compared to experimental data in all conditions. Although there are some models that do give an accurate estimate of the drilling fluid behavior (Guo and Liu, 2011, Lake and Mitchell, 2006). It is important to have a rheological model that accurately reflects the drilling fluid behavior in order to predict how the fluid will behave under all conditions of the wellbore. Therefore the drilling fluid's fluid type must be investigated to be able to construct a model of it. Fluids are classified into two types depending on the it's

relationship between shear stress and shear rate. These two types are called Newtonian and non-Newtonian fluids and they will be described in the following sub-section.

2.3.1 Newtonian Fluids

Newtonian Fluids are ones whose viscosity is not affected by shear rate but is affected by temperature and pressure (Chilingarian and Vorabutr, 1983, Lake and Mitchell, 2006). Water, air, and alcohol are examples of commonly found Newtonian fluids. Newtonian fluids are commonly single phase and made up of small molecules. They are useful for their ability to maintain constant viscosity at constant temperatures and varying shear rates.

The rheological behavior can be described by the following relationship (Schlumberger Limited, n.d.-i, Rehm, 2012):

$$\mu = \frac{\tau}{\dot{\gamma}}$$

(2.3)

Where:

- μ = Viscosity [cP]
- τ = Shear stress [Pa]
- $\dot{\gamma}$ = Shear rate [1/s]

The shear stress is directly proportional to the shear rate as shown in figure 2.3.

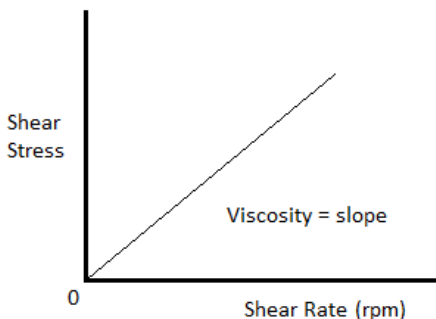


Figure 2.3: Graph showing the linear relationship between shear rate and shear stress of a Newtonian Fluid

2.3.2 Non-Newtonian Fluids

Non-Newtonian Fluids are fluids that are not described by the Newton's law i.e. the shear stress being directly proportional to the shear rate. Viscosity in a non-Newtonian fluid varies at different shear rates and the relationship between shear rate and shear stress is non-linear. Thus, it can behave either more like a solid or more like a liquid depending on the force exerted on it. This behavior makes it ideal as a drilling fluid since there are instances where you want the drilling fluid to behave more like a solid. Since the Newtonian fluid model does not accurately represent the behavior, other models must be used to accurately describe the flow behavior (Rehm, 2012, Schlumberger Limited, n.d.-j). The models that are further used in this thesis, out of the many that have been described in the literature to estimate the rheological parameters, are the Bingham Plastic, Power Law, Herschel-Bulkley, Unified and Robertson-Stiff models.

2.3.2.1 Bingham Plastic Model

A Bingham plastic material is one that behaves like a solid under low stress but flows as a fluid at once the stress reaches yield stress. Once it reaches the threshold yield stress, there is a linear relationship between shear stress and shear rate (Schlumberger Limited, n.d.-a). This is a common model used for drilling fluid. The connection between the parameters is shown in Figure 2.4 where the shear stress-shear rate relationship begins at the yield point.

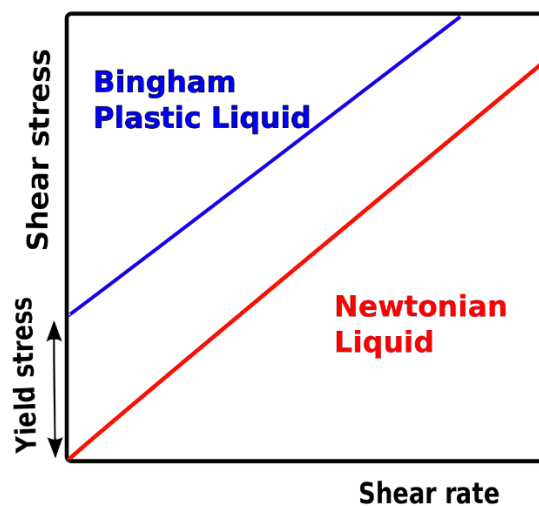


Figure 2.4: Graph showing the relationship between shear stress and shear rate of a Bingham Plastic Fluid versus a Newtonian Fluid

The parameters yield point (YP) and plastic viscosity (PV) can be determined from viscometer dial readings, which is expressed in equation 2.4 and 2.5;

$$PV = \theta_{600} - \theta_{300} \tag{2.4}$$

$$YP = \theta_{300} - PV = 2 \cdot \theta_{300} - \theta_{600} \tag{2.5}$$

The Bingham plastic model then can be expressed mathematically as follows:

$$\tau = YP + PV \cdot \dot{\gamma} \tag{2.6}$$

Where:

- τ = Shear stress [lbf/100 ft²]
- YP = Yield Point [lbf/100 ft²]
- PV = Plastic viscosity [cP]
- $\dot{\gamma}$ = Shear rate [1/s]
- θ_{300} = Viscometer dial reading at 300 RPM [°]
- θ_{600} = Viscometer dial reading at 600 RPM [°]

2.3.2.2 Power-Law Model

Whereas the Bingham Plastic model describes fluids that have a linear relationship between shear stress and shear rate, the Power-Law Model describes fluids that do not show a linear. This model utilizes parameters referred to as consistency index, k , and flow behavior index, n (Belayneh, 2019b, Skjeggstad, 1989). The model can model the behavior of fluids with the following characteristics

- Pseudoplastic fluids, or shear thinning- are fluids whose behavior has a lower viscosity at higher shear rates and have an n of less than 1

- Newtonian fluids where $n=1$ and viscosity are independent of shear rate
- Dilatant fluids, or shear thickening, are fluids where viscosity increases with increasing shear rate and $n>1$.

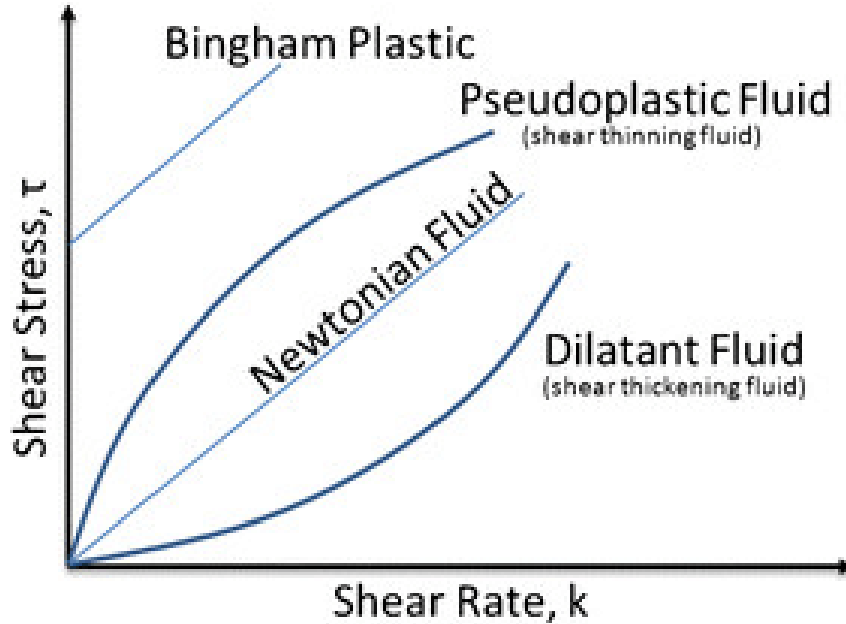


Figure 2.5 Graph showing the relationship between shear stress and shear rate of the Power Law Model

The mathematical expression of the Power Law model is as shown:

$$\tau = k \cdot \dot{\gamma}^n \tag{2.7}$$

Where the parameters k and n are calculated from viscometer dial readings using the equation 2.8 and 2.9:

$$k = \frac{\theta_{300}}{511^n} = \frac{\theta_{600}}{1022^n} \tag{2.8}$$

$$n = 3.32 \log \left(\frac{\theta_{600}}{\theta_{300}} \right) \tag{2.9}$$

Where:

- τ = Shear stress [lbf/100 ft²]
- k = Consistency index [lbs/100 ft²/s]
- $\dot{\gamma}$ = Shear rate [1/s]
- n = Flow behavior index []
- θ_{300} = Viscometer dial reading at 300 RPM [°]
- θ_{600} = Viscometer dial reading at 600 RPM [°]

2.3.2.3 *Herschel-Bulkley Model*

The Herschel-Bulkley Model seeks to model the behavior of fluids that are similar to Bingham Plastic fluids, require a certain amount of stress applied to flow, and do not have a linear relationship between shear stress and shear rate, similar to the Power-Law Model. This is believed to be a better description of drilling fluids and is preferred to both the Bingham Plastic and Power Law Models. The mathematical expression of the model is expressed as (Belayneh, 2019b, Schlumberger limited, n.d.-f):

$$\tau_{HB} = \tau_y + k\dot{\gamma}^n \tag{2.10}$$

Where:

- τ_{HB} = Shear stress for Herschel-Bulkley model [lbf/100ft²]
- τ_y = Yield stress [lbf/100ft²]
- k = Consistency index [lbs/100 ft²/s]
- $\dot{\gamma}$ = Shear rate [1/s]
- n = Flow behavior index [Dimensionless]

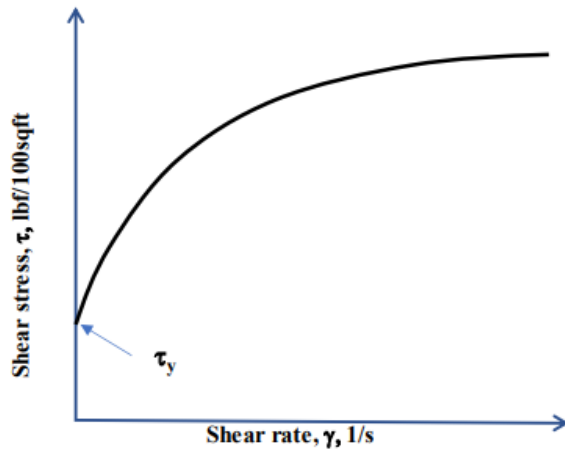


Figure 2.6: Graph showing shear stress and shear rate relationship of the Herschel-Bulkley Model

2.3.2.4 Unified Model

The unified model is a yielded power-law model similar to the Herschel-Bulkley model but is simplified and more suitable for fieldwork. The unified model estimates the yield stress based on the two lowest shear stress data of 3 and 6 RPM, which is the main variation between the models.

The unified model is written as follows (Ochoa, 2006):

$$\tau_{UN} = \tau_{yL} + k\dot{\gamma}^n \quad (2.11)$$

The parameter, τ_{yL} , replaces the yield stress value used in the Herschel-Bulkley model, it refers to the lower shear yield point instead of the yield stress value. The way to calculate based on the dial readings is as follows:

$$\tau_{yL} = (2 \cdot \theta_3 - \theta_6) \cdot 1.066 \quad (2.12)$$

Once the lower shear stress is estimated using equation 2.12, the consistency index (k) and flow index (n) are determined by curve fitting.

2.3.2.5 Robertson-Stiff Model

The Robertson-Stiff model was presented in an SPE journal paper in 1976 by Robertson and Stiff and is considered a more accurate rheological model for drilling fluid than the Herschel-Bulkley model. The model is proposed to be an improved mathematical model for describing the relation between shear stress and shear rate in cement slurries and drilling fluids (Robertson and Stiff, 1976). The model uses parameters referred to as A, B, and C. The Power Law model's k and n parameters are represented by the parameters A and B, respectively, while the shear rate is corrected for by parameter C. Although the model is rarely used in the drilling industry due to the difficulty in calculating these parameters. The basic mathematical model is as follows (Ochoa, 2006):

$$\tau = A(\dot{\gamma} + C)^B \quad (2.13)$$

The term $(\dot{\gamma} + c)$ is considered the effective shear rate and C is calculated by the following equation:

$$C = \frac{\dot{\gamma}_{min} \dot{\gamma}_{max} (\dot{\gamma}^*)^2}{2 \cdot \dot{\gamma}^* - \dot{\gamma}_{max}} \quad (2.14)$$

Where $\dot{\gamma}^*$ is the corresponding shear rate of the geometric average of the shear stress, τ^* , which is calculated from the following equation:

$$\tau^* = \sqrt{\tau_{min} \cdot \tau_{max}} \quad (2.15)$$

The shear stress in the Robertson-Stiff model is found by setting the shear rate to zero and is given in the following equation as τ_0 :

$$\tau_0 = AC^B \quad (2.16)$$

The model is commonly used in its logarithmic form and its output is plotted on a log-log diagram so that it generates a straight line as shown in figure 2.8. This diagram can be used to determine

the A and B parameters, which can then be logarithmically converted in equation 2.21. A and B are equal to the slope and intersection at which $(\dot{\gamma} + C)$ is equal to one when plotting τ verses $(\dot{\gamma} + C)$ (Robertson and Stiff, 1976).

$$\log \tau = \log A + B \cdot \log C$$

(2.17)

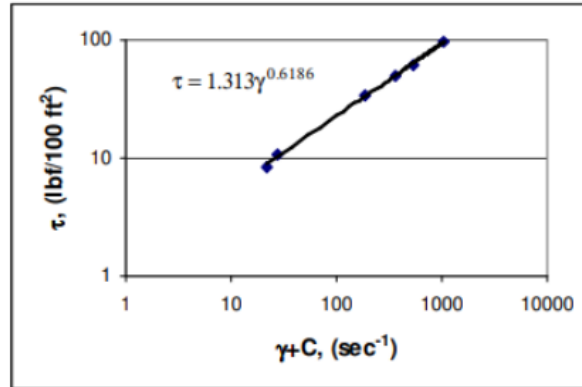


Figure 2.7: Graph showing an example of the Robertson-Stiff Model on a log-log scale

2.4 Viscoelasticity

Viscoelasticity refers to a material's property to exhibit both viscous and elastic characteristics under deformation. The viscoelastic properties enable us to determine the material's gel structure. The gel structure is critical for drilling muds for the drilling fluid to transport cuttings and solid suspensions while the drilling fluid is circulating as well as when it's not circulating. The gel structure also prevents the fluid from invading the reservoir from the annulus of the wellbore while drilling. Viscoelasticity isn't usually tested for out in the field, but it is important to test for while designing and testing novel drilling fluids (Bui et al., 2012).

Viscosity and elasticity are the roots of the word viscoelasticity. While elasticity refers to a solid material's capacity to restore its previous shape and size following deformation, viscosity denotes the resistance to flow of a fluid. When subjected to shear stresses, viscoelastic materials display both elastic and viscous tendencies, indicating that they have both fluid and solid qualities. Hooke's law governs elasticity, while Newtonian fluid law governs the behavior of viscous liquids (Özkaya et al., 2012).

2.4.1 Oscillatory Tests

Oscillatory tests can be performed to test a material's viscoelastic properties. The two-plate model, shown in figure 2.8, which involves a particular amount of material put between a stationary plate and a mobile upper plate with oscillating motion. The sample is sheared as a result of the upper plate moving caused by a driving wheel's revolution. The lower plate is kept stationary by the counterforce, shear stress, and the shear strain is the measured deflection of the shearing process. Given that the preset shear strain stays below a level that can damage the sample's internal structure and produce a non-sinusoidal curve for the ensuing shear stress, two time-dependent sine curves that correspond to both shear forces are generated from this method.

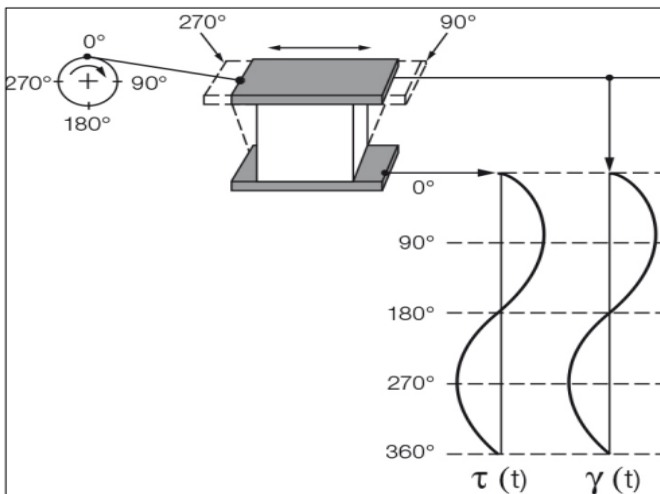


Figure 2.8: Two-Plate Model for an oscillatory test showing ideally elastic behavior in the shear stress and shear strain sine curves

This thesis will utilize an Anton Paar MCR 302 rheometer to perform the rotational oscillatory tests. This process will be described further in subsection 4.2.

2.4.2 Methods for Measuring Viscoelasticity

There are four different oscillatory tests that are often conducted to determine the viscoelastic behavior of a fluid. These tests include (Mezger, 2011):

- Amplitude Sweep

- Temperature Sweep
- Frequency Sweep
- Time Sweep

This thesis will utilize the amplitude sweep tests to evaluate the formulated drilling fluids. Therefore, a more detailed explanation of the two tests will be provided in the following subsection.

2.4.2.1 Amplitude Sweep

The amplitude sweep test is carried out by running an oscillatory test that measures shear stress and shear strain while the amplitude is increased. Temperature and frequency are held constant and the amplitudes are held at each step for a period of time. Before going further into the process of the oscillator test, several viscoelastic parameters must be determined (Anton Paar GmbH, n.d.-b).

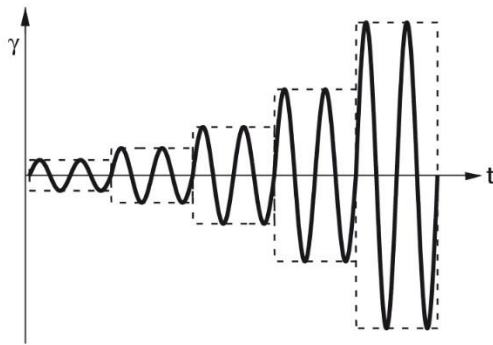


Figure 2.9: Amplitude Sweep example with 5 steps of increased shear strain and amplitudes (Anton Paar GmbH, n.d.-a)

2.4.2.1.1 Shear Stress and Shear Strain

Mentioned previously, the oscillatory tests generate two sine curves that correlate to the preset shear strain and the resulting shear stress. The shear stress and shear strain curves can be expressed as a function of time as follows (Bui et al., 2012):

$$\gamma(t) = \gamma_a \cdot \sin(\omega t)$$

(2.18)

$$\tau(t) = \tau_a \cdot \sin(\omega t + \delta) \tag{2.19}$$

Where:

- γ = Shear strain
- γ_a = Shear rate amplitude, []
- τ = Shear stress [Pa]
- τ_a = Shear stress amplitude [Pa]
- t = Time [s]
- ω = Angular frequency [rad/s]
- δ = Phase shift angle [°]

By combining the equations above, shear stress can be expressed in terms of shear strain by using the sum formula for sine as follows:

$$\tau(t) = \tau_a [\sin(\omega t) \cos(\delta) + \cos(\omega t) \sin(\delta)] \tag{2.20}$$

The formula can then be multiplied by γ_a/γ_a as well as inserting the expression for the storage and loss modulus. This results in the following formulae:

$$\tau(t) = \tau_a \left[\left(\frac{\tau_a}{\gamma_a} \cos(\delta) \right) \sin(\omega t) + \left(\frac{\tau_a}{\gamma_a} \sin \delta \right) \cos(\omega t) \right] \tag{2.21}$$

$$\tau(t) = \tau_a [G' \sin(\omega t) + G'' \cos(\omega t)] \tag{2.22}$$

2.4.2.1.2 The Storage and Loss Modulus

The viscoelastic behavior that reflects the elastic component is known as the storage modulus. In essence, it is the measurement of shearing, or the amount of energy held in a material that has undergone deformation. When the load that created the material's deformation is removed, the unused deformation energy forces the material to return to its original size and shape. The unit of the storage modulus is pascals and is denoted as G' . The storage modulus is equal to the cosine-based expression:

$$G' = \frac{\tau_a}{\gamma_a} \cos(\delta) \tag{2.23}$$

The viscous portion of viscoelastic behavior is reflected by the loss modulus. It is also measured in pascals but is denoted as G'' . The amount of energy that a deformed material expends during deformation is measured by the loss modulus. When the load that created the deformation is released, this energy is wasted. It can alter the structure of the material when in use, and the internal friction created when it flows entirely exhausts the energy. The following sine based expression represents the loss modulus and is also implemented in the shear stress equation:

$$G'' = \frac{\tau_a}{\gamma_a} \sin(\delta) \tag{2.24}$$

2.4.2.1.3 Loss Factor

The loss factor, also referred to as the damping factor, is the proportion of viscous to elastic behavior in viscoelastic systems. According to equation 2.29, the phase shift angle's tangential value is equal to the ratio between the loss and the storage modulus. The behavior of a deformed material can be described by the damping factor. The ideal viscous behavior happens when \tan is infinitely big, whereas the ideal elastic behavior happens when \tan is zero. Additionally, when the damping factor is one, the viscous and elastic components of the viscoelastic behavior are perfectly balanced (Mezger, 2011).

$$\frac{G''}{G'} = \tan(\delta)$$

(2.25)

2.4.2.1.4 The Phase Shift Angle

The phase shift angle, also known as the loss angle, is the difference between the curves that reflect the preset shear strain and the resultant shear stress. It also represents the lag in time between the two sinusoidal curves that serve as functions of time. When compared to the predetermined shear stress curve, the shear strain curve for viscoelastic materials will always display some delay. The loss angle (δ), which is always between 0° and 90° , is the phase lag between the shear stress (τ) and shear strain (γ) curves, as seen in figure 2.10. (Anton Paar

GmbH, n.d.-b, Mezger, 2011).

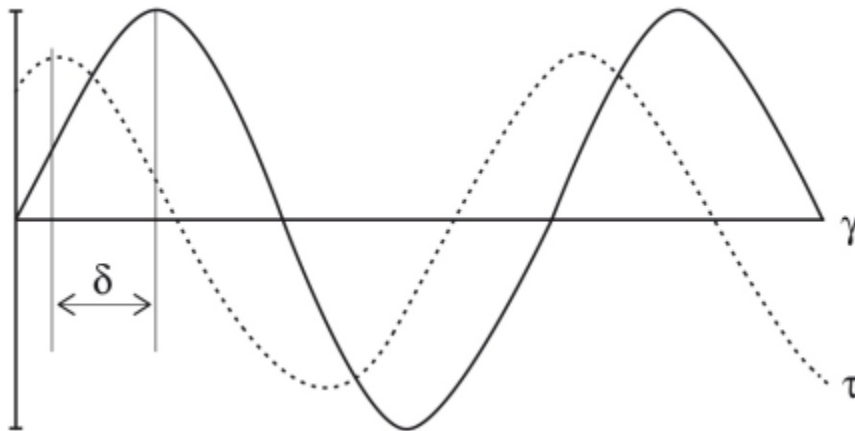


Figure 2.10: Shear strain and resulting shear stress as two sinusoidal functions, offset by phase shift angle (Anton, Paar GmbH, n.d.-b)

2.4.2.2 Amplitude Sweep Test

Amplitude sweeps are commonly presented as a logarithmical diagram where either shear stress or strain is represented on the x-axis and both storage and loss modulus, G' and G'' , are portrayed on the y-axis (Anton Paar GmbH, n.d.-a). An amplitude sweep test can evaluate the gel strength, dynamic yield point and the structural stability. Additionally, they are typically carried out to establish the top limit of the linear viscoelastic range, or LVE range. This range denotes the range of test conditions where the sample's structure can be maintained. At low amplitude values the

values of both G' and G'' are constant until they reach the upper limit of the LVE range where the sample's structure begins to change. The upper limit of the LVE range is represented by (γ_L) in a strain amplitude sweep test (Mezger, 2011). By examining figure 2.11, it can be seen that the sample deforms linearly and viscoelastically up until the limiting strain value. From this point, the LVE range is exceeded, the storage and loss modulus curves begin to deviate, and the deformation becomes non-linear viscoelastic (Bui et al., 2012). The values of G' and G'' and which value is greater is determined by the structural characteristics of the sample. Depending on the structural characteristics of the sample, the curves may also have a point where they crossover. In the illustration below, the diagram to the right is of a solid or gel-like material where G' is larger than G'' . To the right is a liquid sample where G' is smaller than G'' (Anton Paar GmbH, n.d.-a).

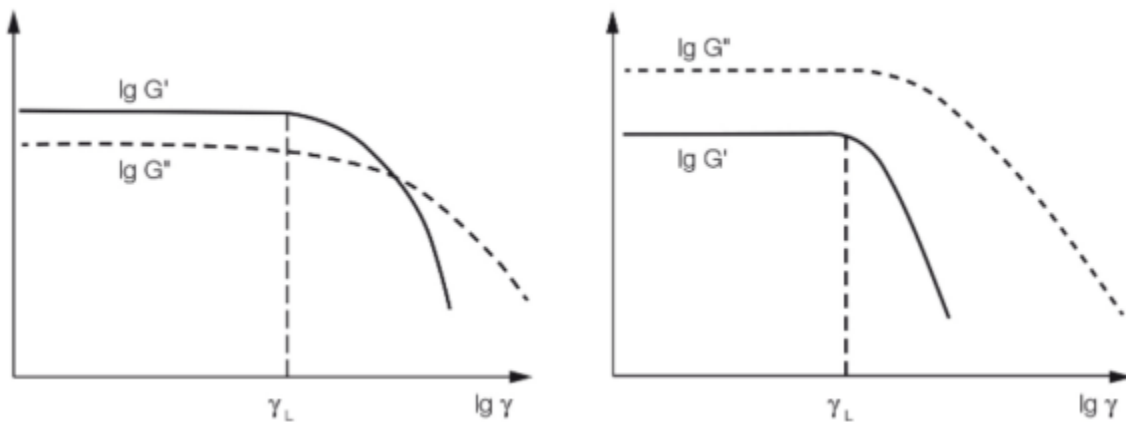


Figure 2.11: Example of results from two amplitude sweep tests showing a gel-like or solid sample (left) or a fluid sample (right)

In some scenarios, the storage and loss modulus remain constant after exceeding the LVE range limit. Rather, the loss modulus G'' may increase until it hits a peak. This pattern suggests that only some of the interior structure of a sample is initially irreversibly deformed, and that the deformation energy absorbed by the internal superstructure before its final dissolution grows. Increasing G'' values may be a result of (Mezger, 2011):

- Long Network bridges
- Unlinked or networked-fixed agglomerates or superstructures
- Mobile single particles
- Relative motion between the molecules

- Flexibility of chains' sides and end pieces

This pattern typically only occurs for polymers with unlinked linear molecules (Mezger, 2011). Figure 2.12 can be used to demonstrate how G moves. At zone 1, the sample will start to show microcracks as the loss modulus rises. The entire sample then ruptures at the crossover point, in zone 2, when the sample exceeds the maximum peak of the curve. By then, the elastic component of viscoelastic behavior has been surpassed by the viscous component (Anton Paar GmbH, n.d.-a).

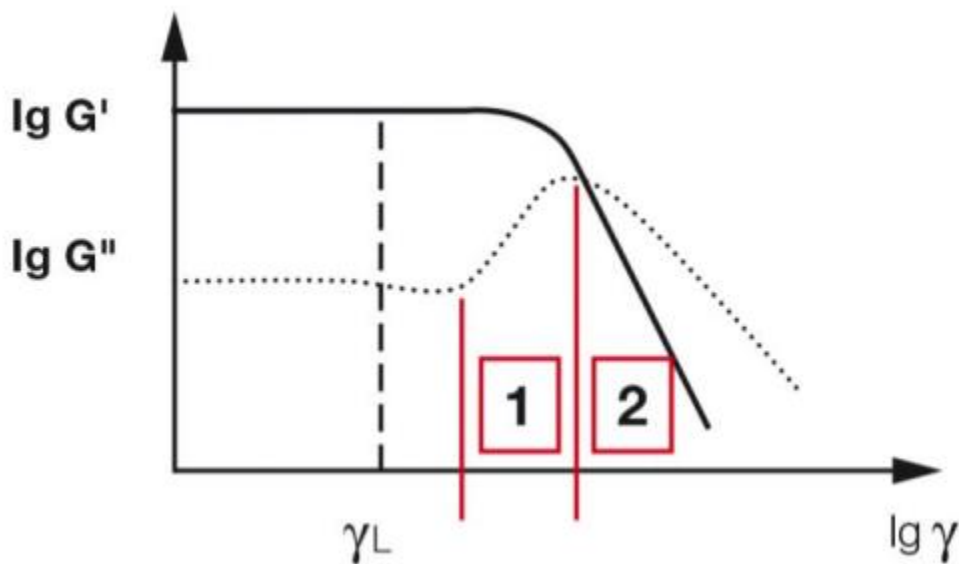


Figure 2.12: Example of an amplitude sweep test where the loss modulus reaches its maximum after exceeding the LVE range (Anton Paar GmbH, n.d.-a)

Amplitude sweeps can deliver information to establish the yield point and flow point of a sample in addition to establishing the LVE range and assessing storage and loss modulus. Regardless of whether the test uses a strain- or a shear-controlled amplitude sweep, the measurement data can also be displayed with shear stress plotted on the x-axis. Figure 2.13 illustrates the determination of the yield point and flow point, denoted as y and f , respectively. The yield point is determined by the upper limit of the LVE range, and the flow point is determined by the intersection of the storage and loss modulus curves. Between the yield point and the flow point, where G' and G'' are balanced and the sample displays behavior that is on the cusp of being liquid,

the material is in a transitional state. G' dominates G'' after that point, indicating that the sample is liquid (Mezger, 2011).

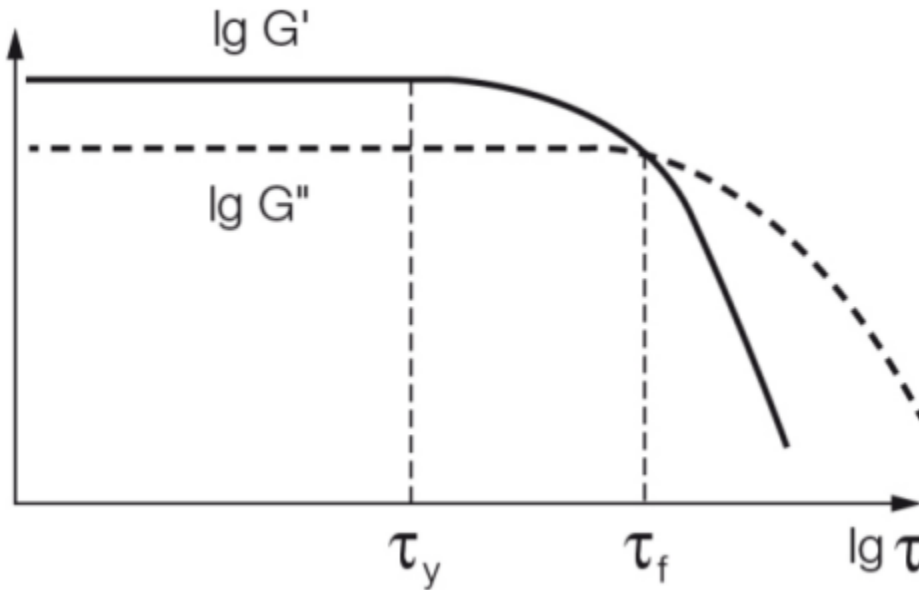


Figure 2.13: Example of an amplitude sweep test where functions of storage and loss modulus are plotted in terms of shear stress (Anton Paar GmbH, n.d.-a)

Table 2.1 provides a summary of a material's behavior under various phase shift angle, storage, and loss modulus conditions. At the flow point, where $G' = G''$ and the phase shift angle is 45° , the proportions of elastic and viscous behavior are indeed equal. The ideal behavior of a material is shown to exhibit optimal viscous flow behavior at $= 90^\circ$ and ideal elastic behavior at $= 0^\circ$. The transition zone between this phase angle interval is where the viscoelastic behavior can be found (Mezger, 2011).

Ideally viscous flow behavior	Viscoelastic liquid behavior	50/50 ratio between viscous and elastic portions	Viscoelastic gel or solid behavior	Ideally elastic behavior
$\delta = 90^\circ$	$90^\circ > \delta > 45^\circ$	$\delta = 45^\circ$	$45^\circ > \delta > 0^\circ$	$\delta = 0^\circ$
$\tan \delta \rightarrow \infty$	$\tan \delta > 1$	$\tan \delta = 1$	$\tan \delta < 1$	$\tan \delta \rightarrow 0$
$G' \rightarrow 0$	$G' < G''$	$G' = G''$	$G' > G''$	$G'' \rightarrow 0$

Table 2.1: The relationship between material behavior, phase shift angle, and storage-and-loss modulus

2.4.3 Static Sag Test

One problem with drilling fluids is called barite sagging, this is when barite particles are precipitated and deposited at the bottom of the wellbore. This occurs when a drilling fluid does not have a sufficient gel structure to suspend the barite particles. In this thesis, the sagging tendencies of the formulated drilling fluids are tested under static conditions to ensure proper gel structure. The static sag was tested according to the following steps

1. The fluid systems were placed into plastic cups and waited at room temperature for one day
2. 10ml of the fluid was taken from the top of the fluid using a syringe and then weighed
3. One milliliter was expelled from the syringe and then the syringe was weighed again. This step was repeated until no more fluid was left in the syringe.
4. Steps 2 and 3 were repeated except the sample of the fluid was taken from the bottom of the cup.
5. The densities of each fluid's samples were calculated using $\rho = m/V$
6. The average values were calculated to estimate the densities at the top and bottom layers.

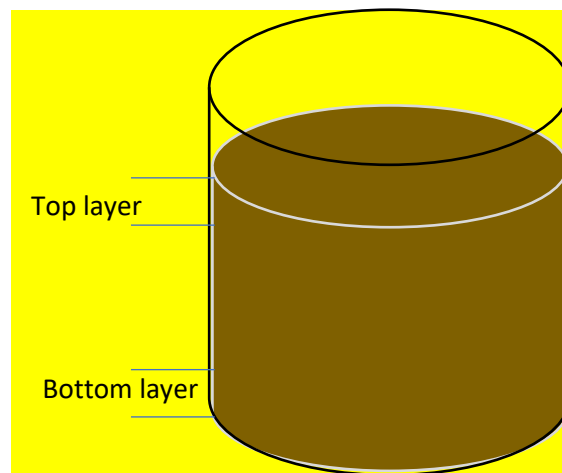


Figure 2.14: Drilling fluids in cup for static sag

The static sag factor is calculated by this formula;

$$sag\ factor = \frac{\rho_{bottom}}{\rho_{top} + \rho_{bottom}} \quad (2.26)$$

The limit for the sag factor is 0.53, if the sag factor is higher than the limit then the drilling fluid has a high sag potential. Otherwise, the fluid system has a sufficient gel structure to hold the particles in suspension.

2.5 Hydraulics Model

The field of hydraulics seeks to study the motion of fluids, some particularly study the motion of fluids within a pipe or in a tank. The foundation of hydraulics' is based in fluid mechanics which is the study of how fluids respond to applied forces (Faber, 2019, Encyclopedia Britannica Inc, 2019). The safety and success of a drilling operation is rooted in fluid hydraulics and the understanding of how the fluids in the wellbore will perform. A hydraulic analysis can address some of the concerns that arise when designing a drilling operation (Guo and Liu, 2011, Whittaker and Exlog, 1985). The following factors are some of the main concerns:

- The downhole ECD lays within the pore- and fracture-gradient
- The required pump pressure to be provided by the mud pump
- Sufficient transport of cuttings
- The bit hydraulic horsepower and jet impact force are maximized by the flow rate

The flow of drilling fluid in a wellbore and the corresponding pressure are critical to maintaining wellbore stability, preventing fluid influx, and the transportation of cuttings. The drilling fluid must provide enough pressure downhole to prevent incidents of well blowouts and kicks. Therefore, precise fluid flow- and pressure-in-the-wellbore predictions are essential for a good drilling fluid system (Mitchell et al., 2011). The performance of the flow is frequently predicted using hydraulic models. The pressure profiles in the annulus and along the entire wellbore can be predicted using such mathematical models. Additionally, they explain how drilling fluids flow. The relationship between flow rate and pressure drop can therefore be established by using hydraulic models to analyze any flow conduit shape, flow regime, or fluid parameters. Numerous

distinct hydraulics models are relevant in rheology. Different types of fluid require different computations in the various models (Guo and Liu, 2011, Hossain and Islam, 2018).

In this thesis, hydraulic simulations were carried out using the Unified model. In a study by Jeyhun Sadigov, where the predictive ability of other models was examined, it was discovered that this specific hydraulics model provided the best correlations of rheological data of drilling fluids (Sadigov, 2013). The parameters and equations required for the Unified hydraulics model for pipe- and annular flow are presented in table 2.2.

Unified Hydraulics Model		
Pipe Flow	Annular Flow	Parameters
$n_p = 3.32 \log \left(\frac{2\mu_p + \tau_y}{\mu_p + \tau_y} \right)$ $k_p = 1.066 \left(\frac{\mu_p + \tau_y}{511} \right)$	$n_p = 3.32 \log \left(\frac{2\mu_p + \tau_y}{\mu_p + \tau_y} \right)$ $n_p = 3.32 \log \left(\frac{2\mu_p + \tau_y}{\mu_p + \tau_y} \right)$	$\mu_p = R_{600} - R_{300}$ $\tau_y = R_{300} - \mu_p$ $\tau_0 = 1.066(2R_3 - R_6)$
$V_p = \frac{24.51q}{D_p^2} \left[\frac{ft}{min} \right]$	$V_p = \frac{24.51q}{D_2^2 - D_1^2} \left[\frac{ft}{min} \right]$	$G = \left(\frac{(3 - \alpha)n + 1}{(4 - \alpha)n} \right) \left(1 + \frac{\alpha}{2} \right)$ <p>For pipe: $\alpha = 0$</p> <p>For annuli: $\alpha = 1$</p>
$N_{Re} = \frac{\rho v_p}{19.36\tau_2}$	$N_{Re} = \frac{\rho v_{p3}}{19.36\tau_2}$	$\tau_w = \frac{(4 - \alpha)}{(3 - \alpha)} \tau_0 + k\gamma_w^n \left[\frac{lbf}{100ft^2} \right]$ $\gamma_w = \frac{1.6Gv}{D_R} [sec^{-1}]$
$f_{laminar} = \frac{16}{N_{Re}}$ $f_{transient} = \frac{16N_{Re}}{(3470 - 1370n_p)}$ $f_{turbulent} = \frac{a}{N_{Re}^b}$	$f_{laminar} = \frac{24}{N_{Re}}$ $f_{transient} = \frac{16N_{Re}}{(3470 - 1370n_p)}$ $f_{turbulent} = \frac{a}{N_{Re}^b}$	$a = \frac{\log(n) + 3.93}{50}$ $b = \frac{1.75 - \log(n)}{7}$
$f_P = (f_{partial}^{12} + f_{laminar}^{12})^{\frac{1}{12}}$	$f_{Pa} = (f_{partial}^{12} + f_{laminar}^{12})^{\frac{1}{12}}$	

$\left(\frac{dP}{dL}\right) = 1.076 \cdot \frac{f_p v_p^2 \rho}{10^5 D_p} \rightarrow \left[\frac{psi}{ft}\right]$ $\Delta P = \left(\frac{dP}{dL}\right) \cdot \Delta L \rightarrow [psi]$	$\left(\frac{dP}{dL}\right) = 1.076 \cdot \frac{f_a v_a^2 \rho}{10^5 (D_2 - D_1)} \rightarrow \left[\frac{psi}{ft}\right]$ $\Delta P = \left(\frac{dP}{dL}\right) \cdot \Delta L \rightarrow [psi]$	$f_{partial} = (f_{transient}^{-8} + f_{turbulent}^{-8})^{-\frac{1}{8}}$
$\Delta P_{Nozzles} = \frac{156qp^2}{(D_{N1}^2 - D_{N2}^2 - D_{N3}^2)^2} \rightarrow [psi]$		

Table 2.2: Summary of equations and parameters used in the Unified Hydraulics Model (Robertson and Stiff, 1976)

2.5.1 Equivalent Circulating Density

Equivalent circulating density (ECD) refers to the pressure in a well created by the circulating drilling fluids (Guo and Liu, 2011). The pressure created by the drilling fluid is depending on several factors including its density, the true vertical depth (TVD) of the well, and whether the fluid is static or dynamic. The hydrostatic pressure, also known as the pressure of static drilling fluids, is the result of adding the mud weight and the well's TVD. ECD is referred to as the effective density when a formation's circulating fluid is considered in relation to the pressure loss brought on by friction between the wellbore wall and the fluid flow (Schlumberger Limited, n.d.-d, Zhongwei et al., 2018). Equation 2.27 provides an expression for it as follows:

$$ECD = MW + \frac{\Delta P_{annulus}}{.0981 \cdot TVD} \quad (2.27)$$

Where:

- MW = Mud weight [sg]
- ΔP = Pressure drop in annulus [bar]
- TVD = True vertical depth [m]

2.5.2 Pump Pressure

The driving force behind a drilling fluid circulation system is the mud pump. Before the pump generates any pump pressure, one must be aware of the drilling fluids' whole circulation path.

Figure 2.17 depicts a typical circulation system and its parts (Guo and Liu, 2011, Schlumberger Limited, n,d-b). As the illustration shows, mud is extracted from the tank into the mud pump and then forced through the standpipe and Kelly, before it finally enters the drill string. Next, the drilling fluid flows through the drill string where it exits at the bottom of the wellbore through bit nozzles. The mud is circulated upwards through the annular space between the string and wellbore wall until it reaches the surface. Then the shale shakers separate the cuttings from the mud. Desanders, desilters, and degassers can be added to remove air, gas, and small particles from the mud. Finally, the clean mud is then pumped back into the mud tank to restart the process (Belayneh, 2019a, Guo and Liu, 2011).

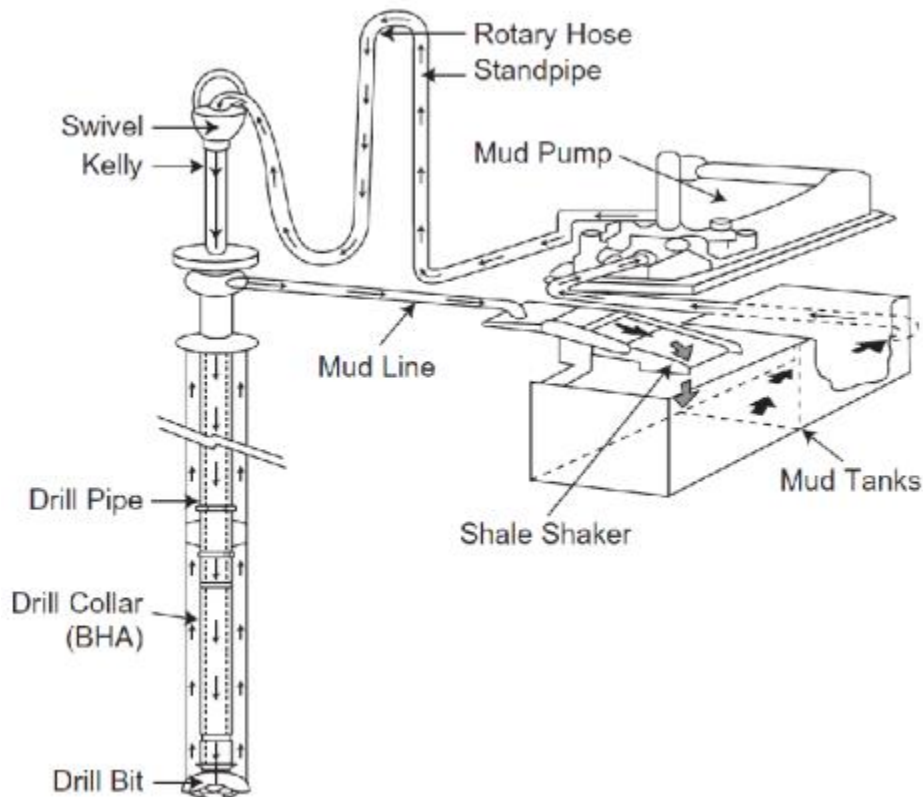


Figure 2.15: Typical drilling fluid circulation system (Guo and Liu, 2011)

As the drilling fluid moves through the circulation system it is exposed to frictional resistance. Figure 2.15 (Zeynalov, 2018) illustrates how the system's pump pressure is decreased by the frictional pressure losses in the components. Therefore, for the drilling fluid to circulate, the

pump pressure needs to be greater than all system pressure losses. Pump pressure can be expressed using the variables provided in figure 2.16 as shown in equation 2.28.

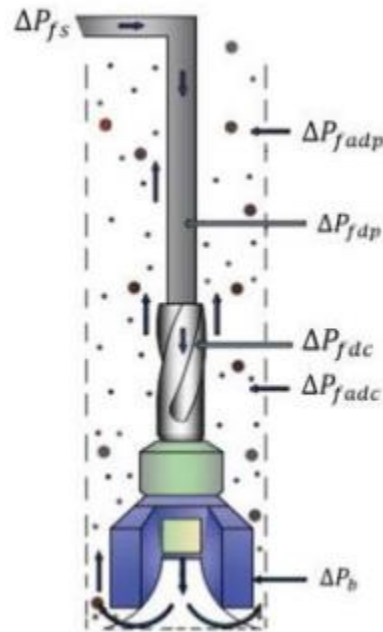


Figure 2.16: Frictional pressure losses in circulating system (Zeynalov, 2018)

$$P_{pump} = \Delta P_{tot} = \Delta P_{fs} + \Delta P_{fadp} + \Delta P_{fdc} + \Delta P_b + \Delta P_{fadc} + \Delta P_{fadp}$$

2.28

Where:

- P_{pump} = Pump pressure [bar]
- ΔP_{tot} = Total frictional pressure loss [bar]
- ΔP_{fs} = Pressure loss in surface flow lines [bar]
- ΔP_{fadp} = Pressure loss in drill pipe [bar]
- ΔP_{fdc} = Pressure loss in drill collar [bar]
- ΔP_b = Pressure loss in nozzles of the drill bit [bar]
- ΔP_{fadc} = Pressure loss in the annular space between the wellbore and drill collar [bar]
- ΔP_{fadp} = Pressure loss in the annulus between the wellbore and drill pipe [bar]

2.6 Tribology and Friction

The study of lubrication, wear, and friction between moving surfaces is known as tribology (Yan, 2013). Wear is the term used to describe the removal of material from a surface as a result of contact, whereas friction is the force that prevents sliding or rolling between two surfaces. On the other hand, lubrication is the procedure used to lessen wear and friction between sliding surfaces. To do this, lubricants are used at the contact points of moving surfaces (Encyclopaedia Britannica Inc., 2017).

2.6.1 Coefficient of Friction and the Coulomb Model

Amontons, a French military engineer, published two fundamental rules of friction in 1699. After researching static and kinetic friction, another French scientist and military engineer named Coulomb developed the third law in the 18th century (Kaarstad et al., 2009). These evolved into the following three laws of friction:

- Shear resistance is proportional to normal load
- Shear resistance is independent of the apparent area of contact between two bodies
- The sliding velocity has no effect on dynamic friction

Antoine Parent defined the following relation to introduce Amonton's work to mechanics (Kaarstad et al., 2009):

$$\tan\theta = \frac{F}{N} \tag{2.29}$$

Where:

- θ = The incline plane
- F = The tangential force
- N = The normal force

Later, Euler demonstrated that the following equation could be used to calculate the coefficient of friction, (Kaarstad et al., 2009):

$$\mu = \tan \theta$$

(2.30)

The definition of coefficient of friction, which is the ratio of normal force to friction force applied to surfaces, is the result of combining equations 2.32 and 2.33. (Kaarstad et al., 2009). Equation 2.34 gives the following expression for the relationship:

$$\mu_i = \frac{F_i}{N}$$

Where:

- F_i = Frictional force
- i = Denotes whether the friction is static or kinetic

As a result, friction can be categorized as either static or kinetic. When two surfaces are not moving in relation to one another, static friction arises. Otherwise, kinetic friction is the force that restricts rolling or sliding between two surfaces (Kaarstad et al., 2009). Figure 2.18 depicts typical behavior of the static and kinetic friction as a function of time.

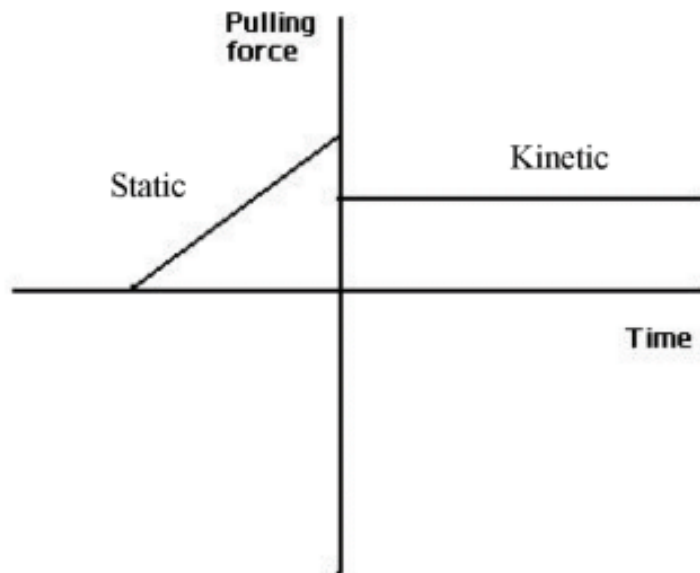


Figure 2.17: Static and kinetic behavior as a function of time

In the petroleum industry, coulomb friction models are frequently used to assess well friction. By relying on a single parameter, the model overlooks the effect of temperature. The parameters in equation 2.34 can be rearranged into the following formula (Kaarstad et al., 2009):

$$Q = \mu \cdot N \tag{2.31}$$

Where Q represents the friction force.

Despite the use of a straightforward one-parameter model, it is important to consider the context in which the coefficient of friction is calculated when presenting its values because it can be affected by a variety of circumstances. Factors like the applied load, the surface roughness, the humidity, the temperature, the speed, and the viscosity can have an impact on these numbers (Kaarstad et al., 2009).

2.6.2 Industrial Application of Friction and Lubrication

To further enhance the material, lubricants are being developed with great care. This is because less friction and wear allow numerous businesses, particularly the petroleum industry, to save a significant amount of energy. High levels of friction during an operation may cause direct or indirect material damage as a result of heat production. The wear resistance of the applied components also has a significant impact on their longevity. Because the coefficient of friction and wear rate are the primary results of such measurements, tribology studies are crucial (Encyclopædia Britannica inc, 2017, Nohava, n.d.).

Friction is a significant factor in the petroleum business, and it is crucial to forecast frictional loads in the wellbore during stages like well planning (Dawson et al., 1984, Kaarstad et al., 2009). As drilling operations become more sophisticated with increased reach and deeper targets, increasing friction has emerged as a significant barrier to further development. Higher penetration rates are possible due to less wellbore friction because mechanical wear and drag forces are reduced (Alshubbar et al., 2017, Alvi et al., 2018, Kaarstad et al., 2009). The coefficient of friction is an important factor since improving drilling performance and extending the period the components can be used will ultimately result in cost savings (Strm and

Belayneh, 2019). Therefore, measurements of the coefficient of friction are made as part of this study's experimental activity.

2.7 Torque and Drag Modelling

The most advantageous time to forecast frictional resistance is during the well's planning stage. In essence, deep and severely deviated wells can be planned to reduce torque and drag, which can then be used as criteria to choose the best well path. Improved drill string components and techniques can be used to accommodate for increased forces, if necessary. Because of this, understanding friction is crucial for ensuring drilling operations are effective and the intended depth is reached (Dawson et al., 1984). Drag forces and excessive torque might be attributed to (Freddie Ruiz, 2015):

- Sloughing Hole
- Sliding friction in the wellbore
- Keyseats
- Tight and poor hole conditions (cuttings accumulation)
- Differential Sticking

As for this thesis, the model based on Aadny's (Aadny, 2006) research is presented. There are various torque and drag models that can be utilized in a simulation. Additionally, the next subsections provide an explanation of the implemented torsional, buckling, and tensile limits.

While drilling, the friction between the drill string and the wellbore is the main source of the drag force. This force is added to the weight of the freely rotating drill string while tripping into or out of the hole. In general, it is greater when the drill string is pulled out of the hole (POOH) and less significant when the drill string is run into the hole (RIH). In order to successfully complete long-reach wells, a smooth path during drilling is preferred. However, this is rarely the case because during drilling, azimuth and inclination frequently vary continuously (Aarrestad, 1994)

The drilling fluids lubricity impacts on the torque and drag will be evaluated. The theory to be implemented is provided in the appendix.

3 Literature Study

This chapter discusses the use of ecologically friendly additives, as well as evaluations of related research from the past.

3.1 Eco Friendly Based Drilling Fluid

Due to the damaging effects of chemicals and non-biodegradable materials, environmental protection is currently a major concern on a global scale. These worries motivate the industry to create formulas for drilling fluid that are environmentally sustainable (Al-Hameedi et al., 2019a).

The issue of waste materials is also becoming more and more problematic in modern society because of the negative consequences they might have on the environment and public safety. To solve these problems, it is essential to establish a substitutional strategy. Instead of discarding these waste elements as undesirable trash, the petroleum sector can make use of them by using them for other uses (Al-Hameedi et al., 2019c). Researchers have recently investigated the use of food waste in drilling fluids (Al-Hameedi et al., 2019b)

Abo Al-Hameedi researched the utility of potato peel powder as a WBN supplement in 2019. According to his investigation, the potato peel increased plastic viscosity, decreased yield point, and reduced filtrate loss (Al-Hameedi et al., 2019a). He also carried out a similar experimental study with powdered palm tree leaves. These findings demonstrated that the modified mud's filtration and alkalinity qualities had been diminished. Additionally, yield point and gel strength were reported to have significantly decreased, suggesting that palm tree leaves might be used as a fluid thinner additive (Al-Hameedi et al., 2019a)

Erwin studied sugarcane and corn cobs as environmentally friendly viscosifying agents in 2005. According to the study's findings, plastic viscosity increased at concentrations between 6 and 10 parts per billion (ppb), although yield point and gel strength decreased (Iranwan et al., 2009).

According to Anietie Okon's research (Okon et al., 2014), drilling fluid loss was decreased by 65% using rice husk at a concentration of 20 ppb compared to 10 ppb of carboxymethyl cellulose. Additionally, more study has been conducted on the extraction of potato starch from potato tubers, leaves from cashew and mango trees, and cellulose from corncobs (Nmegbu and Bari-

Agara, 2014). (Wami et al., 2015). Comparing corncob cellulose to the polymer polyanionic cellulose, it was discovered that the latter greatly reduced fluid loss (PAC). The drilling fluid's rheological qualities were improved by the cashew and mango leaf extracts; however the potato starch had a negative effect on the drilling fluid's rheological and filtering features.

As a pH and corrosion controller, banana peel ash has also been researched as a potential replacement for sodium hydroxide (NaOH). Banana peel ash was shown by Adebowale and Raji to be quite effective at raising pH. (Adebowale A and Raji J, 2015). The same finding was made in Iheagwara's investigation, which revealed that standard caustic soda (sodium hydroxide) and banana peel both have an alkaline effect on drilling fluid (Onwuachi-Iheagwara, 2015).

The study by Al-Hameedi that substituted mandarin peel powder for traditional chemicals in a WBM. YP and PV were significantly decreased in the fluid at concentrations of 3% and 4% MPP. MPP may be used as a fluid loss control agent because it improved filtration characteristics by reducing mud cake thickness and fluid loss, especially for 3% and 4% concentrations. In particular at high concentrations, it was also proposed as a pH reducer (AlHameedi et al., 2019c).

3.2 Nanotechnology

Nanotechnology is the development and application of materials, equipment, and devices on a nanoscopic scale. Nanoparticles are substances with a diameter of one to one hundred nanometers, and their use has produced several technological advances in a number of different fields. One of the most active research areas at the moment is nanotechnology (Cocuzza et al. 2011, Ali et al. 2020). Despite the fact that over the past few decades, nanotechnology has significantly advanced fields like health, biology, and electronics, the petroleum sector has only recently shown an interest in it. Due to the technology's importance in several areas of the business, the use of nanoparticles has grown quickly (Rafati et al., 2018, Cocuzza et al., 2011). Improvements in building and materials as well as in drilling fluids are a few examples of applications for nanotechnology (Hoelscher et al., 2013).

3.3 Nanoparticle Based Drilling Fluids

It is common knowledge that the effectiveness of the drilling fluid used in the wellbore has a significant impact on the outcome and overall cost of a drilling operation. In order to perform effectively, drilling fluid intended for the wellbore should be designed with the wellbore conditions in mind. The mud must be able to withstand more challenging and harsh circumstances as drilling operations become more sophisticated, such as:

- Gas Hydrate Formation
- High Temperature
- Stuck Pipe Conditions
- Clay Swelling
- Limited Operating Window
- Inadequate Hole Cleaning

Due to their superior drilling fluid performance, oil-based drilling fluids have previously handled these conditions. According to 1.1, OBM are not a viable drilling fluid system in use today because they are both expensive and environmentally harmful. In order to address these issues and enhance drilling performance in a way that is both cost-effective and ecologically sustainable, nanoparticle water-based drilling fluids are being developed (Alcázar-Vara, 2018, Lake and Mitchell, 2006, Salih et al., 2016).

A nanoparticle drilling fluid is any drilling fluid that contains one or more nanoparticle additives. Such systems offer fluid qualities that go beyond the changes that may be made by traditional additives, such as increased lubricity, fluid loss inhibition, cuttings conveyance, and shale inhibition. By altering fluid characteristics in response to wellbore conditions, nanoparticles enable fit-for-purpose optimization. One of the primary factors contributing to the higher drilling fluid performance of nanoparticles is their large surface area to volume ratio (Long et al., 2012; Salih et al., 2016).

Nanoparticle use could decrease the need for other pricey additives and enhance drilling fluid efficiency. They are, however, extremely sensitive to changes in the wellbore and other fluid components due to their high reactivity. The rheological and filtration characteristics of a fluid are frequently adversely impacted when nanoparticle concentrations surpass a particular threshold. Additionally, when variations in pH, salinity, and temperature deteriorate the drilling fluid, a lot of nanoparticles induce formation damage and instability due to poor dispersion qualities. Salih et al. (2016); Long et al. (2012)

Recently, oil and gas industries have used nanotechnology with impressive results. Numerous papers that emphasize the usage of nanoparticles as drilling fluid additives have been published. According to Cho's report, a copper nanoparticle improved the thermal conductivity of water (Choi and Eastman, 1995)

Paiaman and Al-Anazi found that mud cake thickness at HTHP environments decreased as a result of adding nano-carbon black particles to the drilling fluid, preventing stuck pipes (Al-Anazi et al., 2009).

According to a study by Tsen and Lin (Tseng and Lin, 2003), TiO₂ nanoparticles made water more viscous. Amanullah examined the same substitution and discovered that the TiO₂ nanoparticle increased the PV and YP (Amanullah et al., 2011)

In his studies on the use of iron oxide magnetic nanoparticles in drilling fluids, Lee discovered that their addition led to a rise in viscosity (Lee et al., 2009).

CuO and ZnO nanoparticles, according to William (William et al., 2014), increased electrical and thermal conductivity and stabilized drilling fluid viscosity at higher temperatures.

According to Contreras' study's findings, iron and calcium-derived nanoparticles in oil-based drilling fluids obstruct porous media under HTHP circumstances and decrease filtering under LPLT settings (Contreras et al., 2014).

4 Experimental Work

The numerous drilling fluid systems that are experimentally evaluated in this thesis will be presented in this chapter, along with a description of all the chemical additives. It will also introduce the experimental procedures and equipment needed to investigate rheology, viscoelasticity, fractionality, and fluid loss.

4.1 Description of Drilling Fluid Additives

Several chemicals were employed to affect the varied drilling fluid properties of the WBM when creating the drilling fluids that were used in the experimental study. All the additives used in drilling fluid compositions are listed in the following subsections.

4.1.1 Bentonite

Bentonite is an absorbent swelling clay that is typically formed from weathering volcanic ash in seawater. It is primarily composed of montmorillonite, a smectite group three-layer clay. Bentonite is a general term rather than an accurate mineralogy since it lacks a clear mineral makeup (Kutlic et al., 2012, Schlumberger Limited, n.d.-g). As can be observed in table 4.1, the main chemical compositions of a typical Wyoming bentonite clay are alumina and silica.

Chemical composition of Wyoming "Volclay"	
<i>Components</i>	<i>Composition in %</i>
Silica, SiO ₂	64.32
Alumina, Al ₂ O ₃	20.74
Cumulative water	5.14
Ferric oxide, Fe ₂ O ₃	3.03
Soda, Na ₂ O	2.59
Magnesia, MgO	2.30
Lime, CaO	0.50
Ferrous Oxide, FeO	0.46
Potash, K ₂ O	0.39
Sulfuric Anhydride	0.35
Titanium Oxide, TiO ₂	0.14
Phosphoric Anhydride	0.01
Other minor constitutes	0.01

Table 4.1: Chemical Composition of Bentonite (Kutlic et al., 2012)

The swelling and thixotropic properties of bentonite, which are used as viscosity enhancers in drilling fluids, are provided by the component montmorillonite. Thus, bentonite can improve the suspension of heavy items and boost a fluid's carrying capacity. Additionally, it can have a positive effect on fluid loss and filter cake qualities (Chilingarian and Vorabutr, 1983, Fink, 2003, Skjeggstad, 1989). Figure 4.1 depicts the three-layer minerals and basic montmorillonite clay structure. Water swells beneath and between the following unit layer of tetrahedral as it is trapped between the two tetrahedral layers.

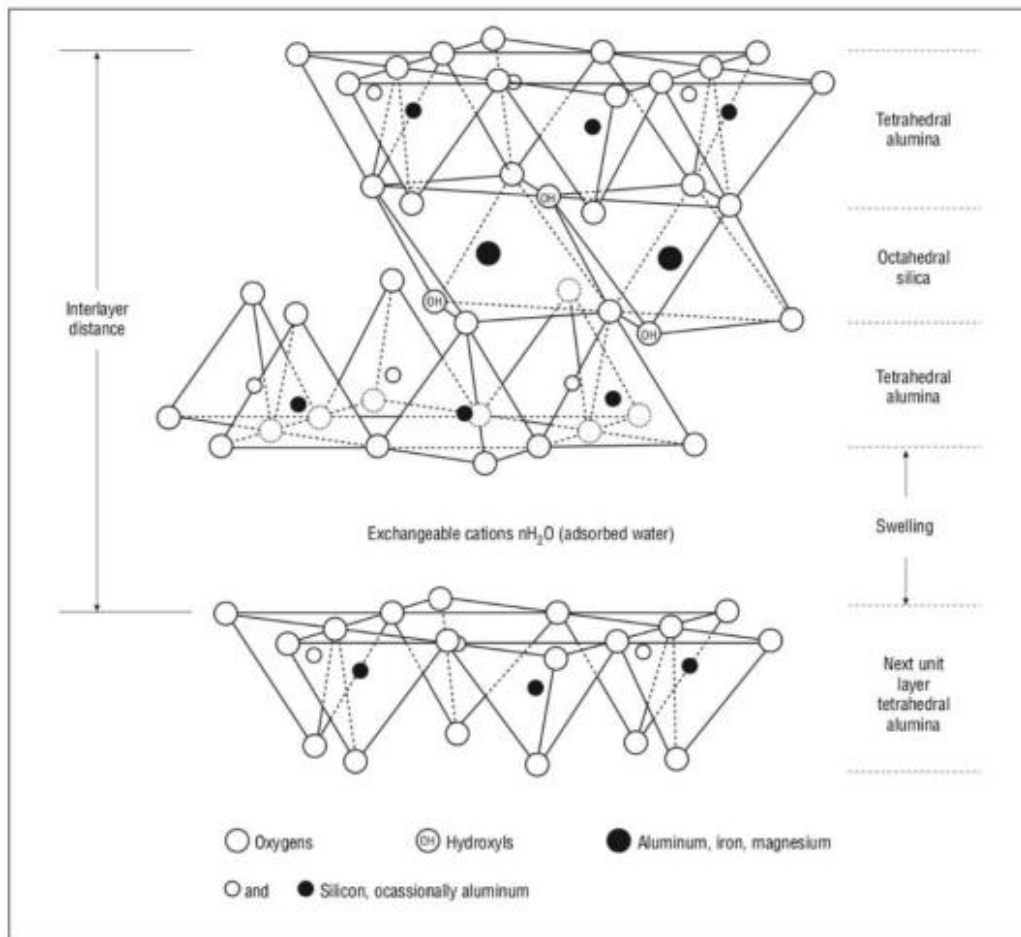


Figure 4.1: Illustration of the basic structure of montmorillonite (Skjeggstad, 1989)

4.1.2 Soda Ash

Soda ash, an alkali water soluble salt, is used in drilling fluids to raise the pH level. The addition can also be used to clean up drilling fluids made of water that have been tainted with calcium ions from gypsum or anhydride formations. Such contamination may lead to pH lowering, clay

flocculation, and polymer precipitation (Schlumberger Limited, n.d.-o). Thus, anhydrous (100%) soda ash will be used in this thesis.

4.1.3 Barite

Barite, a naturally occurring mineral, is frequently added to drilling fluid in order to increase density. The solid has a high specific gravity of 4.2–4.5 and is neither poisonous nor radioactive. Barite is a weighing substance that is frequently used in WBM because it can raise the mud weight to 2.6 sg while keeping the viscosity at a low level. A sufficient hydrostatic head in the wellbore is achieved by incorporating weighing components into drilling fluids (Chilingarian and Vorabutr, 1983; Devereux, 2012; Strand, 1998).

4.1.4 Polymer Additives

Certain clay additives, such as bentonite, can have undesired or inefficient drilling fluid qualities, and in certain cases polymers are preferable to replace or work in conjunction with the clay. Large molecules known as polymers are made up of monomers—repeating units—connected to one another in lengthy chains. The chain length, also known as the molecular weight, and the polymer charge determine the diverse polymers with different functions. By altering the monomers, their coupling, and the quantity of monomers, the molecules can be made to respond to particular drilling conditions. In this instance, the polymers are synthetic, and virtually countless combinations are possible. Additionally, there exist naturally occurring polymers (Devereux, 2012, Strand, 1998).

Polymer additives can be used for a variety of purposes, including:

- Reducing fluid loss
- Increasing viscosity and gelation properties
- Serving as a flocculant or deflocculant
- Acting as a surfactant

The following subsections provide information on the polymers used in this thesis (Skjeggstad, 1989).

4.1.4.1 *Polypac*

The polyanionic cellulose polymer polypac can be used to regulate fluid loss in water-based drilling fluids. It may be used in all WBMs and is still useful at low concentrations. However, when employed in saltwater systems, shales and cuttings, among other materials, need to be encapsulated at higher concentrations. When added to drilling fluid, Polypac creates a thin filter cake with limited permeability, which reduces the likelihood of differential sticking and flow from the wellbore into the formation. There are various sorts of polypacs, such as M-I Swaco's polypac ELV and polypac UL, but the extra qualities are slightly different even if they all typically serve as fluid loss reducers (Schlumberger Limited, n.d.-k).

4.1.4.2 *Pac*

Similar to Polypac, polyanionic cellulose (pac) boosts the viscosity of water-based drilling fluids while still controlling fluid loss. Both polymers are resistant to bacteria, which means they work well in a variety of pH ranges. As a stabilizer, suspending agent, and colloid protector, pac can also be used. As a result, one benefit of the addition is that it enhances the drilling fluid's ability to suspend cuttings and transport them. Additionally, numerous types of polymers are available that have varying degrees of viscosity control (GLOBAL DRILLING FLUIDS & CHEMICALS LTD, n.d.; IRO GROUP INC, n.d.).

4.1.4.3 *Carbopol*

Carbopol is connected to polyacrylic acid polymers, commonly known as carbomers, which are employed in numerous sectors to increase the viscosity of liquids. All of the Carbopol solutions are high molecular weight crosslinked polyacrylic acid polymers. Priscilla (Priscilla et al., 2019) lists stabilization and suspension dispersion as further polymer function areas. A thorough implementation approach is essential for its reproduction because the properties of dispersion are greatly influenced by elements such as reagents, water characteristics, and the mixing process (Lefrançois et al., 2015).

Numerous rheological fluid characteristics, including pH, composition, temperature, aging, manufacturing method, and a function of its concentration, are influenced by carbopol. To maximize the polymer's ability to thicken, bases like potassium hydroxide and sodium hydroxide

(caustic soda) are frequently utilized. Temperature has a negligible impact, nevertheless (Lubrizol Corporation, 2009; Priscilla et al., 2019).

4.1.5 Titanium Nitride Nanoparticle

Titanium nitride was used as the nanoparticle in this thesis that will be added to the drilling fluid. Excellent thermal conductivity, a high melting point (2950 °C), great hardness, and strong chemical stability at high temperatures are all characteristics of titanium nitride nanoparticles. Figure 4.3's SEM image serves as an illustration of the shape of TiN nanopowder. The particles are round and black, as can be observed.

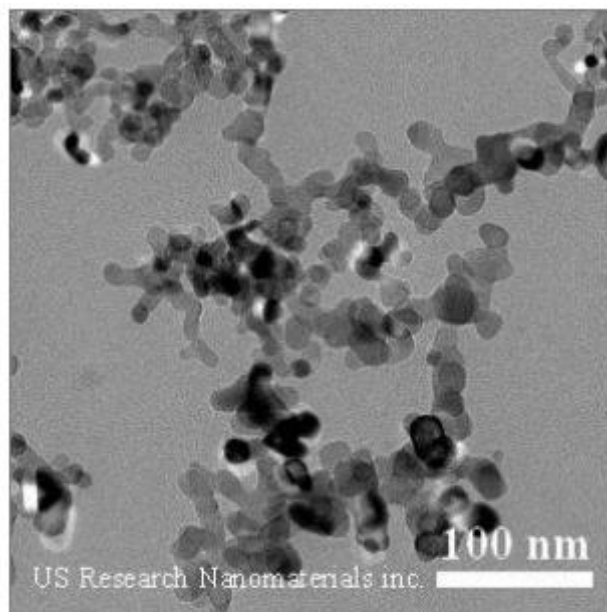


Figure 4.2: TiN Nanoparticles

The TiN additive employed in this thesis is a suspension of nanoparticles in water that was purchased from US Research Nanomaterials (US Research Nanomaterials inc, n.d.). Table 4.2 provides a list of TiN's typical features.

Properties of Titanium Nitride (TiN)	
<i>Purity</i>	>97%
<i>Average Nanoparticle Size</i>	20 nm
<i>Specific Surface Area</i>	48 m ² /g
<i>Melting Point</i>	2950°C
<i>Density, true</i>	5.22 g/cm ³

Table 4.2: Properties of Titanium Nitride

4.1.6 Mandarin Peel Powder

Mandarin peel powder was one of the ecological additives investigated in this study. Despite its usage as an ingredient in food and health goods, the peel of the citrus fruit mandarin is typically classified as food waste. It does, however, show a high mineral concentration. The following information about mandarin peel was reported from a study about the mineral content of the pulp and peel of several citrus fruits (Czech et al., 2020):

Chemicals	Content (mg/100g)
<i>Iron (Fe)</i>	0.33
<i>Zinc (Zn)</i>	0.29
<i>Copper (Cu)</i>	0.05
<i>Manganese (Mn)</i>	0.12
<i>Selenium (Se)</i>	0.00338
<i>Potassium (K)</i>	141
<i>Sodium (Na)</i>	1.09
<i>Calcium (Ca)</i>	37.1
<i>Phosphorus (P)</i>	19.9
<i>Magnesium (Mg)</i>	12.9

Table 4.3: Chemical Content of a Mandarin Peel (Czech et al., 2020)

4.1.7 Chia

Another environmentally friendly addition that was studied in this thesis is Chia seeds. They are widely used in food science because they confer their properties like high-water retention capacity, emulsifying capacity, gelling capacity, stabilizing agent, and viscosity. Chia has a very high mineral content. The following mineral content is from a study conducted by Jet et al.

Protein	16.5	g/100 g	24.2	g/100 g
Total lipid	30.7		40.2	
Ash	4.8		4.77	
Carbohydrate	42.1		26.9	
Dietary fibre	34.4		30.2	
Calcium	631.0	mg/100 g	456	mg/100 g
Iron	7.7		9.18	
Magnesium	335.0		449	
Phosphorus	860.0		919	
Potassium	407.0		726	
Sodium	16.0		0.26	
Zinc	4.6		6.47	
Copper	0.9		1.86	
Manganese	2.7		3.79	

Table 4.4: Composition of Chia Seeds (Jin et al)

4.1.8 Potassium Chloride (KCl)

Potassium Chloride (KCl) is a soluble salt that is used in drilling fluid and stimulation fluid to stabilize clays and shales and inhibit water absorption of the clays. It is especially used when drilling through water-sensitive clays. The ion exchange of KCl provides inhibition by keeping the individual clay platelets in the shale together and holding them together. This also removes water from the drilling fluid. Preventing water absorption of the clays ensures wellbore stability (schlumberger Limited, n.d.-o)

4.1.9 Xanthan

By using a bacteria called *Xanthomonas campestris* to ferment simple sugars, xanthan gum is a polymer that is produced. It belongs to the hydrocolloid family of polymers, which are both water-soluble and hydrophilic, meaning that their molecules are drawn to water. Xanthan gum is used as a thickening agent to make drilling fluid a gel-like consistency. In water-based mud it provides non-Newtonian mud rheology making it efficient at lifting and suspending cuttings even when the drilling fluid is not flowing.

4.2 Experimental Equipment

4.2.1 Hamilton Beach Mixer

All drilling fluid formulas in this thesis were blended using a Hamilton Beach Mixer and mixing cup. There are three different speed options on the device: low, medium, and high. A switch on the device's top allows for simple control of these speed levels. The samples were blended for a few minutes to create a homogeneous combination of the fluid particles before any experimental testing. The mixing of drilling mud is depicted in figure 4.3.



Figure 4.3: Hamilton Beach Mixer blending drilling mud

4.2.2 OFITE Viscometer and Rheology Measurements

Using an OFITE Model 800 viscometer, the rheological parameters of all drilling fluids were assessed. Measurements were made at eight different shear rates, and during the test, a dial window on the top surface of the equipment allowed the user to see the corresponding shear stress for each shear rate. 600, 300, 200, 100, 60, 30, 6, and 3 RPM were the various speeds used in the test, and the measurements were taken in that order. Throughout the measurements, a heating apparatus was used to regulate the fluid's temperature. An OFITE Thermo-cup was used to do this. As a result, the fluids' rheological characteristics were determined at 22°C, 50°C, and 80°C.



Figure 4.4: Ofite Viscometer

4.2.3 Anton Paar Rheometer

Using an Anton Paar MCR 302 rheometer, the rheological and viscoelastic characteristics of the drilling fluid systems were examined. With this apparatus, shear and torsional tests can be carried out in both continuous and oscillatory rotation. A parallel plate setup or the "cup and bob" arrangement can be employed in a test, but for the sake of this experiment, only the parallel plate setup was used. Figure 4.5 shows an Anton Paar rheometer with a parallel plate in the test position.



Figure 4.5: Anton Paar Rheometer

The Anton Paar rheometer was used to analyze temperature sweep and amplitude sweep data. Sweeps of increasing amplitudes (0.1 to 1,000%) were performed while keeping the temperature and angular frequency at 22°C and 10 rad/s, respectively. Results of amplitude sweep tests were used to estimate the structural stability, strength, and dynamic yield point of the fluid system. Regarding the temperature sweep test, it investigated how temperature affected fluid stability and structure. The temperature range for these tests was 20–80°C, and the rotation was constant and continuous.

4.2.4 pH-Meter

With the use of a Mettler Toledo FiveEasy™ pH meter, the pH of the formulations of the water-based drilling fluids was determined. In figure 4.6, the cup to the right shows a glass-membrane electrode that is used to gauge the hydrogen ion potential of fluids. The following is a description of the pH test procedure:

After taking the electrode from the storage solution, rinse it with deionized water. Then, place it in the sample and agitate carefully. After the pH readings have stabilized, read the numbers. Finally, put the electrode back in the storage solution.

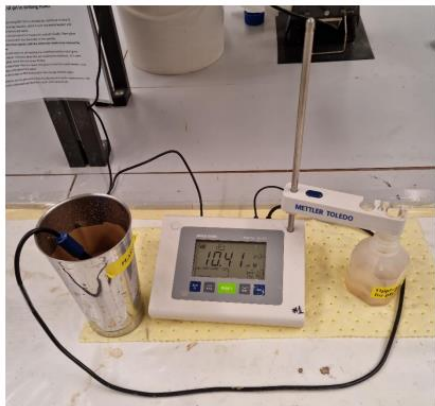


Figure 4.6: pH-meter conducting a pH measurement.

4.2.5 API Static Filter Press and Fluid Loss Measurement Procedure

The API Static Filter Press is used to obtain the filtrate loss results. The API Static Filter Press is composed of a metallic cell that is composed of a variety of mechanical parts and then it is attached to the pressure tubing. The base cap with a filtrate tube, the cell body, the top cap (connected to the pressure tubing), and the measurement cylinder are all shown in Figure 4.7. A

sealed cell body that had been filled with fluid was placed in the API static filter press as part of the filtrate procedure. A measuring cylinder was positioned beneath the filtrate tube during testing to calculate the volume of fluid lost. The filtrate testing period was then set to 7 minutes and 30 seconds, and 100 psi of pressure was then delivered to the system. The measuring container continued to fill with fluid drips until 7.5 minutes had passed. The fluid loss volume from the cylinder and the removal of the filter paper from the cell body were done in order to determine the mud cake features and filtration properties, as shown in the picture below.



Figure 4.7: API Static Filter Press

4.2.6 Tribometer and Frictional Measurement

Using a CSM tribometer, the frictional characteristics of drilling fluid systems including suspensions of nanoparticles were studied. The so-called pin-on-disc methodology is applied in a pin-on-disc tribometer. It has a metal ball with a diameter of 6 millimeters manufactured of chromium steel. The frictional measurements were made using a computer-controlled equipment at 22°C for 10 minutes with a force of 5 N moving at 3 cm/s. All friction experiments were done numerous times for each fluid system to establish repeatability and calculate numerical averages.



Figure 4.8: CSM tribometer instrument used for friction tests

4.2.7 Haver EML 200 Digital Sieve Shaker

MPP was created using the Heaver EML 200 digital sieve shaker, which is covered in more detail in 4.4.1. A motor inside of this instrument releases vibrations at a predetermined rate and duration. As seen in figure 4.5, several sieves are stacked on top of one another and attached between two bars. Five metal sieves were used in this thesis, with the top sieve having a mesh size of >350 microns and the bottom sieve having a mesh size of 90 microns. The following image includes mesh sizes 90 μm , 106 μm , 180 μm , 250 μm and 350 μm . The particles fall through the sieves as the sieve shaker begins to vibrate until they reach a mesh size that they cannot fit through.

The MPP was put on the upper sieve, which was a 350 m sieve, to the maximum of 200 grams.

The shaker was then adjusted for intensity, intervals, and timing. The sieving process was set at an intensity of 8, zero intervals, for a total of 10 minutes. The powder was consequently divided into five distinct samples, each of which represented a mesh size range between two sieves. As previously noted, subsection 4.4.1 provides a more detailed explanation of how the mandarin peel is prepared.



Figure 4.9: Siever shaker shaking mandarin peel powder

4.3 Drilling Fluid Formulation

In this study, three different base fluids were used in order to study the effects of chia. The first being bentonite based, as it is the most used type of water-based mud. The next two base fluids used are potassium chloride-based drilling fluid. Potassium muds are used when drilling through water-sensitive shales and are commonly used in drilling operations in the North Sea. The first potassium mud uses polypac and pac as filtration control additives and the other formulation uses xanthan gum as an additive.

4.3.1 Bentonite Based Drilling Fluid Formulation

First, the reference fluid to be used to compare to samples that contained chia. The formula used, was based off a formulation that was used in Lene Fattnes's study on flat rheology drilling fluids. The additives and their amounts are included in table 4.5 and the procedure of making this drilling fluid is described in table 4.6. The table provides the additive's mixing order and the mixing method and duration of mixing. First, the soda ash is stirred into the water until it is fully dissolved. Next, the bentonite is added gradually while mixing to avoid flocculation. Then, PolyPac and Pac are added to the mixture and the mixture is blended for five minutes. The barite is then added to the mixture and mixed for ten minutes. Finally, the Carbopol is added and mixed

for five minutes. Throughout this process the inside of the mixing cup is scraped down to ensure that all additives are thoroughly incorporated into the mixture. The final mixture was poured into glass bottles and stored at room temperature.

Chemical Additive [g]	Reference Bentonite
Water	350
Bentonite	10
Soda Ash	3.2
Polypac	1
Pac	.5
Barite	150
Carbopol	.08

Table 4.5: Content of the bentonite reference fluid

Chemicals	Method of Mixing
Water	Poured into the Mixing Cup
Soda Ash	Manually stirred into the based mud with a spoon until all the soda ash is fully dissolved into the water
PolyPac and Pac	Mixed with the Hamilton Beach Mixer for 5 minutes at low speed
Bentonite	Mixed with the Hamilton Beach Mixer for 5 minutes at low speed
Barite	Mixed with the Hamilton beach Mixer for 10 minutes at high speed
Carbopol	Mixed with the Hamilton Beach Mixer for 5 minutes at high speed

Table 4.6: Mixing procedure of the bentonite reference fluid

For each sample this procedure was followed. After making the bentonite base fluid the chia is added. Three different preparation methods of chia were used for this study; uncooked, cooked and fermented. The uncooked chia is raw chia that is measured and directly added to the final mixture of the bentonite base fluid and mixed thoroughly using a Hamilton Beach mixer. The cooked chia is mixed at the beginning with the 350g of water and cooked on the stove until the water came to a boil. The water that was boiled off was replaced with cold water and then the rest of the steps to make the bentonite base fluid were followed.

In order to characterize the uncooked chia in bentonite-based drilling fluid, different amounts of uncooked chia were added to each sample. Only one sample was created for the cooked and

fermented preparations in order to compare it to the uncooked chia. They both contained two grams of chia. Below is Table 4.7 listing the samples and the amount of chia added to each sample.

Sample	Amount of Chia Added [g] to the Reference Fluid	Weight % of chia in total mixture
Reference Fluid	0	0
Sample 1	.2	.04%
Sample 2	.4	.08%
Sample 3	.6	.12%
Sample 4	.8	.16%
Sample 5	1	.19%
Sample 6	1.5	.29%
Sample 7	2	.39%
Sample 8	3	.58%
Cooked Sample	2	.39%
Fermented Sample	2	.39%

Table 4.7: Amount of chia in each bentonite-based sample

4.3.2 Potassium Based Mud with Polypac and Pac

The additives and their amounts are included in table 4.8 and the procedure of making this drilling fluid is described in table 4.9. The table provides the additive's mixing order and the mixing method and duration of mixing. First, the soda ash and KCl are stirred into the water until they are both fully dissolved. Then, PolyPac and Pac are added to the mixture and the mixture is blended for five minutes. The barite is then added to the mixture and mixed for ten minutes. Finally, the Carbopol is added and mixed for five minutes. Throughout this process the inside of the mixing cup is scraped down to ensure that all additives are thoroughly incorporated into the mixture. The final mixture was poured into glass bottles and stored at room temperature.

Chemical Additive [g]	Reference Potassium Mud with Polypac and Pac
Water	350
Soda Ash	.5
PolyPac	2.2
Pac	1.1
KCl	25
Barite	143
Carbopol	.08

Table 4.8: Content of Potassium mud reference fluid made with PolyPac and Pac

Chemicals	Method of Mixing
Water	Poured into the Mixing Cup
Soda Ash and Potassium Chloride (KCl)	Manually stirred into the based mud with a spoon until all the soda ash and KCl is fully incorporated
PolyPac and Pac	Mixed with the Hamilton Beach Mixer for 5 minutes at low speed
Barite	Mixed with the Hamilton beach Mixer for 10 minutes at high speed
Carbopol	Mixed with the Hamilton Beach Mixer for 5 minutes at high speed

Table 4.9: Mixing Procedure of Potassium Chloride based fluid

There were two chia preparations that were tested with this fluid, cooked and uncooked. The chia was prepared the same as the uncooked and cooked chia in the bentonite-based fluid. The table below shows the amount of chia added to each sample.

Sample	Amount of Chia [g] added to the reference fluid
Uncooked	2
Cooked	2

Table 4.10: Chia content of the samples made with Potassium Chloride and Polypac and Pac

4.3.3 KCl Based Mud with Xanthan Gum

The additives and their amounts are included in table 4.11 and the procedure of making this drilling fluid is described in table 4.12. The table provides the additive’s mixing order and the mixing method and duration of mixing. First, the soda ash and KCl are stirred into the water until they are both fully dissolved. Then, the Xanthan gum is added to the mixture and the mixture is blended for five minutes. The barite is then added to the mixture and mixed for ten minutes. Finally, the Carbopol is added and mixed for five minutes. Throughout this process, the inside of the mixing cup is scraped down to ensure that all additives are thoroughly incorporated into the mixture. The final mixture was poured into glass bottles and stored at room temperature.

Chemical Additive [g]	Reference Potassium Mud with Polypac and Pac
Water	350
Soda Ash	.5
Xanthan Gum	1.5
KCl	25
Barite	143
Carbopol	.08

Table 4.11: Content of Potassium Chloride reference fluid with Xanthan Gum

Chemicals	Method of Mixing
Water	Poured into the Mixing Cup
Soda Ash and Potassium Chloride (KCl)	Manually stirred into the based mud with a spoon until all the soda ash and KCl is fully incorporated
Xanthan Gum	Mixed with the Hamilton Beach Mixer for 5 minutes at low speed
Barite	Mixed with the Hamilton beach Mixer for 10 minutes at high speed
Carbopol	Mixed with the Hamilton Beach Mixer for 5 minutes at high speed

Table 4.12: Mixing Procedures of Potassium Chloride and Xanthan Gum Reference Fluid

There were two chia preparations that were tested with this fluid, cooked and uncooked. The chia was prepared the same as the uncooked and cooked chia in the bentonite-based fluid. The table below shows the amount of chia added to each sample.

Sample	Amount of Chia [g] added to the reference fluid	Weight Percent of Chia as total of mixture
Reference	0	n/a
Uncooked Sample 1	2	.38%
Cooked Sample 1	1	.2%
Cooked Sample 2	2	.38%
Cooked Sample 3	3	.57%

Table 4.13: Amount of chia per sample in Potassium Chloride and Xanthan Gum fluids

5 Results

This chapter includes all the findings from the experimental work and testing of mud that has been enhanced with the environmentally friendly additives of chia and mandarin peel powder. Review and evaluation of measurements of pH, conductivities, rheology, viscoelasticity, filtrate loss, and friction are performed.

5.1 Characterization of Chia in Bentonite-Based Water-based Mud

This section presents the experimental results obtained from the process of characterizing the effect of chia on water-based drilling fluid. Varying amounts of chia were added to the base formulation of water-based mud in order to study the effects of chia. In addition, other drilling fluid additives were utilized to improve the rheological properties as discussed in section (3.??). To start, eight samples with varying amounts of uncooked chia were used to observe the effects of chia on rheological properties.

5.1.1.1 *Effect of Chia on Rheological Properties*

The first test was on rheological properties and the mud was designed to be made with water, bentonite, PolyPac, Pac, barite, Carbopol, and varying amounts of uncooked chia. The rheology of the samples was measured within a few days of creating each sample. The plastic viscosity and yield stress of the various samples are show in figures 5.1 and 5.2. These were calculated based on the Bingham Plastic model and were computed using viscosity measurements that were obtained at 20°C, 50°C and 80°C. Additionally, the line connecting the three points is to provide a visual representation of the anticipated yield stress profile of the fluid systems and will be used for all rheological plots presented in this thesis.

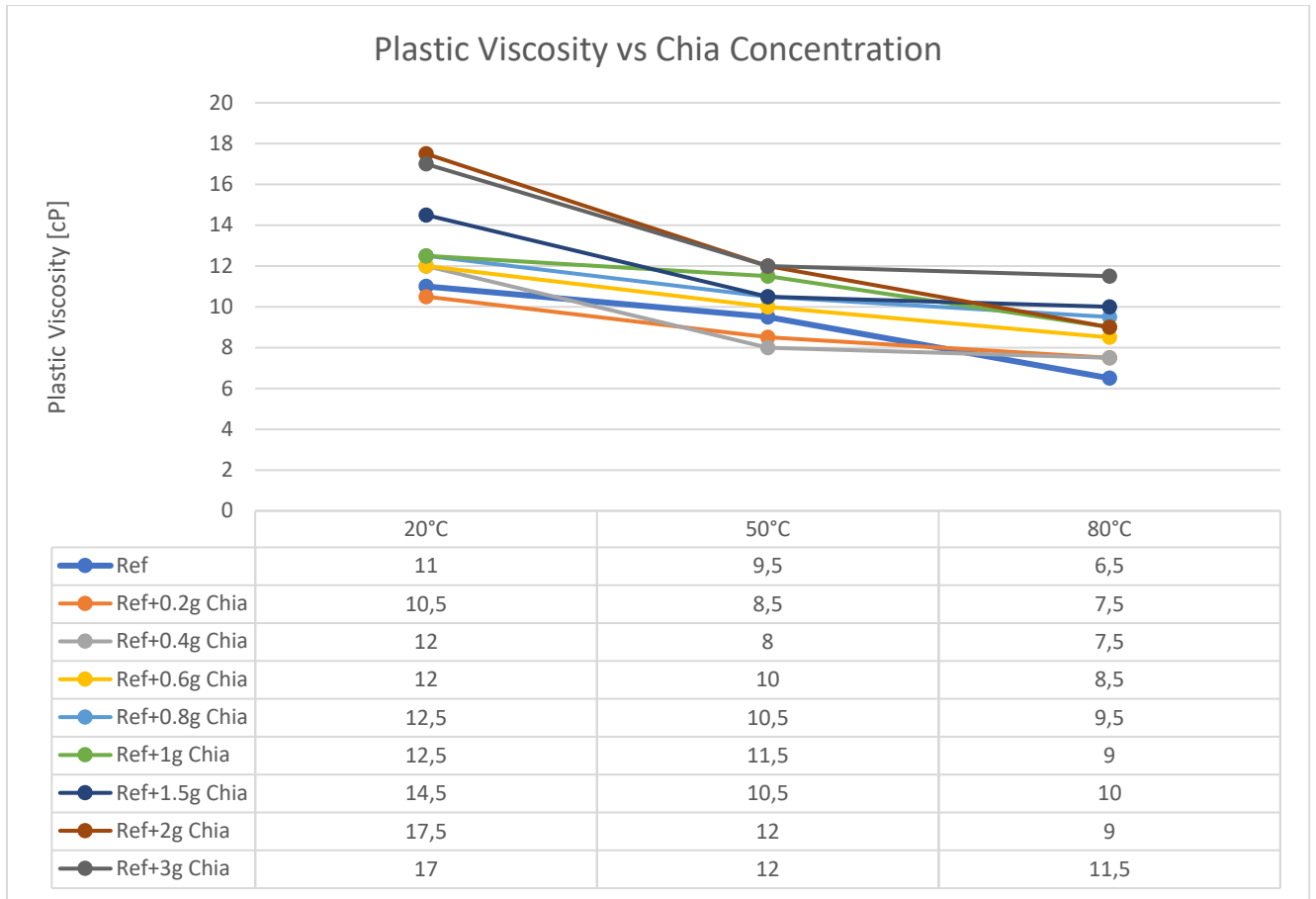


Figure 5.1: Plastic Viscosity vs Chia Amount in Bentonite

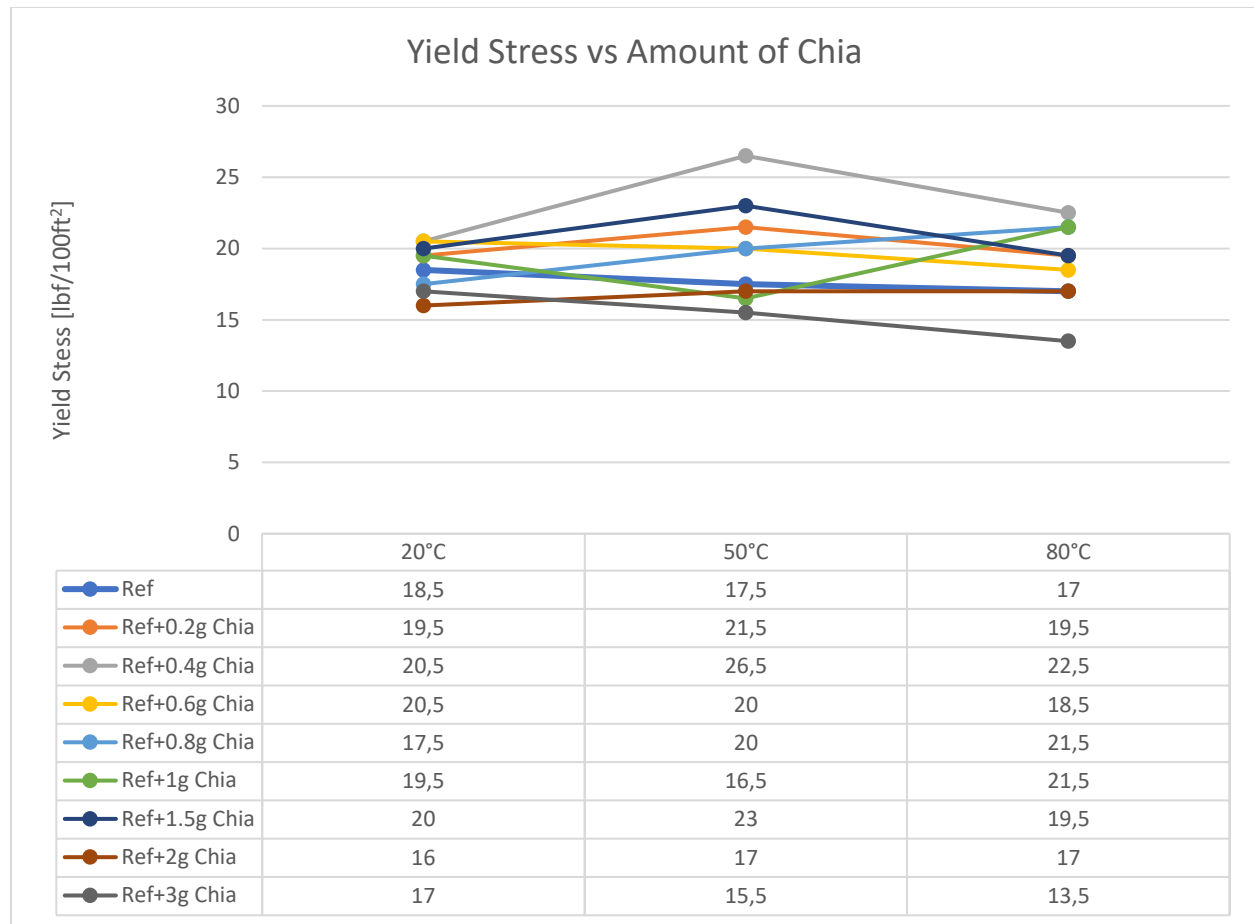


Figure 5.2: Yield Strength vs Amount of Chia in Bentonite

As observed in figure 5.1, the addition of chia generally increases the plastic viscosity of the sample at each temperature. The amount that it increases the viscosity is non-linear with added chia. In figure 5.2, it can be seen that the addition of chia also increases the yield stress. Some of these samples exceed the range of 11-20 lbf/ft² which is the common limit in the field to ensure efficient cuttings transport. Furthermore, none of the systems except for Ref+2g Chia exhibited stable yield stress across the entire temperature range. Ref+2g Chia was closer to being thermally stable than the reference fluid with no chia. Therefore this system will be studied further.

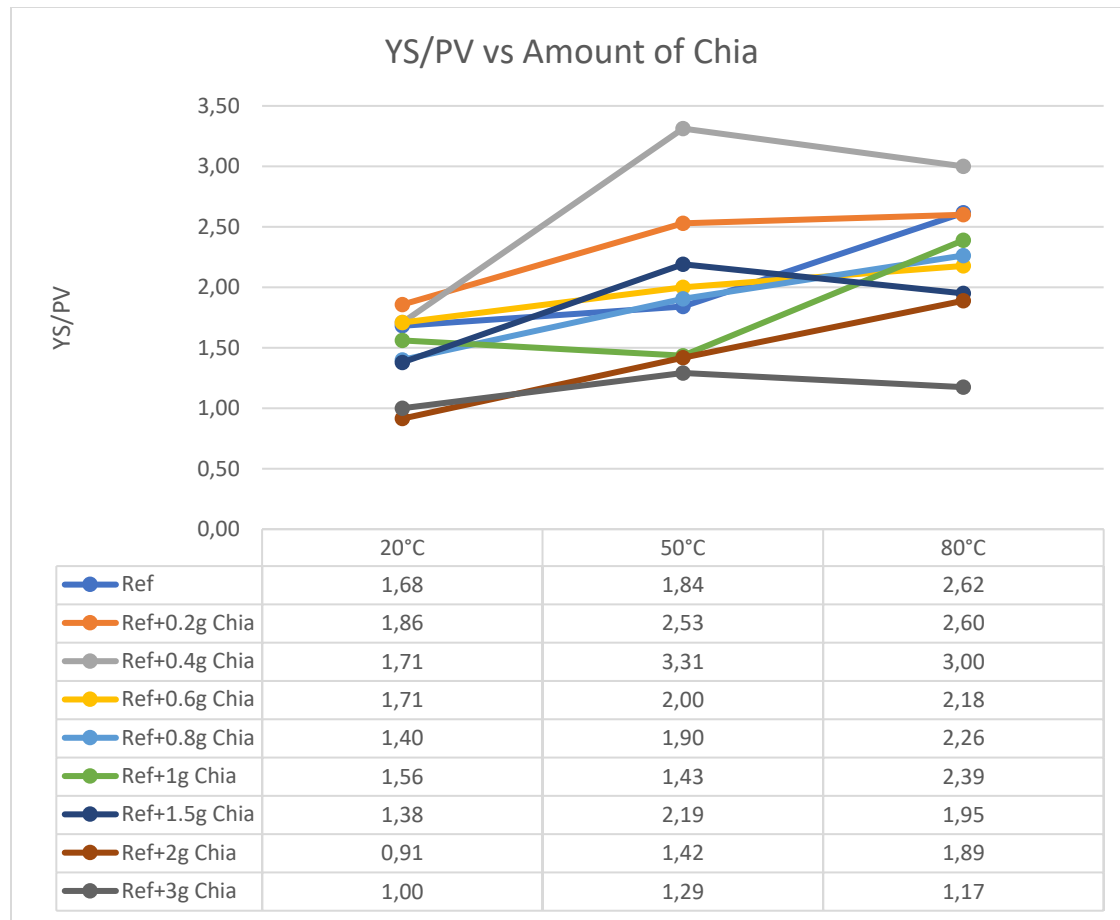


Figure 5.3: YS/PV vs Chia Amount

Figure 5.3 shows the ratio of yield stress to plastic viscosity which is said to predict the carrying capacity of a drilling fluid where the higher the ratio the higher the carrying capacity. Lower additions of chia appear to increase this ratio at lower temperatures but at higher temperatures it lowers the ratio thus lowering the carrying capacity.

5.1.2 Effect of Amount of Chia on Sag Factor

The second test done to characterize chia was a sag factor test. This was done by taking samples at the top of the sample and measuring their weight and volume and then taking samples at the bottom of the sample and measuring their weight and volume. Then the density of the top and bottoms were calculated, as well as an average of all the fluid’s density samples. Then the ratio of density at the top versus the density at the bottom was calculated. A sag factor of less than .5 implies that there is no sedimentation of the weighting material and a sag factor of higher than

0.53 indicates solid settlement and inadequate suspension properties. An acceptable sag factor ranges from 0.50 to 0.53. All of these samples fall below the upper limit of the range and a few are below the acceptable range. A few of the samples had a sag factor of less than 0.5. Figure 5.5, is a picture of the samples; reference, reference+1g chia, and reference+2g chia, that show sediment settling as well as the increase in air bubbles as more chia was added to the reference fluid. The amount of air bubbles trapped within the fluid leads to concern about the filtrate loss of the fluid, the filtrate loss will be tested in section 5.4.

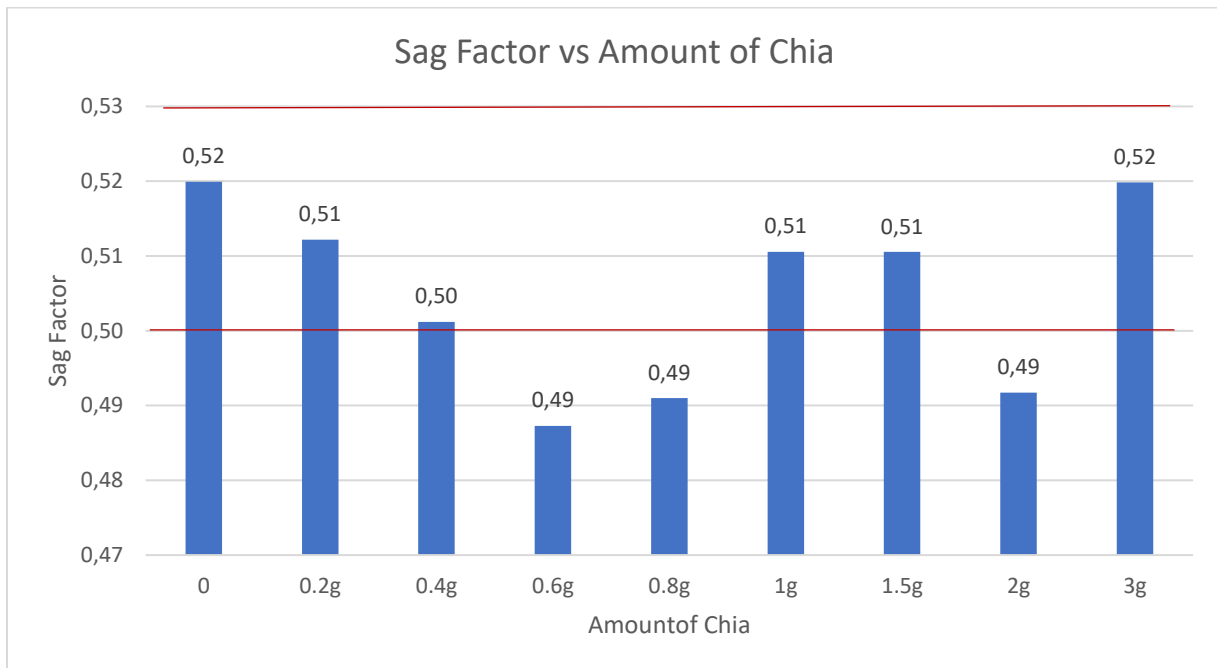


Figure 5.4: Sag Factor vs Amount of Chia in Bentonite Systems



Figure 5.5: Pictures of the sample from left; reference, reference +1g chia, reference +2g chia

5.1.3 Effect of Chia Preparation on Rheology

Next the question of does the preparation of the chia effect its rheological properties was investigated. As discussed in section 4, there were three preparation methods that were investigated; cooked, uncooked and fermented. The cooked chia was boiled before combined with the drilling fluid. The uncooked chia was added raw, and the fermented chia was allowed to ferment before being tested. The preparation effects on plastic viscosity and yield strength are shown in figures 5.4 and 5.5. Plastic viscosity and yield strength were calculated using shear stress and rpm data from a viscometer. The viscometer data is presented in the appendix.

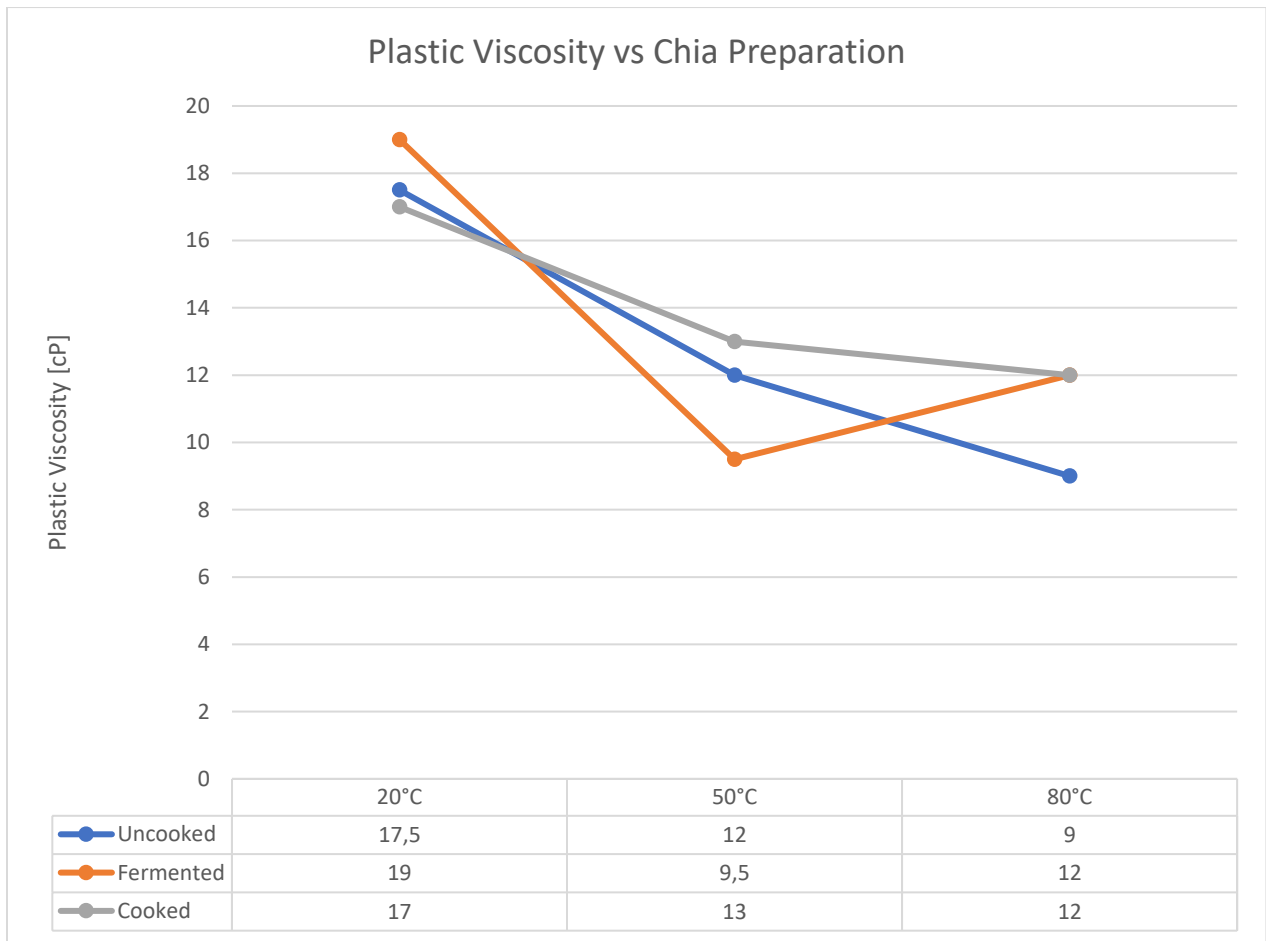


Figure 5.6: Plastic Viscosity vs Chia Preparation in Bentonite

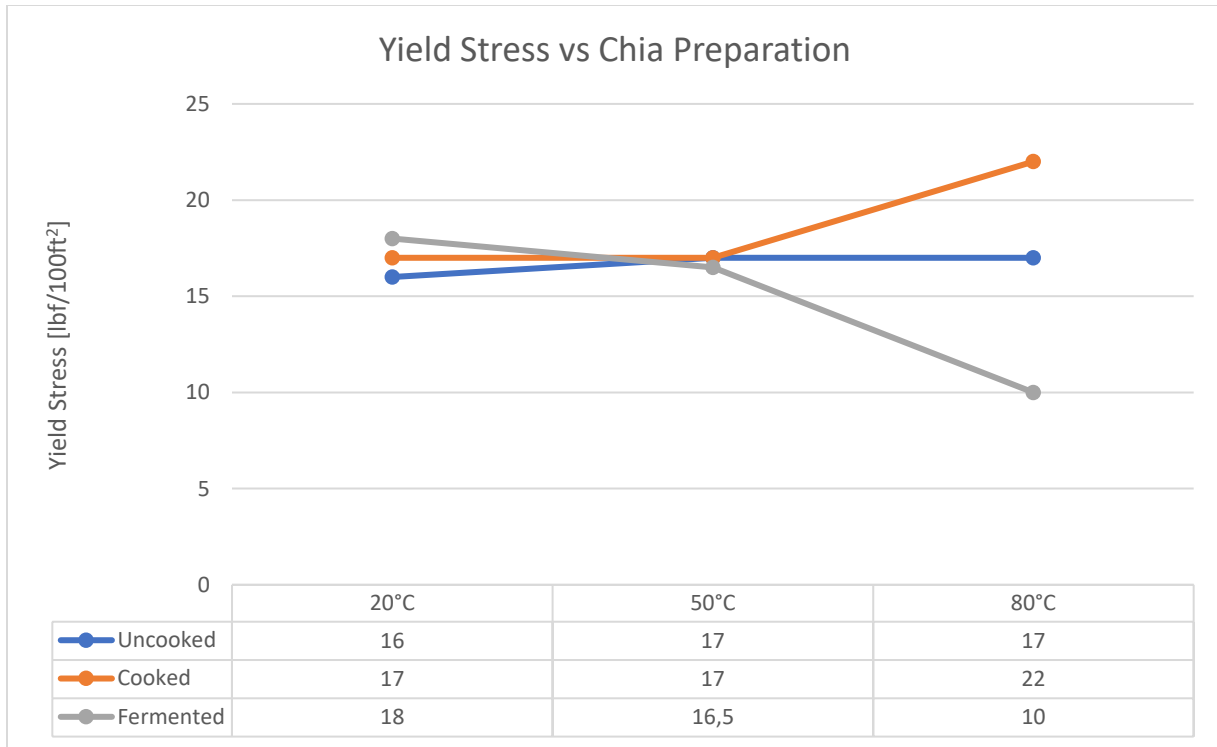


Figure 5.7: Yield Stress vs Chia Preparation in Bentonite

The preparation of the chia had little effect on plastic viscosity but it did affect the thermal stability of the fluid. Only the uncooked chia sample was thermally stable across the temperature range with the other two preparations being unstable across the temperature range. Also, the cooked chia sample exceeded the acceptable range for yield stress as it had a value of 22 lbf/100 ft² and the acceptable range is 11-20lbf/100ft². The preparation of the chia had some affect on the carrying capacity of the fluid as shown in figure 5.7, where the cooked chia sample had a greater YS/PV ratio than the uncooked sample at 50°C. The fermented sample had a lower ratio than the other two preparation methods at 50°C and 80°C.

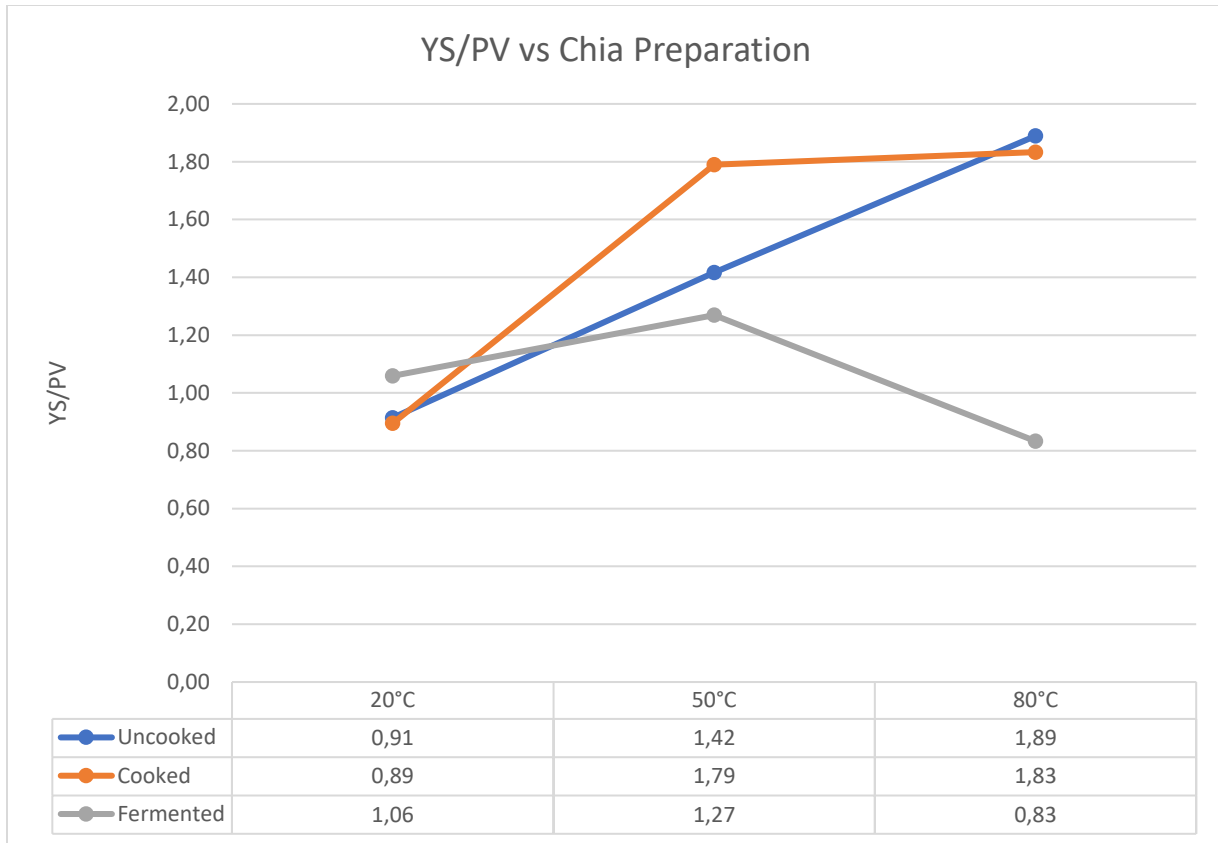


Figure 5.8: YS/PV vs Chia Preparation

5.1.4 Effect of Chia Preparation on Sag Factor

Next, the sag factor of the uncooked and cooked chia samples were measured to ensure that the sag factor fell within the acceptable range of 0.5-0.53. The sag factor was measured on samples that had not undergone any testing and had remained at room temperature as well as samples that had underwent rheology testing at 50°C and 80°C and are notated as “exposed to heat”. The uncooked samples have sag factor values that fall within the acceptable range and at the cooked

chia sample that had been exposed to heat had a value of 0.55 which is above the acceptable range.

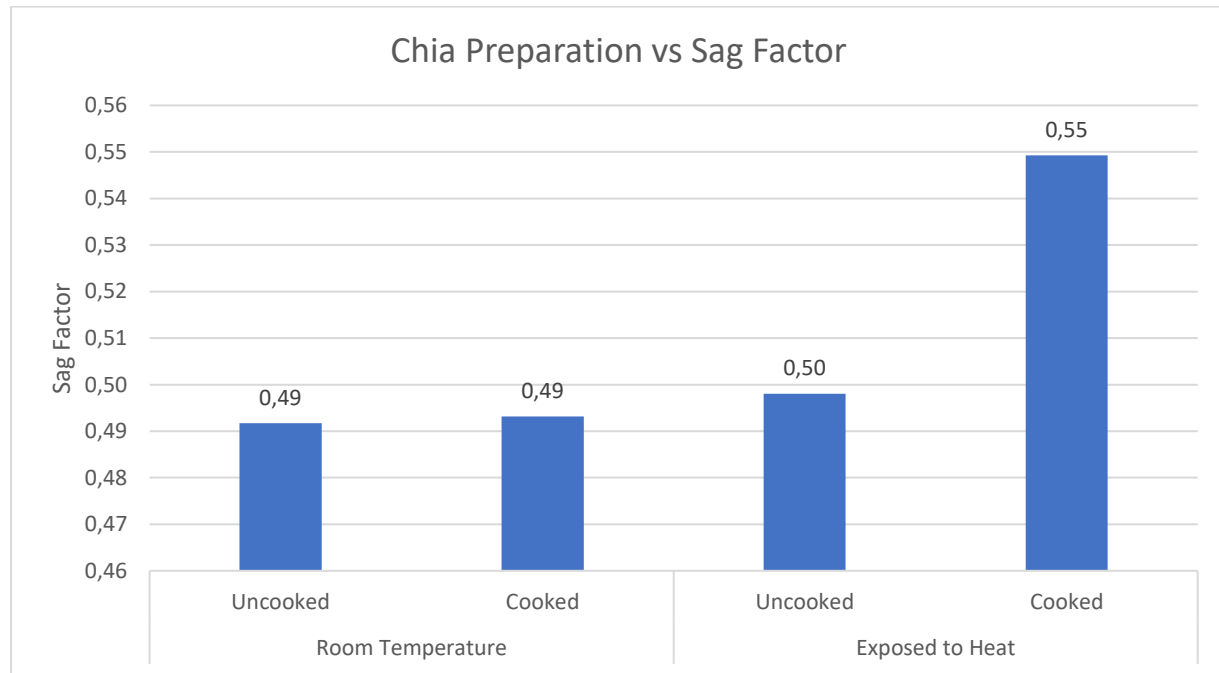


Figure 5.9: Chia Preparation vs Sag Factor in Bentonite

5.2 Characterization of Chia in Potassium Chloride based Drilling Mud

This section covers the characterization and development of a Potassium Chloride (KCl) based drilling fluid with the addition of chia as an additive. The aim was to find a formulation that was thermally stable while being within the acceptable sag factor range.

5.2.1 Chia Characterization in Pac/Polypac

This KCl-based formulation of drilling fluid was made to be similar to the bentonite formulation used, in that it uses the same additives as it had flat rheological characteristics. First, chia preparation was investigated to see if it had a different effect on KCl-based drilling fluid than the bentonite-based drilling fluid.

5.2.1.1 Rheology

Two preparations of chia were tested in the KCl-based drilling fluid, uncooked and cooked. The cooked chia was boiled prior to its addition to the drilling fluid and the uncooked was added raw.

The rheological properties were measured within a couple days of making the sample. The figures below show plastic viscosity and yield stress calculations for both chia preparations at various temperatures. These calculations were calculated using shear stress and rpm data from a viscometer. The viscometer data is presented in the appendix.

Figure 5.10 shows the plastic viscosity data and it can be observed that the cooked chia fluid has a lower viscosity than the uncooked chia fluid at all temperatures. Furthermore, figure 5.11 shows the yield stress data which shows that the yield stress for the cooked chia fluid has a lower yield stress than the uncooked chia fluid. Both fluids had yield stress that is below the acceptable range of 10-20 lbf/100ft². This means that this formulation must be altered to be within the acceptable range for yield stress.

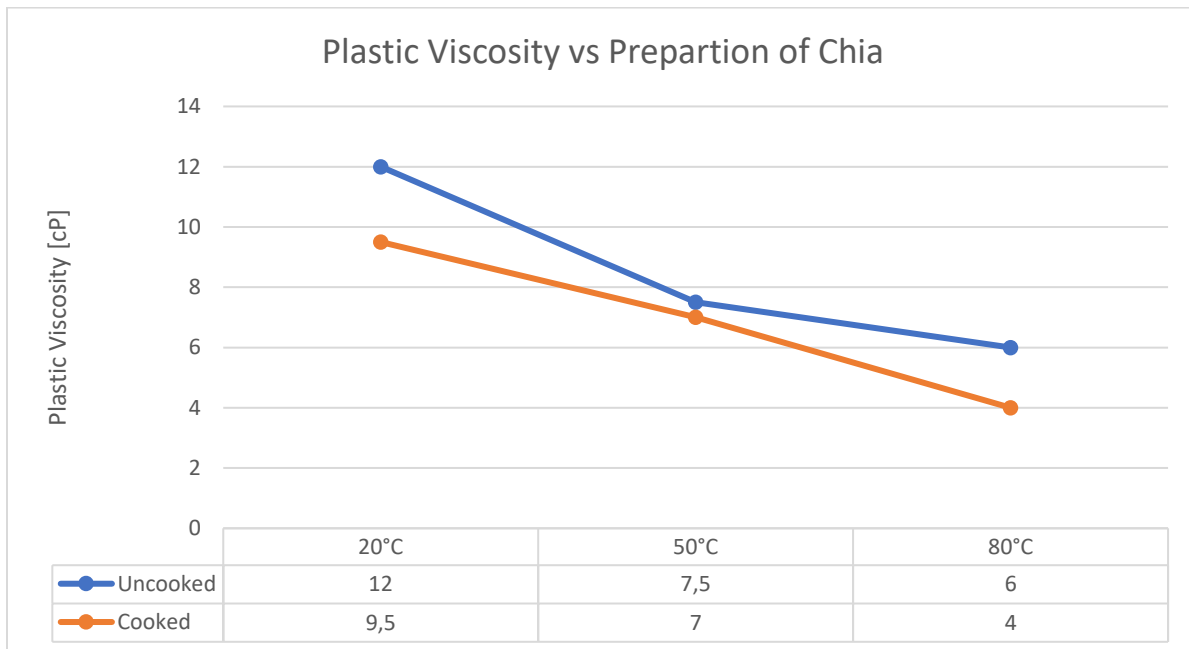


Figure 5.10: Plastic Viscosity vs Chia Preparation in KCl-Pac/Polypac System

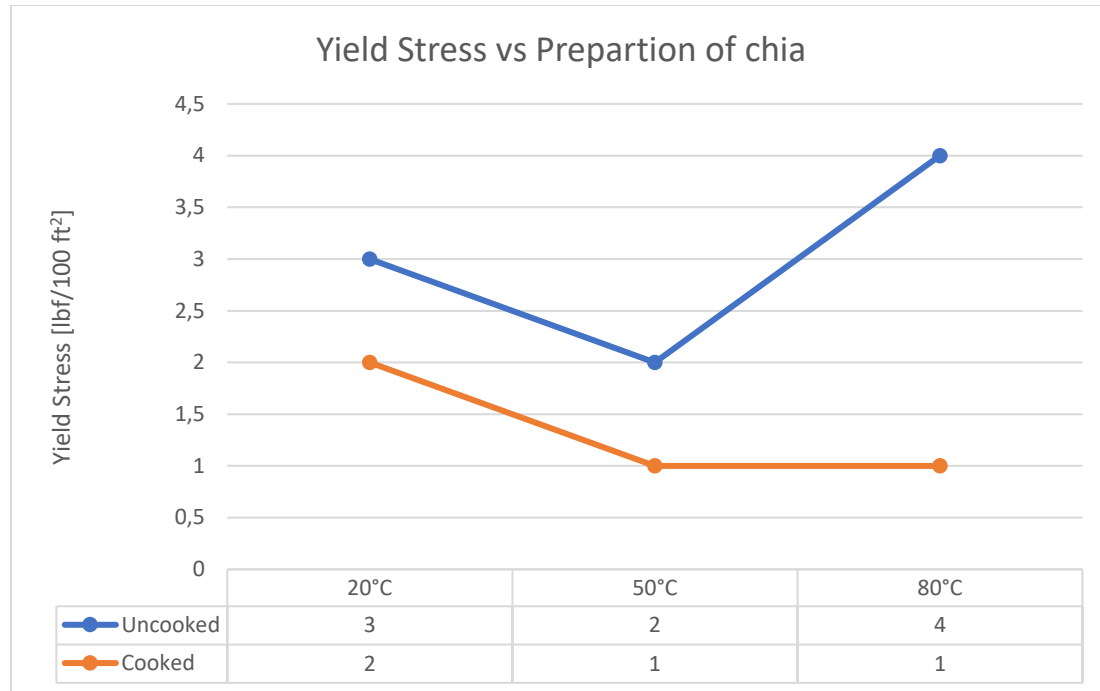


Figure 5.11: Yield Strength vs Chia Preparation in KCl-Pac/Polypac System

5.2.1.2 Sag Factor

After the two KCl-based fluids with different preparations of chia were tested with a viscometer, their sag factor was calculated. This was done by taking samples at the top of the sample and measuring their weight and volume and then taking samples at the bottom of the sample and measuring their weight and volume. Then the density of the top and bottoms were calculated, as well as an average of all the fluid’s density samples. Then the ratio of density at the top versus the density at the bottom was calculated. The sag factor was measured on samples that had not undergone any testing and had remained at room temperature as well as samples that had undergone rheology testing at 50°C and 80°C and are notated as “exposed to heat”. All the samples had sag factors that were above the acceptable range of 0.5 to 0.53. This means that their suspension capabilities were not acceptable to be used as a drilling fluid. Therefore, to reduce the sag factor a change to the formulation must be made. Figure 5.13 contains a photo of the sample that contained 2g uncooked chia and its reformulation that also contained 2g uncooked chia but xanthan gum instead of pac and polypac which will be covered in the next section. The photo illustrates the amount of sediment settling that the samples exhibited and why reformulation was necessary.

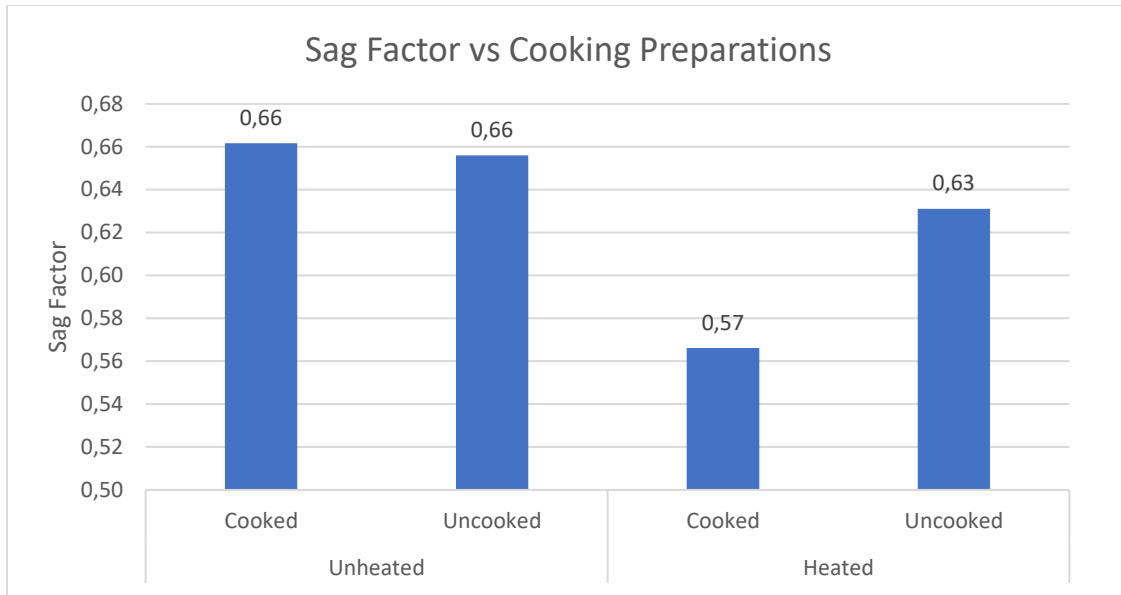


Figure 5.12: Sag Factor vs Cooking Preparations in KCl-Pac/Polypac System



Figure 5.13: Picture of two samples containing 2g uncooked chia, the left containing Pac and PolyPac and the right containing Xanthan Gum

5.2.2 Effect of Chia on Potassium Chloride-based Mud with Xanthan Gum

In order to obtain yield stress and sag factor values that fall within acceptable ranges, the next formulation of Potassium Chloride-based drilling mud used Xanthan Gum as a replacement for PolyPac and Pac. The first formulation with Xanthan Gum used 2.14g of Xanthan Gum to test if it was a proper substitute. After testing the rheological properties, the amount of xanthan gum was

decreased to 1.5g. Next, the preparation of chia was investigated using 2g of chia per sample as well as one sample with no chia to use as a reference fluid.

5.2.2.1 Chia Preparation effects on Rheology

Three samples were tested in this round of formulation; a sample with 1.5g XG and 2g uncooked chia, a sample with 1.5g XG and 2g uncooked chia, as well as a sample with 2.14g XG and 2g uncooked chia. The sample with 2.14g XG was made first and based off visual investigation of the fluid, it was decided to make more samples with less xanthan gum. It was still included in testing as to ensure its disqualification from further testing. These samples were tested with a viscometer to gather data on its shear stress at different RPMs at various temperatures, diagrams with this data are in the appendix. Using that data, plastic viscosity, yield stress, low shear yield stress and the ratio of yield stress to plastic viscosity was calculated by using the Bingham Plastic model. These calculations are shown in the following figures.

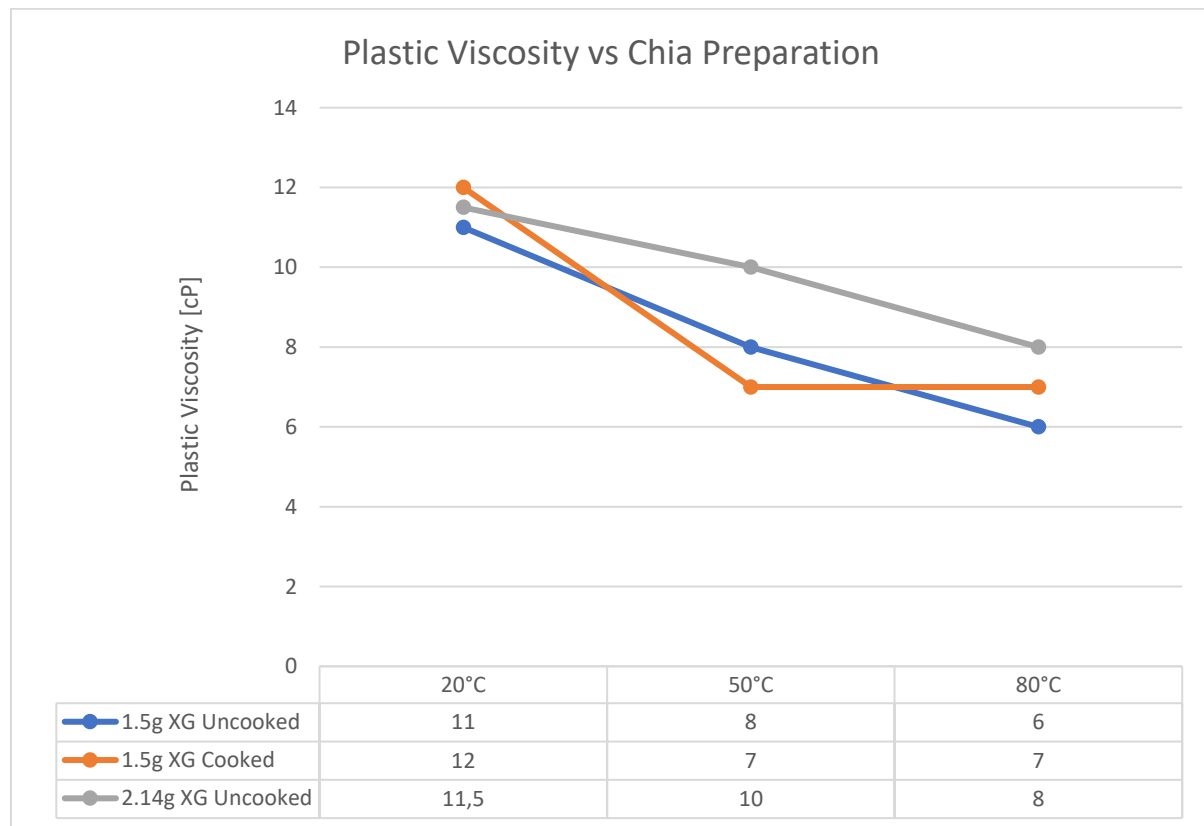


Figure 5.14: Plastic Viscosity vs Chia Preparation in KCl-Xanthan Gum System

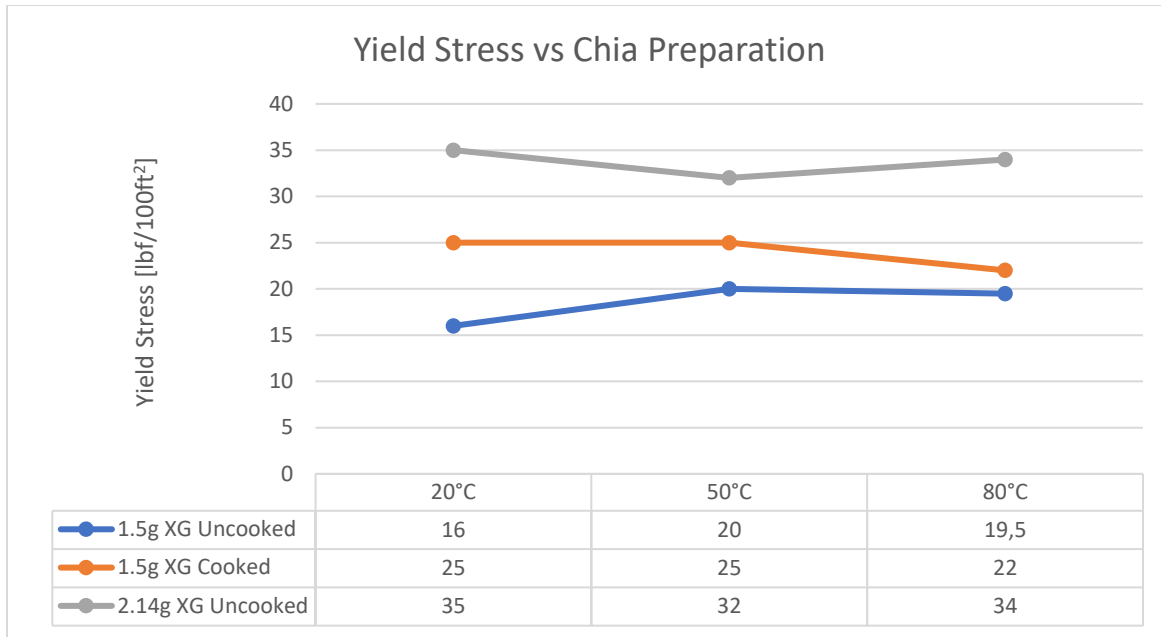


Figure 5.15: Yield Stress vs Chia Preparation in KCl-Xanthan Gum System

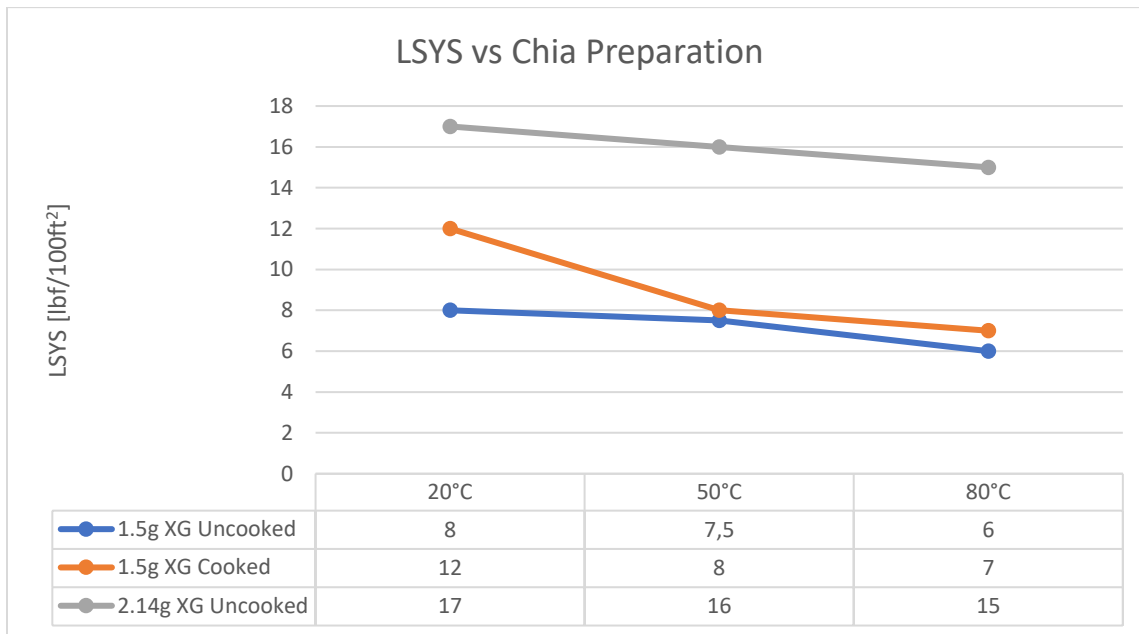


Figure 5.16: Low Shear Yield Stress vs Chia Preparation in KCl-Xanthan Gum System

Figure 5.14 shows the plastic viscosity where it can be observed that the sample with 2.14g XG had a higher plastic viscosity than the sample with 1.5g XG at all temperatures. It also had high plastic viscosity than the cooked chia sample at the higher temperatures. There was little difference in plastic viscosity between the cooked and uncooked chia samples with 1.5g XG. Figure 5.15 and figure 5.16 shows the samples' yield stress values and lower shear yield stress

values, where it can be observed that the sample with 2.14g XG had much higher yield stress values than the samples with 1.5g XG. These yield stress values far exceed the range of acceptable yield stress values to warrant further testing. The samples with 1.5g XG had similar yield stress and lower shear yield stress values, with the cooked chia having slightly higher values. They both had yield stress values that slightly exceed the acceptable 10-20 lbf/100ft² range for yield stress values, but only slightly and the effect of varying the amount of chia will be tested later. Although, the sample with cooked chia showed thermal stability so, only cooked chia will be used in further investigations of KCl-based fluids with Xanthan Gum.

Below is figure 5.15 which shows the ratio of yield stress over plastic viscosity which is a predictor of the carrying capacity of the fluid. The cooked chia had generally higher values than the uncooked chia with the same amount of xanthan gum except at 80 °C where they were similar. The sample with 2.14g XG had higher values except at 50 °C where the cooked chia sample had a slightly higher value.

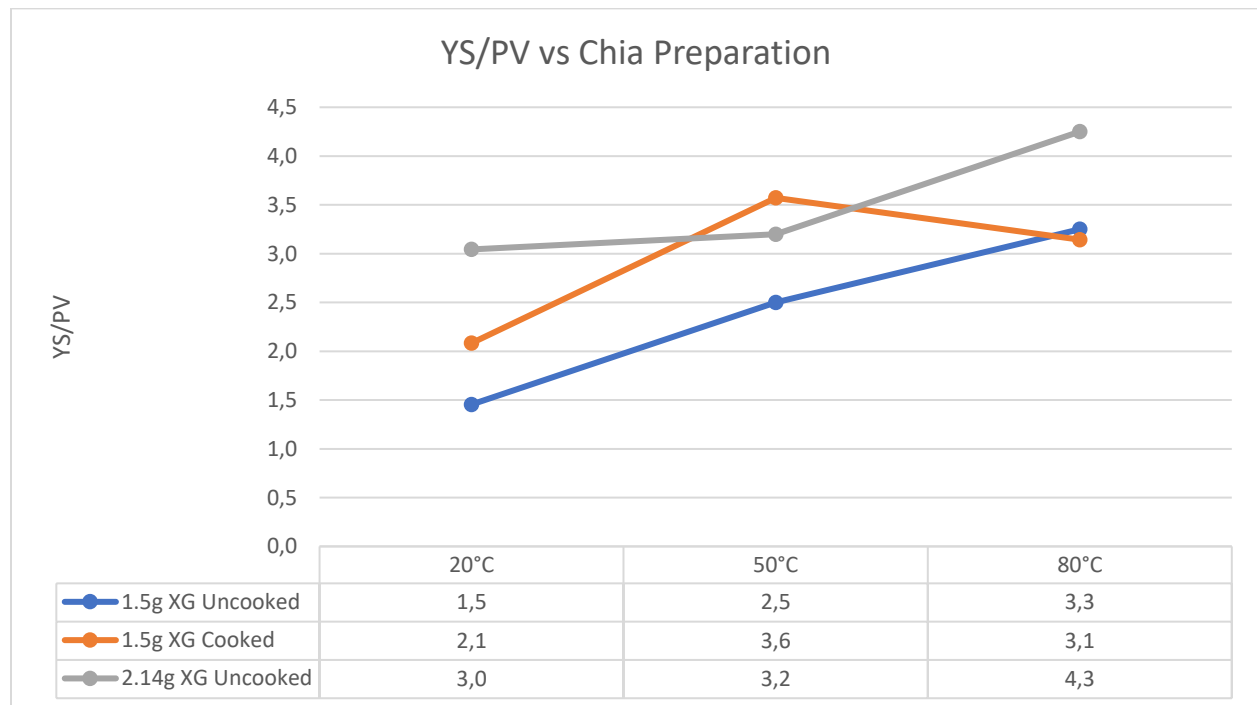


Figure 5.17: YS/PV vs Chia Preparation in KCl-Xanthan Gum System

5.2.2.2 Effect of Chia Preparation on Sag Factor

Next, the three samples were tested for Sag Factor to ensure that they didn't experience sedimentation. The procedure for testing sag factor has been explained previously. These fluids were tested with samples that had previously been at room temperature and samples that had been exposed to heating during the viscometer tests. All of the samples had sag factor values that were within side the acceptable range of 0.5 to 0.53, with an exception being the sample with 2.14g XG which's room temperature sample had a slightly lower sag factor of 0.48. This could be that the xanthan gum had suspended some heavier particles at the top of the fluid. Figure 5.19 contains a photo containing the samples; KCl+2.14g XG, KCl+1.5g XG + 1g Chia, KCl+1.5g XG +2g Chia. The photo illustrates that the sample containing 2.14g XG experienced no sedimentation but the samples containing 1.5g XG did. The samples containing 1.5g XG also showed signs of increasing air bubbles with increased amounts of chia.

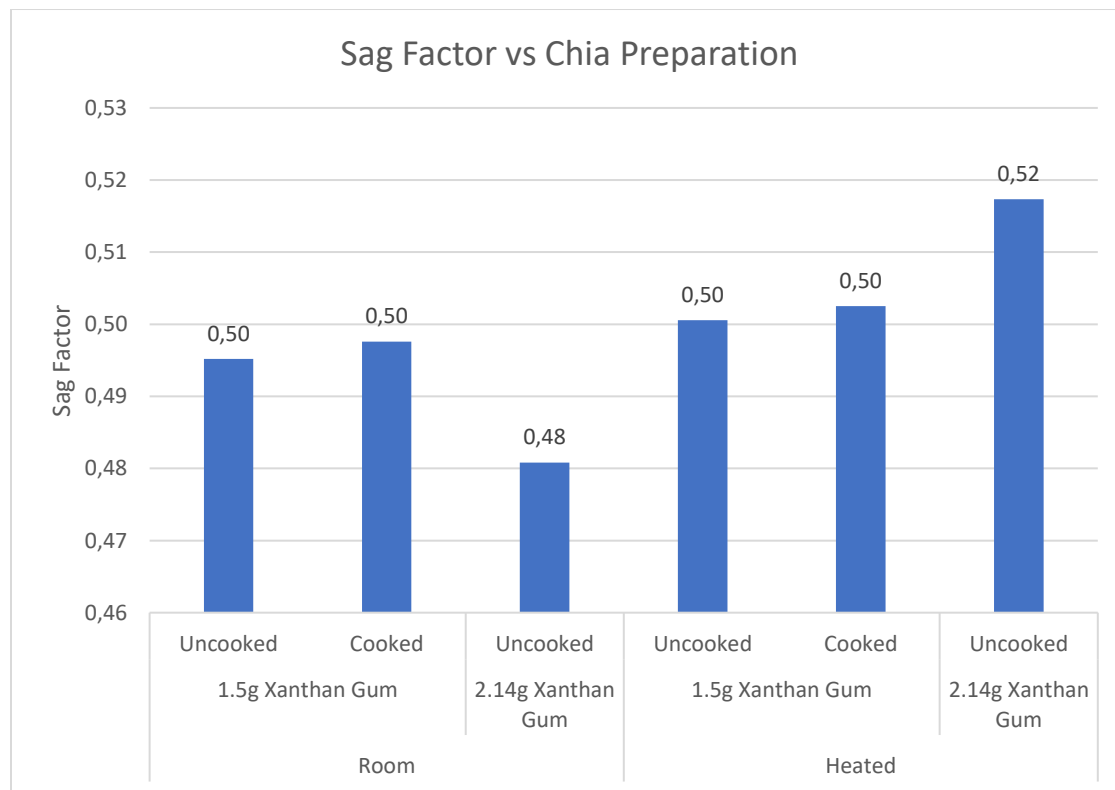


Figure 5.18: Effect of Chia Preparation on Sag Factor in KCl-based system with Xanthan Gum



Figure 5.19: Picture containing the samples from left; KCl+2.14g XG, KCl+1.5g XG + 1g Chia, KCl+1.5g XG +2g Chia

5.2.2.3 Effect of Chia Amounts in KCl with Xanthan Gum

Next, in order to characterize the effects of chia on KCl-based drilling fluid, the amount of chia in each sample is varied. As shown in the previous section, the cooked chia preparation method resulted in a thermally stable fluid, only cooked chia will be used in the samples studied in this section. The samples that are tested in this section include a reference fluid that does not contain chia, reference +1g chia, reference + 2g chia, and reference + 3g chia. In this section, the rheological properties are being investigated and the samples were tested with a viscometer in order to study the plastic viscosity, yield stress, low shear yield stress and the ratio of YS/PV. These were calculated based on the Bingham Plastic model and were computed using viscosity measurements that were obtained at 20°C, 50°C and 80°C, this data is presented in the appendix.

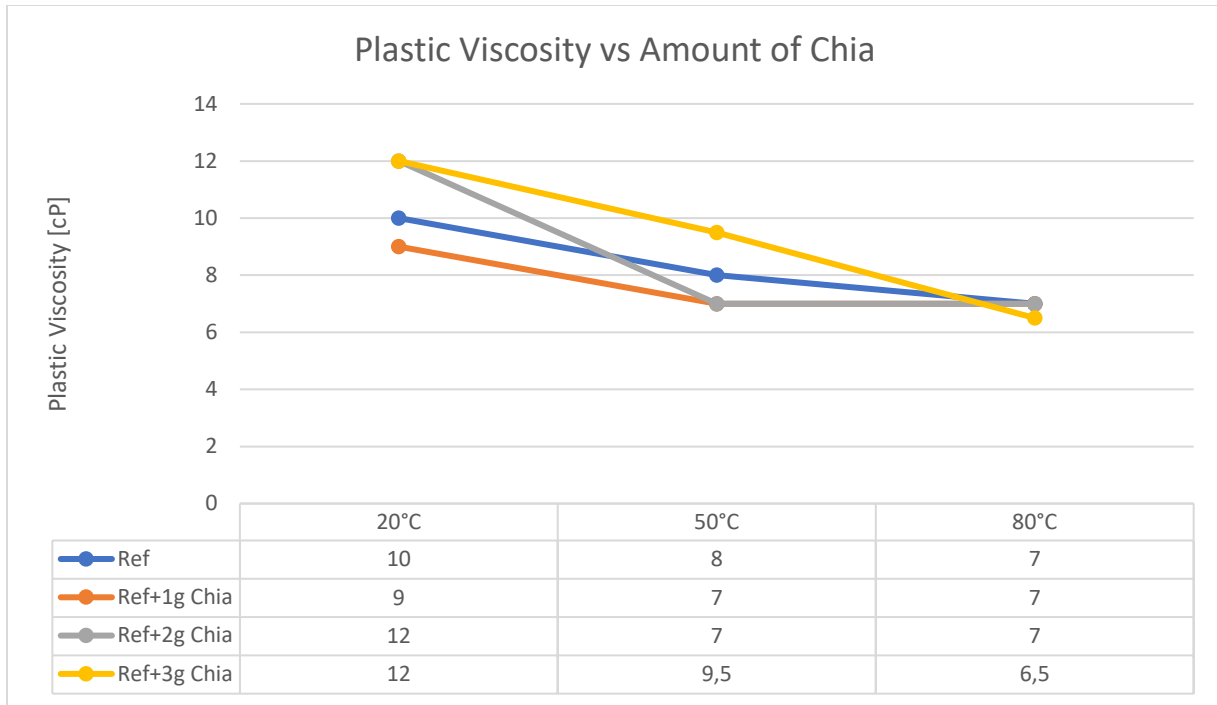


Figure 5.20: Plastic Viscosity vs Amount of Chia in KCl-Xanthan Gum System

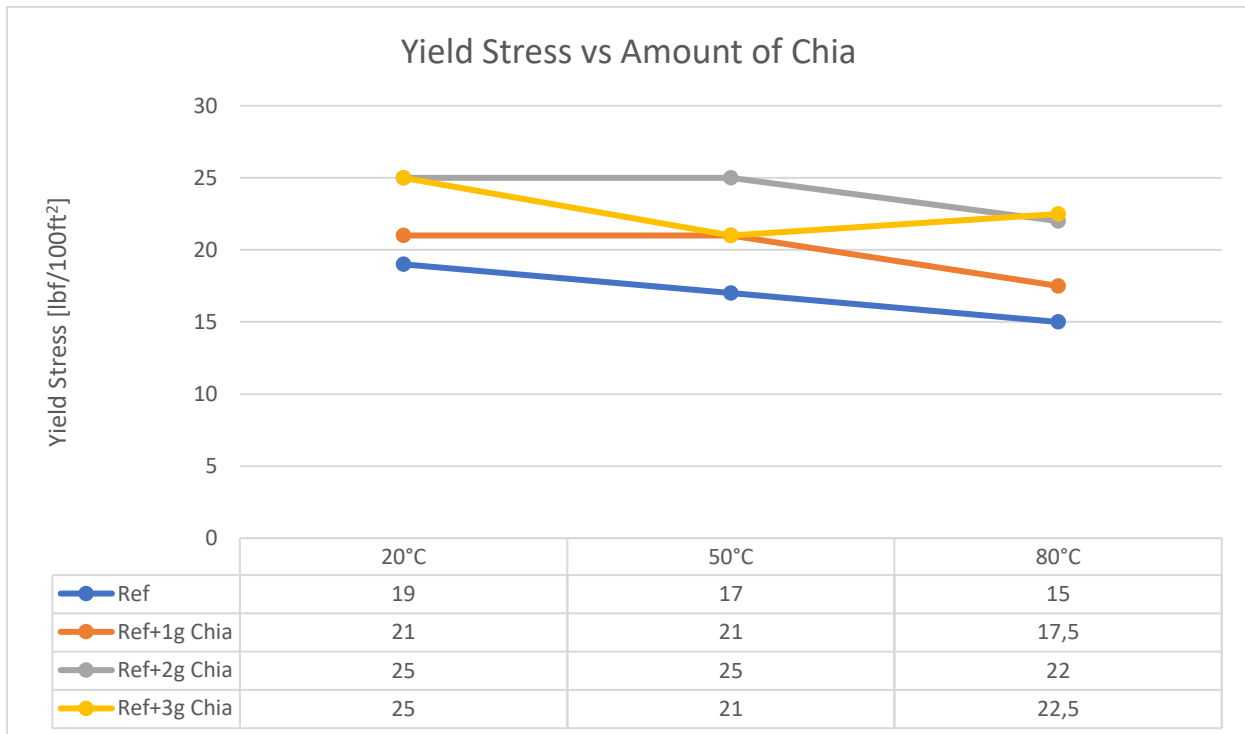


Figure 5.21: Yield Stress vs Amount of Chia in KCl-Xanthan Gum system

As observed in figure 5.20, the amount of chia had no significant effect on the plastic viscosity of the fluid. Figure 5.21 shows that the amount of chia increases the yield stress of the fluid, but not linearly. All the samples had yield stress that were above the desirable range of 11-20 lbf/100ft² to ensure efficient cutting transport, although the chia did make the fluid more thermally stable than the sample without chia. Below is figure, 5.22, which shows YS/PV, which is also a predictor of carry capacity. All of the samples containing chia had a ratio above the reference fluid, but there is not a linear correlation between the amount of chia and the increase of the ratio.

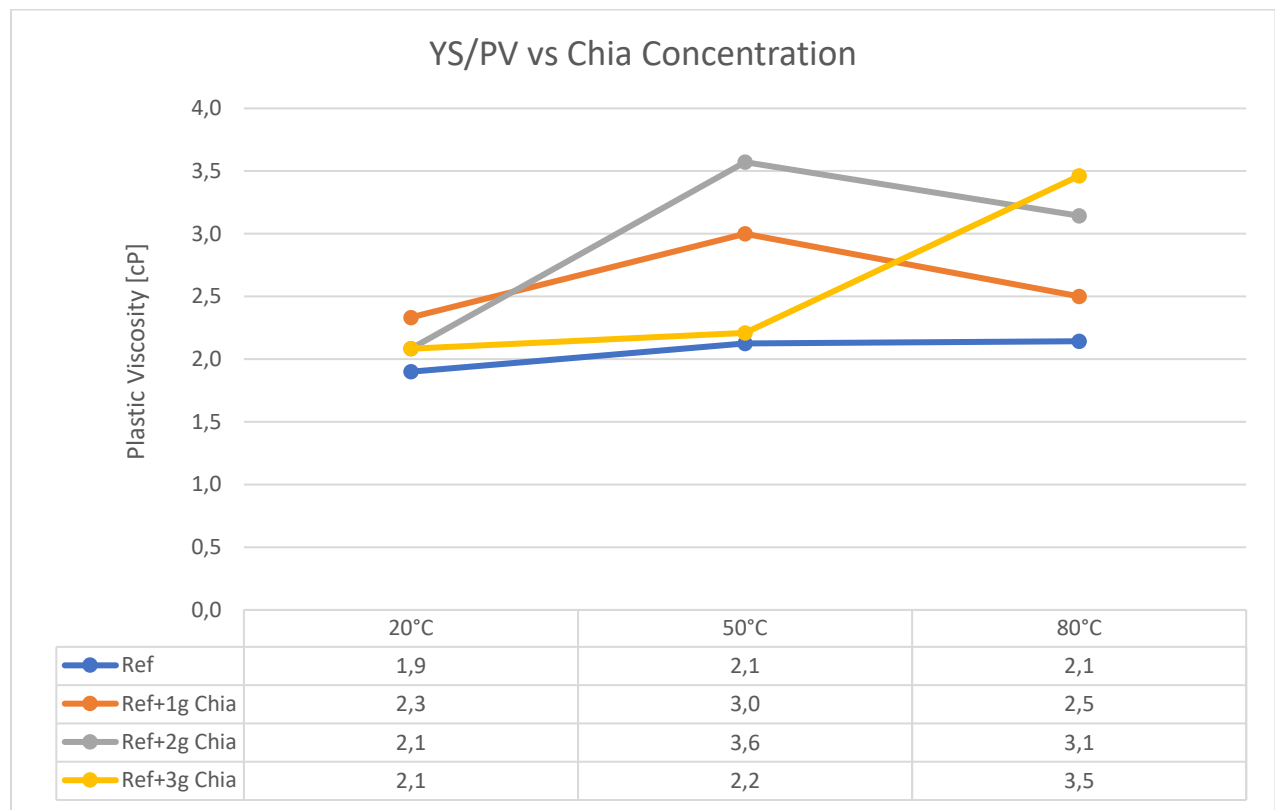


Figure 5.22: YS/PV vs Amount of Chia in KCl-Xanthan Gum system

5.2.2.4 Effect of Amount of Chia on Sag Factor

Next the sag factor of the samples was investigated to ensure that the fluid had proper suspension abilities. The sag factor was measured on samples that had not been used for other testing and had only been sitting at room temperature since they were created. All of the samples had sag factors that fell within acceptable ranges.

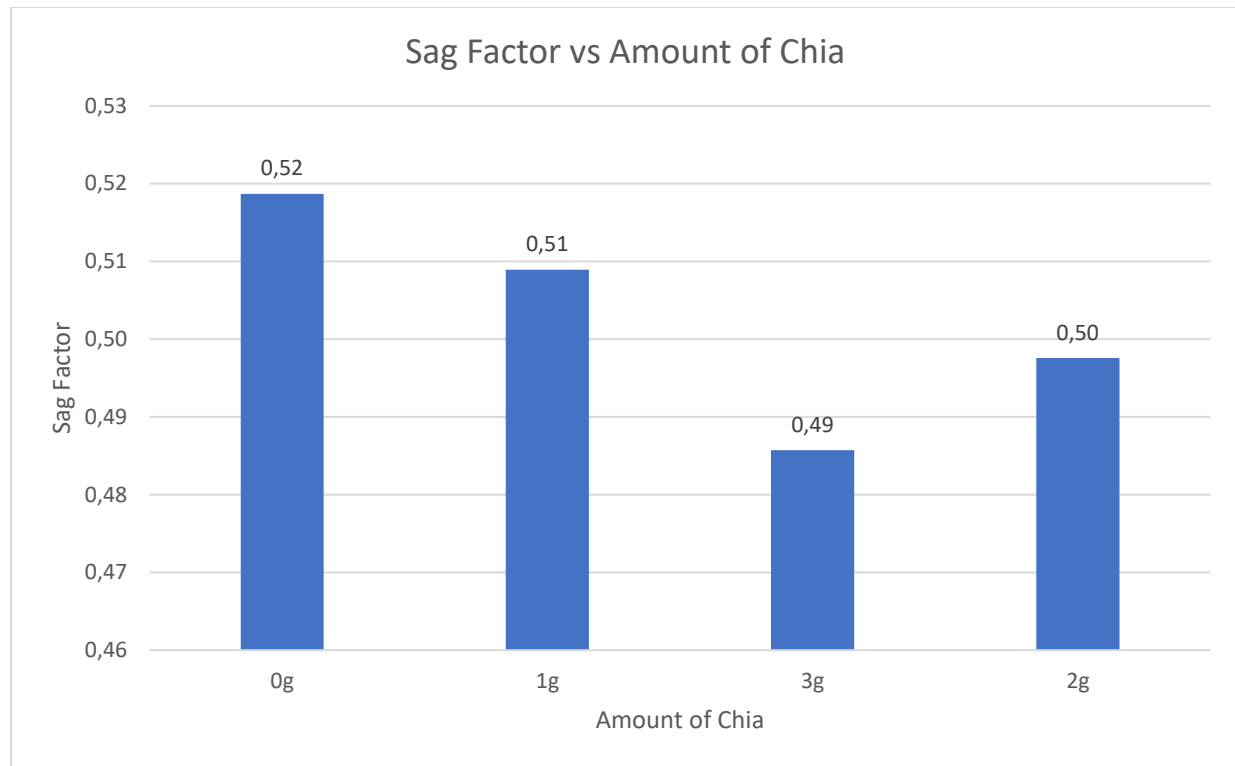


Figure 5.23: Sag Factor vs Amount of Chia in KCl-Xanthan Gum system

5.3 The Addition of Mandarin Peel Powder

It was decided to add mandarin peel powder (MPP) as there were concerns over the filtrate loss of the fluid due to the amount of air bubbles that were seen in the prepared samples. A previous study done by Petter Havnen showed that MPP decreased filtrate loss in water-based drilling fluids. This section will first investigate whether the mandarin peel powder causes thermally stable fluid to no longer be thermally stable, and ensure that its sag factor has not increased beyond acceptable levels.

5.3.1 Rheology

Mandarin was added to improve filtrate loss that will be covered in the next section, but first the rheological data was investigated to ensure that the fluid remained thermally stable. For bentonite 3 samples with varying amounts of mandarin peel powder were compared to the thermally stable sample that contained 2g of uncooked chia and will be called the reference fluid.

For the KCl-based fluid the reference fluid is the sample which contained 3g of cooked chia and it will be compared to a sample that added 1g of mandarin peel powder to it. Figures

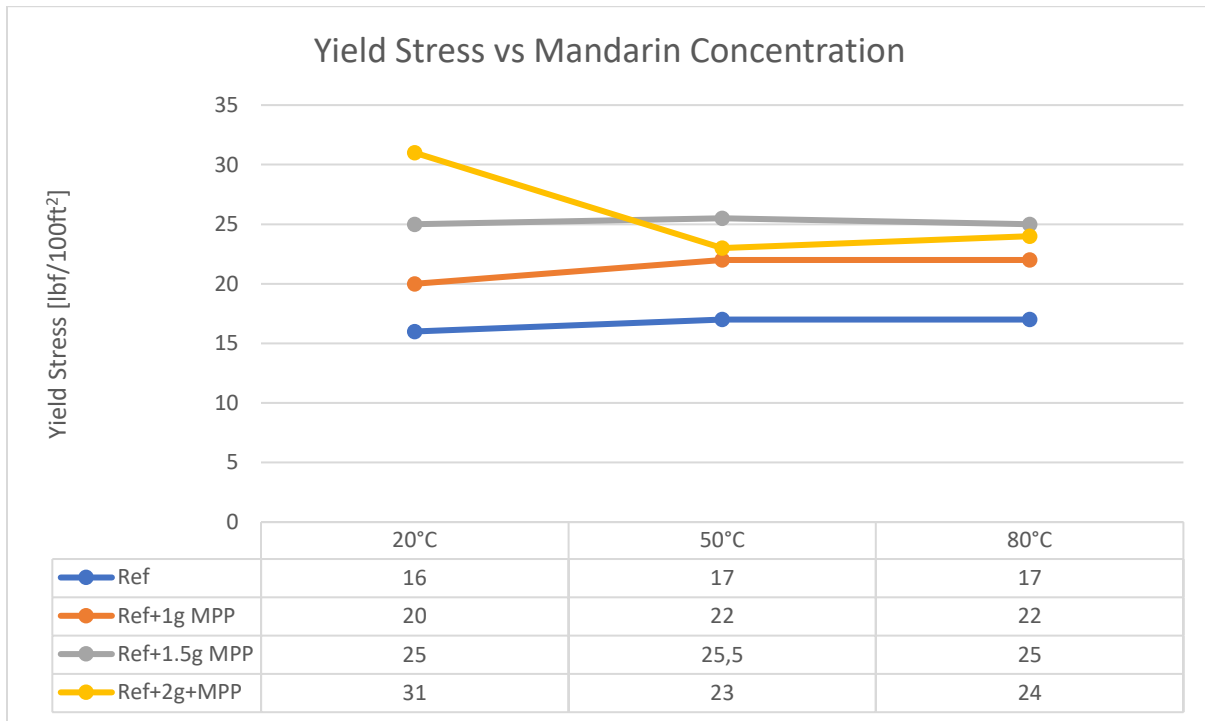


Figure 5.24: Yield Stress vs Amount of Mandarin in Bentonite-based fluid

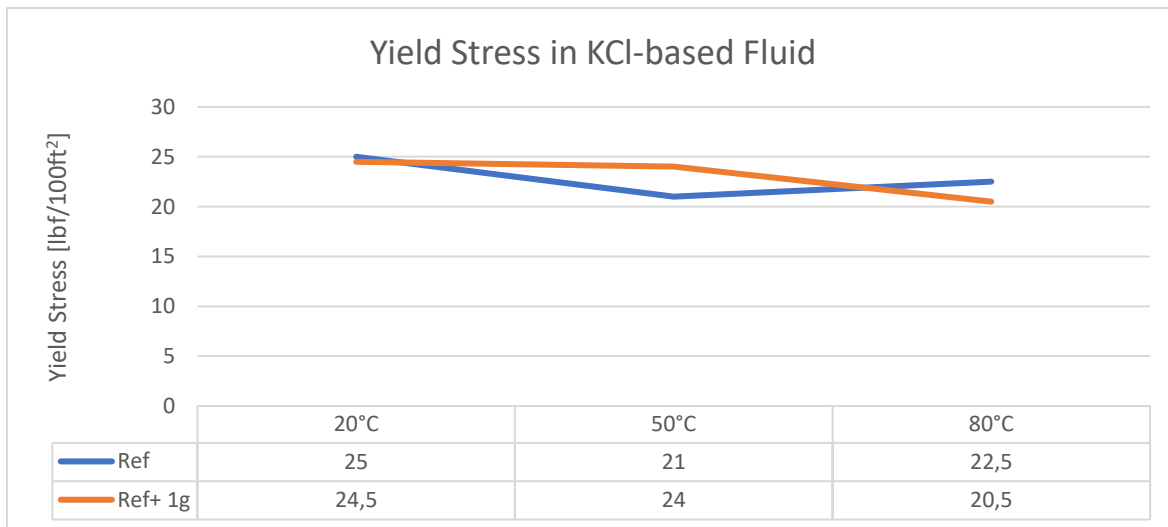


Figure 5.25: Yield Stress vs Mandarin Addition in KCl-Based Fluid

Figures 5.24 and 5.25 show the effect of Mandarin on the fluids. It can be observed that the addition of mandarin increased the yield stress in bentonite in an almost linear fashion while

remaining thermally stable, except for reference+2g MPP. In the KCl-based fluid, the yield stress was approximately the same in both the fluid which contained mandarin and the one that did not contain mandarin. They were also both similarly thermally stable. Figures 5.26 and 5.27 below, show the effect of mandarin on the fluids carrying capacity. In both fluids, the mandarin did not have a significant effect on the carrying capacity except for in bentonite with the sample reference+2g MPP which had higher carrying capacity at 20°C and 80°C.

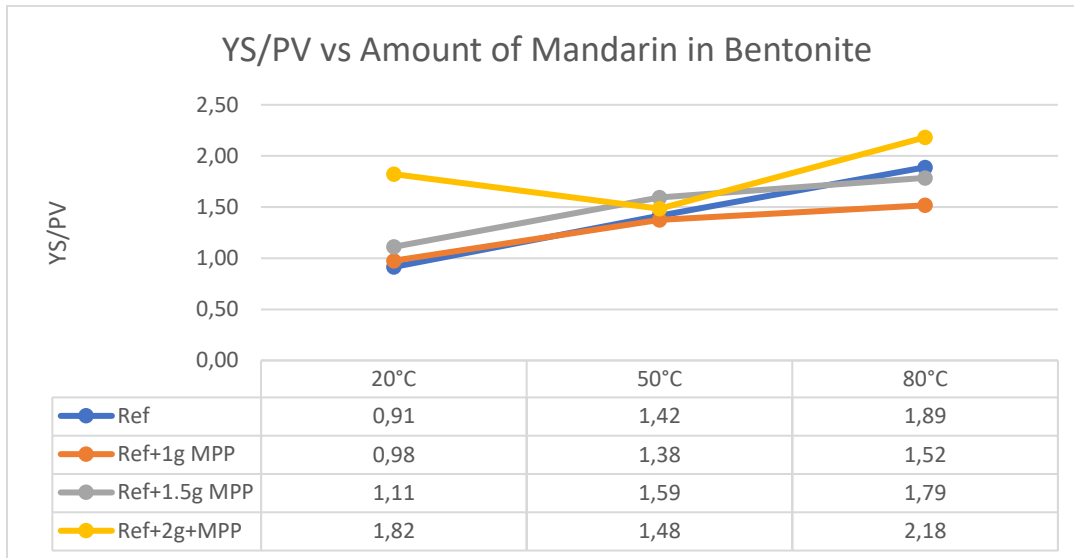


Figure 5.26: YS/PV vs Amount of Mandarin in Bentonite

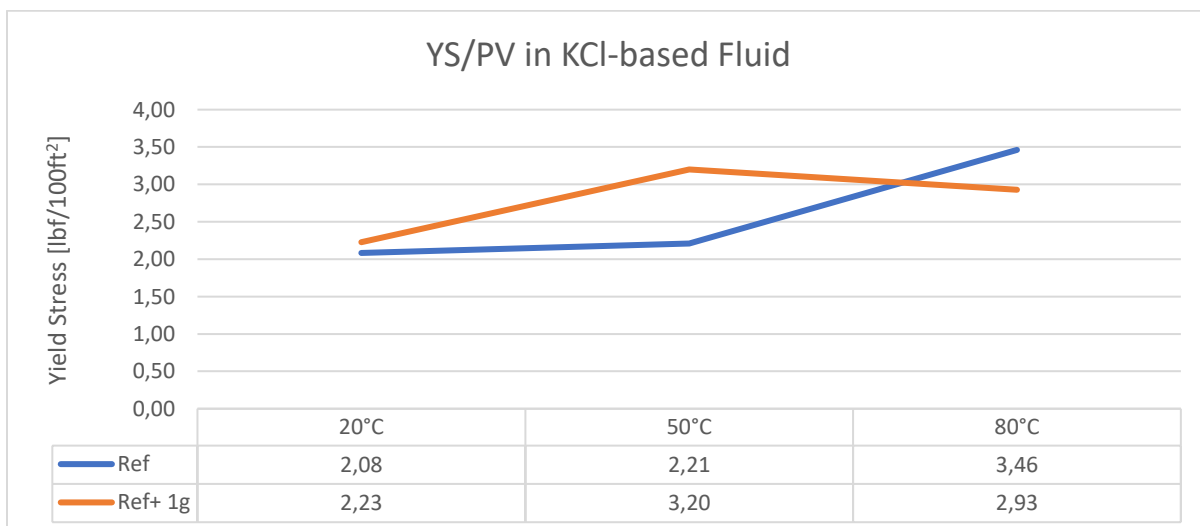


Figure 5.27: YS/PV vs Addition of Mandarin in KCl-based fluid

5.3.2 Effect of Mandarin on Sag Factor

Sag Factor was investigated to verify the suspension abilities of the fluid and to ensure there wasn't too much sedimentation of the particles. Figures 5.28 and 5.29 show a graph of the sag factor of each sample. As it can be seen from the graphs, all the samples had sag factors that were within the acceptable range. It appears that mandarin peel powder does not have a noticeable effect on the suspension abilities of the fluid. Figure 5.30 is a picture of the samples from left to right; Reference, Ref+1.5g MPP, and Ref+2g MPP. In this picture the effects of the mandarin peel powder can be seen in that there is a decreased amount of air bubbles within the fluid. This should affect the amount of filtrate loss, and that will be investigated in the next section.

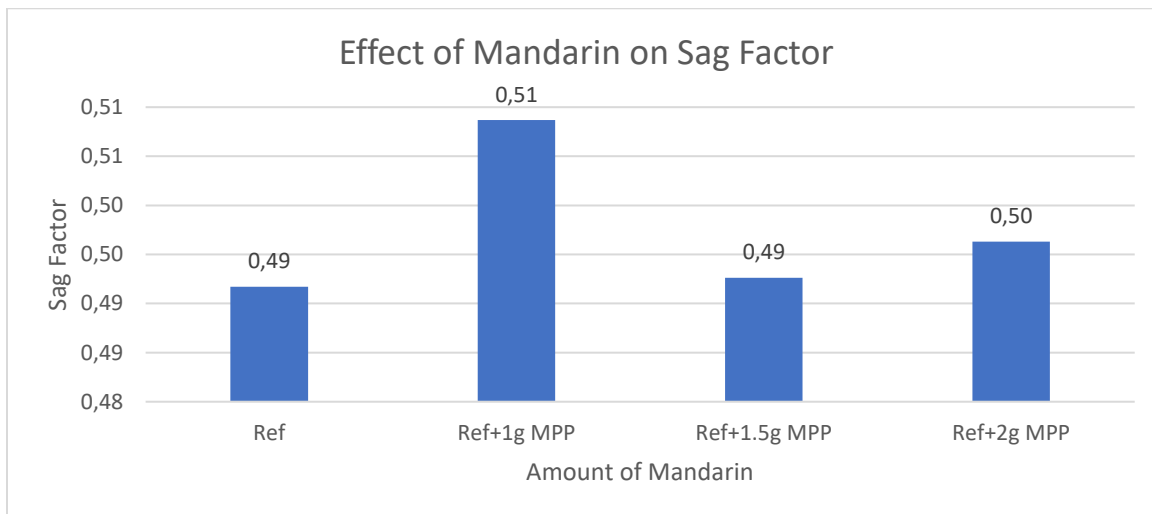


Figure 5.28: Effect of Mandarin on Sag Factor in Bentonite

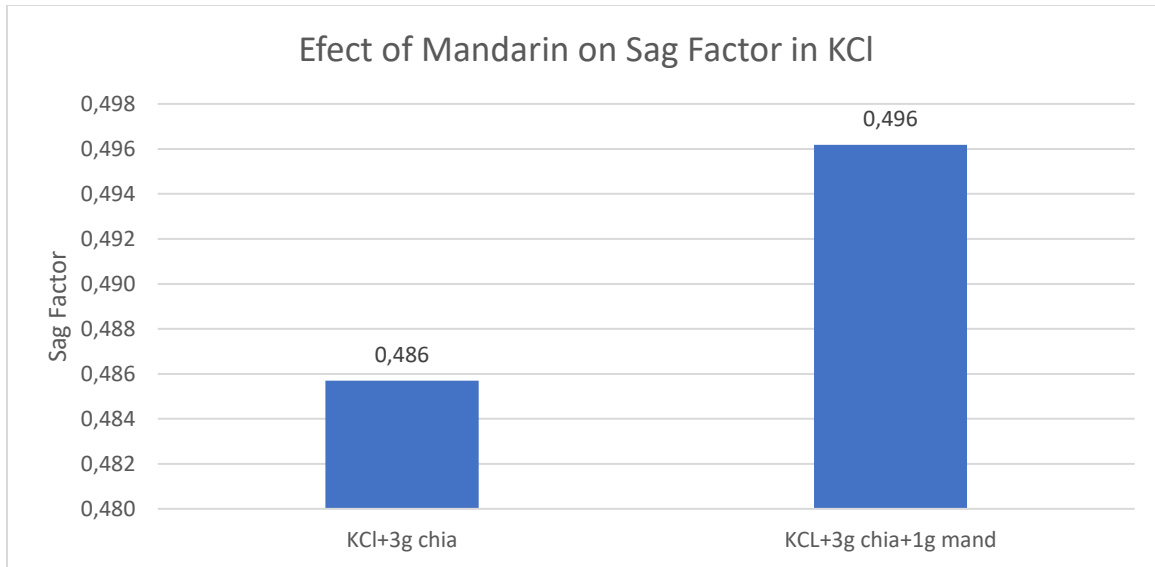


Figure 5.29: Effect of Mandarin on Sag Factor in KCl



Figure 5.30: Photo of the samples from left to right; Ref, Ref+1.5g MPP, and Ref+2g MPP

5.4 Filtrate Loss

Filtrate loss of the samples was done according to the method described in section 4.2.5 and was tested on three different sets of samples. The first set, shown in figure 5.31, is investigating the addition of uncooked chia, the second set, shown in figure 5.32, investigates the effect on varying amounts of mandarin peel powder on top of the thermally stable system of the sample that contained 2g of uncooked chia in the bentonite-based drilling fluid. The third set shown in figure 5.33, investigated varying amounts of chia in the KCl-based fluid and then one sample which contained 3g of cooked chia and 1g of mandarin peel powder.

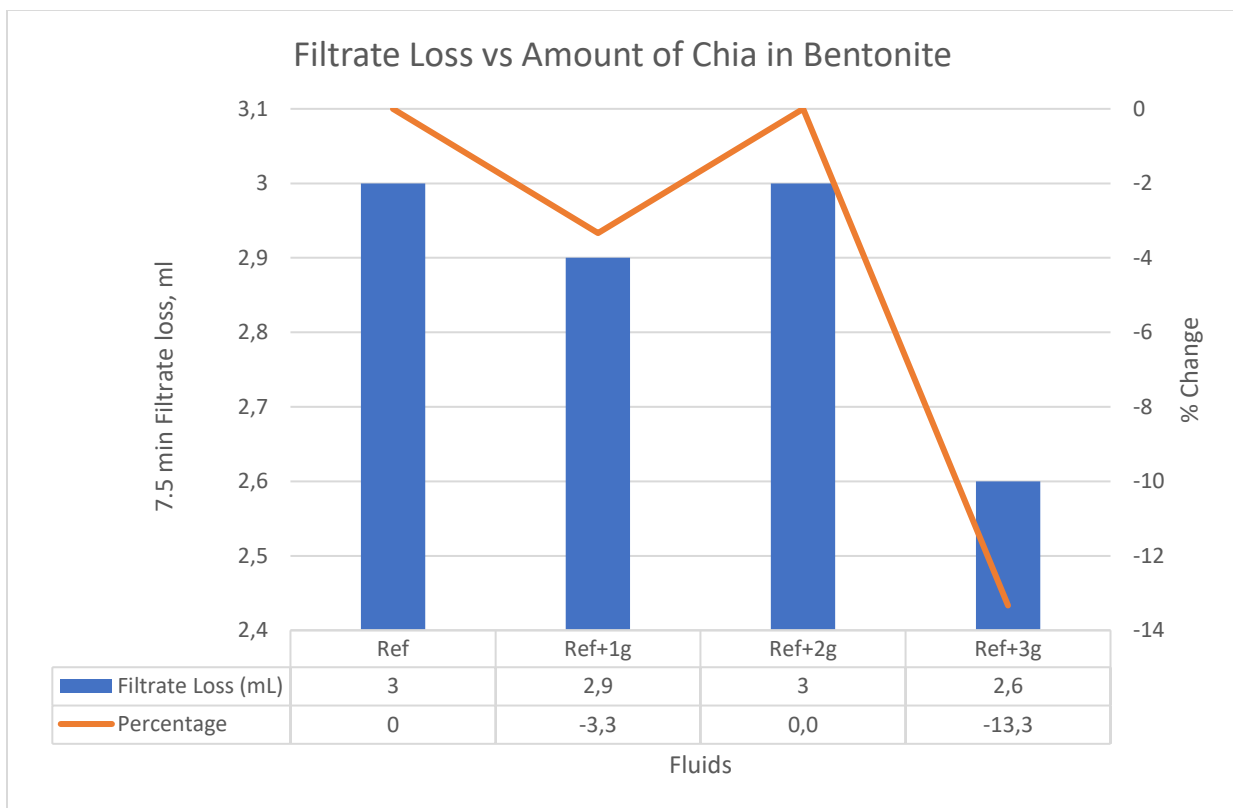


Figure 5.31: Filtrate Loss vs Amount of Chia in Bentonite

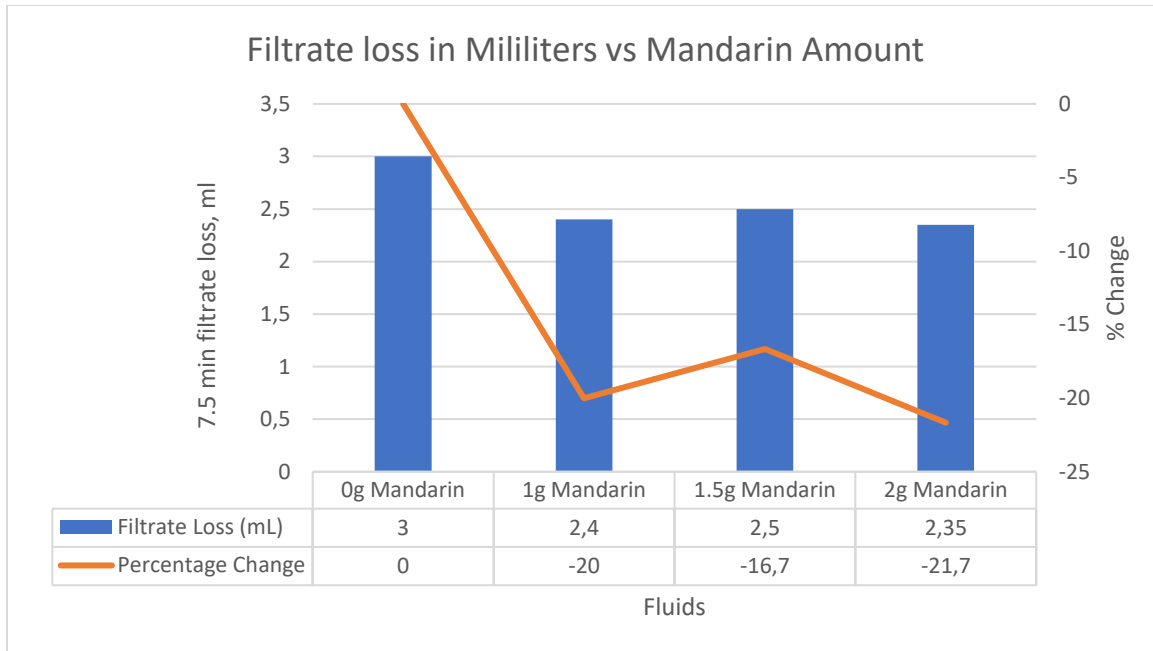


Figure 5.32: Filtrate Loss vs Amount of Mandarin in Bentonite

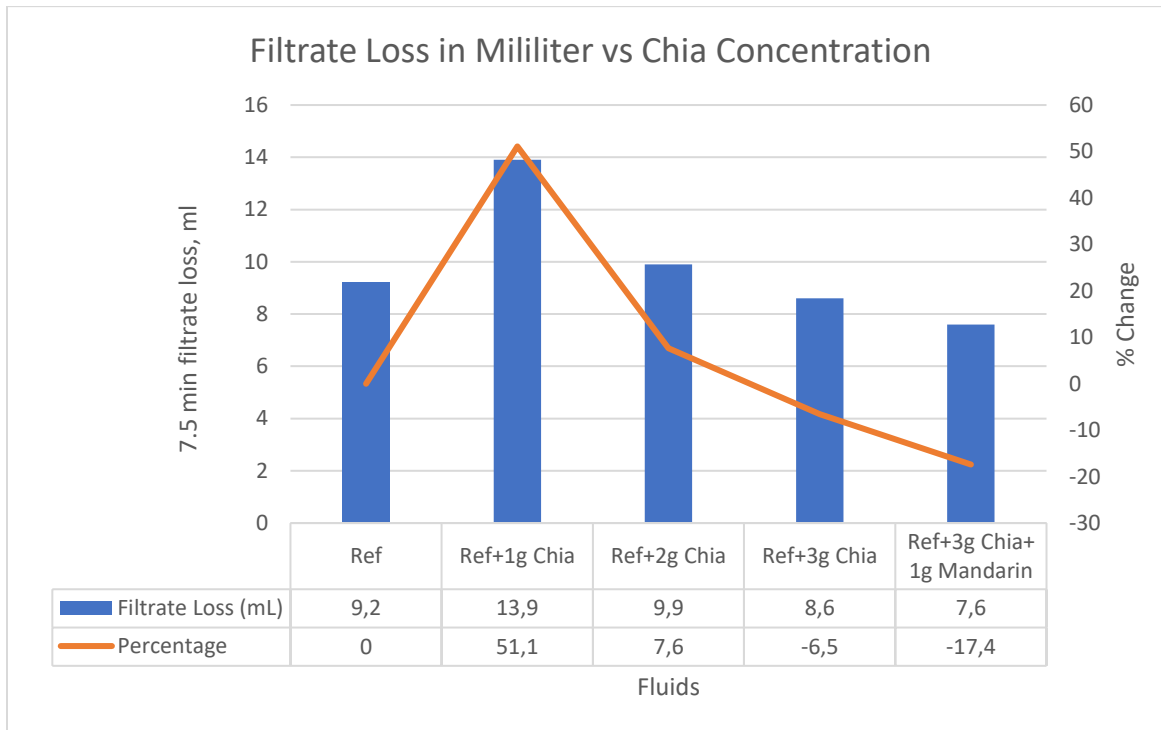


Figure 5.33: Filtrate Loss vs Amount of Chia and Mandarin Peel Powder in KCl

In Figure 5.31 it can be seen that low additions of chia has little to no effect on filtrate loss in the bentonite-based drilling fluid and that the addition of 3g of chia decreased the filtrate lost by

13.3%. Figure 5.32 shows that the addition of mandarin peel powder decreased the filtrate lost by an average of 20%, but it does not suggest that adding more mandarin decreases the amount of filtrate lost. Figure 5.33 shows that in the KCl-based drilling fluid, the addition of 1g of chia increased the filtrate lost by approximately 50% and the addition of 2g of chia increased the filtrate lost by 7.6%. Although the addition of 3g of chia decreased the filtrate lost by 6.5%. The addition of mandarin had a great effect similar to its effect in the bentonite-based drilling fluid, of a decrease of 17% in filtrate lost.

5.5 Ecological Replacement of Polymers for Filtrate Loss

One of the concerns with using ecological additives is whether they can replace environmentally harmful additives. The samples that showed the least amount of filtrate loss were investigated further as to how much of the additives Pac, PolyPac, and Xanthan Gum could be removed and still show similar decreases in filtrate loss. It was found that these additives could be decreased by a third and still show similar decreases in filtrate loss. Tables 5.1 and 5.2 show the decrease in Pac, PolyPac, and Xanthan Gum and the amount and percentage decrease in filtrate loss from the reference samples.

Sample	Bent Ref	Ref+2g Chia +2g MPP	Ref+2g Chia+2g MPP with reduced Pac and PolyPac
Pac (g)	.5	.5	.33
PolyPac (g)	1	1	.67
Chia (g)	0	2	2
Mandarin (g)	0	2	2
Filtrate Loss (mL)	3	2.35	2.6
% Reduction	n/a	21.7	13.3

Table 5.1: Effect of Reduction of Pac and Polypac in Bentonite

Sample	KCl Ref	Ref+3g Chia +1g MPP	Ref+3g Chia+1g MPP with reduced Xanthan Gum
Xanthan Gum (g)	1.5	1.5	1
Chia (g)	0	3	3
Mandarin (g)	0	1	1
Filtrate Loss (mL)	9.2	7.6	8.3
% Reduction	n/a	17.4	9.8

Table 5.2: Effect of Reduction of Xanthan Gum in KCl

5.6 Amplitude Sweep Tests

Amplitude sweep tests were done to investigate the effects on the flow and yield point of chia and mandarin on the bentonite and KCl drilling fluid systems. The Anton Paar rheometer plotted the storage and loss modulus curves as well as shear stress. From there damping angle was calculated and then flow point and yield point. First the effect of chia on the bentonite system will be presented, then the effect of mandarin on the bentonite system, and then the effect of chia and mandarin on the KCl system.

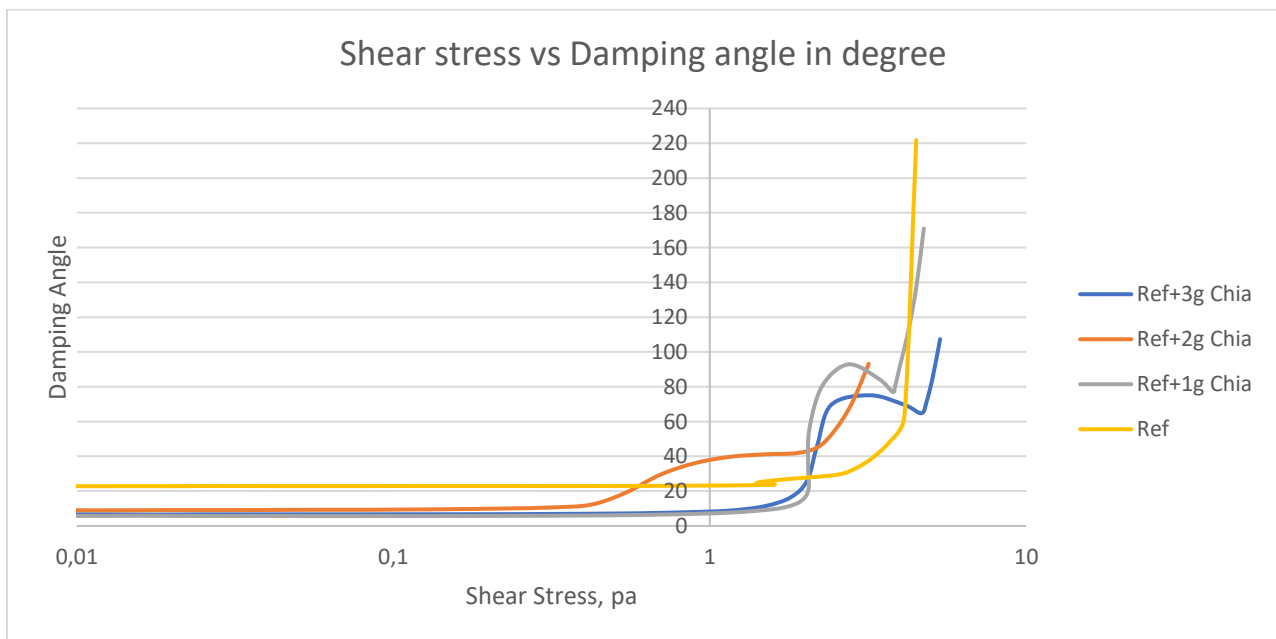


Figure 5.34: Shear Stress vs Damping Angle in Bentonite

	Flow Point	Yield Point
Ref	3.269	0.759
Ref+1g Chia	4.482	0.895
Ref+2g Chia	4.822	1.027
Ref+3g Chia	5.043	1.4

Table 5.3: Flow Point and Yield Point vs Amount of Chia in Bentonite

Figure 5.34 and table 5.3 above, show the effect of chia in the bentonite-based drilling fluid on damping angle, flow point and yield point compared to the reference fluid that did not contain chia. It can be observed that the more chia added, the higher the flow point and yield point.

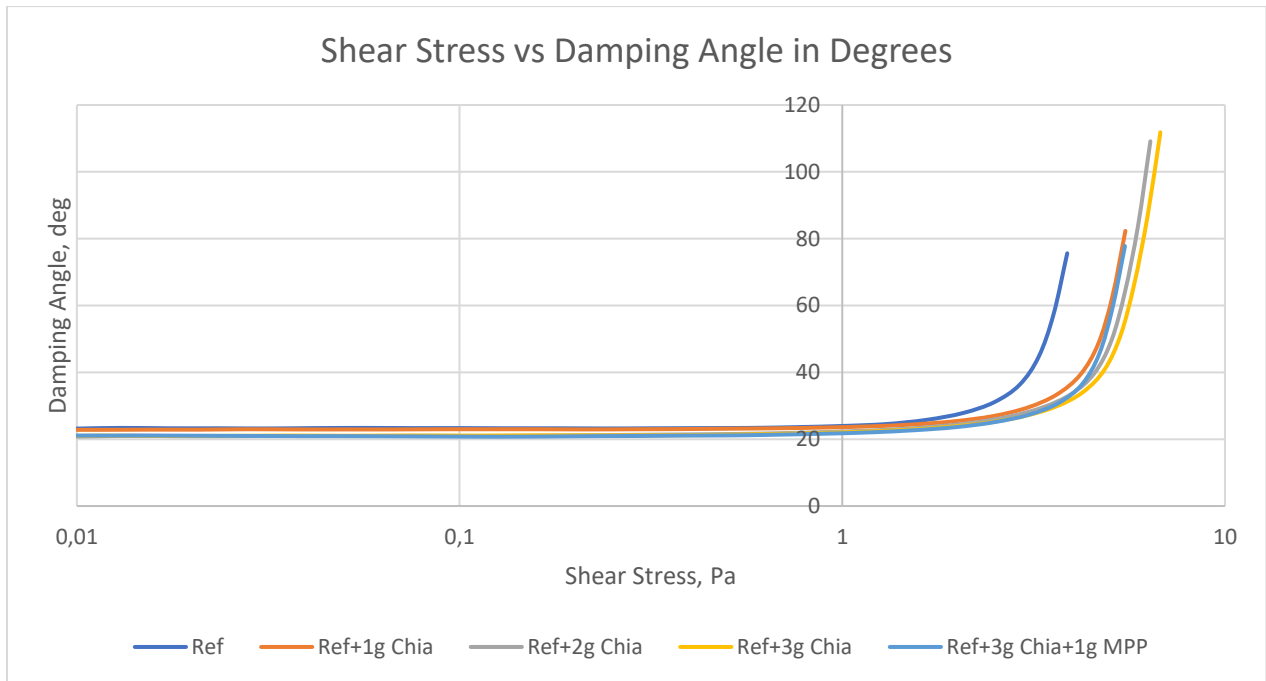


Figure 5.35: Shear Stress vs Damping Angle vs Amount of Chia in KCl

	Flow Point	Yield Point
Ref	3.54	1.41
Ref+1g Chia	2.05	1.16
Ref+2g Chia	2.17	0.31
Ref+3g Chia	2.18	.44
Ref+3g Chia+1g MPP	4.67	1.19

Table 5.4: Flow Point and Yield Point vs Amount of Chia in KCl

Figure 5.35 and table 5.4 show the effect of chia and mandarin on the KCl-based drilling fluid regarding damping angle, flow point and yield point. It can be observed that every addition of

chia decreased the flow point and yield point of the fluid. The addition of mandarin increased the flow point and yield point.

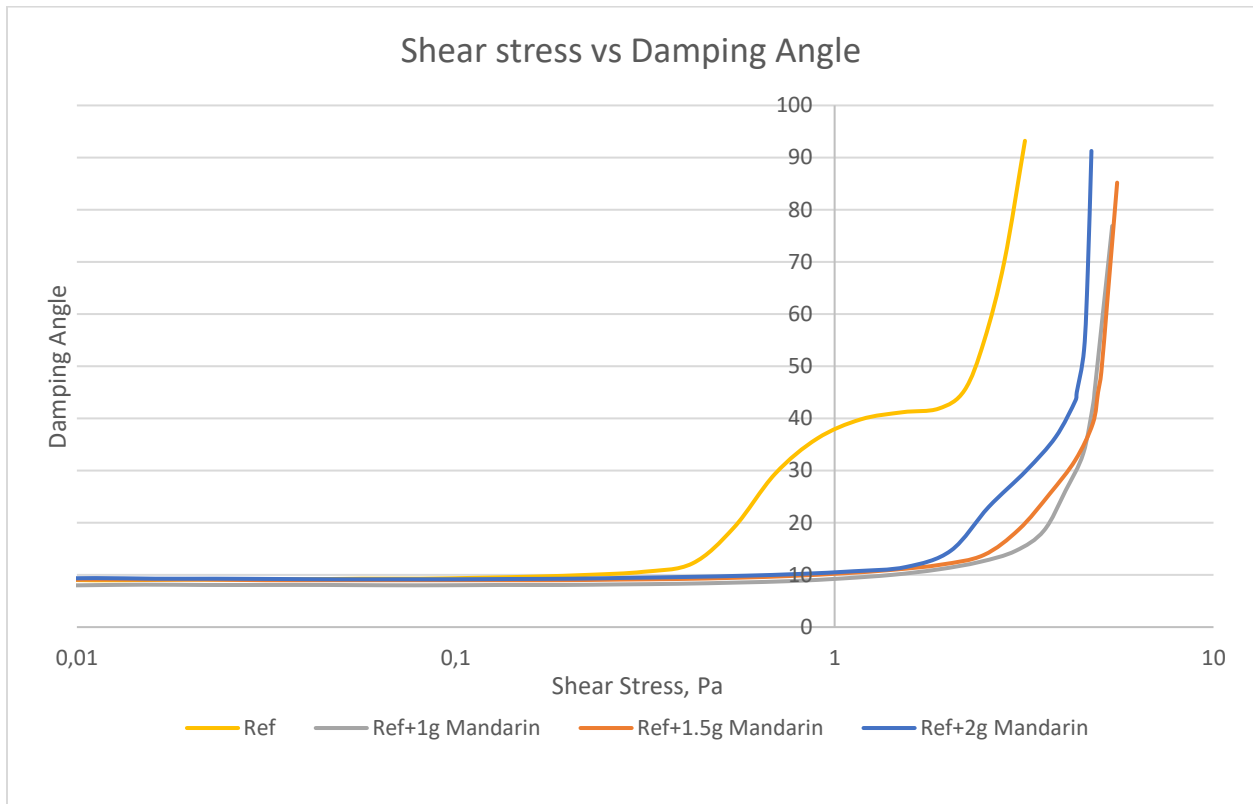


Figure 5.36: Shear Stress vs Damping Angle vs Amount of Mandarin

	Flow Point	Yield Point
Ref	4.82	1.03
Ref+1g MPP	4.85	0.39
Ref+1.5g MPP	4.96	0.54
Ref+2g MPP	4.35	0.58

Table 5.5: Flow Point vs Yield Point vs Amount of Mandarin

Figure 5.36 and table 5.5 show the effect of mandarin on the bentonite system regarding flow point and yield point. The edition of mandarin did not have a noticeable impact on flow point but did lower the yield point non-linearly.

5.7 Ecological Replacement of Polymers for Filtrate Loss

One of the concerns with using ecological additives is whether they can replace environmentally harmful additives. The samples that showed the least amount of filtrate loss were investigated

further as to how much of the additives Pac, PolyPac, and Xanthan Gum could be removed and still show similar decreases in filtrate loss. It was found that these additives could be decreased by a third and still show similar decreases in filtrate loss. Tables 5.6 and 5.7 show the decrease in Pac, PolyPac, and Xanthan Gum and the amount and percentage decrease in filtrate loss from the reference samples.

Sample	Bent Ref	Ref+2g Chia +2g MPP	Ref+2g Chia+2g MPP with reduced Pac and PolyPac
Pac (g)	.5	.5	.33
PolyPac (g)	1	1	.67
Chia (g)	0	2	2
Mandarin (g)	0	2	2
Filtrate Loss (mL)	3	2.35	2.6
% Reduction	n/a	21.7	13.3

Table 5.6: Effect of Reduction of Pac and Polypac in Bentonite

Sample	KCl Ref	Ref+3g Chia +1g MPP	Ref+3g Chia+1g MPP with reduced Xanthan Gum
Xanthan Gum (g)	1.5	1.5	1
Chia (g)	0	3	3
Mandarin (g)	0	1	1
Filtrate Loss (mL)	9.2	7.6	8.3
% Reduction	n/a	17.4	9.8

Table 5.7: Effect of Reduction of Xanthan Gum in KCl

Rheological measurements were also done on the samples with reduced Pac and PolyPac and reduced Xanthan gum to investigate the effects. In bentonite, reducing the pac and polypac by a third resulted in a nearly thermally stable fluid in regard to yield stress as shown in figure 5.37. The yield stress was higher than the reference fluid and less than the sample with the full amount of Pac and PolyPac. The plastic viscosity as shown in figure 5.38 showed the same trend.

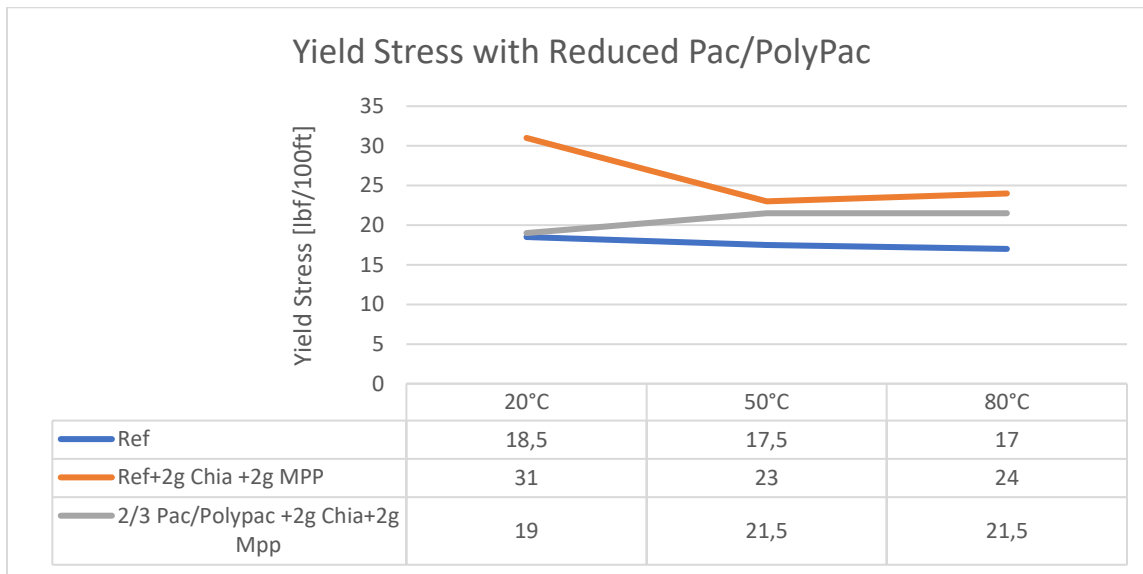


Figure 5.37: Yield Stress with Reduced Pac/PolyPac

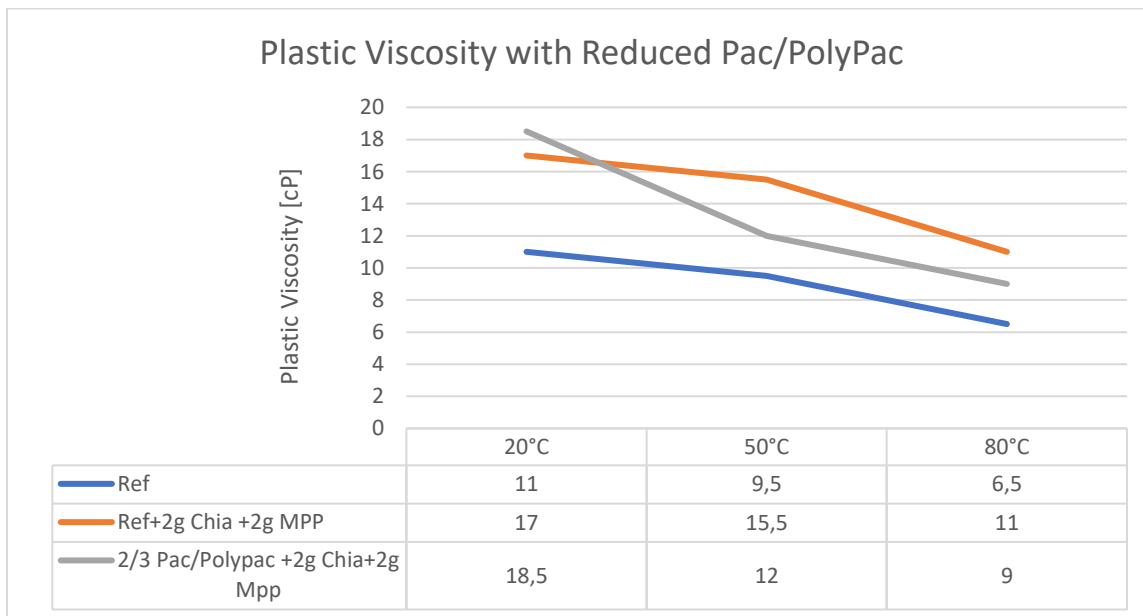


Figure 5.38: Plastic Viscosity with Reduced Pac/PolyPac

For the KCl-based system, reducing the xanthan gum brought the yield stress to the same as the reference fluid, and the plastic viscosity slightly less than the reference fluid and the fluid with the full amount of xanthan gum. These results can be seen in figures 5.39 and 5.40.

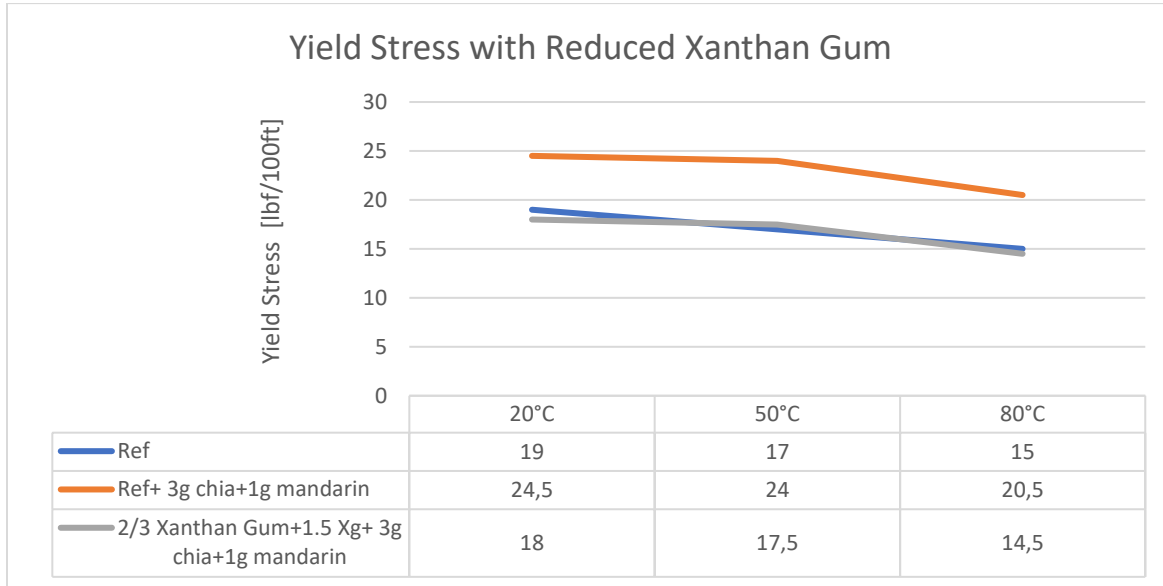


Figure 5.39: Yield stress with Reduced Xanthan Gum

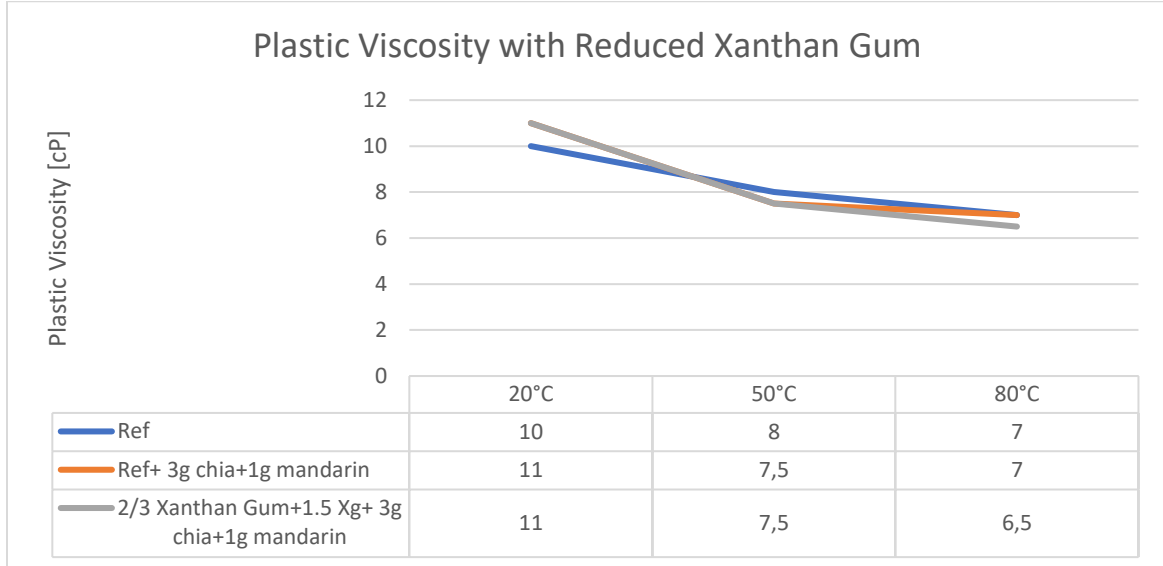


Figure 5.40: Plastic Viscosity with Reduced Xanthan Gum

Next the samples were tested with the rheometer to investigate the effects on the flow point and yield point. For the bentonite-based fluid, the flow point was increased with the reduction in pac and polypac and the yield point was the same as the reference fluid. For the KCl-based

fluid, the flow point was decreased and the yield point was decreased from the sample with the full amount of xanthan gum and 3g chia and 1g MPP.

Drilling fluids	Flow Point	Yield Point
Ref	3,54	1,41
Ref+2g Chia+2g MPP	4,36	0,58
Reduced Pac and Polypac+2g Chia+2g MPP	4,51	1,41

Table 5.8: Flow and Yield Point for reduced Pac and Polypac

Drilling fluids	Flow Point	Yield Point
Ref	3,27	0,76
Ref+3g Chia+1g MPP	4,67	1,89
Reduced XG+3g Chia+1g MPP	2,56	1,07

Table 5.9: Flow and Yield Point for reduced Xanthan Gum

5.8 Effect of Chia, Mandarin, and TiN nanoparticles on lubricity of KCl Drilling Fluid

Here, the best drilling fluid has been selected to evaluate its lubricity property. The best fluid was based off its thermal stability and filtration properties. It was decided that kcl ref+3g Chia+1g MPP was the best fluid. To further improve the lubricity of the best drilling fluid it was decided to add nanoparticles. The nanoparticle choice was based on the previous study done by Petter Havnen studying MPP and nanoparticles where he used Titanium Nitride nanoparticles. A few formulations were tested to find the best concentration, but these tests are omitted from this study. The best concentration was found to be 0.02wt% TiN. The performance was compared with chia and mandarin free KCL based. Table 5.10 shows the formulation of the drilling fluid including TiN nanoparticles.

Additives	Ref	Ref+3g Ch+1g M	Ref+3g Ch + 1gM +0.02wt% TiN
Water [g]	350	350	350
KCL [g]	25	25	25
XG [g]	1.5	1.5	1.5
Soda ash [g]	0.5	0.5	0.5
Barite [g]	143	143	143
Chia [g]	-	3	3
Mandarin peel [g]	-	1	1
Carbopol [g]	0.1	0.1	0.1
TiN [wt%]			0.02

Table 5.10: Formulation of KCl with TiN nanoparticles

Figure 5.41 show the grinded 3g chia. As shown in Table 5.10, Chia contains a higher concentration lipid, which is fat. After the chia was ground, as shown in figure 5.41, it appeared

wet and oily. To assess its lubricity further, the ground chia was mixed with 350 ml and cooked. The resulting oil on the fluid surface and the wall is shown in Figure 5.42



Figure 5.41: Ground Chia for lubricity test

Figure 5.42: Photo of the resulting oil from the ground chia

Several lubricity tests have been performed and the average values are reported. Figure xx shows the results. As shown the addition of 3g Chia and 1g Mandarin Peel reduced the lubricity of the reference drilling fluid by about 34%. The addition of 0.02 wt % TiN nanoparticle on the chia and mandarin based drilling fluid reduced the lubricity by 41.5% as compared with the reference fluid.

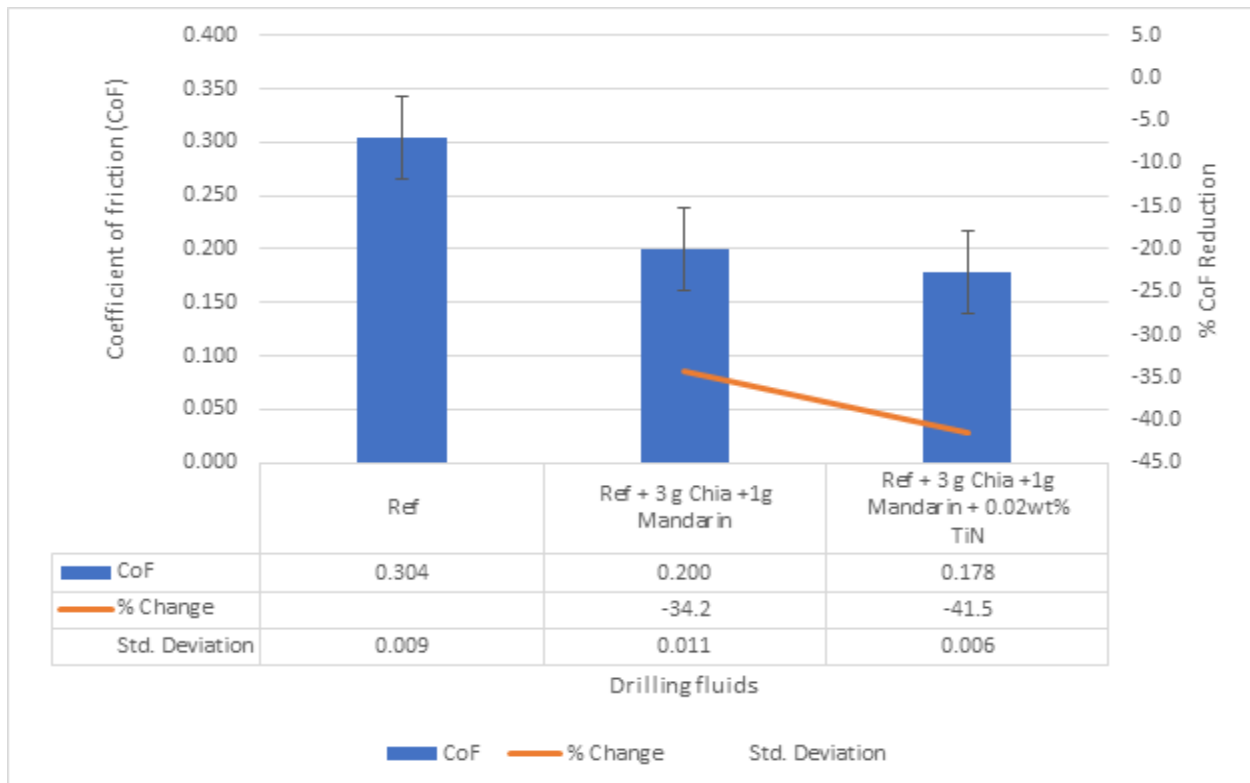


Figure 5.43: Averaged Results from Lubricity Tests

6 Hydraulics Simulations and Rheology Modelling

Rheological modelling was performed for the best performing flat rheology system in the three different categories of; bentonite-based fluid, bentonite-based fluid containing mandarin, and KCl-based fluid. Wellbore simulation studies such as hydraulics and torque and drag simulations were done on the initial fluid formulation and a select few other samples that will be covered in their specific sections. For the hydraulics simulation, the ECD and pump pressure of these fluids were calculated based on the Unified Hydraulics model as described in section.

6.1 Hydraulic Performance Simulation

It is important to conduct hydraulic analyses of drilling fluids that are to be used in drilling fluid operations to ensure that the fluid will not lead to lost circulation, kick, or even a potential blow-out. As mentioned in section 2.5, the ECD is a critical parameter that should be kept above the pore pressure and below the fracture gradient. However, the pump pressure is also necessary to circulate the drilling fluid and provide proper cuttings transport can also affect the wellbore pressure. As it is so vital in drilling operations, it has become customary to perform hydraulics simulations. In this section, the effect of chia is investigated as well as the effect of mandarin peel powder on both the bentonite-based drilling fluid and KCl-based drilling fluid. The simulations utilize a set experimental well set-up and flow rate that will be described in the next subsection

6.1.1 Simulation Set-Up

The well design for the hydraulics simulations is presented in figure 6.1. An Excel calculator was used to perform the simulations and uses the parameters of an 8.5'' vertical well with a total depth of 10,000 feet. Both the mud pump and tank are assumed to be directly in contact with the drill string so that the surface pressure loss is neglected. Additionally, the drill string only consists of a 5'' OD x 4.8'' ID drill pipe and a drill bit with three nozzles. During the simulation the mud weight is set at 1.3 sg while the flow rate of the drilling fluid is varied between 50 to 600gpm. The drilling fluids included in the hydraulics performance simulation will be described in their respective subsections as well as the viscosity measurements that were inputted into the simulator. The simulations were done at 22 °C, 50 °C and 80 °C for all systems. It was also assumed that there are no cuttings and no rotation of the drill string.

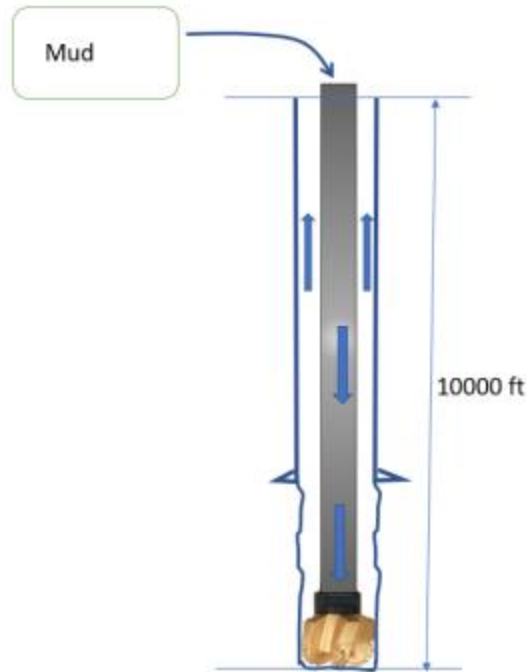


Figure 6.1: Well setup for the hydraulics performance simulation

6.1.2 Chia in Bentonite

The fluids included in this section include the reference fluid with no chia, reference+1g Chia, reference +2g chia, reference +3g chia. The viscometer dial readings that were used are shown in table 6.1 and table 6.2. The ECD results are shown for all these fluids and the pump pressure of the best performing thermally stable fluid is shown. The pump pressure results for the other fluids are presented in the appendix.

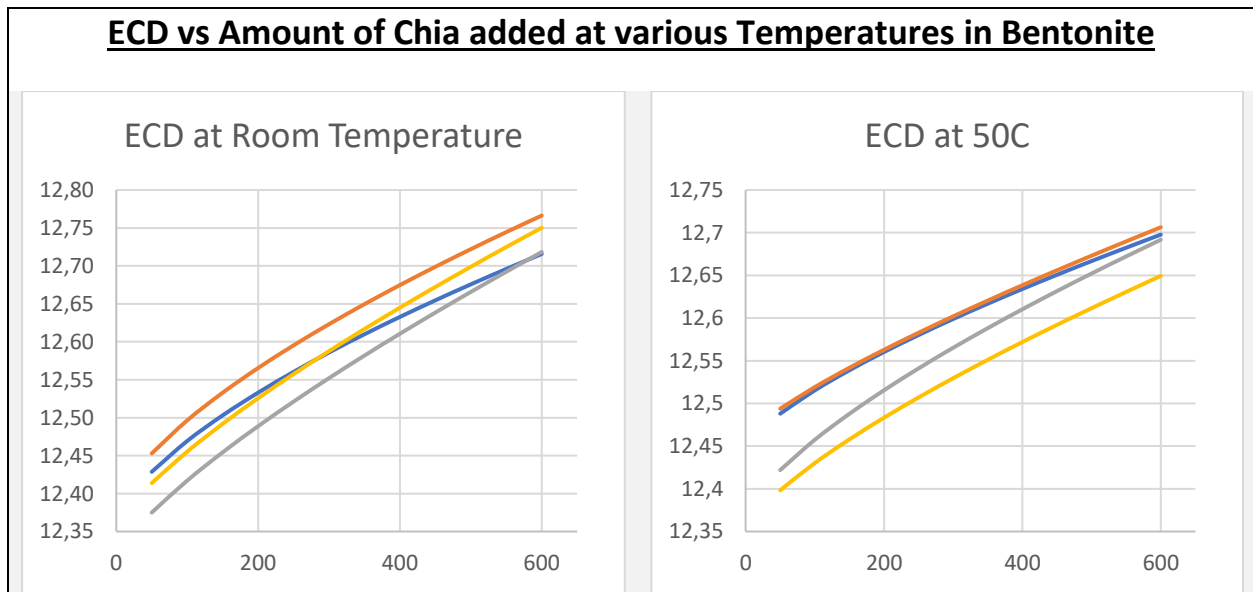
RPM	REF			REF+1g Chia		
	22°C	50°C	80°C	22°C	50°C	80°C
600	40.5	36.5	30	44.5	39.5	39.5
300	29.5	27	23.5	32	28	30.5
200	23.5	23.5	20.5	26.5	24	26
100	19	19.5	16.5	20	19	21
6	10.5	12.5	11	11	12.5	14
3	10	12	10.5	10.5	12	13.5

Table 6.1: Summary of Chia in Bentonite viscometer dial readings applied in hydraulics simulation

RPM	REF+2g Chia			REF+3g Chia		
	22°C	50°C	80°C	22°C	50°C	80°C
600	51	41	35	51	39.5	36.5
300	33.5	29	26	34	27.5	25
200	26	24	23	27.5	23.5	21
100	19	18	18	21	18	17
6	9	10.5	10.5	10	10	9.5
3	8.5	10	10	9.5	9.5	8.5

Table 6.2: Summary of Chia in Bentonite viscometer dial readings applied in hydraulics simulation (cont.)

The simulation results for the equivalent circulating density of the reference fluid and a range of chia amounts are shown in figure 6.2. The figure shows three graphs showing the ECD as a function of flow rate for the selected fluids at 20, 50 and 80 °C. The results show that at room temperature, the sample with 3g of chia had lower ECD than the reference fluid at all temperature points and flow rates, but the sample with 1g of chia had an on average higher ECD than the reference fluid. The sample with 2g of chia had a lower ECD at the lower temperatures of 20 and 50 °C, but a slightly higher ECD at 80°C. The highest difference came with ref+1g chia at 80°C with a 1.3% increase in ECD.



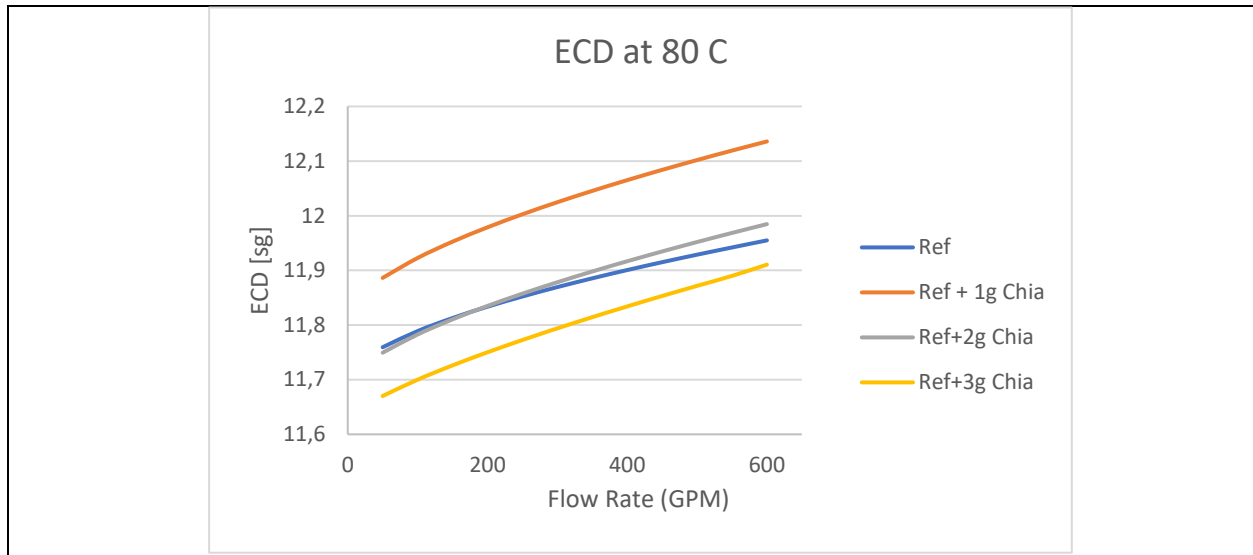


Figure 6.2: ECD at various Temperatures vs Amount of Chia in Bentonite-based Drilling fluid

When it came to pump pressure, chia did not have a noticeable effect, therefore only the best performing's fluid's pump pressure results are shown in figure 6.3 with the rest being displayed in the appendix. The pump pressure is graphed as a function of flow rate at the three different temperatures it was simulated at. It is observed that the effect of temperature on the total pressure loss is relatively small with it only slightly decreasing the pump pressure but still overall remained stable.

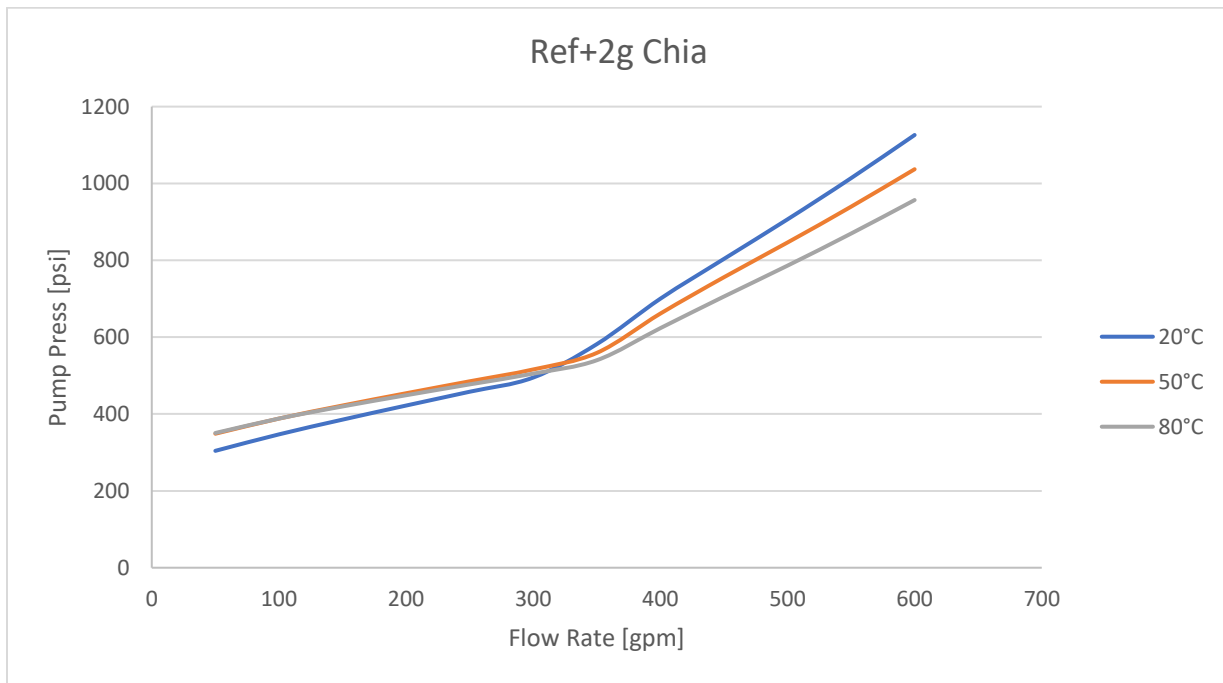


Figure 6.3: Pump Pressure vs Flow rate for Ref+2g Chia

6.1.3 ECD and Pump Pressure with MPP in Bentonite

The fluids included in this section include the reference fluid that is the base-bentonite fluid +2g chia referred to as “ref” in this section, ref+1g MPP, ref+1.5g MPP, ref+2g MPP. The viscometer dial readings that were used are shown in table 6.3 and table 6.4. The ECD results are shown for all these fluids and the pump pressure of the best performing thermally stable fluid is shown. The pump pressure results for the other fluids are presented in the appendix.

RPM	REF			REF+1g MPP		
	22°C	50°C	80°C	22°C	50°C	80°C
600	51	41	35	61	54	51
300	33.5	29	26	40.5	38	36.5
200	26	24	26	34	31.5	30.5
100	19	18	18	24	22.5	23
6	9	10.5	10.5	16	12	12
3	8.5	10	10	10	11	11

Table 6.3: Summary of Mandarin in Bentonite viscometer dial readings applied in hydraulics simulation

RPM	REF+1.5g MPP			REF+2g MPP		
	22°C	50°C	80°C	22°C	50°C	80°C
600	70	57.5	53	65	54	46
300	47.5	41.5	39	48	38.5	35
200	38.5	34.5	33.5	36	32.5	29
100	27.5	25.5	26	27	24.5	23.5
6	12.5	12	14	12	12.5	13.5
3	10.5	11.5	13.5	11	11.5	13

Table 6.4: Summary of MPP in Bentonite viscometer dial readings applied in hydraulics simulation (Cont.)

The simulation results for the equivalent circulating density of the reference fluid and a range of Mandarin Peel Powder (MPP) amounts are shown in figure 6.4. The figure shows three graphs showing the ECD as a function of flow rate for the selected fluids at 20, 50 and 80 °C. The results show that at room temperature and 50 °C, the samples with MPP had lower equivalent circulating densities than the fluid which did not contain MPP. The ECD’s decreased non-linearly with increasing amounts of MPP. The largest percentage decreases of ECD were at low flow rates and the sample with 1g of MPP had the largest percentage decrease of 3.2% and 4% at 50gpm at room temperature and 50 °C respectively. This trend changes at 80 °C where the samples with

MPP had higher ECDs than the sample containing no MPP. The percentage increase of ECD increased with increasing flow rates with the sample containing 1.5g MPP having the highest percentage difference at 600gpm with a 4.3% increase.

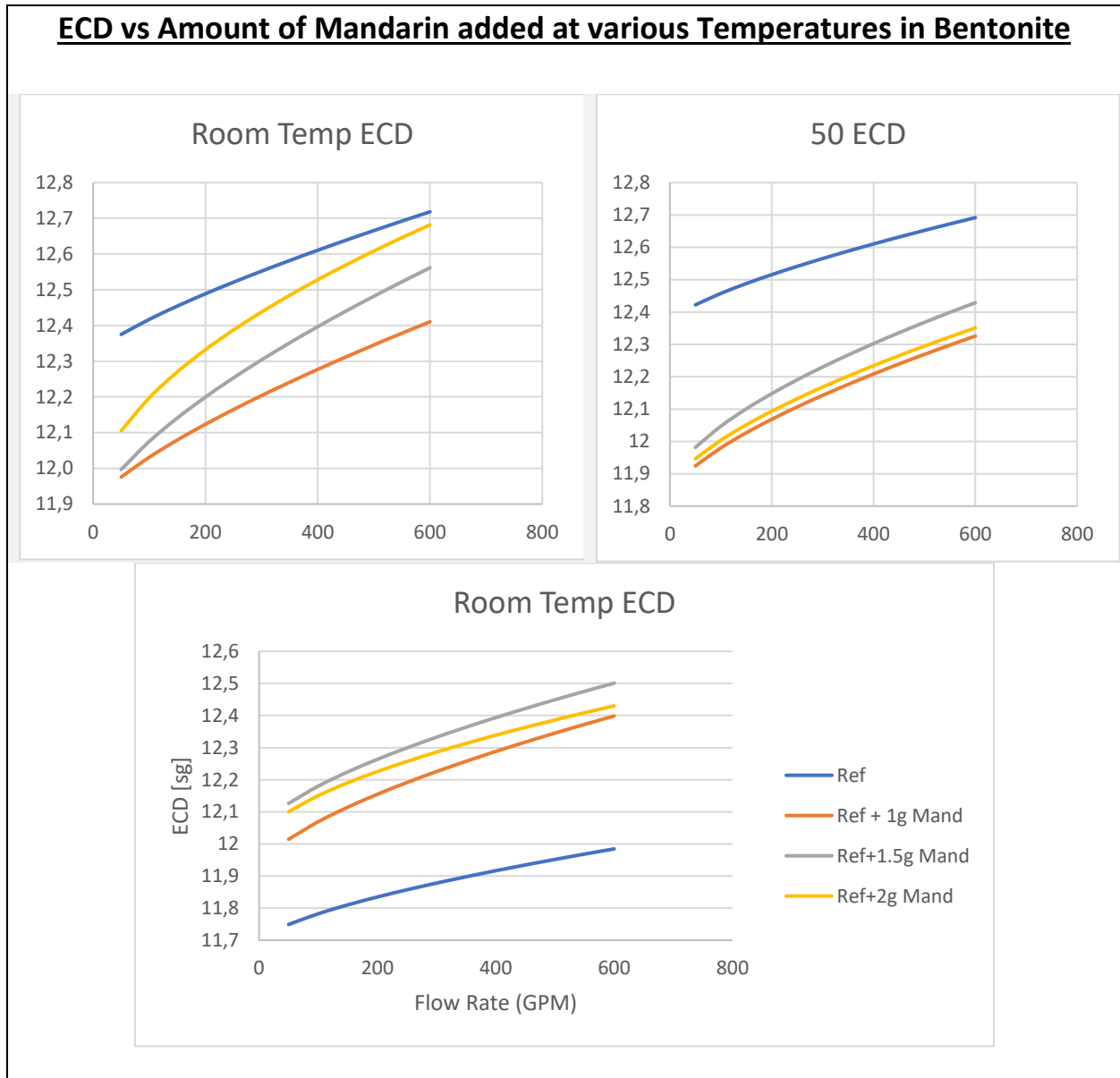


Figure 6.4: ECD vs Amount of Mandarin added at various temperatures in Bentonite

The simulation results for the pump pressures of the reference fluid and a range of Mandarin Peel Powder (MPP) amounts are shown in figure 6.5. The figure shows three graphs showing the pump pressure as a function of flow rate for the selected fluids at 20, 50 and 80 °C. The results

show that at all temperatures, the samples containing MPP had higher pump pressures. The highest increase in pump pressures happened at lower flow rates and the increase happened non-linearly with respect to amount of mandarin added.

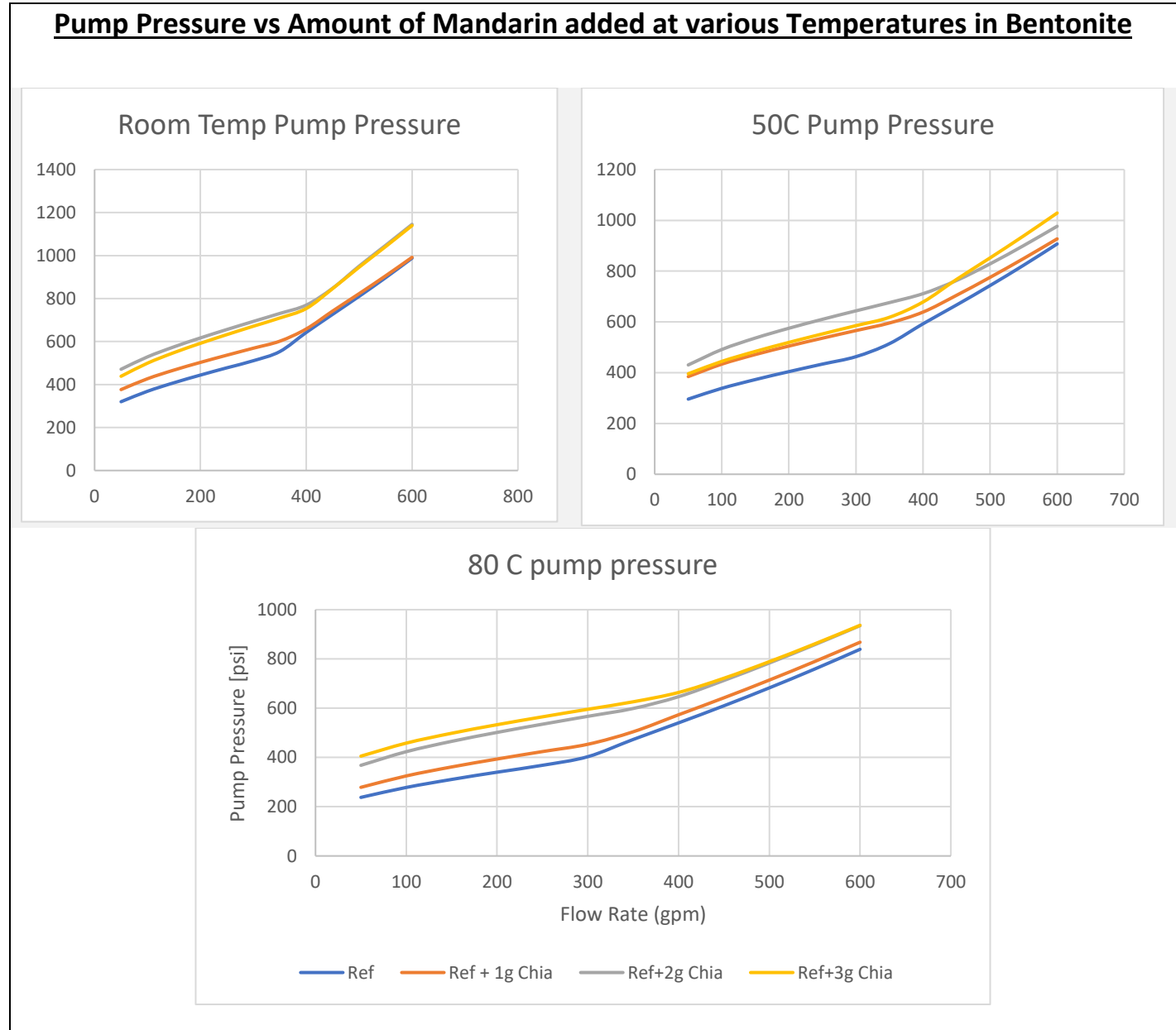


Figure 6.5: Pump Pressure vs amounts of MPP at various temperatures in Bentonite

6.1.4 Chia and Mandarin in KCl-based drilling fluid

The fluids included in this section include the reference fluid that is the base-KCl Fluid with no chia, ref+1g chia, ref +2g chia, ref+3g chia, and ref +3g chia +1g MPP. The viscometer dial readings that were used are shown in table 6.5 and table 6.6. The ECD results are shown for all these fluids and the pump pressure of the best performing thermally stable fluid is shown. The pump pressure results for the other fluids are presented in the appendix.

RPM	REF			REF+1g Chia		
	22°C	50°C	80°C	22°C	50°C	80°C
600	39	33	29	39	35	31.5
300	29	25	22	30	28	24.5
200	25	21	19	26	24.5	21.5
100	20	17	15.5	21	20	17.5
6	9.5	8	7	11	10.5	8.5
3	8.5	7.5	6	10	9.5	7

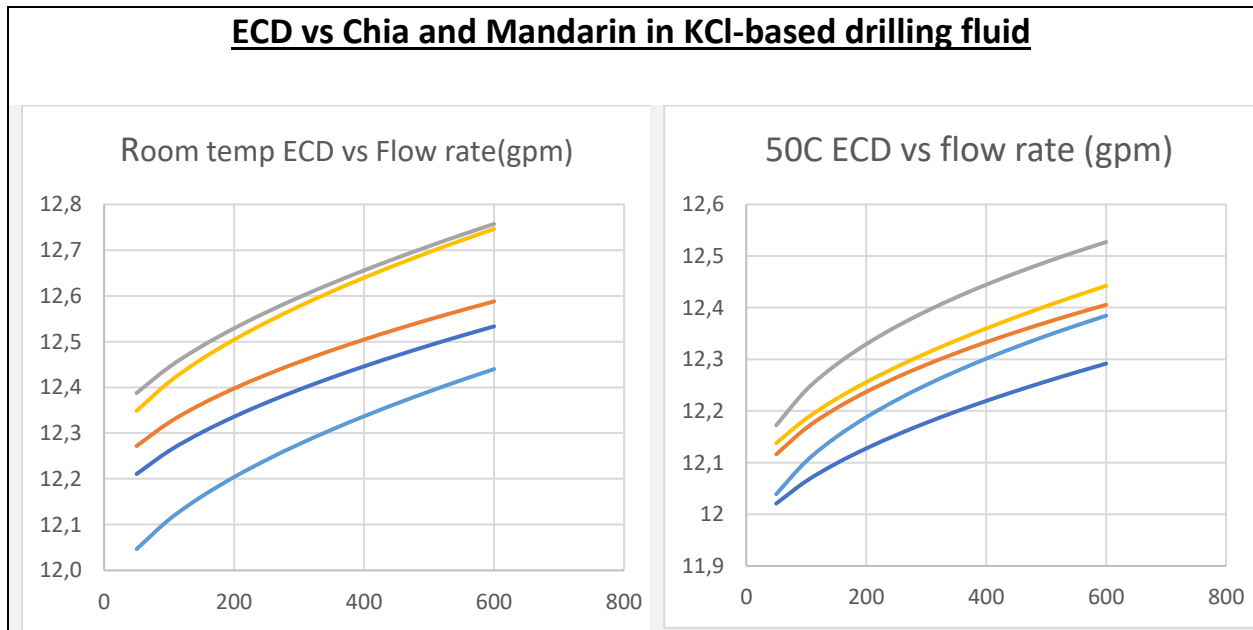
Table 6.5: Summary of Chia and MPP in KCl viscometer dial readings applied in hydraulics simulation

RPM	REF+2g Chia			REF+3g Chia			Ref+3g Chia +1g MPP		
	22°C	50°C	80°C	22°C	50°C	80°C	22°C	50°C	80°C
600	49	39	36	49	40	35.5	46.5	39	34.5
300	37	32	29	37	30.5	29	35.5	31.5	27.5
200	32	28	25.5	31.5	17.5	26	30	26.5	24.5
100	26	23	21	25	22.5	22	23.5	20.5	19.5
6	14	12	11	12.5	12	11	11.5	11.5	10
3	13	10	9	11.5	11	10	10.5	10	8.5

Table 6.6: Summary of Chia and MPP in KCl viscometer dial readings applied in hydraulics simulation (cont.)

The simulation results for the equivalent circulating density of the reference fluid and a range of chia amounts, as well as ref+3g chia+1g MPP are shown in figure 6.6. The figure shows three

graphs showing the ECD as a function of flow rate for the selected fluids at 20, 50 and 80 °C. The results show that at room temperature, the samples containing chia had a higher ECD than the reference fluid with ref+1g Chia having the lowest increase in ECD and ref+2g having the highest increase. The sample containing 1g of MPP had a decrease in ECD with the highest decrease being at lower flow rates. At 50 °C, the samples containing chia and MPP shown increased ECDs compared to the reference fluid. The sample containing MPP had the lowest percentage increase with the sample containing 1g of Chia having the lowest increase out of the samples only containing chia. The highest percentage increase being the sample containing 2g of chia. At 80 °C, the samples containing chia and MPP also had increased ECDs compared to the reference, but the sample containing 1g of MPP had the highest percentage increase and the sample containing only 1g of chia had the lowest percentage increase.



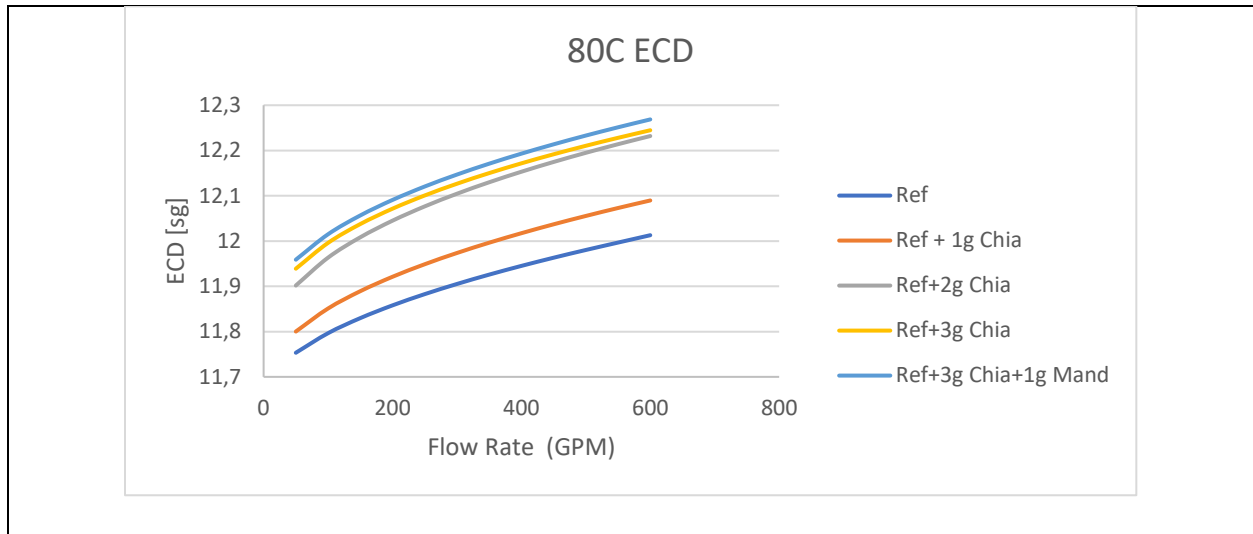


Figure 6.6: ECD vs Amount of Chia in KCl

The simulation results for the pump pressures of the reference fluid and a range of chia amounts and ref+3g chia+1g MPP are shown in figure 6.7. Only the pump pressure results for 80 °C are shown as there was little change in pump pressures across different temperatures and it was the most representative. The results at other temperatures are shown in the appendix. It can be seen that the addition of chia and mandarin increased the pump pressure at all flow rates non-linearly. Figure 6.8 isolates the results for ref+3g chia+1g MPP as it is thermally stable and shows that the pump pressure remained relatively stable across various temperature points.

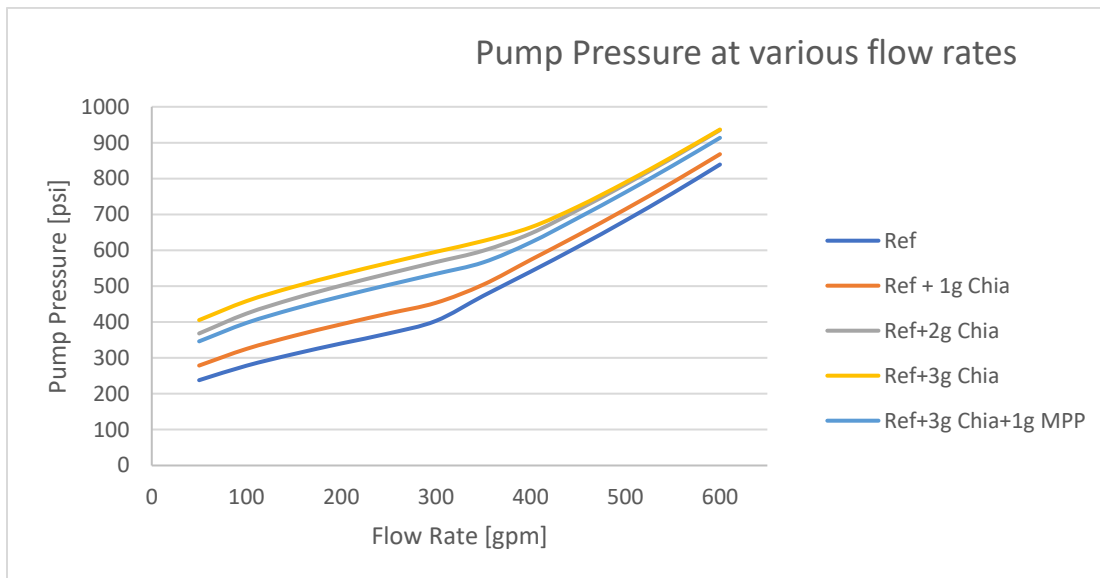


Figure 6.7: Pump Pressure at various flow rates in KCl

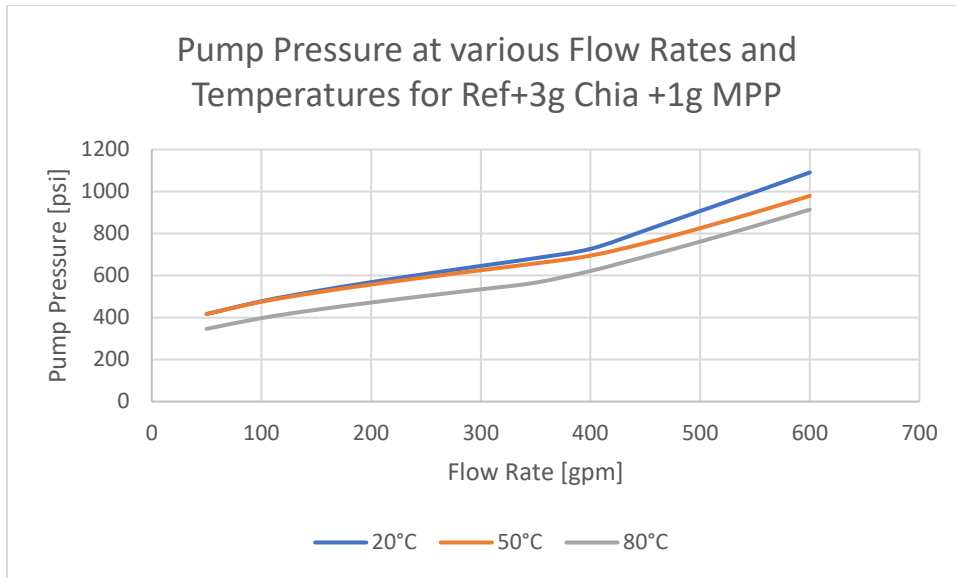


Figure 6.8: Pump Pressure results for Ref+3g Chia+1g MPP

6.2 Rheological Modeling

Rheological modeling was done to determine which rheological model would best reflect the flow characteristics of the best thermally stable systems, as well as to investigate the effect of temperature on their rheological parameters. The calculations and modeling were done using an excel calculator which used viscometer dial readings and shear rates. The excel calculator then calculated the parameters for each model and the percentage difference from the actual measurements. The rheological models that the samples will be compared to are;

- Bingham Plastic model
- Power Law model
- Herschel-Bulkley model
- Unified model
- Robertson-Stiff model

The excel calculator used the equations presented in section 2.3, where the rheological models are presented. The Newtonian model will not be compared to as it is not relevant to drilling fluids.

6.2.1 Best-Fit Rheological Model for Bentonite

The sample that was chosen to be investigated is Ref+2g Chia+2g MPP, as it was thermally stable and showed good filtrate loss results. The viscometer dial readings for this fluid that were used for the calculations are shown in table

Figure 6.9 presents the percentage deviation between the actual measurements and the model prediction for each of the rheological models at 20°C, 50°C and 80°C, as well as the average across the temperatures for each of the models. The Robertson-Stiff, Unified, and Herschel Bulkley models provide the most accurate description of the rheological properties with an average deviation of 1.35%, 2.57%, and 3.21% respectively. The Bingham Plastic Model provided the least accurate description with an average of 14.5% deviance. The Robertson-Stiff model is the best-fit rheological model for the fluid as it had the smallest deviance both overall and at each temperature.

Ref+2g Chia+2g MPP			
RPM	20°C	50°C	80°C
Θ_{600}	65	54	46
Θ_{300}	48	38.5	35
Θ_{200}	36	32.5	29
Θ_{100}	27	24.5	23.5
Θ_6	12	12.5	13.5
Θ_3	11	11.5	13

Table 6.7: Viscometer Dial Readings for Ref+2g Chia+2g MPP

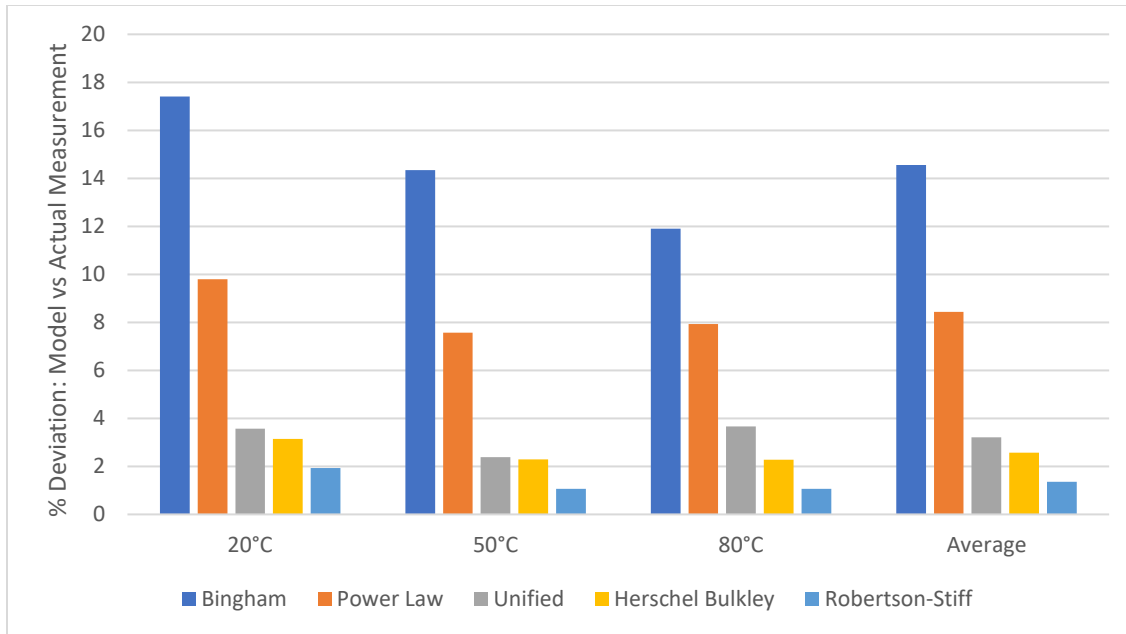


Figure 6.9: % Deviation between model prediction and actual values

The predictions provided by each rheological model versus the viscometer dial reading measurements are presented in the appendix, whereas the corresponding parameters and percentage deviations are provided in the tables 6.8,6.9, and 6.10.

Model	τ_0, τ_y, A	k, C	n, B	μ_p, μ	Error	cP
Herschel Bulkley	10,510	0,397	0,733		3,145	
Unified	10,670	0,341	0,757		3,575	
Power Law		6,208	0,329		9,793	
Bingham	15,848			0,0569	17,406	27,244
Robertson and Stiff	1,688	33,0156	0,535		1,931	

Table 6.8: Model parameters at 20°C

Model	τ_0, τ_y, A	k, C	n, B	μ_p, μ	Error	cP
Herschel Bulkley	11,179	0,387	0,700		2,289	
Unified	11,204	0,378	0,703		2,382	
Power Law		7,138	0,281		7,577	
Bingham	15,721			0,044	14,344	21,115
Robertson and Stiff	2,073	38,099	0,475		1,063	

Table 6.9: Model parameters at 50°C

Model	τ_0, τ_y, A	k, C	n, B	μ_p, μ	Error	cP
Herschel Bulkley	13,029	0,264	0,723		2,280	
Unified	13,338	0,159	0,803		3,661	
Power Law		8,744	0,230		7,934	
Bingham	16,606			0,035	11,902	16,519
Robertson and Stiff	2,789	44,554	0,409		1,069	

Table 6.10: Model parameters at 80°C

6.2.2 Temperature Effects on Rheological Parameters in Bentonite

Table 6.13 presents a summary of all the rheological parameters for the sample, ref+2g chia+2g MPP, that was tested as well as the percentage deviations caused by the increasing temperatures. Based on the information in the table, the following observations were made for each of the models:

Herschel-Bulkley Model

It is observed from the rheological modeling that the yield stress of the fluid increases with temperature, which means that greater shear stress values are required to initiate flow at higher temperatures. Although the higher temperatures led to lower consistency index values and flow behavior index values. Also, the fluid is implied to be pseudoplastic as all the n -values are below 1.

Unified Model

The unified model shows higher shear yield points than the Herschel-Bulkley model and that they increase with temperature. The consistency index and flow behavior index did not follow a trend across temperatures. The unified model's results are very similar to the Herschel-Bulkley model's parameters which is most likely related to the fact that the unified model is a simplification of the Herschel-Bulkley flow equation.

Power Law Model

The Power Law model showed the trend that increasing the temperature led to greater differences in values. Also the k -values are larger than the values obtained by the Herschel-Bulkley and Unified models whereas the n -values are smaller. The smaller n -values imply that the

fluid is more shear-thinning and it can be seen in the appendix that the Power Law model assumed that the fluid is more shear thinning than it is.

Bingham Plastic Model

The Bingham Plastic Model was the least accurate rheological model, however it showed small changes in yield stress across temperatures, with only a slight increase at 80 °C. The plastic viscosity decreased with increasing temperature.

Robertson-Stiff Model

The Robertson-Stiff model was the most accurate of the rheological models, but it was observed that the A-parameter, which resembles the k-value of the other models, increased by 65% from 20 °C to 80 °C. The B parameter, which is similar to the n-value of the other models, decreased as the temperature increased and all the B-values were below 1 which indicates pseudoplastic behavior.

Model		20 °C	50 °C	80 °C
Herschell-Bulkley	tau0	10,510	11,179	13,0287
	%dev		6,4	24,0
	K	0,397	0,387	0,264
	%dev		-2,5	-33,5
	n	0,733	0,699	0,7226
	%dev		-4,6	-1,4
Unified	tauyL	10,67	11,204	13,338
	%dev		5,0	25,0
	k	0,341	0,378	0,159
	%dev		10,9	-53,4
	n	0,7571	0,7034	0,8031
	%dev		-7,1	6,1
Power Law	k	6,208	7,138	8,744
	%dev		15,0	40,9
	n	0,329	0,281	0,229
	%dev		-14,6	-30,4
Bingham Plastic	tauy	15,848	15,721	16,606
	%dev		-0,8	4,8
	mup	0,057	0,044	0,0264
	%dev		-22,8	-53,7
Robertson-Stiff	A	1,686	2,073	2,789
	%dev		23,0	65,4
	C	33,0156	38,099	44,554
	%dev		15,4	34,9
	B	0,535	0,475	0,409
	%dev		-11,2	-23,6

Table 6.11: Summary of all rheological parameters for Ref+2g chia+2g MPP

6.2.3 Best-Fit Rheological Model for KCl

The sample that was chosen to be investigated is Ref+3g Chia+1g MPP, as it was thermally stable and showed good filtrate loss results. The viscometer dial readings for this fluid that were used for the calculations are shown in table

Ref+3g Chia+1g MPP			
RPM	20°C	50°C	80°C
Θ_{600}	46.5	39	34.5
Θ_{300}	35.5	31.5	27.5
Θ_{200}	30	26.5	24.5
Θ_{100}	23.5	20.5	19.5
Θ_6	11.5	11.5	10
Θ_3	10.5	10	8.5

Table 6.12: Viscometer Dial Readings for Ref+3g Chia+1g MPP

Figure 6.13 presents the percentage deviation between the actual measurements and the model prediction for each of the rheological models at 20°C, 50°C and 80°C, as well as the average across the temperatures for each of the models. The Robertson-Stiff, Bingham Plastic, and Power Law models provide the most accurate description of the rheological properties with an average deviation of 3.5%, 3.1%, and 1.8% respectively. The Bingham Plastic Model provided the least accurate description with an average of 18.3% deviance. The Robertson-Stiff model is the best-fit rheological model for the fluid as it had the smallest deviance both overall and at each temperature.

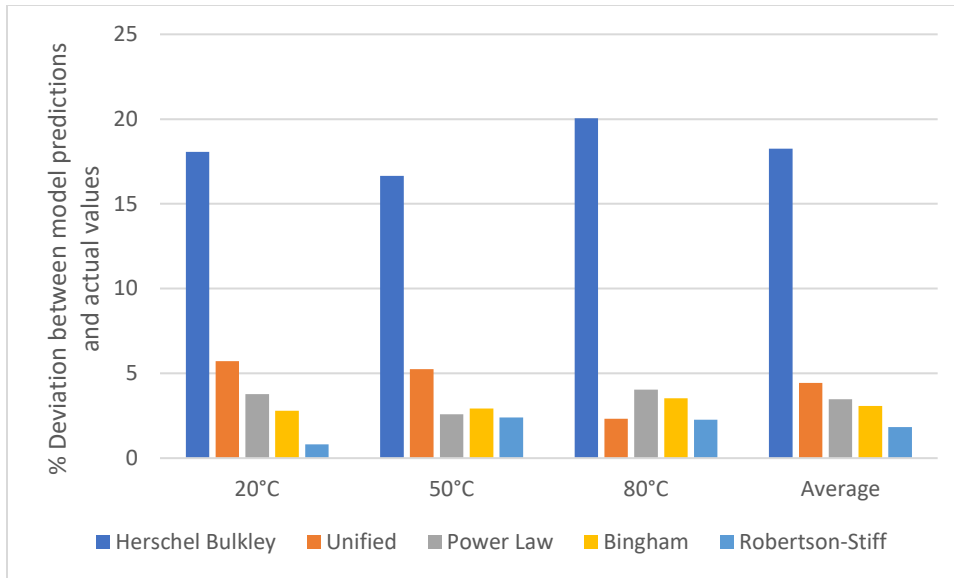


Figure 6.10: Percent deviations of model predictions from actual measurements

The predictions provided by each rheological model versus the viscometer dial reading measurements are presented in the appendix, whereas the corresponding parameters and percentage deviations are provided in the tables 6.10, 6.11, and 6.12

Model	τ_0, τ_y, A	k, C	n, B	μ_p, μ	Error	cP
Herschel Bulkley	9,824	0,530	0,636		2,796	
Unified	10,137	0,401	0,680		3,778	
Power Law		6,667	0,277		5,729	
Bingham	15,211			0,037	18,057	17,859
Robertson and Stiff	2,785	24,531	0,415		0,822	

Table 6.13: Model parameters at 20°C

Model	τ_0, τ_y, A	k, C	n, B	μ_p, μ	Error	cP
Herschel Bulkley	9,275	0,652	0,575		2,923	
Unified	9,070	0,753	0,553		2,593	
Power Law		6,830	0,250		5,249	
Bingham	14,414			0,030	16,657	14,364
Robertson and Stiff	2,919	27,217	0,384		2,398	

Table 6.14: Model parameters at 50°C

Model	τ_0, τ_y, A	k, C	n, B	μ_p, μ	Error	cP
Herschel Bulkley	7,238	0,914	0,513		3,529	
Unified	7,469	0,791	0,535		4,033	
Power Law		5,825	0,259		2,328	
Bingham	13,086			0,026	20,042	12,640
Robertson and Stiff	3,310	15,333	0,349		2,269	

Table 6.15: Model parameters at 80°C

6.2.1 Temperature Effects on Rheological Parameters in Bentonite

Table 6.16 presents a summary of all the rheological parameters for the sample, ref+3g chia+1g MPP, that was tested as well as the percentage deviations caused by the increasing temperatures. Based on the information in the table, the following observations were made for each of the models:

Herschel-Bulkley Model

It is observed from the rheological modeling that the yield stress of the fluid decreases with temperature, which is the opposite as the bentonite system. The K-values increased with increasing temperatures whereas the n-values decreased. Also, the fluid is implied to be pseudoplastic as all the n-values are below 1.

Unified Model

The unified model shows higher shear yield points than the Herschel-Bulkley model and that they decrease with temperature. The consistency index and flow behavior index showed the same trends as the Herschel-Bulkley Model. The unified model's results are very similar to the Herschel-Bulkley model's parameters which is most likely related to the fact that the unified model is a simplification of the Herschel-Bulkley flow equation.

Power Law Model

The Power Law model showed the trend that increasing the temperature led to greater differences in values. Also the k-values are larger than the values obtained by the Herschel-Bulkley and Unified models whereas the n-values are smaller. The smaller n-values imply that the

fluid is more shear-thinning and it can be seen in the appendix that the Power Law model assumed that the fluid is more shear thinning than it is.

Bingham Plastic Model

The Bingham Plastic Model was the least accurate rheological model, however it showed small changes in yield stress across temperatures, with only a slight increase at 80 °C. The plastic viscosity decreased with increasing temperature.

Robertson-Stiff Model

The Robertson-Stiff model was the most accurate of the rheological models, but it was observed that the A-parameter, which resembles the k-value of the other models, increased by 18% from 20 °C to 80 °C. The B parameter, which is similar to the n-value of the other models, decreased as the temperature increased and all the B-values were below 1 which indicates pseudoplastic behavior.

Model	Column1	20	50	80
Herschel-Bulkley	tau0	9,824	9	7,237
	%dev		-5,6	-26,3
	K	0,5298	0,6519	0,9139
	%dev		23,0	72,5
	n	0,6361	0,5747	0,513
	%dev		-9,7	-19,4
Unified	tauYL	10,136	9,069	7,469
	%dev		-10,5	-26,3
	k	0,401	0,7532	0,7912
	%dev		87,8	97,3
	n	0,679	0,553	0,535
	%dev		-18,6	-21,2
Power Law	k	6,665	6,83	5,824
	%dev		2,5	-12,6
	n	0,277	0,249	0,259
	%dev		-10,1	-6,5
Bingham Plastic	tauY	15,211	14,414	13,086
	%dev		-5,2	-14,0
	mup	0,037	0,03	0,0264
	%dev		-18,9	-28,6
Robertson-Stiff	A	2,785	2,919	3,31
	%dev		4,8	18,9
	C	24,531	27,217	15,332
	%dev		10,9	-37,5
	B	0,418	0,384	0,349
	%dev		-8,1	-16,5

Table 6.16: Summary of all rheological parameters in KCl

6.3 Torque and Drag Simulation

Simulations should be performed prior to drilling any well to ensure a safe and successful drilling operation. Safe operational windows are defined in order to ensure that the torsional and tensile limits are not exceeded while running into the well or tripping out. Extended reach, horizontal and deviated wells are especially dangerous as there is increased contact between the drilling string and wellbore which increases friction resistance.

Drillings fluids are tested to determine their lubricity, in this study a CSM tribometer was used. The lubricity of a drilling fluid is critical in lowering the friction of a drilling string and bit to lower the torque and drag forces that occur within the wellbore. The lubricity data can be used to perform torque and drag simulations to evaluate the effective tension, torque, stress during tripping in, and stress during tripping out. In this thesis, Microsoft Excel was used for the simulations. Only the KCl-based drilling fluid was studied in this torque and drag simulation. Three drilling fluids were tested, KCl-reference fluid, ref+0.02wt% TiN, and ref+3g chia+1g MPP+0.02wt% TiN.

6.3.1 Simulation Assumptions and Setup

The assumptions made in this thesis are that the drill pipe is static off bottom, static on bottom, RIH, and POOH as boundary conditions at the bit. The well consisted of a 5" E-75 19.50 lb/ft drill pipe. The well design was kept constant for all the drilling fluids tested. Other well data that was used to construct the simulation in Excel is shown in table 11. The measured coefficient of frictions, shown in table 12, were then used in the simulation.

Well Data		Drillpipe Data:	
L_{KOP} [m]	850	w_{DP} [kN/m]	0.285
$L_{Straight\ inclined, DP}$ [m]	2000	OD [m]	0.127
L_{BHA} [m]	785	ID [m]	0.109
Hole Diameter [m]	0.2116	σ_{yield} [kN/m ²]	517000
R [m]	500	BHA Data:	
α (angle) [radians]	1.31	w_{BHA} [kN/m]	1.154
α (angle) [degrees]	75	OD [m]	0.171
		ID [m]	0.102
		σ_{yield} [kN/m ²]	758000

Figure 6.11: Estimated well data applied to the simulated well

Fluid	Coefficient of Friction
Ref	0.304
Ref+3g Chia+1g MPP	0.200
Ref+3g Chia+1g MPP+0.02wt% TiN	0.178

Figure 6.12: Coefficient of Friction for samples used in simulation

6.3.2 Effect of Chia, Mandarin, and TiN nanoparticles on Torque and Drag

The results from the torque and drag simulations are shown in figures 13 and 14. The blue vertical line in the torque simulation represents the torque limit and is denoted as make-up torque. The

simulated torques during pulling out are represented as solid lines and the dashed lines are for tripping in. It can be observed that all of the fluids are within the torque limit and that the addition of chia, mandarin, and 0.02 wt% TiN decreased the torque at both tripping in and pulling out. Figure 14 shows the simulated tension simulations, including the tensions when tripping in and pulling out of hole. At each side of the graph are the tensile limit and buckling limit for both rotating and non-rotating strings. All the fluids fell within the safe operating limits. Although it can be seen that the addition of the additives and especially the TiN nanoparticles, increased the tension during tripping in to the hole and lowered the tension while pulling out of the hole. Or, simply, the fluid containing TiN nanoparticles is better positioned within the safe operating window.

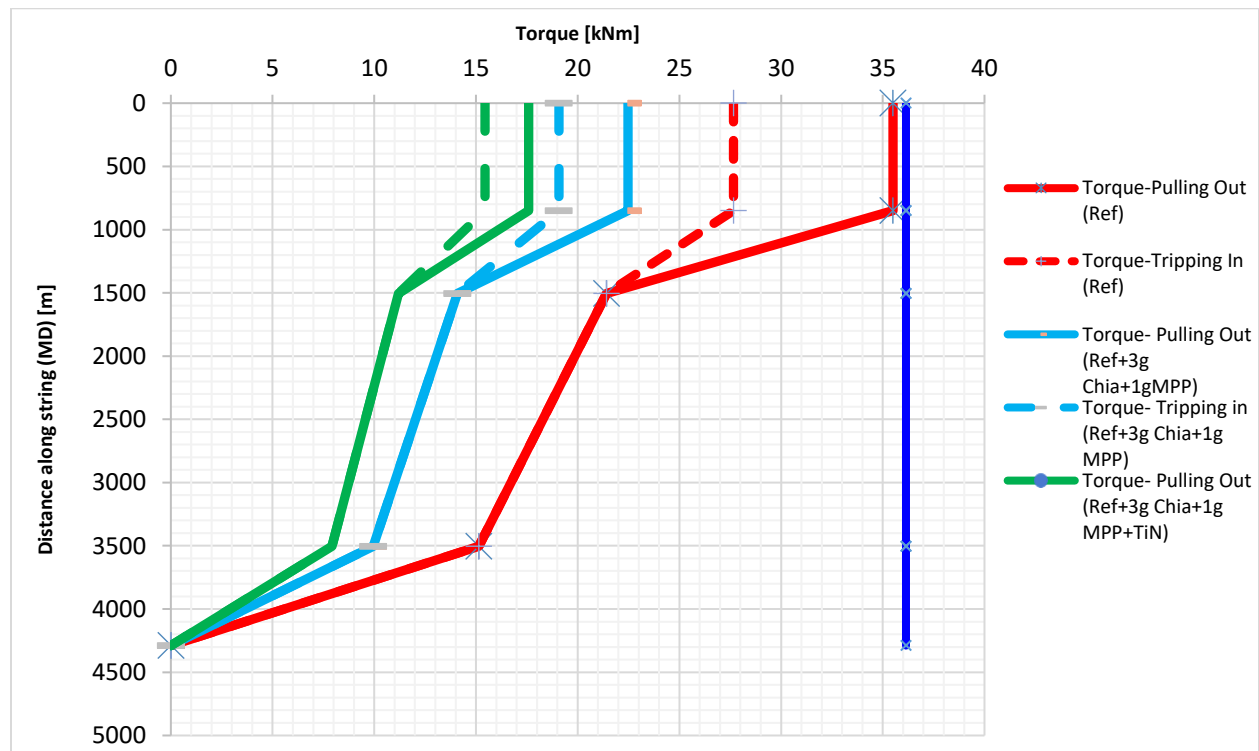


Figure 6.13: Torque Simulations

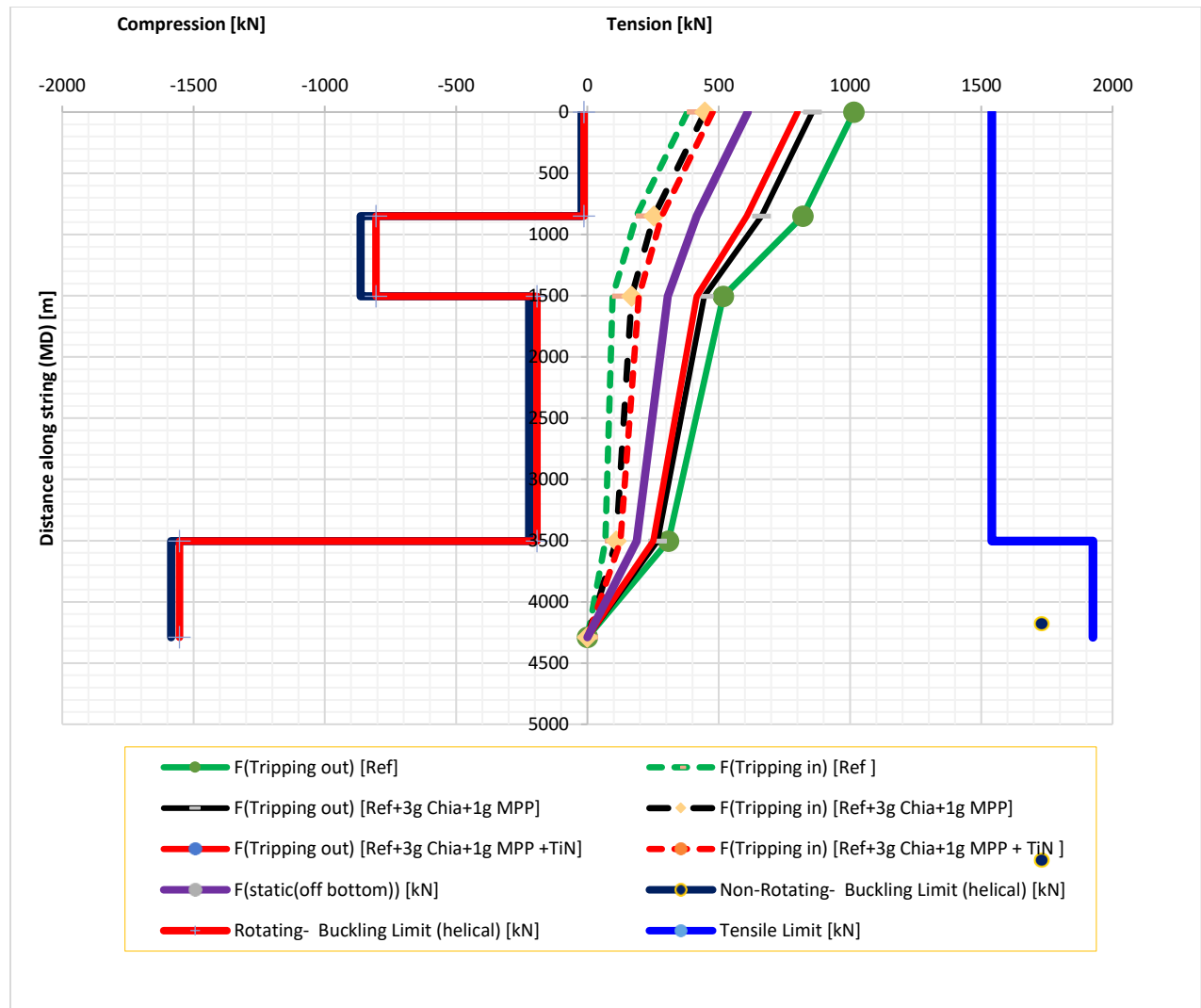


Figure 6.14: Drag Simulations

The important values from the simulation results are summarized in table 13. It can be seen that the addition of chia and mandarin led to a 34.2% decrease in friction, and the addition of TiN decreased it by an additional 7%. The decrease in torque was similar to the decrease in friction. The forces in the drill string are pushed toward the buckling and tensile limit when the coefficient of friction rises. According to these findings, larger coefficients of friction result in higher torque and drag forces, which increase the risk of string damage and limit the amount of offset that drilling operations may achieve.

	CoF	Torque		Effective Tension	
		Lowering	Pullout	Lowering	Pullout
Ref	0.304	36	28	1015	381
Ref+3g Chia+1g MPP	0.200	22	19	857	448
% Change from Ref	-34.2	-36.7	-31	-15.6	17.5
Ref+3g Chia+1g MPP + 0.02 wt% TiN	0.178	20	17	826	463
% Change from Ref	-41.5	-44.1	-38	-18.6	21.6

7 Summary and Discussion

This section will provide a summary and discussion of the results obtained during experimental work and simulation studies. Additionally, some limitations and uncertainties related to the fluid measurements will also be discussed.

7.1 Drilling Fluid Characterization

The water-based drilling fluids were characterized using rheological, filtration, viscoelastic, and frictional measurements. The rheological properties were obtained at 22°C, 50°C and 80°C using an OFITE Model 8 viscometer and an Anton Paar MCR 302 rheometer was utilized to obtain the viscosity and amplitude sweep of the samples. A static filter press was used to obtain filtration measurements and a CSM tribometer was used to measure the frictional properties of the fluids. Sag factor was also measured using a scale and syringes. Further descriptions of these equipment and tests were described in section 2.4.

7.1.1 The Bentonite-based Drilling Fluid

This study utilized a drilling fluid formulation that was tested in two prior studies done by Petter Havnen (Havnen, 2022) and Lene Fattnes (Fattnes, 2020), where a bentonite based WBM formulation provided a thermally stable rheology system. It was utilized as the reference fluid in order to study the effect of chia, MPP and then TiN nanoparticles. This study investigated various concentrations of chia, as well as different preparations of chia.

Rheological Measurements and Sag Factor

Initially, various amounts of chia were added to the water-based drilling fluid with the objective of studying the effects and obtaining a thermally stable fluid. Next, upon finding a concentration that had thermally stable rheological properties, the preparation of chia was investigated. It was found that in the Bentonite-system, 2g of uncooked chia provided such characteristics. Next, MPP was added as it was found in Petter Havnen's study that it improved filtrate loss properties, and it was found that it retained its thermally stable properties. As shown in figure 7.1.

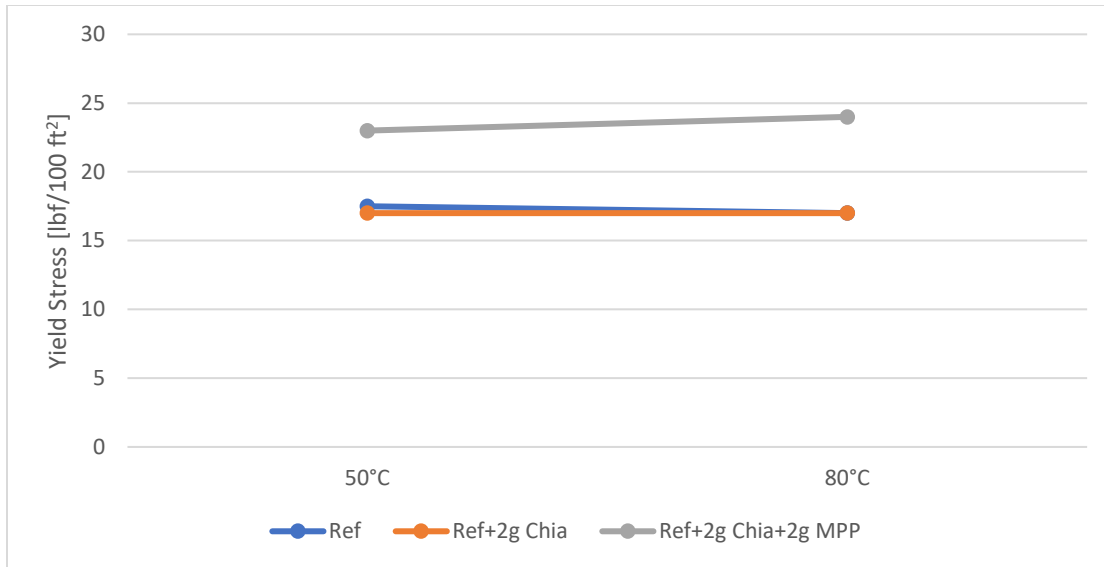


Figure 7.1: Bingham Yield Stress of best bentonite-based fluids at 50°C and 80°C

The addition of the Chia worked as a thickening agent and increased the viscosity of the fluid as seen in figure 7.2. Chia did not affect the yield stress in a linear or predictable manner with increased concentration of chia added.

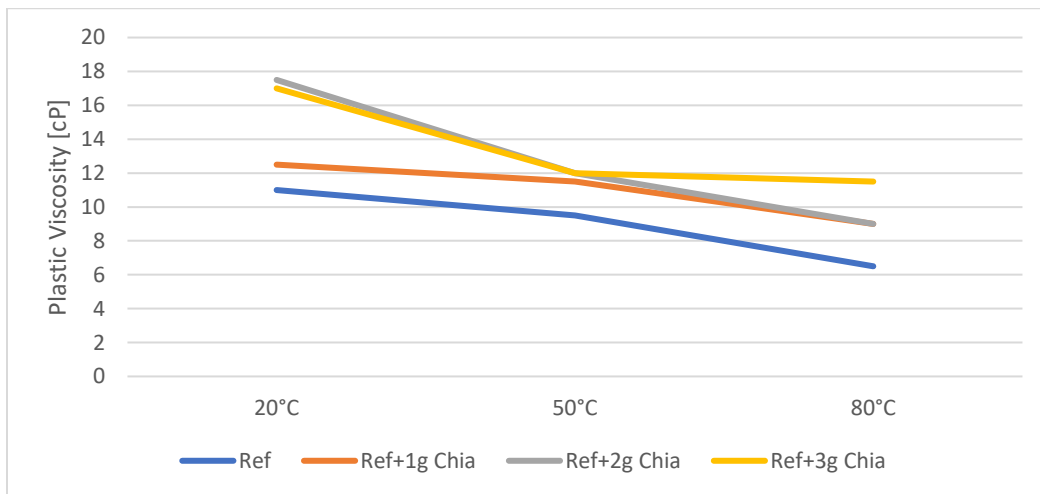


Figure 7.2: Plastic Viscosity and Chia additions at 20°C, 50°C, and 80°C

The preparation of the chia was investigated after finding the concentration of chia that had thermally stable rheological properties. It was found that uncooked chia was the only preparation that led to thermal stability, as shown in figure 7.3

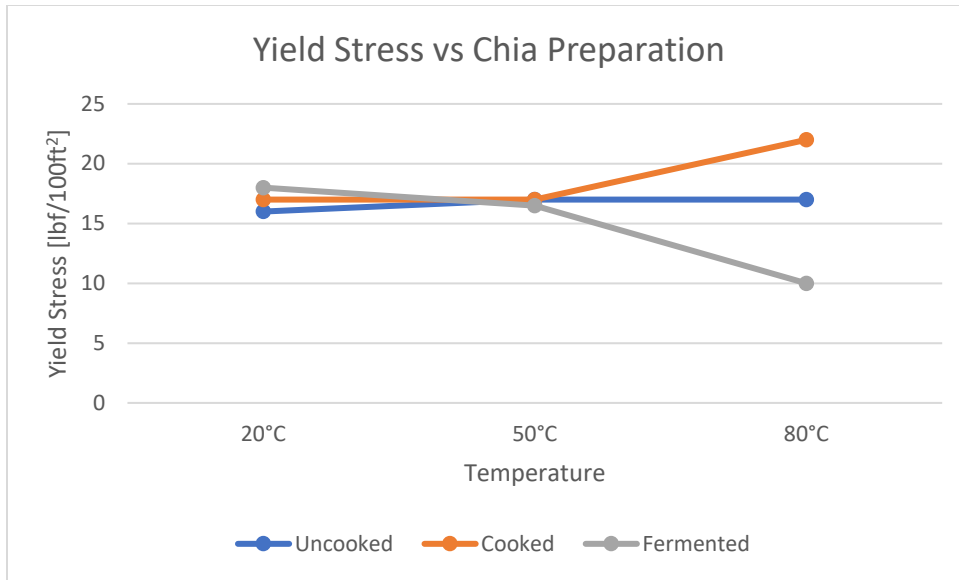


Figure 7.3: Yield Stress vs Chia Preparation at 20°C, 50°C, and 80°C

The addition of the MPP worked as a thickening agent and it increased the viscosity and yield stress of the fluid, as seen in figure 7.4. Although it did increase the yield stress and viscosity non-linearly with addition of the MPP.

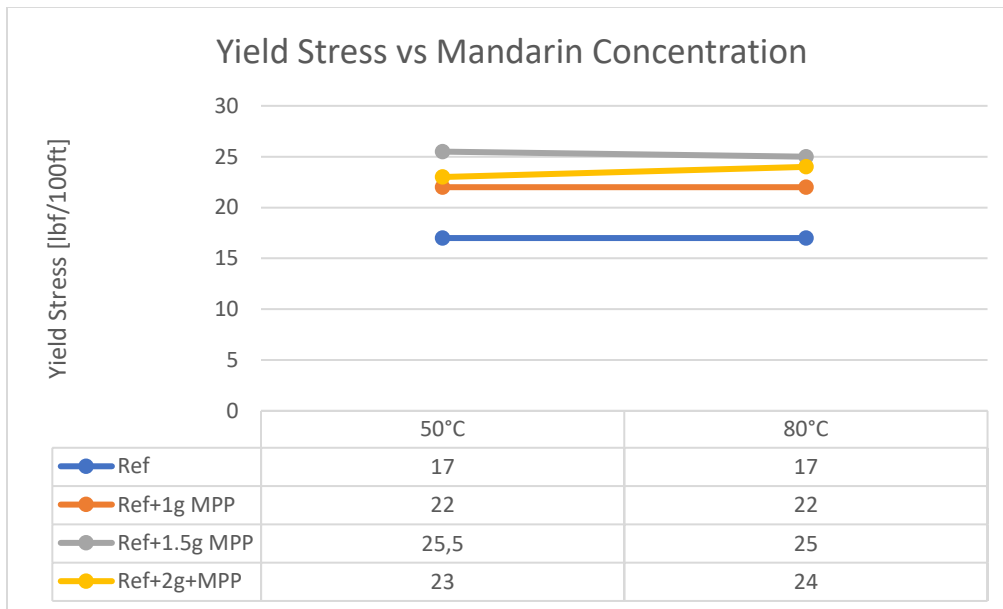


Figure 7.4: Yield Stress vs Mandarin Concentration at at 50°C, and 80°C

All the samples were tested for Sag factor to ensure that they had proper gelling abilities and did not show sedimentation tendencies. All the samples, fell within the proper range for sag factor.

Filtrate Measurements

Mandarin Peel Powder was added to the reference fluid including chia to improve its filtration properties. The addition of chia to the reference fluid had little to no impact on filtration. The mandarin peel powder decreased the filtrate loss by around 20% as seen in table 7.3. With the greatest decrease in filtrate loss with 2g MPP at a 21.7% reduction.

	Ref	Ref+2g Chia+2g MPP	Ref+2g Chia+1g MPP	Ref+2g Chia+1.5g MPP	Ref+2g Chia+2g MPP
Filtrate Loss (mL)	3	3	2,4	2,5	2,35
Percentage Change	n/a	0	-20	-16,7	-21,7

Table 7.1: Chia and Mandarin Effect on Filtrate Loss in Bentonite-based fluid

Viscoelastic Measurements

The effect of chia and mandarin peel powder were both investigated using the viscometer. The fluid containing chia and the fluid containing chia and mandarin peel powder showed gel-like characteristics. The addition of chia lowered the flow and yield point of the fluid which means that the fluid will be irreversibly deformed at lower shear rates and the viscous behavior prevails earlier with greater amounts of chia. The opposite was observed with the addition of MPP which increased the yield stress and flow point values of the fluid. Both effects occurred non-linearly.

7.1.2 The KCl-Based Drilling Fluid

The KCl-based drilling fluid was based off the bentonite-based fluid but with slight changes in the formulation. The first formulation included Pac and PolyPac as additives but these were then replaced with Xanthan Gum as the Pac and Polypac formulations were not thermally stable and had sag factors that were outside the acceptable range. This study investigated various concentrations of chia, as well as different preparations of chia.

Rheological Measurements and Sag Factor

Initially, different preparations of chia were tested as to determine which preparation to continue with for the rest of the study. After finding the preparation of chia that best works in

the KCl-based fluid, different concentrations were investigated to see which concentration resulted in the best thermally stable fluid. The cooked chia, was determined to be the most thermally stable as shown in figure 7.5.

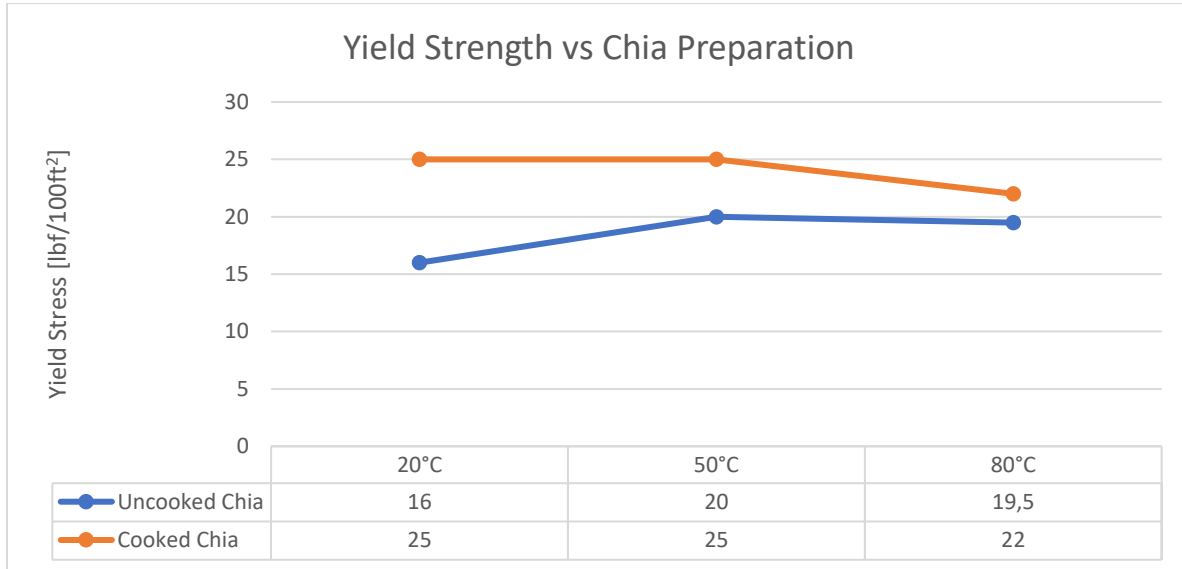


Figure 7.5: Yield Strength vs Chia Preparation

The addition of chia increased the yield stress in a non-linear manner, but it did not affect the viscosity of the fluid in a linear or predictable manner with increased concentrations of chia. The yield stress of increasing amounts of chia can be seen in figure.

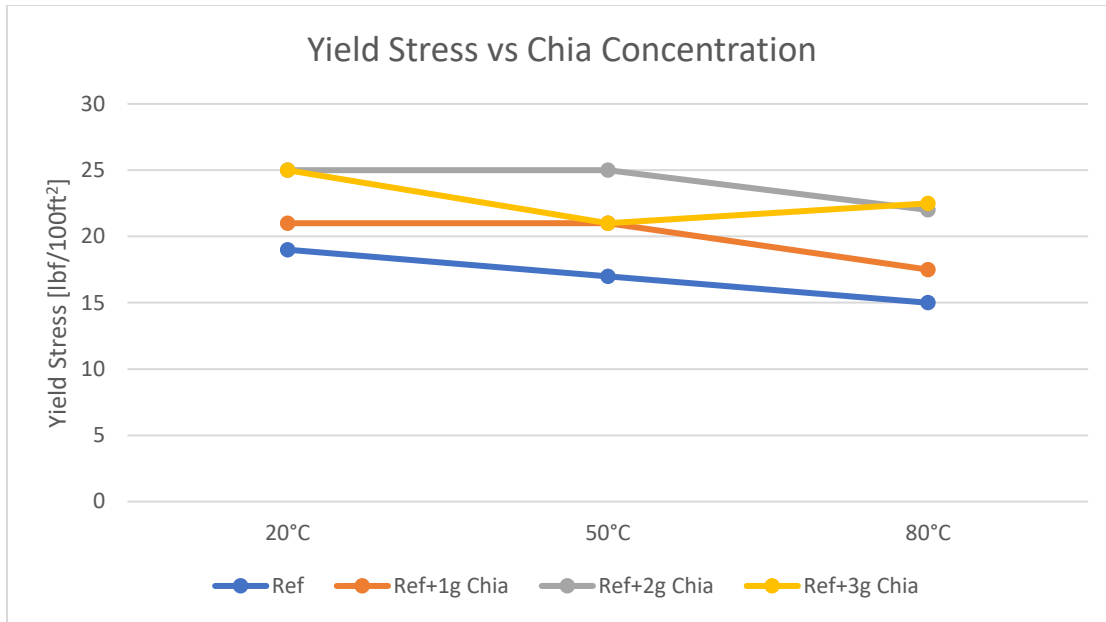


Figure 7.6: Yield Stress vs Chia Concentrations in KCl-based fluid

The addition of MPP, was due to its filtration properties that were studied in the bentonite-based fluid. It did not affect the plastic viscosity or yield stress in the KCl-based fluid. Figure 7.7 shows the effect of MPP on the yield stress. Also, all the samples were tested for Sag Factor to ensure that they had proper gelling abilities and they all had sag factors that fell within the proper range.

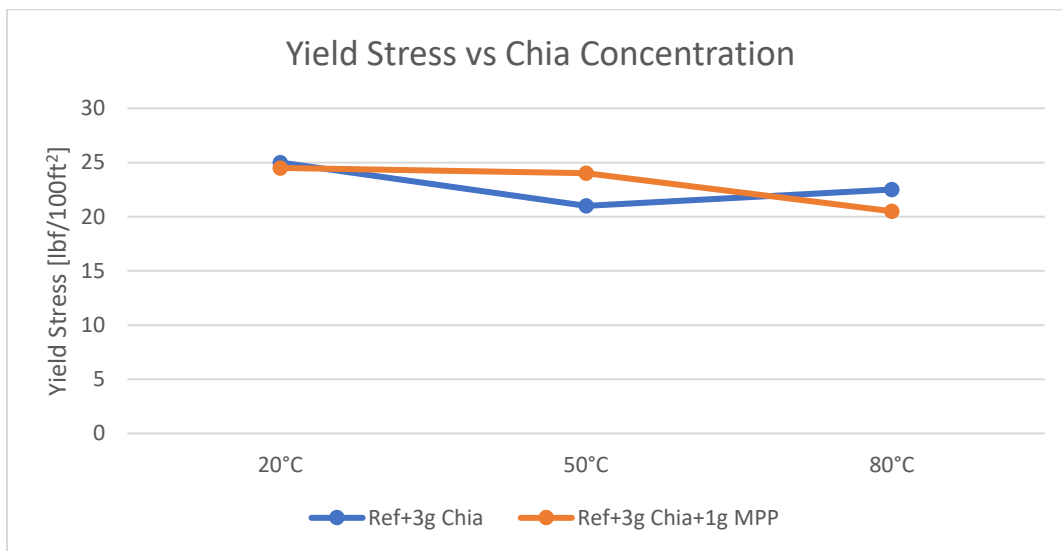


Figure 7.7: Yield Stress and the addition of MPP

Filtrate Measurements

Mandarin Peel Powder was added to the reference fluid including chia to improve its filtration properties. The addition of chia at first increased the volume of filtrate loss and then at the addition of 3g of chia it decreased the amount of filtrate loss. The addition of mandarin led to a 17.4% in filtrate loss as seen in table

Chia	Ref	Ref+1g Chia	Ref+2g Chia	Ref+3g Chia	Ref+3g Chia+ 1g Mandarin
Filtrate Loss (mL)	9,2	13,9	9,9	8,6	7,6
Percentage	0	51,1	7,6	-6,5	-17,4

Table 7.2: Chia and Mandarin Effect on Filtrate Loss in KCl-based fluid

Viscoelastic Measurements

The effect of chia and MPP were both investigated using the viscometer. The fluid containing chia and the fluid containing both chia and MPP showed gel-like characteristics. The addition of chia increased the flow and yield point of the fluid which means that the fluid will be irreversibly deformed at higher shear rates and the viscous behavior prevails later with greater amounts of chia. The addition of MPP slightly lowered the flow point but increased the yield point.

7.1.3 Chia and Mandarin Peel Powder as a Replacement for other additives

The possibility of replacing Pac and PolyPac in the bentonite-base fluid and xanthan gum in the KCl-base fluid was investigated. The results of this investigation are in the subsequent sections

7.1.3.1 Replacing Pac and PolyPac in Bentonite-Based Fluid

It was found that the addition of 2g Chia and 2g MPP was able to replace a third of the Pac and PolyPac with little effect on the yield stress and plastic viscosity. Figure 7.6 shows the effect on yield stress.

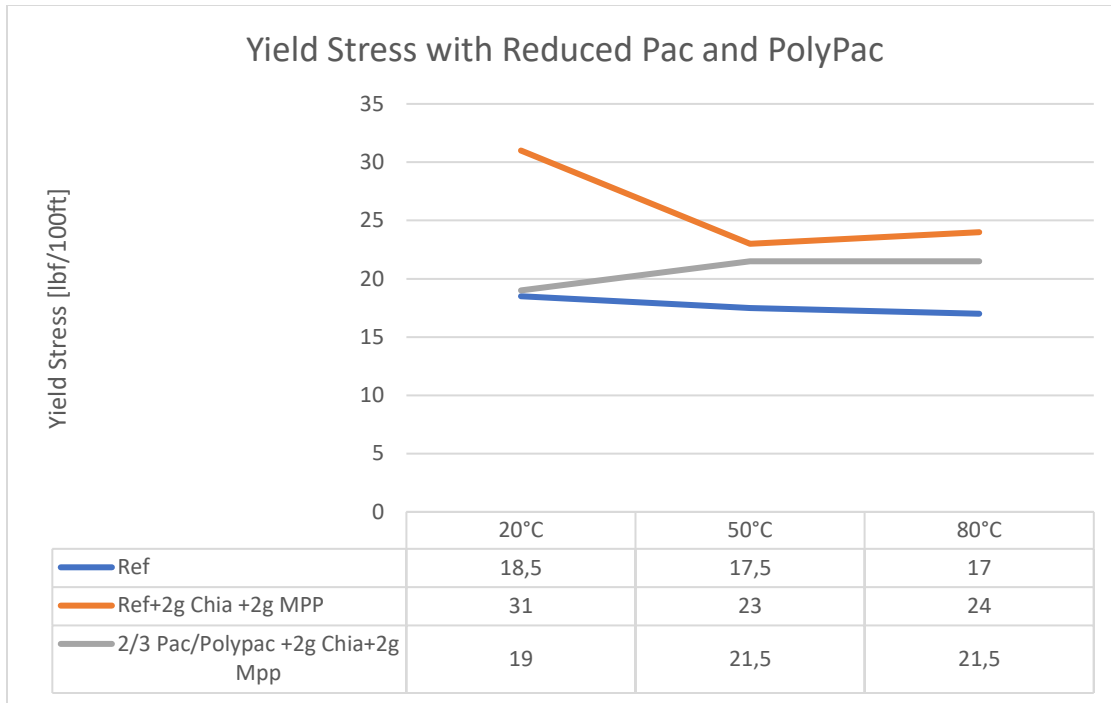


Figure 7.8: Yield Stress with Reduced Pac and PolyPac

For filtrate loss, the reduction of Pac and PolyPac showed a small increase in filtrate loss compared to the sample containing the full amount of Pac and Polypac

	Ref	Ref+2g Chia+2g MPP	2/3 of Pac and PolyPac and 2g Chia+2g MPP
Filtrate Loss (mL)	3	2,35	2,6
Percentage	n/a	-21,7	-13,3

Table 7.3: Filtrate Loss and reduced Pac and PolyPac

When the flow point and yield point was tested with the rheometer, reducing the Pac and PolyPac led to an increase in the flow point and the same yield point as the reference fluid as shown in table 7.4.

Drilling fluids	Flow Point	Yield Point
Ref	3,54	1,41
Ref+2g Chia+2g MPP	4,36	0,58
Reduced Pac and Polypac+2g Chia+2g MPP	4,51	1,41

Table 7.4: Flow Point and Yield Point with Reduced Pac and PolyPac

7.1.3.2 Replacing Xanthan Gum in KCl-Based Fluid

It was found that the addition of 3g Chia and 1g MPP was able to replace a third of the Xanthan Gum with little effect on the plastic viscosity. The reduction of xanthan gum did lead to yield stress that was approximately the same as the reference fluid with the full amount of xanthan gum.

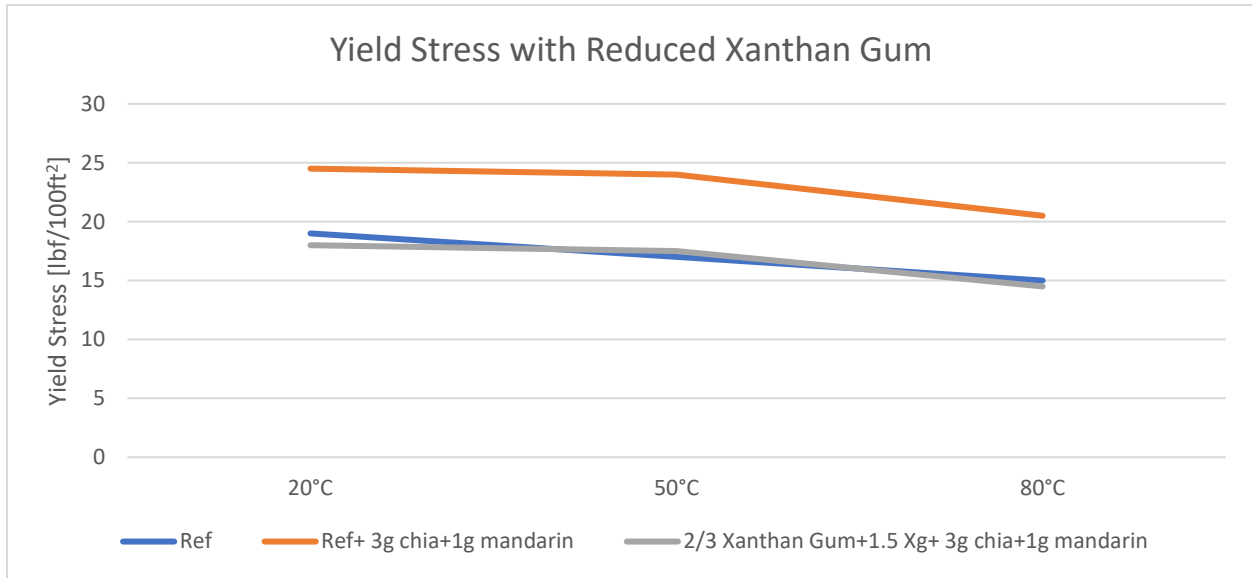


Figure 7.9: Yield Stress with Reduced Xanthan Gum

For filtrate loss, the reduction of xanthan gum showed a decrease in the volume of filtrate lost compared to the fluid containing the full amount of xanthan gum with 3g Chia and 1g MPP. However, it did show a 9.8% decrease compared to the reference fluid as shown in table 7.5.

	Ref	Ref+3g Chia+1g MPP	2/3 Xanthan Gum +3g Chia+ 1g MPP
Filtrate Loss (mL)	9,2	7,6	8,3
Percentage	0	-17,4	-9,8

Table 7.5: Filtrate Loss and Reduced Xanthan Gum

When the flow point and yield point was tested with the rheometer, reducing the Xanthan Gum led to a decrease in the flow point and an increase in the yield point from the reference fluid as shown in table 7.6.

	Flow Point	Yield Point
Ref	3,27	0,76
Ref+3g Chia+1g MPP	4,67	1,89
Reduced XG+3g Chia+1g MPP	2,56	1,07

Table 7.6: Flow Point and Yield Point with reduced Xanthan Gum

7.2 Performance Evaluation

Rheological modeling was performed on the best performing thermally stable fluids that showed good filtration properties. Hydraulic simulations were performed on a range of fluids to investigate the effects of chia and mandarin. Torque and Drag simulations were conducted on the initial fluid formulation and nanoparticle enhanced systems. In the hydraulic simulation, the ECD and pump pressure of these fluids were examined based on the unified hydraulics model that was described in section 2.3.

7.2.1 Hydraulics

Hydraulic performance investigations were done on a range of fluids to investigate the effect of varying concentrations of chia and mandarin. The simulation of the ECD and pump pressure was conducted at 22, 50 and 80°C. The simulation was conducted using an excel spreadsheet and a well that was described in depth in section 2.5. The fluids that were included in the results fall into these three groups:

- Varying concentrations of chia in bentonite reference fluid
- Varying concentrations of MPP in bentonite reference+2g Chia
- Varying concentrations of Chia, and 3g chia +1g MPP in KCl reference fluid

Bentonite-based Fluids

By examining the results that were shown in section 6.1. The addition of chia did not cause a significant difference in pump pressure. Ref+2g chia, did show thermal stability of the pump pressure across the three temperatures. The addition of MPP did lead to an overall increase in pump pressures across all temperatures. For ECD, the addition of chia led to a decrease in ECD across all temperatures and showed slight less variability across temperatures. The addition of MPP led to a decrease in ECD across all temperatures and shown thermal stability properties.

KCl-based Fluids

For the KCl-based fluids, the addition of chia led to an overall increase in pump pressures across all flow rates and temperatures. The addition of chia did lead to the system being slightly more thermally stable. The addition of MPP decreased pump pressures across all temperatures and especially at higher flow rates and was more thermally stable than the samples only containing chia. For ECD, the addition of chia led to a slight increase across all temperature ranges and was equally or slightly more thermally stable than the reference fluid. The addition of MPP decreased the ECD and was thermally stable.

7.2.2 Rheology Modeling

The best thermally stable fluid bentonite-based fluid and KCl-based fluid were used for rheological modeling in order to find which rheological best fit their flow behavior. The Robertson-Stiff model was found to be most accurate for both. Though the Unified and Herschel-Bulkley models were found to be good fits for the bentonite-based fluid. The Bingham-Plastic and Power-Law models were the next best fit for the KCl-based fluid.

7.2.3 Torque and Drag Simulation

Torque and drag simulations were performed to investigate the frictional properties of chia, mandarin and was then supplemented by TiN nanoparticles. The frictional measurements were then used to investigate the affect on torque and effective tension. The addition of chia and mandarin decreased the coefficient of friction by 34% and then adding TiN nanoparticles decreased the coefficient of friction by 41% from the reference fluid. The simulation showed that both torque and effective tension were improved by chia, mandarin and TiN nanoparticles. During tripping in and pulling out of the string, the torque and drag forces were moved in the opposite direction of the load limits. This indicated that lowering the coefficient of friction results in better torque and drag performance.

7.3 Limitations and Uncertainties

Due to restrictions, uncertainties, and assumptions relating to the used instruments and calculations, all experimental measurements will have some degree of inaccuracy. The necessity of minimizing and accounting for sources of error cannot be overstated because doing so will

reduce the reliability and reproducibility of the data generated. Some aspects are easier to control than others, but the degree to which the potential errors can be controlled varies.

Chemical Additive Measurements

The amount of chemical that is actually measured and added to the drilling fluid will be affected by the use of an uncalibrated and/or low precision weight balance with a low number of decimals. Therefore, employing a high accuracy weight balance and regularly performing calibrations can help to reduce the possibility of error. However, the quantity of additive added to the drilling fluids may still fluctuate significantly as a result of very tiny particle losses to the environment, such as those that take place during mixing.

Viscometer Measurements

The applied viscometer should be routinely calibrated to reduce the chance of errors when measuring the viscosity of the fluids. The same approach should be used throughout the whole investigation. The following things can also cause mistakes in the readings on the viscometer dial:

- Temperature variations,
 - It is generally known that temperature influences the dial readings on a viscometer, and that the viscosity of most bentonite fluids rise as the temperature rises.
- Dynamic Sag
 - As particles settle to the bottom of the measuring cup, this leads to lower dial readings on the viscometer
- Inhomogeneous fluid
 - Inhomogeneous fluids can cause variations in the viscometer reading because the properties of the fluids differ depending on which part of the fluid is sampled

Rheometer Measurements

Oscillatory amplitude sweeps were carried out using the Anton Paar MCR 302 rheometer. The following variables may have an impact on how accurate these measures are:

- Dried out sample
 - Depending on how much the sample has dried out, different characteristics may show
- An Inhomogeneous fluid
 - Data points may fluctuate as a result of the fluid's viscoelastic properties could vary within the fluid
- Error in gap size
 - A mistake in gap size can prevent the sample from contacting both plates

Hydraulics Simulations

When running the hydraulics simulations, several assumptions were made for simplicity. The simulated well is unrealistic since these assumptions, which are stated in section 6.1, neglect a number of characteristics of an actual drilling process. The assumptions were accepted as the goal of the simulation study was to compare the hydraulic performance of the drilling fluids in relation to one another. However, because the simulation research is reliant on the viscometer dial readings and the density of the drilling fluid, any mistakes in these measurements could cause the pump pressure and ECD to be incorrect.

8 Conclusion

The purpose of this thesis was to investigate the effect of chia, mandarin peel powder and TiN nanoparticles on the properties of both a bentonite-based reference fluid and a KCl-based reference fluid. Their performance was experimentally tested in terms of rheology, viscoelasticity, filtrate loss and pH. In addition frictional properties was measured in samples containing chia, mandarin peel powder and TiN nanoparticles. Further investigation of the chia and MMP enhanced fluid's performance was conducted through hydraulic modeling. Torque and Drag simulations were also performed on the samples containing chia, MPP, and TiN nanoparticles

The effect of chia and mandarin peel powder on bentonite-based drilling fluid

- From the rheological measurements, it was observed that uncooked chia should be used to attain thermally stable rheology characteristics
- The addition of chia could provide thermally stable rheology characteristics and worked as a viscosifier.
- Results from the rheological measurements indicated that the addition of .39wt% Chia provided the most thermally stable fluid
- The addition of chia led to an increase in gelling abilities and the fluids containing chia did not experience sedimentation outside of the acceptable range
- The addition of MPP provided thermally stable rheology characteristics and led to increased viscosity
- The addition of MPP led to enhanced filtration abilities
- From the oscillatory amplitude sweeps, it was observed that all fluids exhibited a gel-like structure and thus possess viscoelastic properties.
- Rheological modeling found that the fluid was best represented by the Robertson-Stiff model.
- The hydraulics simulation verified the thermal stability of both chia and mandarin, as both the resulting pump pressure and ECDs were stable with increasing temperature.

The effect of chia and mandarin peel powder on KCl-based drilling fluid

- From the rheological measurements, it was observed that cooked chia should be used to attain thermally stable rheology characteristics
- The addition of chia could provide thermally stable rheology characteristics and worked as a viscosifier.
- Results from the rheological measurements indicated that the addition of 0.57wt% Chia provided the most thermally stable fluid
- The addition of chia led to an increase in gelling abilities and the fluids containing chia did not experience sedimentation outside of the acceptable range
- The addition of MPP provided thermally stable rheology characteristics
- The addition of MPP led to enhanced filtration abilities
- From the oscillatory amplitude sweeps, it was observed that all fluids exhibited a gel-like structure and thus possess viscoelastic properties.
- Rheological modeling found that the fluid was best represented by the Robertson-Stiff model.
- The hydraulics simulation verified the thermal stability of both chia and mandarin, as both the resulting pump pressure and ECDs were stable with increasing temperature.

It should be emphasized that these findings are based on how these environmentally friendly additives and nanoparticle suspensions affected the water-based drilling fluids formulated in this thesis. The chemical additives may respond differently when added to different base fluids or when subjected to other pressure and temperature ranges. Additionally, the impact of concentrations outside the purview of this thesis are unknown.

9 References

- ADEBOWALE A & RAJI J 2015. Local content supplements as an alternative to imported corrosion control additives for drilling mud treatment. *Proceedings of the international academic conference for sub-Saharan Africa transformation and development*, 3.
- AHMET ORAL, B. O., MEHMET OZER, 2015. *2nd International Congress on Energy Efficiency and Energy Related Materials*.
- AL-ANAZI, A., MIRZAEI-PAIAMAN, A., BEDAIWI, E. & AL-ANAZI, B. 2009. Polymer Injection for Water Production Control through Permeability Alteration in Fractured Reservoir. *NAFTA*, 60.
- AL-HAMEEDI, A. T., ALKINANI, H. H., DUNN-NORMAN, S., ALASHWAK, N. A., ALSHAMMARI, A. F., ALKHAMIS, M. M., W. ALBAZZAZ, H., MUTAR, R. A. & ALSABA, M. T. Environmental Friendly Drilling Fluid Additives: Can Food Waste Products be Used as Thinners and Fluid Loss Control Agents for Drilling Fluid? SPE Symposium: Asia Pacific Health, Safety, Security, Environment and Social Responsibility, 2019a. D021S005R004.
- AL-HAMEEDI, A. T., ALKINANI, H. H., DUNN-NORMAN, S., ALBAZZAZ, H. W. & ALKHAMIS, M. M. Insights into Eco-Friendly and Conventional Drilling Additives: Applications, Cost Analysis, Health, Safety, and Environmental Considerations. SPE Symposium: Asia Pacific Health, Safety, Security, Environment and Social Responsibility, 2019b. D022S009R004.
- AL-HAMEEDI, A. T., ALKINANI, H. H., DUNN-NORMAN, S. & HAMOUD, Z. A. Investigation Study of the Effectiveness of Eggshells Powder as a Multifunctional Eco-Friendly Additive in Water-Based Fluid. 54th U.S. Rock Mechanics/Geomechanics Symposium, 2020a. ARMA2020-1157.
- AL-HAMEEDI, A. T. T., ALKINANI, H. H., ALBAZZAZ, H. W., DUNN-NORMAN, S. & ALKHAMIS, M. M. 2020b. Insights into the applications of waste materials in the oil and gas industry: state of the art review, availability, cost analysis, and classification. *Journal of Petroleum Exploration and Production Technology*, 10, 2137-2151.
- AL-HAMEEDI, A. T. T., ALKINANI, H. H., DUNN-NORMAN, S., AL-ALWANI, M. A., ALSHAMMARI, A. F., ALKHAMIS, M. M., MUTAR, R. A. & AL-BAZZAZ, W. H. 2019c. Experimental investigation of environmentally friendly drilling fluid additives (mandarin peels powder) to substitute the conventional chemicals used in water-based drilling fluid. *Journal of Petroleum Exploration and Production Technology*, 10, 407-417.

- AL-HAMEEDI, A. T. T., ALKINANI, H. H., DUNN-NORMAN, S., ALKHAMIS, M. M. & FELIZ, J. D. 2020c. Full-set measurements dataset for a water-based drilling fluid utilizing biodegradable environmentally friendly drilling fluid additives generated from waste. *Data Brief*, 28, 104945- 104945.
- ALCÁZAR-VARA, L. A. 2018. Drilling Fluids For Deepwater Fields: An Overview. IntechOpen.
- ALI, J. A., KALHURY, A. M., SABIR, A. N., AHMED, R. N., ALI, N. H. & ABDULLAH, A. D. 2020. A state-of-the-art review of the application of nanotechnology in the oil and gas industry with a focus on drilling engineering. *Journal of petroleum science & engineering*, 191, 107118.
- ALSHUBBAR, G. D., CORYELL, T. N., ATASHNEZHAD, A., AKHTARMANESH, S. & HARELAND, G. The Effect of Barite Nanoparticles on the Friction Coefficient and Rheology of Water Based Mud. 51st U.S. Rock Mechanics/Geomechanics Symposium, 2017. ARMA2017-0147.
- ALVI, M. A., BELAYNEH, M., SAASEN, A. & AADNØY, B. S. The Effect of Micro-Sized Boron Nitride BN and Iron Trioxide Fe₂O₃ Nanoparticles on the Properties of Laboratory Bentonite Drilling Fluid. SPE Norway One Day Seminar, 2018. D011S011R002.
- AMANULLAH, M., AL-ARFAJ, M. K. & AL-ABDULLATIF, Z. Preliminary Test Results of Nanobased Drilling Fluids for Oil and Gas Field Application. SPE/IADC Drilling Conference and Exhibition, 2011. SPE-139534-MS.
- AMANULLASH, M. Screening and Evaluation of Some Environment-Friendly Mud Additives To Use in Water-Based Drilling Muds. E&P Environmental and Safety Conference, 2007. SPE-98054- MS.
- ANTON PAAR GMBH. n.d.-a. *Amplitude sweeps* [Online]. Available: <https://wiki.anton-paar.com/pl/zmienne-amplitudy/> [Accessed].
- ANTON PAAR GMBH. n.d.-b. *Basics of rheology* [Online]. Available: <https://wiki.anton-paar.com/en/basics-of-rheology/> [Accessed].
- ANTON PAAR GMBH. n.d.-c. *How to measure viscosity* [Online]. Available: <https://wiki.anton-paar.com/en/how-to-measure-viscosity/#c16709> [Accessed 7. February 2023].
- ANTON PAAR GMBH. n.d.-d. *Rotational viscometry* [Online]. Available: <https://wiki.anton-paar.com/en/rotational-viscometry/> [Accessed 25. January 2023].
- BELAYNEH, M. 2006. A review of buckling in oil wells, Aachen, Shaker Verlag University of Stavanger.
- BELAYNEH, M. 2016. Advanced drilling engineering lecture note. Stavanger: University of Stavanger.
- BELAYNEH, M. 2019a. Drilling Equipment, in Advanced Drilling Engineering and Technology, lecture notes. Stavanger: University of Stavanger.
- BELAYNEH, M. 2019b. Hydraulics and cuttings transport, in Advanced Drilling Engineering and Technology, lecture notes. Stavanger: University of Stavanger.

- BOVÉ, A.-T. & SWARTZ, S. 2016. Starting at the source: Sustainability in supply chains. Available: <https://www.mckinsey.com/business-functions/sustainability/our-insights/starting-at-the-source-sustainability-in-supply-chains>.
- BUI, B. T., SAASEN, A., MAXEY, J. E., OZBAYOGLU, M. E., MISKA, S. Z., YU, M. & TAKACH, N. E. Viscoelastic Properties of Oil-Based Drilling Fluids. 2012.
- CHILINGARIAN, G. V. & VORABUTR, P. 1983. *Drilling and drilling fluids*, Amsterdam, Elsevier.
- CHOI, S. U. S. & EASTMAN, J. 1995. *Enhancing thermal conductivity of fluids with nanoparticles*.
- COCUZZA, M., PIRRI, F., ROCCA, V. & VERGA, F. Is The Oil Industry Ready For Nanotechnologies? Offshore Mediterranean Conference and Exhibition, 2011. OMC-2011- 070.
- CONTRERAS, O., HARELAND, G., HUSEIN, M., NYGAARD, R. & ALSABA, M. Application of In-House Prepared Nanoparticles as Filtration Control Additive to Reduce Formation Damage. SPE International Symposium and Exhibition on Formation Damage Control, 2014. D021S010R003.
- CZECH, A., ZARYCKA, E., YANOVYCH, D., ZASADNA, Z., GRZEGORCZYK, I. & KŁYS, S. 2020. Mineral Content of the Pulp and Peel of Various Citrus Fruit Cultivars. *Biological Trace Element Research*, 193, 555-563.
- DAWSON, R., FRIESEN, D. B. & JOHANCSIK, C. A. 1984. Torque and Drag in Directional Wells-Prediction and Measurement. *Journal of petroleum technology*, 36, 987-992.
- DEVEREUX, S. 1998. *Practical well planning and drilling manual*, Tulsa, Okla, PennWell.
- DEVEREUX, S. 2012. *Drilling technology in nontechnical language*, Tulsa, Okla, PennWell.
- DRILLINGFORMULAS.COM. 2016. *pH in Drilling Mud (Water Based Mud)* [Online]. Available: <https://www.drillingformulas.com/ph-in-drilling-mud-water-based-mud/> [Accessed].
- ELKATATNY, S. 2018. Enhancing the Stability of Invert Emulsion Drilling Fluid for Drilling in HighPressure High-Temperature Conditions. *Energies (Basel)*, 11, 2393.
- ENCYCLOPEADIA BRITANNICA INC. 2019. Hydraulics [Online]. Available: <https://www.britannica.com/science/hydraulics> [Accessed].
- ENCYCLOPÆDIA BRITANNICA INC. 2017. tribology [Online]. Available: <https://www.britannica.com/science/tribology> [Accessed].
- ENCYCLOPÆDIA BRITANNICA INC. n.d. Drilling mud [Online]. Available: <https://www.britannica.com/technology/drilling-mud/additional-info#history> [Accessed 30. January 2023].
- FABER, T. 2019. *fluid mechanics* [Online]. Available: <https://www.britannica.com/science/fluid-mechanics> [Accessed].

- FATTNES, L. 2020. *New Nanoparticle Based Drilling Fluid Formulation and Characterization: Experimental and Simulation Studies*. University of Stavanger.
- FINK, J. 2015. *Petroleum Engineer's Guide to Oil Field Chemicals and Fluids*. Second ed.: Gulf Professional Publishing.
- FINK, J. K. 2003. *Oil Field Chemicals*, Kidlington, Kidlington: Elsevier Science & Technology. FREDDIE RUIZ. 2015. Prediction Technique. Available from: <http://www.pvisoftware.com/blog/tag/drillstring-drag/>.
- GLOBAL DRILLING FLUIDS & CHEMICALS LTD. n.d. PAC LV [Online]. Available: <https://www.oil-drilling-fluids.com/pac-lv> [Accessed].
- GUO, B. & LIU, G. 2011. *Applied drilling circulation systems: hydraulics, calculations, and models*, Amsterdam, Elsevier Gulf Professional Publ.
- HAIDER, S., MESSAOUD-BOUREGHDA, M.-Z., AKNOUCHE, H., AKKOUCHE, A., HAMMADI, L. & SAFI, B. 2018. An ecological water-based drilling mud (WBM) with low cost: substitution of polymers by wood wastes. *Journal of petroleum exploration and production technology*, 9, 307-313.
- HAVNEN, P. 2022, *New Eco-Friendly and Nanoparticle Based Drilling Fluid Formulation and Characterization*. University of Stavanger.
- HOELSCHER, K. P., YOUNG, S., FRIEDHEIM, J. & DE STEFANO, G. Nanotechnology Application in Drilling Fluids. Offshore Mediterranean Conference and Exhibition, 2013. OMC-2013-105.
- HOSSAIN, M. E. & ISLAM, M. R. 2018. *Drilling Engineering Problems and Solutions: A Field Guide for Engineers and Students*, Somerset, Somerset: John Wiley & Sons, Incorporated.
- IRANWAN, S., AZMI, A. & SAAID, M. 2009. Corn cobs and sugar cane waste as viscosifier in drilling fluid. *Pertanika J Sci Technol* 17:173–181.
- IRO GROUP INC. n.d. *Viscosifier* [Online]. Available: <https://www.irooildrilling.com/Viscosifier/PAC.htm> [Accessed].
- KOLLE, G. & MESEL, R. 1998. *Brønnvæsker : for VK1 brønnteknikk*, Nesbru, Vett & viten.
- KUTLIC, A., BEDEKOVIC, G. & SOBOTA, I. 2012. Bentonite processing/ Oplemenjivanje bentonita. *Rudarsko-geološko-naftni zbornik*, 24, 61-56.
- KAARSTAD, E., AADNOY, B. S. & FJELDE, T. A Study of Temperature Dependent Friction in Wellbore Fluids. SPE/IADC Drilling Conference and Exhibition, 2009. SPE-119768-MS.
- LAKE, L. W. & MITCHELL, R. F. 2006. *Petroleum Engineering Handbook: Drilling Engineering*, Richardson, Richardson: Society of Petroleum Engineers.
- LEE, J. K., CHYU, M. K. & NTCE, A. NTCE-1804 : Use of magnetic nanoparticles for smart drilling fluids. 2009.

- LEFRANÇOIS, P., IBARBOURE, E., PAYRÉ, B., GONTIER, E., LE MEINS, J.-F. & SCHATZ, C. 2015. Insights into Carbopol gel formulations: Microscopy analysis of the microstructure and the influence of polyol additives. *J. Appl. Polym. Sci*, 132, 42761-n/a.
- LONG, L., XIANGUANG, X., JINSHENG, S., XUBO, Y. & YINGMIN, L. Vital Role of Nanomaterials in Drilling Fluid and Reservoir Protection Applications. Abu Dhabi International Petroleum Conference and Exhibition, 2012. SPE-160940-MS.
- LUBRIZOL CORPORATION. 2009. Neutralizing Carbopol®* and Pemulen™* Polymers in Aqueous and Hydroalcoholic Systems. Available: https://www.lubrizol.com/-/media/Lubrizol/Health/TDS/TDS237_Neutralizing_Carbopol_Pemulen_in_Aqueous_Hydroalcoholic_Systems--PH.pdf.
- MANSOOR, H. H., DEVARAPU, S., SAMUEL, R., SANGWAI, S., PONMANI, S. 2022. Investigation of chia based copper oxide nanofluid for water based drilling fluid: An experimental approach, *Journal of Natural Gas Science and Engineering*, 107, 104775
- MATERION BRUSH INC 2017. CURRENT EVENTS: ELECTRICAL AND THERMAL CONDUCTIVITY.
- MCCOREMICK, R. 2015. *Why pH Levels are Important When Mixing Drill Mud* [Online]. Available: <http://blog.fordia.com/blog/why-ph-levels-are-important-when-mixing-drill-mud> [Accessed].
- MEZGER, T. G. 2011. *The rheology handbook: for users of rotational and oscillatory rheometers*, Hannover, Vincentz.
- MIRHAJ, S. A. A., KAARSTAD, E. & AADNOY, B. S. S. Minimizing Friction In Shallow Horizontal Wells. IADC/SPE Asia Pacific Drilling Technology Conference and Exhibition, 2010. SPE-135812-MS.
- MITCHELL, R. F., MISKA, S. & SOCIETY OF PETROLEUM, E. 2011. *Fundamentals of drilling engineering*, Richardson, Tex, Society of Petroleum Engineers.
- NMEGBU, G. & BARI-AGARA, B. 2014. Evaluation of Corn Cob Cellulose and its Suitability for Drilling Mud Formulation. *International Journal of Engineering Research and Applications*, 4.
- NOHAVA, J. n.d. Applications of tribometers, tribology, friction and wear studies in polymer industry.
- OCHOA, M. Analysis of drilling fluid rheology and tool joint effect to reduce errors in hydraulics calculations. 2006.
- OKON, A. N., UDOH, F. D. & BASSEY, P. G. Evaluation of Rice Husk as Fluid Loss Control Additive in Water-Based Drilling Mud. SPE Nigeria Annual International Conference and Exhibition, 2014. SPE-172379-MS.
- OMOTIOMA, M., EJKEME, P. & MBAH, G. 2014. Comparative Analysis of the Effects of Cashew and Mango Extracts on the Rheological Properties of Water Based Mud. 56-61.

- ONWUACHI-IHEAGWARA, P. N. 2015. Comparative Analysis of the Use of Banana Peels and NaOH in Ph Control In Nigerian Clays. *Journal of the Nigerian Association of Mathematical Physics*, 30, 197-202.
- PARIZAD, A. & SHAHBAZI, K. 2016. Experimental investigation of the effects of SnO₂ nanoparticles and KCl salt on a water base drilling fluid properties. *Can. J. Chem. Eng*, 94, 1924-1938.
- PLASTECH PLUS INC. 2014. *THE DIFFERENCE BETWEEN DRILLING FLUID AND DRILLING MUD* [Online]. Available: <http://www.pvcplus.com/news/the-difference-between-drilling-fluid-and-drilling-mud.aspx> [Accessed].
- PRISCILLA, R. V., M. COSTA, C., S. FONSECA, B., F. NACCACHE, M. & DE SOUZA MENDES, P. 2019. Rheological Characterization of Carbopol® Dispersions in Water and in Water/Glycerol Solutions. *Fluids (Basel)*, 4, 3.
- RAFATI, R., SMITH, S. R., SHARIFI HADDAD, A., NOVARA, R. & HAMIDI, H. 2018. Effect of nanoparticles on the modifications of drilling fluids properties: A review of recent advances. *Journal of petroleum science & engineering*, 161, 61-76.
- REHM, B. 2012. *Underbalanced drillin : limits and extremes*, Houston, TX, Gulf Pub. Co.
- ROBERTSON, R. E. & STIFF, H. A. 1976. An Improved Mathematical Model for Relating Shear Stress to Shear Rate in Drilling Fluids and Cement Slurries. *Society of Petroleum Engineers journal*, 16, 31-36.
- S. KHATANIAR, G. A. CHUKWU & HUA XU 1994. Evaluation of rheological models and application to flow regime determination International journal of rock mechanics and mining sciences & geomechanics abstracts, 32, 155-164.
- SADIGOV, J. 2013. *Comparisons of rheology and hydraulics prediction of mud systems in concentric and eccentric well geometry*. University of Stavanger.
- SALIH, A. H., ELSHEHABI, T. A. & BILGESU, H. I. Impact of Nanomaterials on the Rheological and Filtration Properties of Water-Based Drilling Fluids. SPE Eastern Regional Meeting, 2016. SPE-184067-MS.
- SCHLUMBERGER LIMITED. n.d.-a. Bingham plastic model [Online]. Available: https://glossary.oilfield.slb.com/en/terms/b/bingham_plastic_model [Accessed 17. February 2023].
- SCHLUMBERGER LIMITED. n.d.-b. circulation system [Online]. Available: https://glossary.oilfield.slb.com/en/terms/c/circulation_system [Accessed 21. February 2023].
- SCHLUMBERGER LIMITED. n.d.-c. Drilling fluids [Online]. Available: https://glossary.oilfield.slb.com/en/terms/d/drilling_fluid [Accessed].
- SCHLUMBERGER LIMITED. n.d.-d. ECD [Online]. Available: <https://glossary.oilfield.slb.com/en/terms/e/e cd> [Accessed 15. February 2023].
- SCHLUMBERGER LIMITED. n.d.-e. Fluid loss [Online]. Available: https://glossary.oilfield.slb.com/en/terms/f/fluid_loss [Accessed 20. January 2023].

- SCHLUMBERGER LIMITED. n.d.-f. Herschel-Bulkley fluid [Online]. Available: https://glossary.oilfield.slb.com/en/terms/h/herschel-bulkley_fluid [Accessed 13. February 2023].
- SCHLUMBERGER LIMITED. n.d.-g. Montmorillonite [Online]. Available: <https://glossary.oilfield.slb.com/en/terms/m/montmorillonite> [Accessed 14. February 2023].
- SCHLUMBERGER LIMITED. n.d.-h. Mud Weight [Online]. Available: https://glossary.oilfield.slb.com/en/terms/m/mud_weight [Accessed 25. January 2023].
- SCHLUMBERGER LIMITED. n.d.-i. Newtonian fluid [Online]. Available: https://glossary.oilfield.slb.com/en/terms/n/newtonian_fluid [Accessed 12. February 2023]
- SCHLUMBERGER LIMITED. n.d.-j. Non-Newtonian fluid [Online]. Available: https://glossary.oilfield.slb.com/en/terms/n/non-newtonian_fluid [Accessed 15. February 2023].
- SCHLUMBERGER LIMITED. n.d.-k. POLYPAC UL [Online]. Available: <https://www.slb.com/drilling/drilling-fluids-and-well-cementing/drilling-fluids/drilling-fluid-additives/filtration-reducers/polypac-ul-ultralow-viscosity-cellulose#related-information> [Accessed].
- SCHLUMBERGER LIMITED. n.d.-l. Rheology [Online]. Available: <https://glossary.oilfield.slb.com/en/terms/r/rheology> [Accessed 18. January 2023].
- SCHLUMBERGER LIMITED. n.d.-m. Shear rate [Online]. Available: https://glossary.oilfield.slb.com/en/terms/s/shear_rate [Accessed 20. January 2023].
- SCHLUMBERGER LIMITED. n.d.-n. Shear stress [Online]. Available: https://glossary.oilfield.slb.com/en/Terms/s/shear_stress.aspxS [Accessed 20. January 2023].
- SCHLUMBERGER LIMITED. n.d.-o. Soda ash [Online]. Available: https://glossary.oilfield.slb.com/en/terms/s/soda_ash [Accessed].
- SCHLUMBERGER LIMITED. n.d.-p. Thixotropy [Online]. Available: <https://glossary.oilfield.slb.com/en/terms/t/thixotropy> [Accessed 19. January 2023].
- SCHLUMBERGER LIMITED. n.d.-q. Water-based mud [Online]. Available: https://glossary.oilfield.slb.com/en/terms/w/water-base_mud [Accessed 20. January 2023].
- SCHLUMBERGER LIMITED. n.d.-r. Yield point [Online]. Available: https://glossary.oilfield.slb.com/en/terms/y/yield_point [Accessed 22. January 2023].
- SCRIBD INC. 2018. Drill String Failure Prevention [Online]. Available: <https://www.slideshare.net/hshobeyri/slb-drill-stringfailure> [Accessed].
- SHAKEEL, A., KIRICHEK, A. & CHASSAGNE, C. 2020. Yield stress measurements of mud sediments using different rheological methods and geometries; an evidence of two-step yielding. *Marine geology*, 427, 106247.

- SKJEGGESTAD, O. 1989. *Boreslamteknologi : teori og praksis*, Bergen, Alma Mater.
- SMITH, S. R., RAFATI, R., SHARIFI HADDAD, A., COOPER, A. & HAMIDI, H. 2018. Application of aluminium oxide nanoparticles to enhance rheological and filtration properties of water based muds at HPHT conditions. *Colloids and surfaces. A, Physicochemical and engineering aspects*, 537, 361-371.
- STRAND, S. 1998. Øvinger i bore-og brønnvæsker. Høgskolen i Stavanger.
- TIMILSENA, Y., ADHIKARI, R., KASAPIS, S., ADHIKARI, B. 2015. Rheological and microstructural properties of the chia seed polysaccharide, *International Journal of Biological Macromolecules*, 81, 991-999.
- TSENG, W. J. & LIN, K.-C. 2003. Rheology and colloidal structure of aqueous TiO₂ nanoparticle suspensions. *Materials Science and Engineering: A*, 355, 186-192.
- US RESEARCH NANOMATERIALS INC. n.d. Titanium Nitride (TiN) Nanopowder / Nanoparticles 5wt% Water Dispersion (TiN, 99.2+%, 20nm) [Online]. Available: <https://www.us-nano.com/inc/sdetail/44801> [Accessed].
- WAMI, E., PIUS, J. & NMEGBU, G. 2015. Drilling Mud Formulation Using Potato Starch (Ipomoea Batatas). *International Journal of Engineering Research and Applications*, 5, 48-54.
- WATTS, D. & BAGHERPOUR, J. 2015. *Drilling fluid types* [Online]. Available: https://petrowiki.spe.org/Drilling_fluid_types [Accessed 20. January 2023].
- WHITTAKER, A. & EXLOG 1985. *Theory and application of drilling fluid hydraulics*, Dordrecht, Reidel.
- WILLIAM, J. K. M., PONMANI, S., SAMUEL, R., NAGARAJAN, R. & SANGWAI, J. S. 2014. Effect of CuO and ZnO nanofluids in xanthan gum on thermal, electrical and high pressure rheology of water-based drilling fluids. *Journal of Petroleum Science and Engineering*, 117, 15-27.
- WILLIAMSON, D., CULLUM, D., ESPEY, S. & PREBENSEN, O. I. 2013. *The Defining Series: Drilling Fluid Basics* [Online]. Available: <https://www.slb.com/resource-library/oilfield-review/defining-series/defining-drilling-fluids> [Accessed 25. January 2022].
- WU, J. & JUVKAM-WOLD, H. C. Study of Helical Buckling of Pipes in Horizontal Wells. SPE Production Operations Symposium, 1993. SPE-25503-MS.
- YAN, Y. 2013. Bio-tribocorrosion in biomaterials and medical implants. Portland: Portland: Ringgold, Inc.
- ZHANG, J., CHEN, G., YANG, N. W. & WANG, Y. G. 2014. Preparation of Nitration-oxidation Lignosulfonate as an Eco-friendly Drilling Fluid Additive. *Petroleum science and technology*, 32, 1661-1668.
- ZHENG, Y., AMIRI, A. & POLYCARPOU, A. A. 2020. Enhancements in the tribological performance of environmentally friendly water-based drilling fluids using additives. *Applied surface science*, 527, 146822.

ZHONGWEI, H., GENSHENG, L., SHOUCENG, T., XIANZHI, S., MAO, S. & SUBHASH, S. 2018. Chapter Five - Flow Behavior and Friction Characteristics of Fluid Flow in Coiled Tubing. Elsevier Inc.

ÖZKAYA, N., LEGER, D., GOLDSHEYDER, D. & NORDIN, M. 2012. *Fundamentals of Biomechanics Equilibrium, Motion, and Deformation*, Cham, Springer International Publishing.

AADNOY, B. S., FAZAEIZADEH, M. & HARELAND, G. 2010. A 3D Analytical Model for Wellbore Friction. *Journal of Canadian petroleum technology*, 49, 25-36.

AADNØY, B. S. 2006. *Mechanics of drilling*, Aachen, Shaker Verlag.

AARRESTAD, T. V. 1994. Torque and Drag-Two Factors in Extended-Reach Drilling. *Journal of petroleum technology*, 46, 800-803

10 Appendices

10.1 Torque

While drilling, the friction between the drill string and the wellbore is the main source of the drag force. This force is added to the weight of the freely rotating drill string while tripping into or out of the hole. In general, it is greater when the drill string is pulled out of the hole (POOH) and less significant when the drill string is run into the hole (RIH). In order to successfully complete long-reach wells, a smooth path during drilling is preferred. However, this is rarely the case because during drilling, azimuth and inclination frequently vary continuously (Aarrestad, 1994)

The three primary sections of the applicable well trajectory considered in this study are vertical, bend, and inclination. Figure 10.1 shows this well design, with the relevant forces numerically labeled 1 through 5.

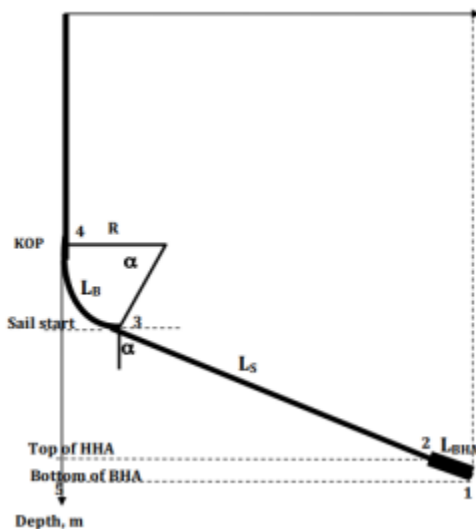


Figure 10.1: Typical simulation well trajectory

Furthermore, while the drill string is static, frictional forces do not apply. As a result, the drill string's static weight is broken up into various pipe sections, as shown in figure 10.1. Table 10.1 provides an overview of the various sections and their static weight calculations.

Static Weight of the Drill String	
At the bottom of the bottom hole assembly (BHA)	$F_{1,static} = WOB$
On top of the bottom hole assembly (BHA) α = the incline angle from the vertical	$F_{2,static} = F_{1,static} + w_{BHA,Buoyant}L_{BHA} \cos \alpha$
On top of the sail section	$F_{3,static} = F_{2,static} + w_{DP,buoyant}L_{DP} \cos \alpha$
At the Kick-Off Point (KOP) R= the radius of the curvature	$F_{4,static} = F_{3,static} + w_{DP,buoyant}R \sin \alpha$
On the top of the string	$F_{5,static} = F_{4,static} + w_{DP,bouyant}L_{KOP}$

Table 10.1: Static Weight of the Drill String

10.1.1 Drag in Straight Inclined/Horizontal Section

Furthermore, while the drill string is static, frictional forces do not apply. As a result, the drill string's static weight is broken up into various pipe sections, as shown in figure 10.2. Table 10.2 provides an overview of the various sections and their static weight calculations.

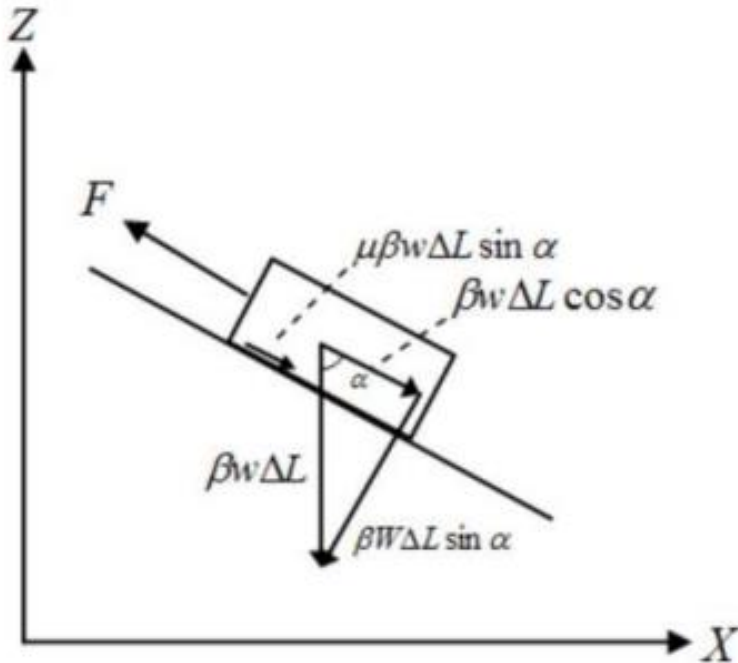


Figure 10.2: Force balance example for a pipe being pulled along a straight surface (Aadnoy et al., 2010)

The drill string's many sections can express the forces shown above. Since there is no WOB at the bottom of the BHA, there is no force there. The buoyancy factor, BHA length, string angle, and whether the string is dragged (+) or lowered (-) into the wellbore all affect the force at the top of the BHA. It also depends on the force at the bottom of the BHA. The force at the top of the sail section is comparable to the force at the top of the BHA, with the exception that the string element uses the length, weight, and force from the bottom of the drill pipe (Aadnoy, 2006). Table 10.2 contains a list of the expressions and arguments.

Forces in Straight Incline or Horizontal Section	
At the bottom of the bottom hole assembly (BHA)	$F_1 = 0$
On top of the Bottom Hole Assembly (BHA)	$F_2 = F_1 + \beta w_{BHA} \Delta L_{BHA} (\cos \alpha \pm \sin \alpha)$
On top of the sail section	$F_3 = F_2 + \beta w_{DP} \Delta L_{DP} (\cos \alpha + \mu_\alpha \sin \alpha)$
Buoyancy Factor	$\beta = 1 - \left(\frac{\rho_{mud}}{\rho_{string}} \right)$

Table 10.2: Forces in Straight Incline or Horizontal Section

10.1.1.1 Drag in Bended Part of the Wellbore

The build-up bend will be further discussed because the torque and drag simulation conducted later in this thesis does not contain a drop-off curve. The build-up bend is depicted in figure 10.2 on top of the bent portion, and a more thorough illustration is displayed in figure 10.3

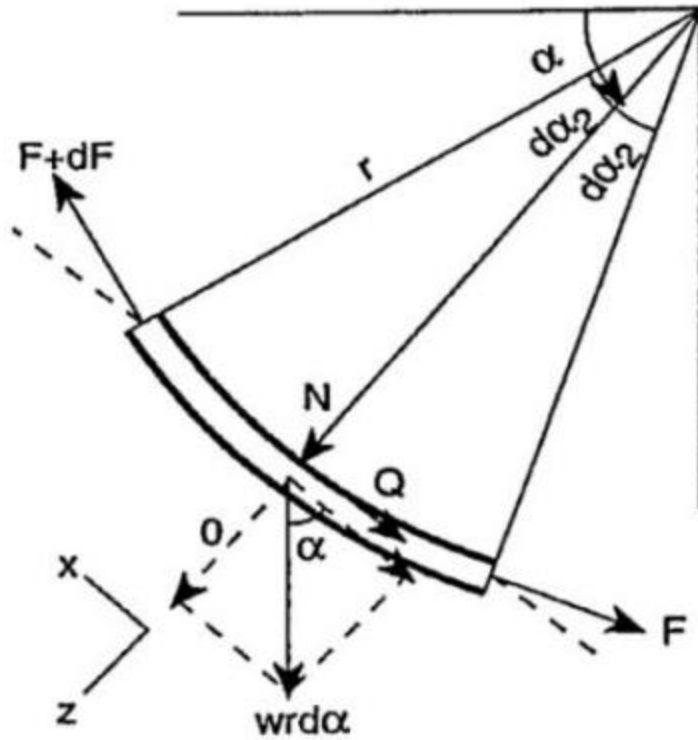


Figure 10.3: Example of a build-up bend section force free body diagram (Aadnoy, 2006)

The mathematical computations of the various forces in the bending region are shown in Table 10.3. It reflects the force used to pull and lower the string on top of the build-up section. Friction coefficient μ_0 is determined between the pipe and the wellbore wall while the drill string is stationary. Nevertheless, depending on whether the drill string is moving axially or tangentially, the friction coefficient value will change. Additionally, the friction coefficient varies with pipe radius when a drill string is moving. The table below also takes these variables into account (Belayneh, 2016, Aadny, 2006).

Forces in the Build-Up Sections of the String	
On top of the build-up section due to pull out of the string	$F_{4,pullout} = (F_{3,pullout} + w_{DP,buoyant}R \sin \alpha)e^{\mu_a \alpha}$
Drag on top of the build-up section due to lowering of the string	$F_{4,lowering} = \left(F_{3,lowering} + \frac{w_{DP,buoyant}R}{1 + \mu_a^2} \left((1 - \mu_a^2) \sin \alpha - 2\mu_a \cos \alpha \right) \right) e^{-\mu_a} + \frac{2\mu_a w_{DP,buoyant}R}{1 + \mu_a^2}$
Axial friction coefficient equation for drag calculations	$\mu_a = \mu_0 \cdot \frac{V_a}{\sqrt{(\Omega r_i)^2 + v_a^2}}$ <p>V_a = axial velocity of drilling string</p> <p>r = outer radius of i (drill pipe or BHA)</p> <p>$\Omega = \frac{2\pi n}{60}$ = revolution per minute where n is the number of rotations per minute</p>

Table 10.3: Forces in the Build Up sections of the string

10.1.1.2 Drag in the Vertical Section

In essence, the force acting on the string is equal to the weight of the vertical segment plus the total of all forces acting below it. The following can be used to express the drag (Aadny, 2006):

$$F_{5i} = F_{4i} + w_{dp,buoyant} L_{KOP} \tag{10.1}$$

10.1.2 Torque

The moment necessary to rotate the drill string and surpass the rotational frictional resistance created in the wellbore and at the bit is referred to as torque in the scope of drilling operations. This friction develops during the interaction of the drill bit with the formation as well as the pipe and wellbore casing. Fundamentally, torque is a function of radius, frictional forces, normal force, and friction coefficient. Torque loss is not present in vertical wells. However, issues with torque in extended reach drilling (ERD) wells can prevent the advancement of drilling operations. Additionally, Aadny's model's torque forces are expressed in many sections related to the well design (Aadny, 2006).

10.1.2.1 *Torque in the Straight Sail Section*

Reviewing the well trajectory shown in figure 10.2, the torque can be expressed by each section. The torque at the bottom of BHA is equal to the torque-on-bit (TOB) in the straight sail portion. Consequently, zero torque is generated when the bit is at the bottom. Torque therefore equals the normal moment, which is expressed with the friction factor t , at the top of the BHA and the sail section. The axis forces have no impact on torque at the straight, inclined, or horizontal portions of the wellbore. The torque calculations still hold true when there are no axial forces in the string since the string's rotational direction is irrelevant. Table 2.6 contains a list of torque equations (Aadnoy, 2006).

Torque in the Straight Section	
At the bottom of the BHA	$T_1 = TOB$ <p style="text-align: center;">When the bit is off the bottom: $TOB = 0$</p>
At the top of the BHA	$T_2 = T_1 + \mu_t w_{BHA, buoyant} L_{BHA} r_{BHA} \sin \alpha$
On top of the sail section	$T_3 = T_2 w_{DP, buoyant} L_{DP} r_{DP} \sin \alpha$
The Axial Friction coefficient equations for torque calculations	$\mu_a = \mu_0 \cdot \frac{V_a}{\sqrt{(\Omega r_i)^2 + v_a^2}}$
	<p>V_a = axial velocity of drill string</p> <p>r = outer radius of i (drill pipe or BHA)</p> <p>$\Omega = \frac{2\pi n}{60}$ = revolution per minute where n is the number of rotations per minute</p>

Table 10.4: Torque in the Straight Section

10.1.2.2 Torque in the Build-Up Bend section

The drag value at the top of the sail section (at KOP) and the direction of the axial string movement are both determinants of the torque's magnitude in the build-up section. Equation 9.2 provides the mathematical expression (Aadnoy, 2006).

$$T_4 = T_3 + \mu_t r_{DP} \left((F_{3,i} + w_{dp, buoyant} R \sin \alpha) \alpha + 2w_{DP, buoyant} R (1 - \cos \alpha) \right) \quad (10.2)$$

Where i represents the pullout or lowering of the string

10.1.2.3 Torque in the vertical part of the wellbore

The forces exerted on the wellbore's vertical segment act at a zero-degree angle. Therefore, the torque at the top of the vertical portion is thus just equal to the torque of KOP, and the expression in equation 2.36 becomes zero (Aadny, 2006):

$$T_5 = T_4 \tag{10.3}$$

10.1.3 Torsional and Tensile Limits

The drill string needs to be strong enough to withstand the loads it will experience in the wellbore in order to provide a safe drilling operation. A drill string mechanics program that will specify a well's safe operating window can be created during the well planning process. Torsion and tensile limitations determine the safe operating window. Failure in the pipe body and tool joints are often the results of exceeding the tensile and torsional limitations. Belayneh, 2019b; Ahmet oral, 2015

Tensile failure happens when the load applied exceeds the yield strength of the drill string's weakest component, while torsional failure happens when the compressive stress exceeds the string's critical buckling load (Scribd Inc, 2018, Mirhaj et al., 2010). Friction becomes a key factor in a wellbore that is subject to torsional and tensile limits because it causes pipe buckling and failure at lower compressive and tensile stresses. Higher weight on bit (WOB) cannot be applied if higher ROP and torque on bit (TOB) are necessary if compressive forces are strong. Higher tensile loads, on the other hand, might distort a material permanently or change its stability. Material failure and pipe failure will potentially result from surpassing the string's yield strength (Belayneh, 2019b, Mirhaj et al., 2010).

The yield force, which is equal to the pipe's yield stress multiplied by its cross-sectional area, is what determines the tensile limit. The yield force (F_y) is multiplied by a safety factor, which is typically equal to ($\frac{8}{7}$), as a precaution. The yield force equation is therefore provided as follows (Belayneh, 2016):

$$F_y = \frac{A\sigma_y}{SF} \tag{10.4}$$

10.1.3.1 Buckling Limit

Drill string issues are frequently connected to extended reach drilling (ERD) operations' use of drill strings. Due to the wells' high slope, the wellbore wall carries most of the weight of the drill pipe. This

results in WOB loss because only a very small part of the weight in the drill pipe goes in that direction. Drill collars are utilized when the WOB is sufficient, which increases the compression on the drill string and increases the risk of the drill string buckling (Wu and Juvkam-Wold, 1993). Most of the pipes used to drill the ERD-wells are long and light, which renders them susceptible to compression stresses and results in buckling. Drilling ERD wells becomes challenging and occasionally impossible due to buckling since it locks up the drill string and inhibits further string extension (Belayneh, 2006; Aadnoy, 2006). Once the pipe has exceeded its critical buckling load, it will first experience sinusoidal buckling, then helical buckling, and in the worst-case scenarios, lockup. The latter situation prohibits the string from advancing deeper into the wellbore due to frictional resistance. In figure 10.4 below, the first and second phases of buckling are depicted.

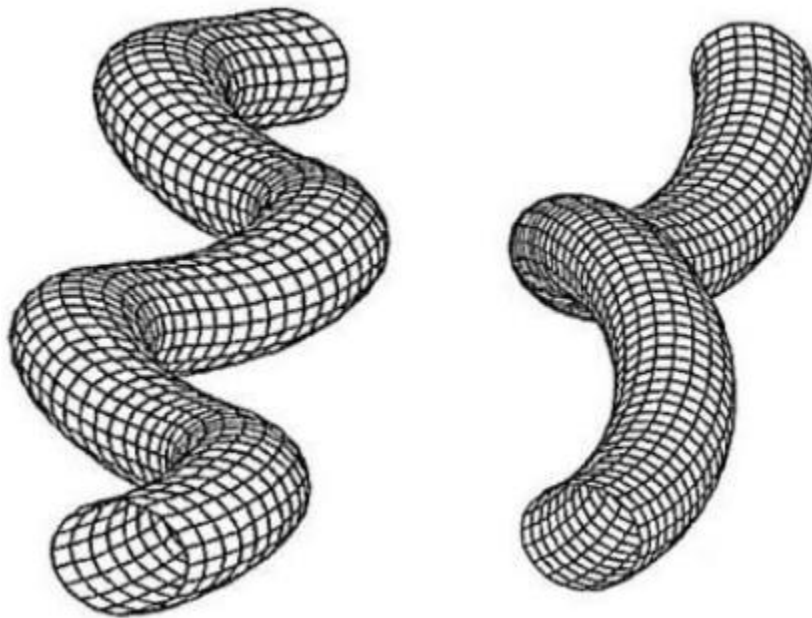


Figure 10.4: Helical Buckling Illustrations

The buckling models can be defined for non-rotating and rotating wellbore circumstances which are described in the following subsections.

Non-Rotating Helical Buckling Models:

The following equation was developed to account for vertical buckling in the wellbore (Belayneh, 2006):

$$F_{Helical} = 5.55(E_{DP}I_{DP}W_{DP,buoyant}^2)^{\frac{1}{3}} \quad (10.5)$$

Where:

- E = Young's modulus
- I = The moment of inertia

The following equations were derived for the critical helical buckling in the build-up section:

$$F_{sinusoidal} = \frac{2E_{DP}I_{DP}k}{r} \left(1 + \sqrt{\frac{W_{DP,bouyant} \sin \alpha r}{E_{DP}I_{DP}k^2}} \right) \quad (10.6)$$

$$k = \frac{1}{R} \quad (10.7)$$

$$F_{helical} = 2.828427 \cdot F_{sinusoidal} \quad (10.8)$$

Where:

- r = Radial clearance between the hole and the outer diameter of the drill pipe
- R = Radius of bended section

A model for the critical buckling of the string in the straight inclined/horizontal part of the wellbore was created based on the energy principle and is represented as follows (Belayneh, 2006):

$$F_{i,helical} = 2\sqrt{2}(E_i I_i)^{\frac{1}{2}} \left(\frac{1}{r_x} \right)^{\frac{1}{2}} \quad (10.9)$$

Where:

- i = The relevant part of DP, and BHA
- r_x = Radius between i and hole

Rotating Helical Buckling Loads

The above buckling models are only valid when the drill string is rotating. The critical buckling load, however, is decreased when torque is applied to the string when rotation is incorporated into the system (Belayneh, 2006).

$$F_{rotating} = F_{non-rotating} \left(1 - \frac{T_{surface}}{\sqrt{\frac{E_i I_i F_{non-rotating}}{2}}} \right)$$

(10.10)

10.2 Rheology Data

10.2.1 Effect of Chia and Mandarin on Bentonite-based drilling fluid

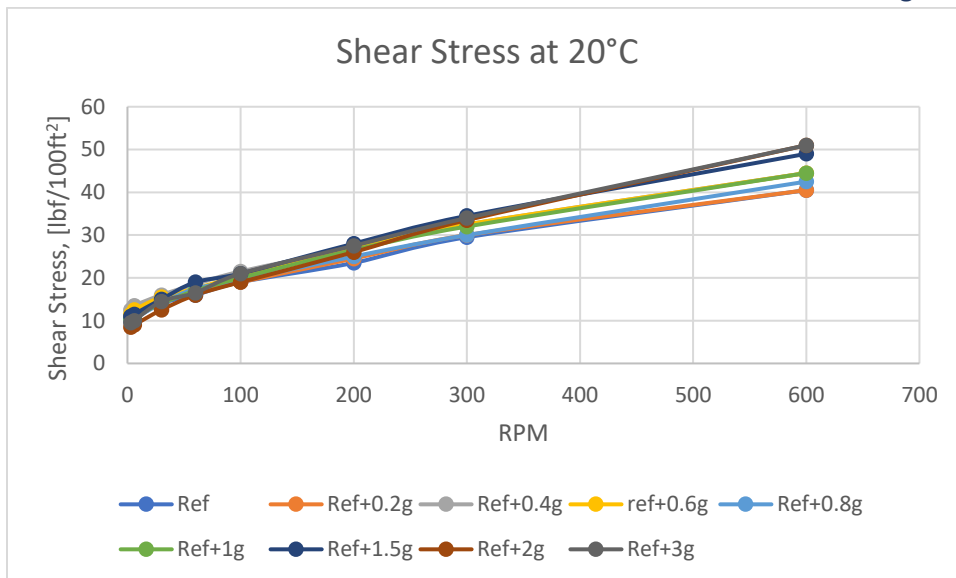


Figure 10.5: Viscometer data at 20°C of bentonite reference fluid and chia

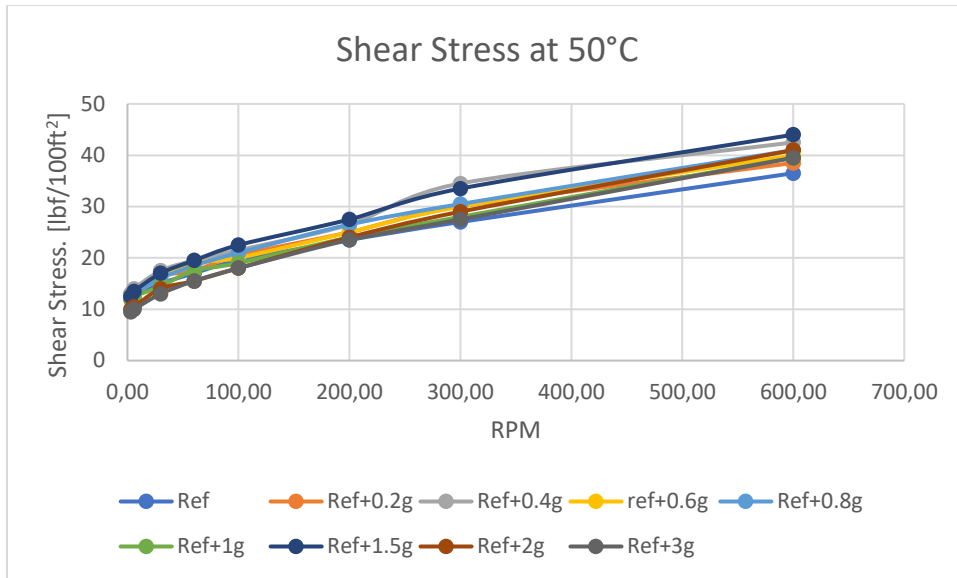


Figure 10.6: Viscometer Data at 50°C of bentonite reference fluid and chia

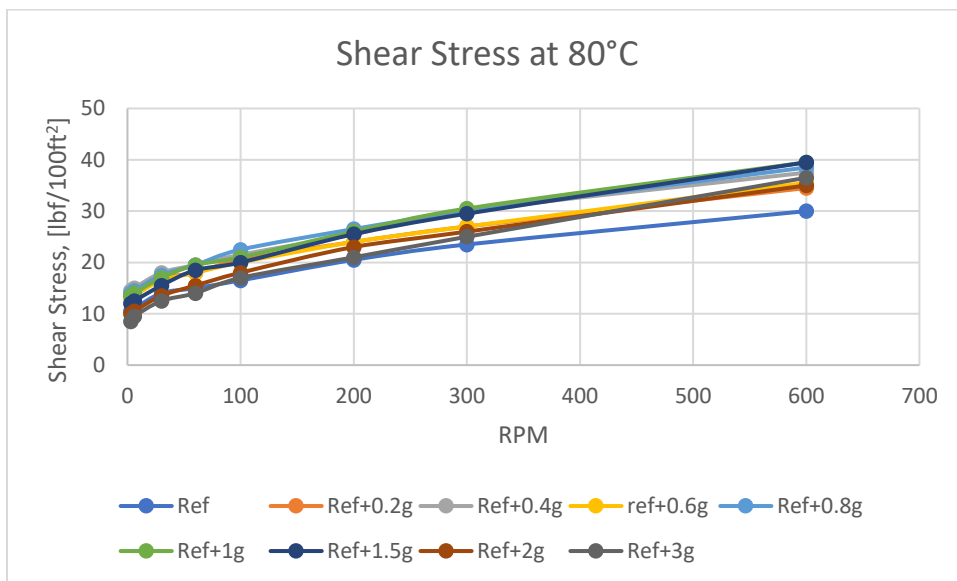


Figure 10.7: Viscometer Data at 80°C of bentonite reference fluid and chia

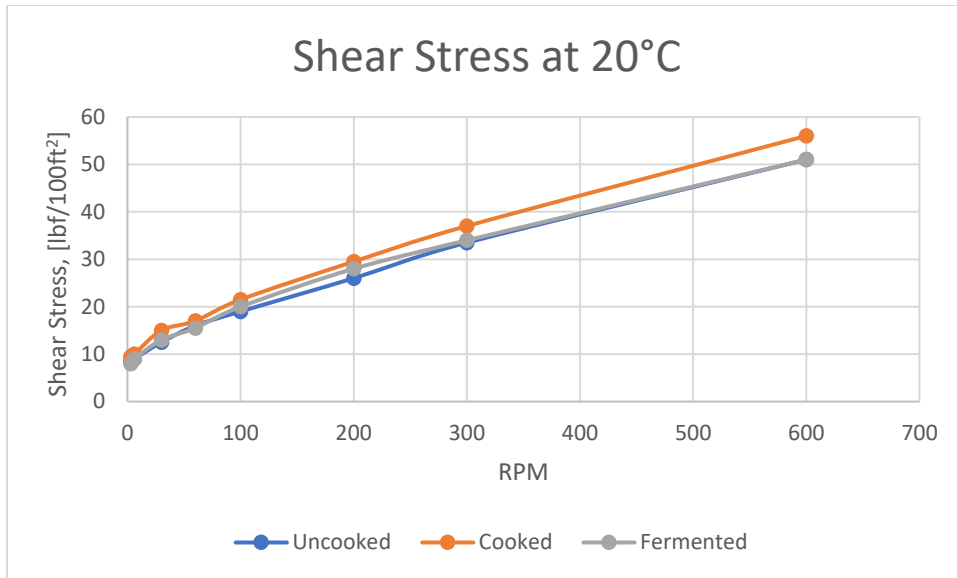


Figure 10.8: Viscometer data at 20°C of bentonite reference fluid and chia preparation

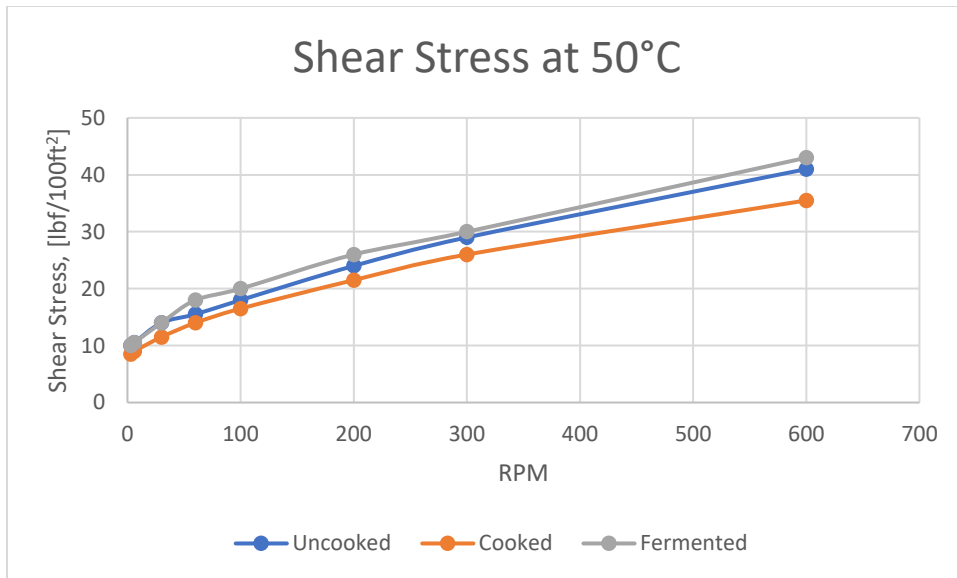


Figure 10.9: Viscometer data at 50°C of bentonite reference fluid and chia preparation

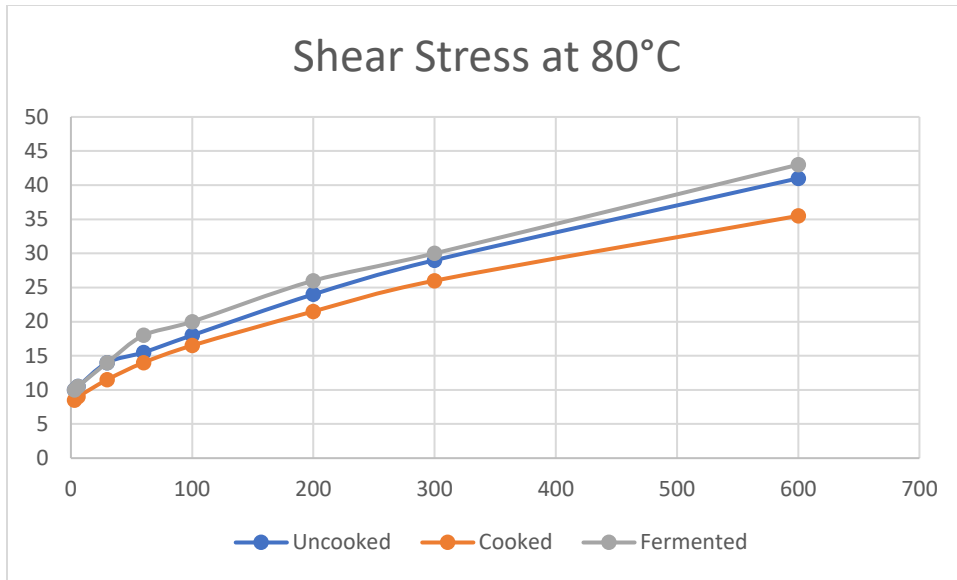


Figure 10.10:Viscometer data at 80°C of bentonite reference fluid and chia preparation

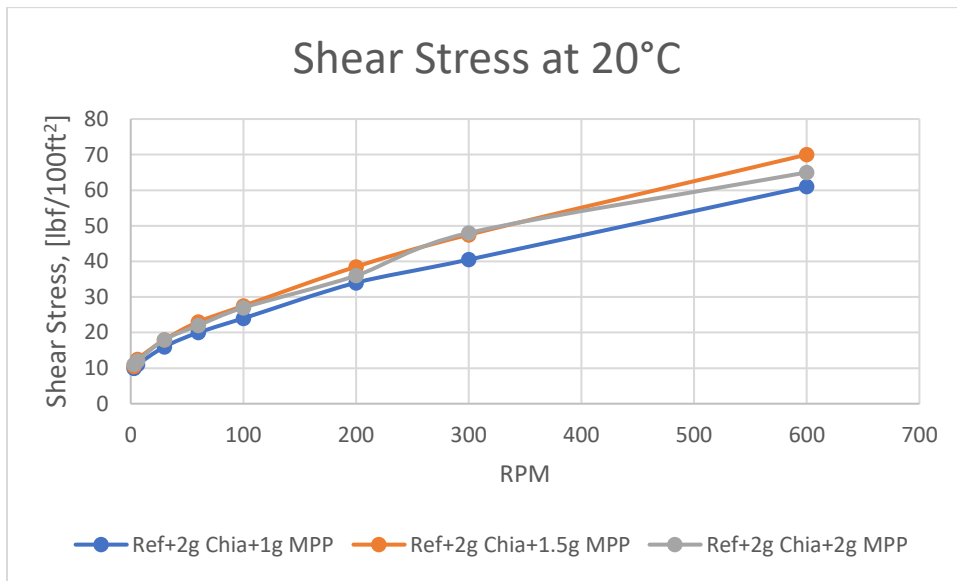


Figure 10.11:Viscometer data at 20°C of bentonite reference fluid and MPP

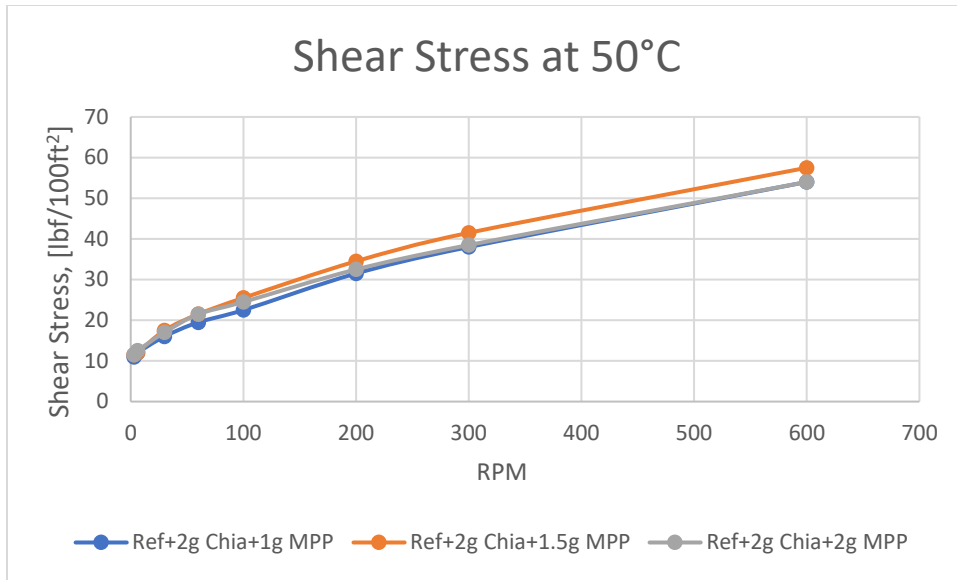


Figure 10.12:Viscometer data at 50°C of bentonite reference fluid and MPP

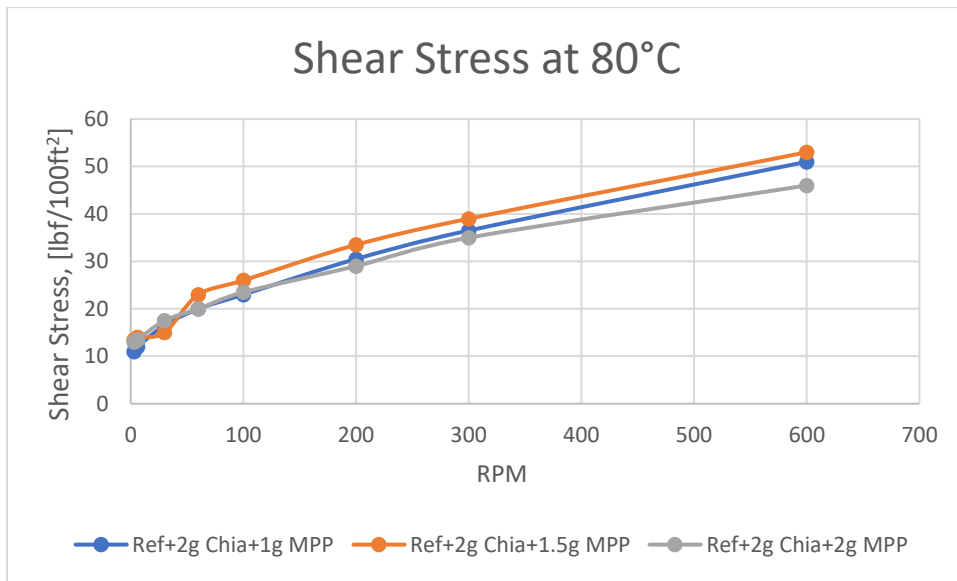


Figure 10.13:Viscometer data at 80°C of bentonite reference fluid and MPP

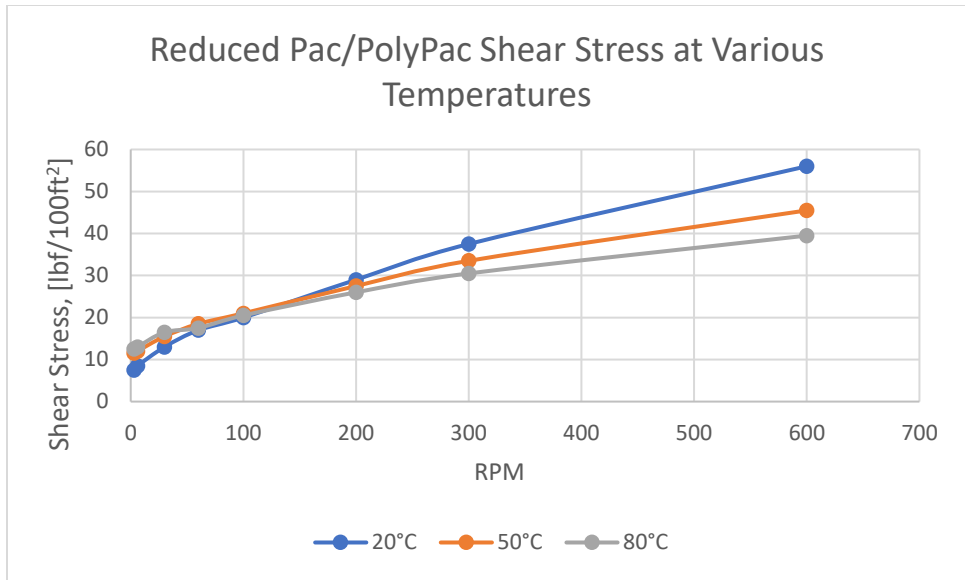


Figure 10.14: Viscometer data for reduced Pac and PolyPac in Bentonite

10.2.2 Effect of Chia and Mandarin on rheology data

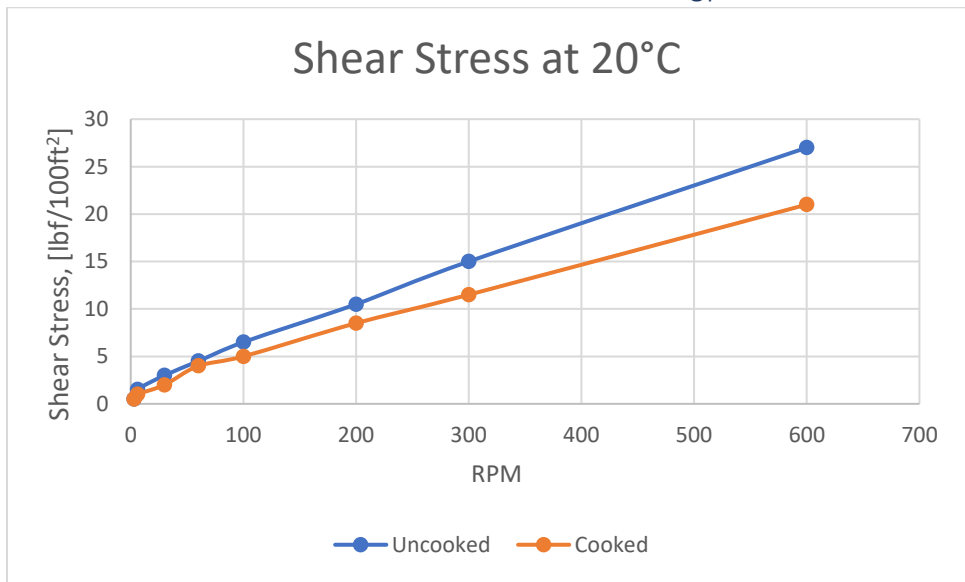


Figure 10.15: Viscometer data at 20°C of KCl and Pac/Polypac reference fluid and chia preparation

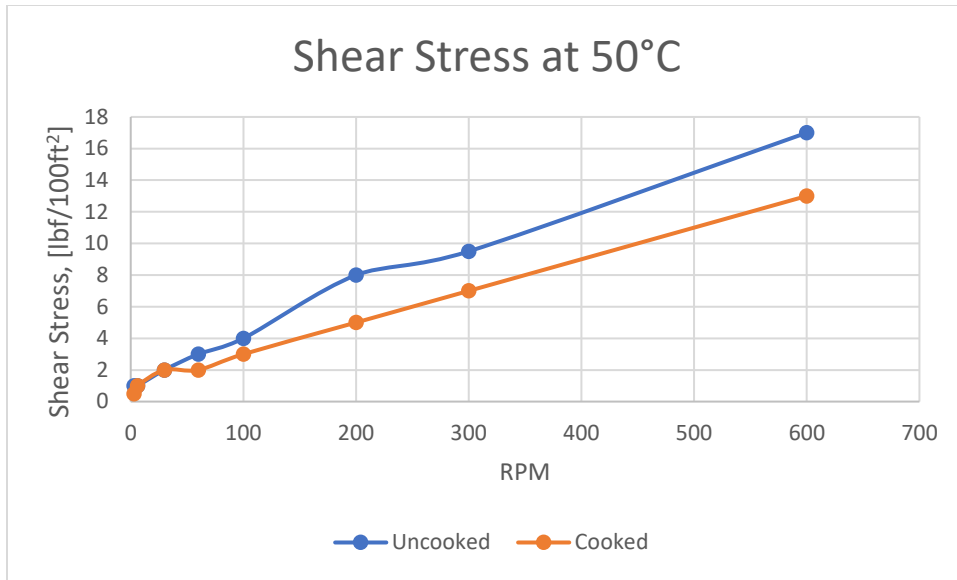


Figure 10.16:Viscometer data at 50°C of KCl and Pac/Polypac reference fluid and chia preparation

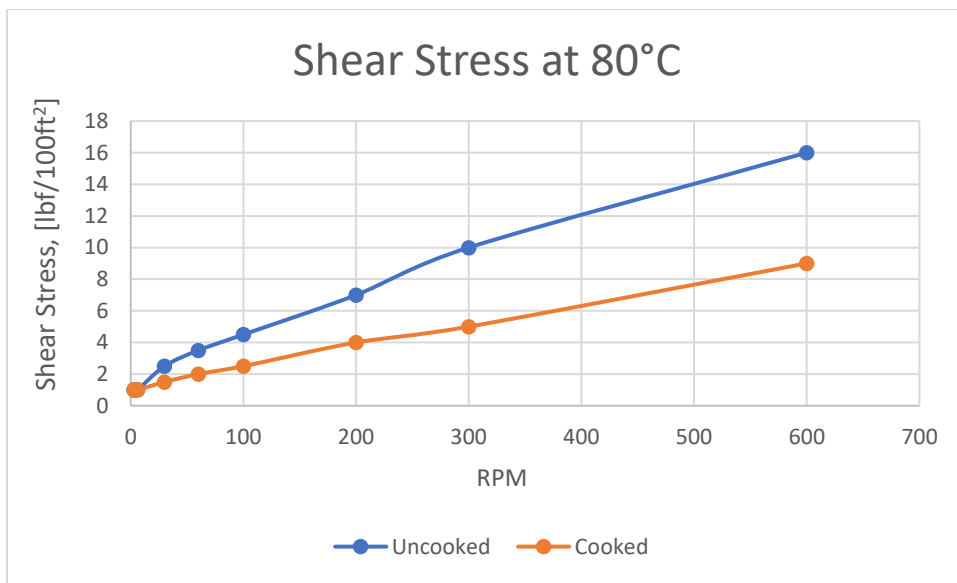


Figure 10.17:Viscometer data at 80°C of KCl and Pac/Polypac reference fluid and chia preparation

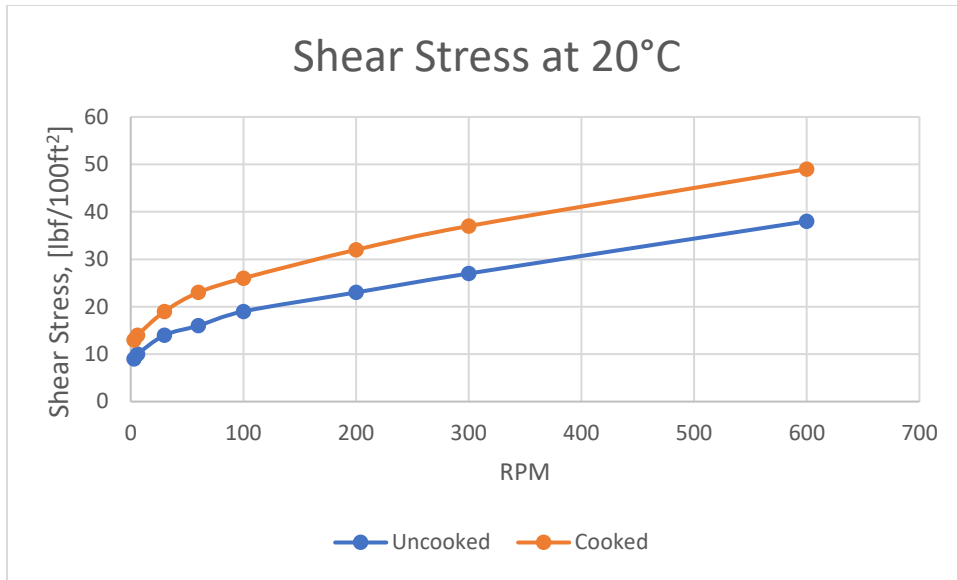


Figure 10.18:Viscometer data at 20°C of KCl and Xanthan Gum reference fluid and chia preparation

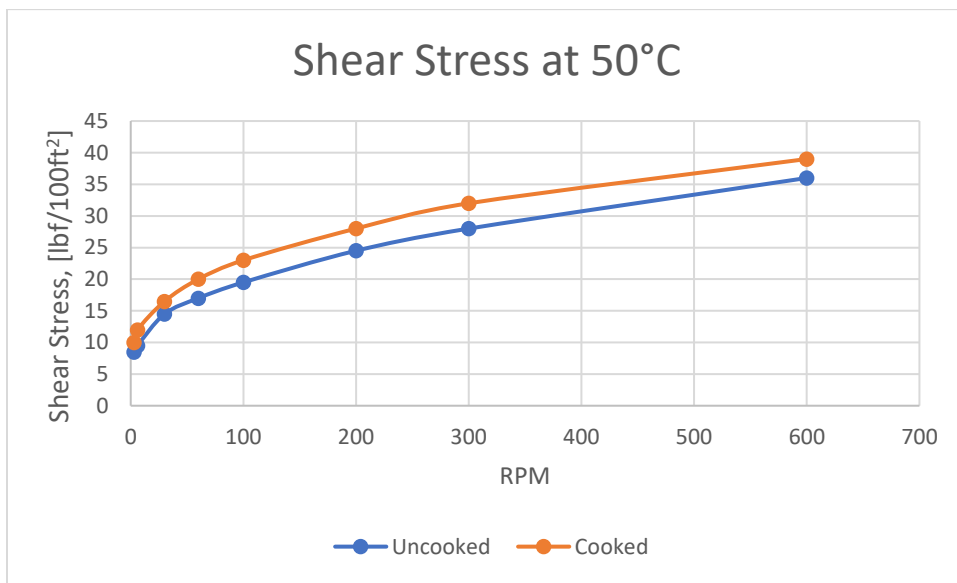


Figure 10.19:Viscometer data at 50°C of KCl and Xanthan Gum reference fluid and chia preparation

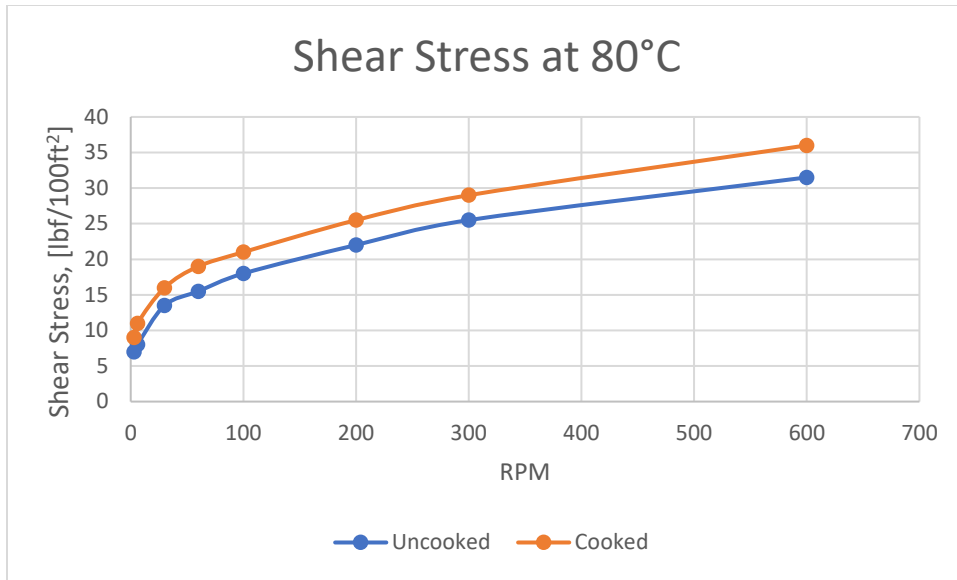


Figure 10.20: Viscometer data at 50°C of KCl and Xanthan Gum reference fluid and chia preparation

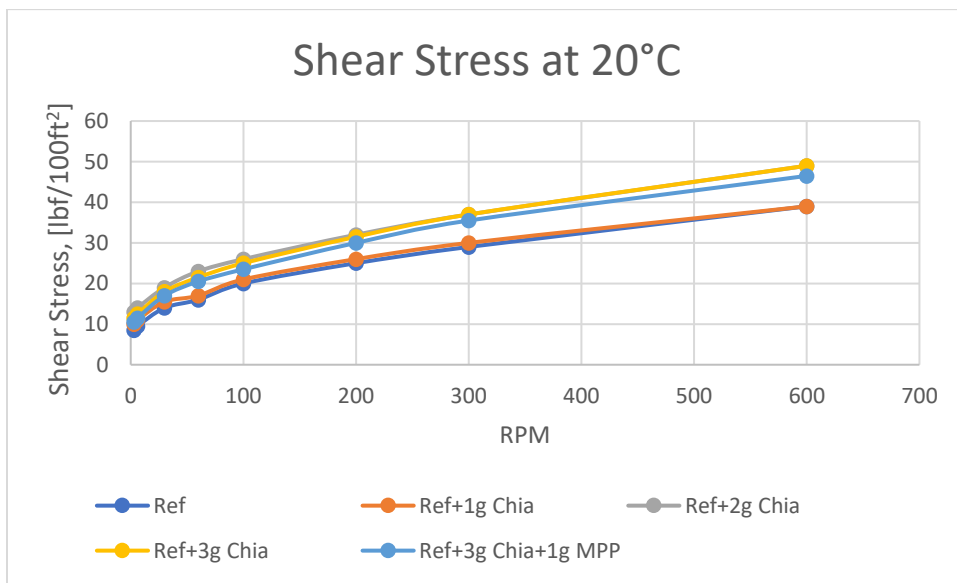


Figure 10.21: Viscometer data at 20°C of KCl and Xanthan Gum reference fluid and chia and MPP

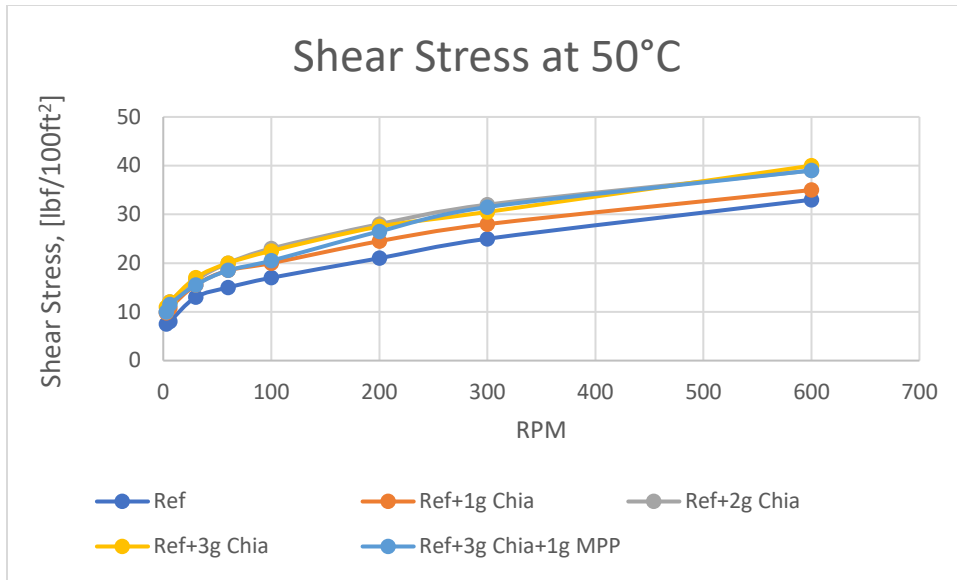


Figure 10.22:Viscometer data at 50°C of KCl and Xanthan Gum reference fluid and chia and MPP

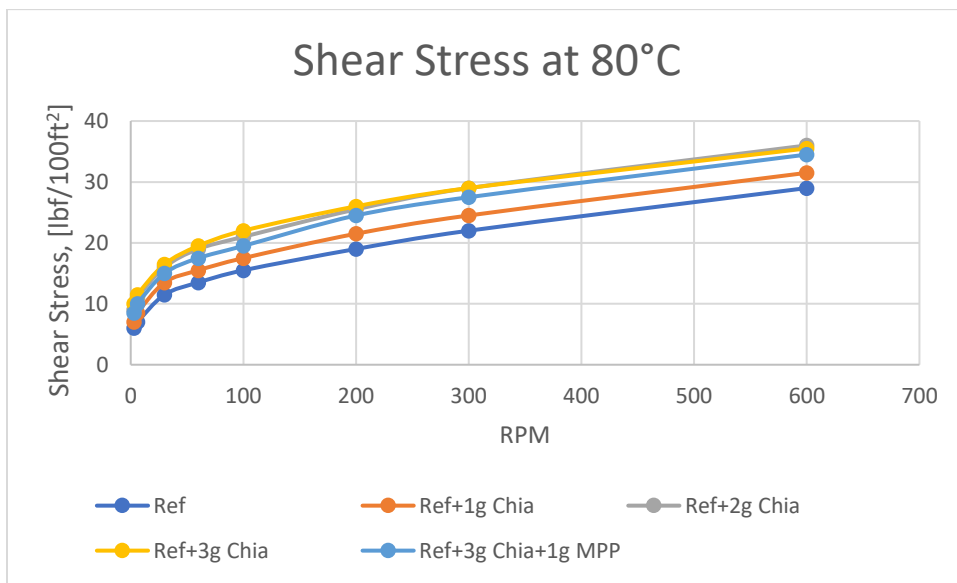


Figure 10.23:Viscometer data at 80°C of KCl and Xanthan Gum reference fluid and chia and MPP

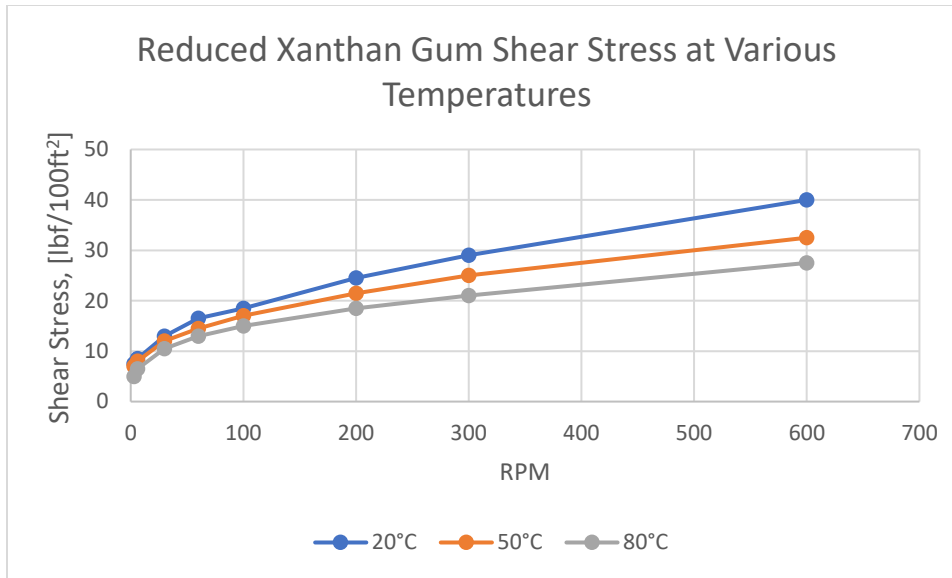


Figure 10.24: Viscometer data of reduced Xanthan Gum at Various Temperatures

10.3 Sag Factor Data

Top										
Vol	Ref	Ref+0,2 g Chia	Ref+0,4 g Chia	Ref+0,6 g Chia	Ref+0, 8 Chia	Ref+1 g Chia	Ref+1, 5 Chia	Ref+2g Chia uncooke d	Ref+2 g Chia cooke d	Ref+3 g Chia
10	n/a	n/a	n/a	n/a	n/a	n/a	n/a	19,15	19,33	18,86
9	n/a	n/a	n/a	n/a	n/a	n/a	n/a	17,87	18,04	17,24
8	n/a	n/a	n/a	n/a	n/a	n/a	n/a	16,56	16,68	16,23
7	n/a	n/a	n/a	n/a	n/a	n/a	n/a	15,25	15,37	15,01
6	n/a	n/a	n/a	n/a	n/a	n/a	n/a	14,03	14,07	13,75
5	12,6	12,59	12,67	12,88	12,82	12,58	12,5	12,72	12,82	12,39
4	11,42	11,22	11,44	11,41	11,57	11,32	11,3	11,41	11,4	11,15
3	9,97	10,12	9,94	10,21	10,3	9,92	10,04	10,09	10,11	9,78
2	8,73	8,72	8,69	8,85	8,91	8,74	8,69	8,73	8,79	8,57
1	7,38	7,44	7,41	7,5	7,57	7,41	7,47	7,5	7,54	7,37
Mass syringe	5,92	5,9	5,87	5,88	5,88	5,9	5,93	5,88	5,91	5,92

Table 10.5: Top Sag Factor Data for Chia in Bentonite

Bottom										
Vol	Ref	Ref+0,2 g Chia	Ref+0,4 g Chia	Ref+0,6 g Chia	Ref+0, 8 Chia	Ref+1 g Chia	Ref+1, 5 Chia	Ref+2g Chia uncooke d	Ref+2 g Chia cooke d	Ref+3 g Chia
10	n/a	n/a	n/a	n/a	n/a	n/a	n/a	19	19,34	19,28
9	n/a	n/a	n/a	n/a	n/a	n/a	n/a	17,76	17,94	18,06
8	17,1 5	16,9	16,92	16,79	16,83	16,67	16,9	16,29	16,56	16,68
7	15,6 7	15,57	15,53	15,49	15,51	15,41	15,55	15,17	15,29	15,37
6	14,3 6	14,25	14,24	14,18	14,2	14,11	14,22	13,81	14	14,1
5	13,0 5	12,96	12,83	12,89	12,88	12,86	12,88	12,59	12,68	12,78
4	11,7 9	11,7	11,45	11,43	11,57	11,57	11,61	11,24	11,26	11,44
3	10,3 4	10,37	10,19	10,11	10,24	10,23	10,27	9,95	9,96	10,13
2	9,01	8,93	8,84	8,66	8,96	8,95	8,87	8,61	8,64	8,89
1	7,67	7,74	7,54	7,4	7,6	7,64	7,56	7,39	7,4	7,58
Mass syring e	5,87	5,92	5,94	5,91	5,92	5,89	5,89	5,9	5,91	5,87

Table 10.6: Bottom Sag Factor Data for Chia in Bentonite

Top				Bottom		
Vol	Ref+2g Chia+1g mandarin	Ref+2g Chia+1.5g mand	Ref+2g Chia+2g mand	Ref+2g Chia+1g mandarin	Ref+2g Chia+1.5g mand	Ref+2g Chia+2g mand
10	18,96	19,15	18,95	19,24	19,15	19,14
9	17,71	17,74	17,65	17,96	17,89	17,88
8	16,42	16,61	16,44	16,64	16,64	16,53
7	15,15	15,27	15,2	15,33	15,26	15,24
6	13,88	13,98	13,94	14,03	13,96	13,89
5	12,57	12,68	12,62	12,74	12,6	12,61
4	11,32	11,36	11,36	11,4	11,28	11,32
3	10	10,11	10,21	10,03	9,99	10
2	8,71	8,87	8,87	8,85	8,71	8,8
1	7,36	7,54	7,65	7,54	7,42	7,48
Mass syringe	5,9	5,87	5,91	5,89	5,92	5,9

Table 10.7: Top and Bottom Sag Factor Data for MPP in Bentonite

Vol	Kcl pac/polypac cooked	Kcl pac/polypac uncooked	Kcl pac/polypac cooked	Kcl pac/polypac uncooked
10	16,57	16,55	27,33	26,05
9	15,55	15,47	25,33	24,19
8	14,48	14,4	23,31	22,22
7	13,45	13,38	21,16	20,45
6	12,37	12,35	18,98	18,52
5	11,37	11,33	16,99	16,33
4	10,3	10,21	14,71	14,39
3	9,26	9,18	12,56	12,28
2	8,2	8,14	10,31	10,19
1	7,13	7,11	8,13	8,06
Mass syringe	5,85	5,9	5,9	5,93

Table 10.8: KCl with Pac and Polypac top and bottom sag factor data

Top							
Vol	Ref+2g Chia Cooked	Ref+2g Chia uncooked	Ref	Ref+2g XG +2g Chia	Ref +1g chia	Ref+3g chia	KCL+3g Chia+1g Mandarin
10	-	19,21	19,17	19,45	19,14	19,45	19,33
9	18,07	17,89	17,8	18,01	17,84	18,21	18,02
8	16,69	16,67	16,48	16,7	16,52	16,95	16,85
7	15,49	15,36	15,24	15,35	15,26	15,41	15,5
6	14,07	14,03	13,85	14,16	13,96	14,3	14,17
5	12,69	12,76	12,57	12,69	12,65	13,09	12,85
4	11,42	11,43	11,32	11,47	11,29	11,75	11,57
3	10,08	10,11	9,94	10,19	10,02	10,42	10,29
2	8,78	8,81	8,74	8,85	8,7	9,07	8,94
1	7,38	7,48	7,41	7,59	7,39	7,7	7,57
Mass syringe	5,9	5,85	5,92	5,89	5,93	5,9	6

Table 10.9: Top Sag Factor data for KCl with Xanthan Gum, Chia and MPP

Bottom							
Vol	Ref	Ref+2g Chia Cooked	Ref+2g Chia uncooked	Ref+2g XG +2g Chia	Ref +1g chia	Ref+3g chia	KCL+3g Chia+1g Mandarin
10	19,45	19,4	19,35	19,09	19,41	19,36	19,31
9	18,06	18,05	17,95	17,79	18,09	18,15	18,03
8	16,82	16,79	16,6	16,49	16,78	16,87	16,73
7	15,46	15,48	15,3	15,15	15,51	15,48	15,42
6	14,14	14,17	13,98	13,79	14,14	14,09	14,17
5	12,82	12,83	12,69	12,52	12,83	12,71	12,82
4	11,51	11,5	11,44	11,22	11,45	11,37	11,49
3	10,09	10,13	10,15	9,84	10,12	10,04	10,19
2	8,86	8,79	8,83	8,59	8,73	8,68	8,85
1	7,49	7,51	7,38	7,24	7,4	7,37	7,49
Mass syringe	5,91	6,01	5,91	5,95	5,86	5,88	6

Table 10.10: Bottom Sag Factor data for KCl with Xanthan Gum, Chia and MPP

10.4 Results from Hydraulics Simulations

10.4.1 Annular Pressure Loss

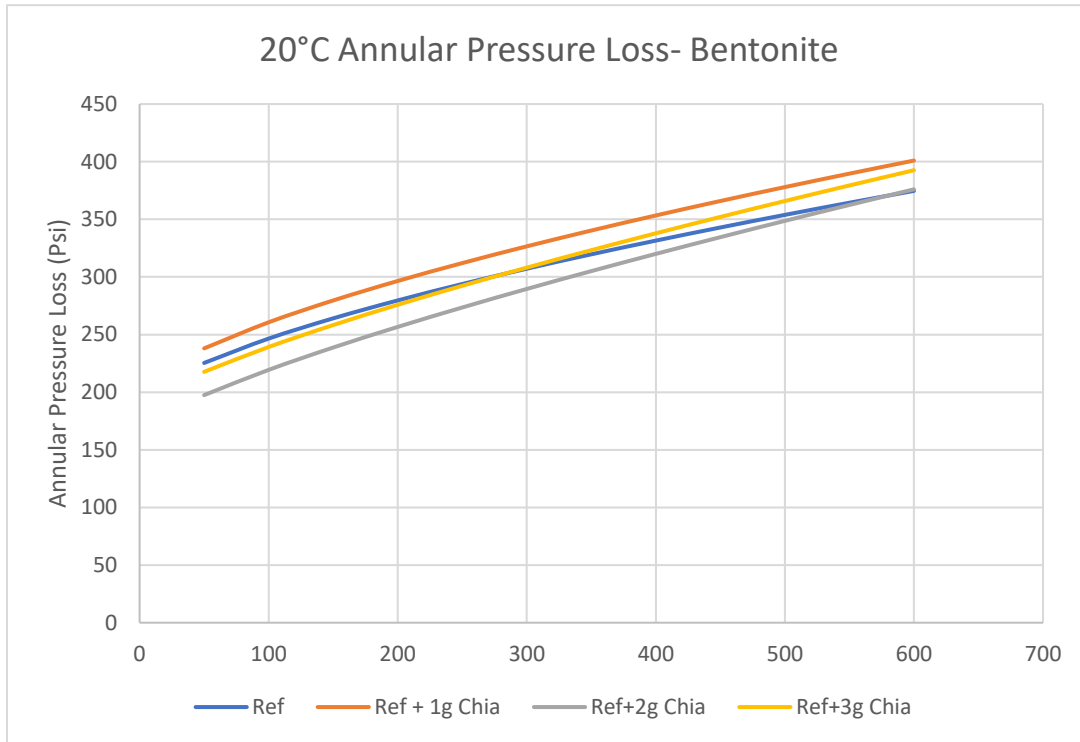


Figure 10.25: Annular Pressure Loss of chia in bentonite at 20°C

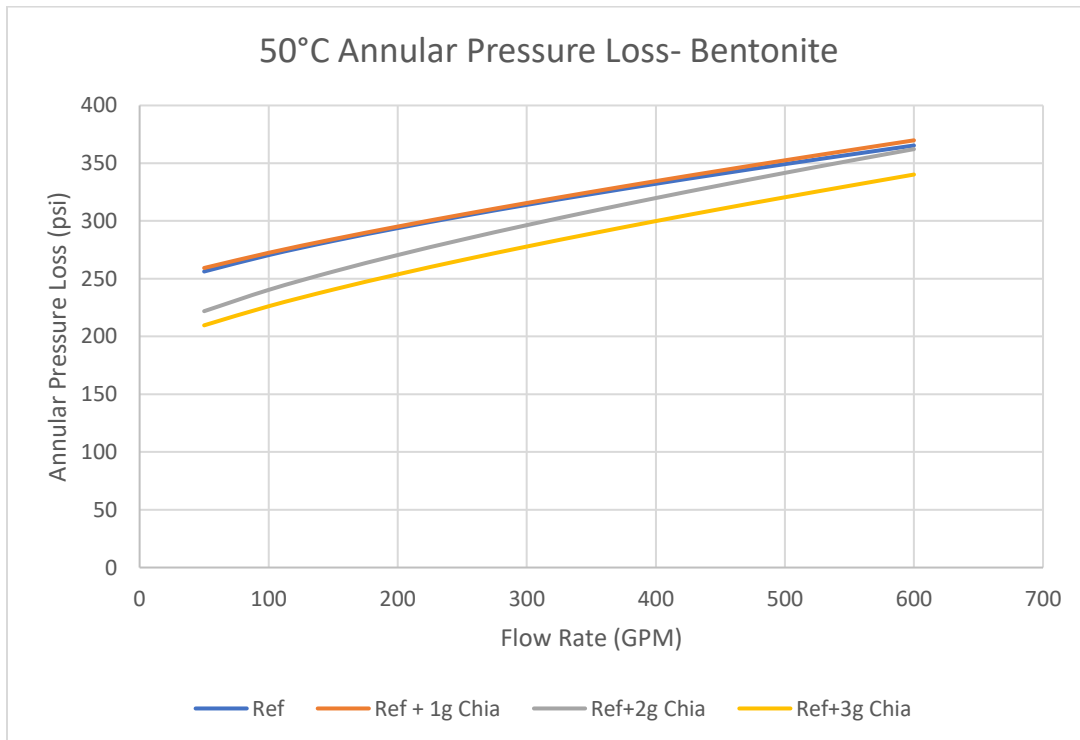


Figure 10.26: Annular Pressure Loss of chia in bentonite at 50°C

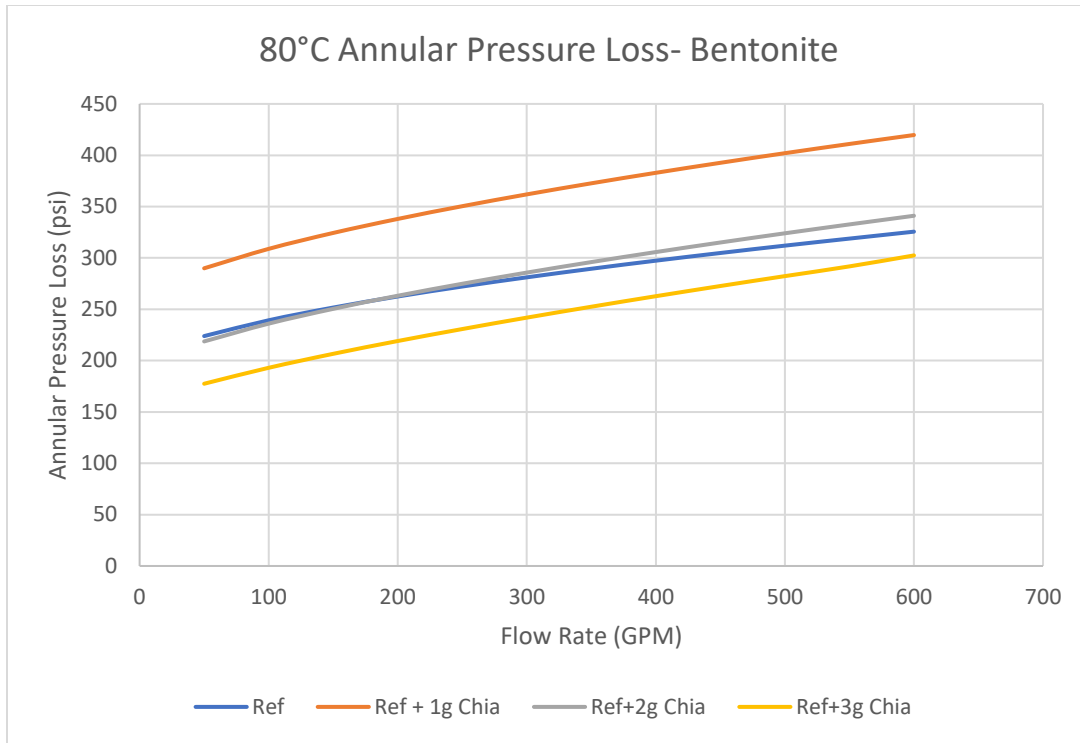


Figure 10.27: Annular Pressure Loss of chia in bentonite at 80°C

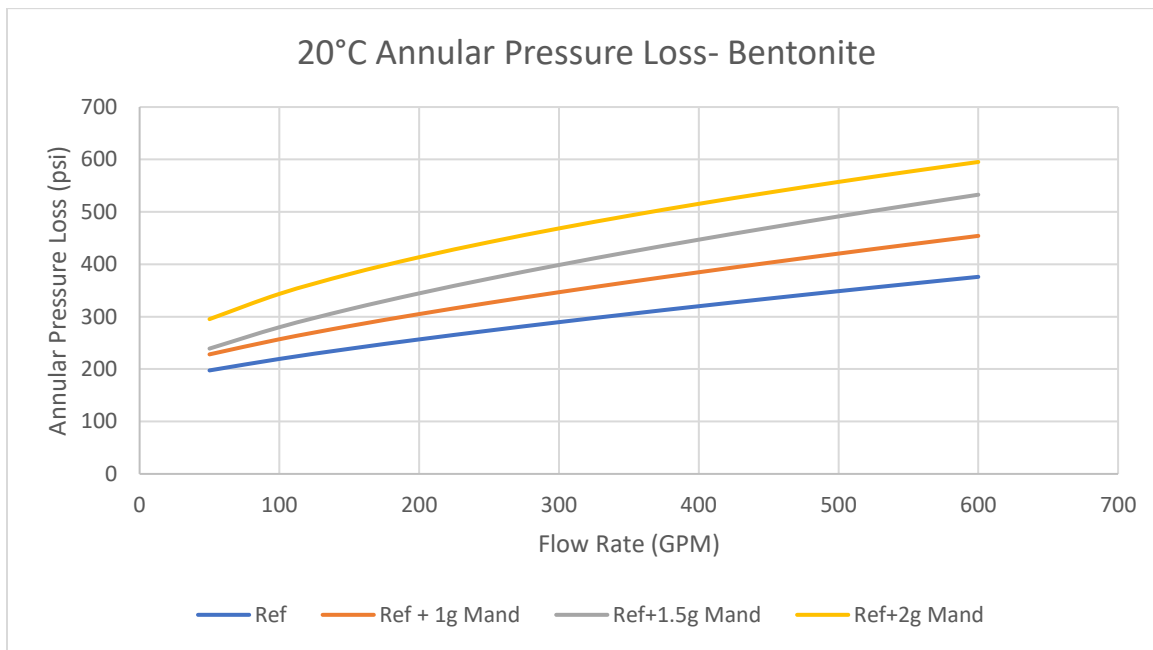


Figure 10.28: Annular Pressure Loss of MPP in bentonite at 20°C

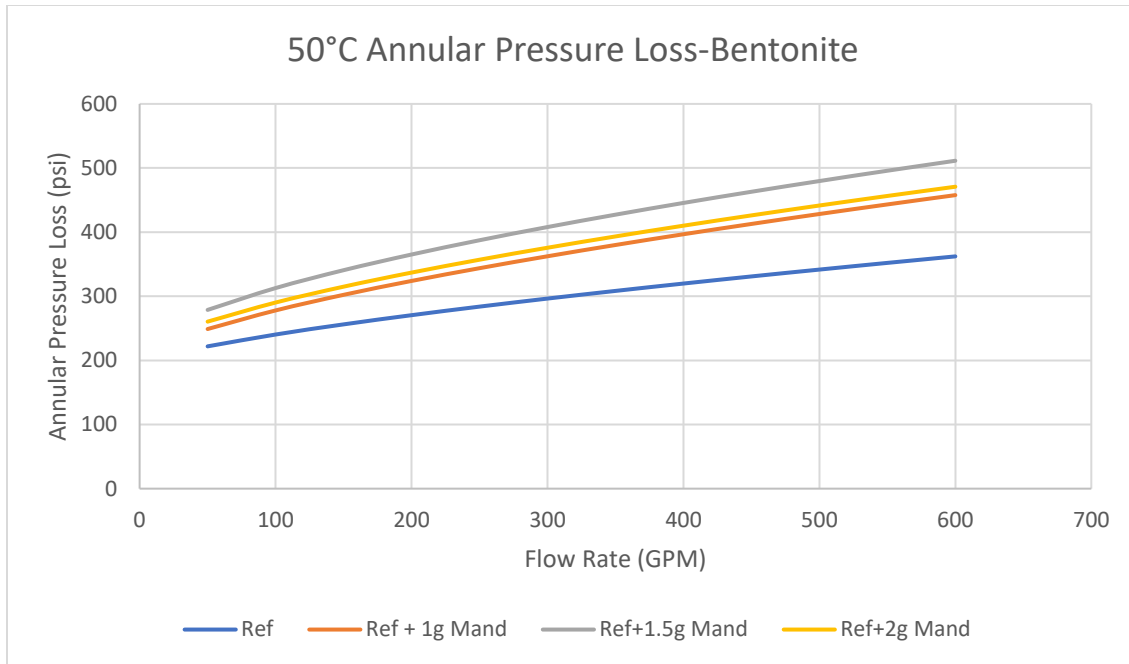


Figure 10.29: Annular Pressure Loss of MPP in bentonite at 50°C

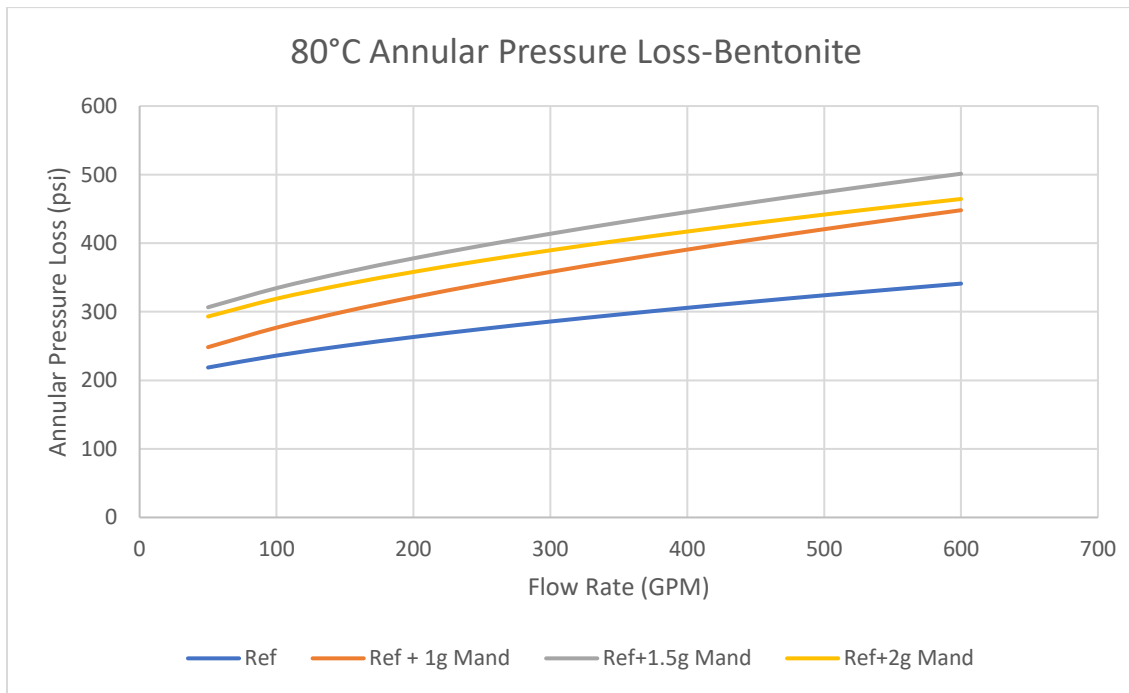


Figure 10.30: Annular Pressure Loss of MPP in bentonite at 80°C

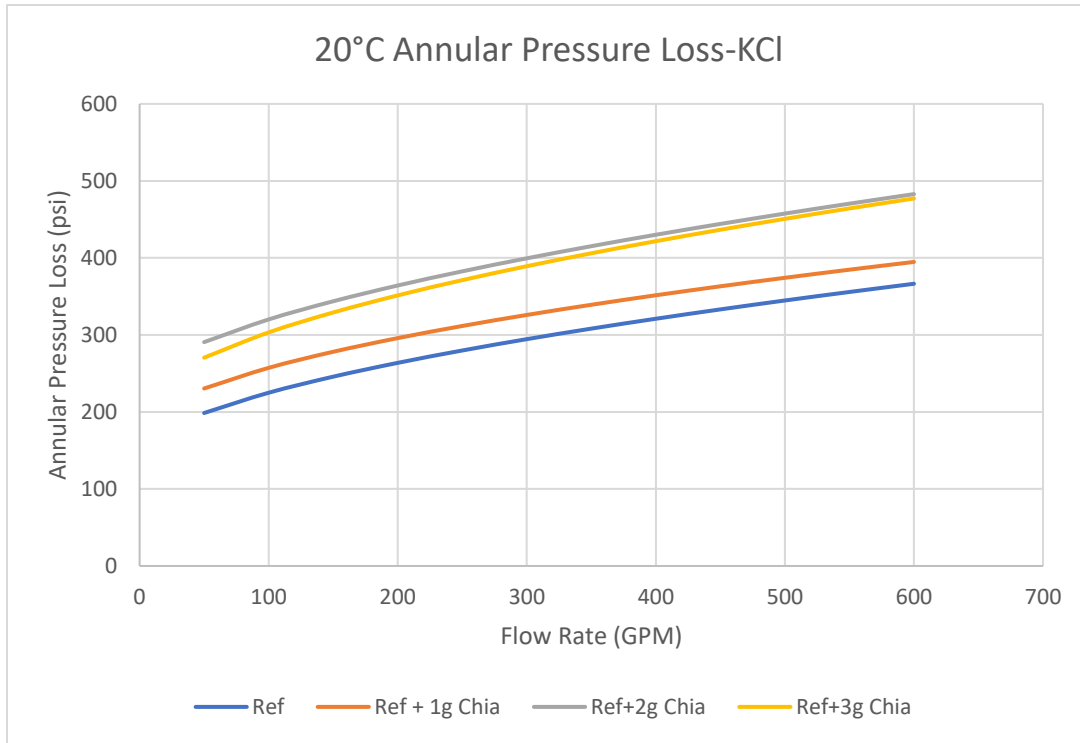


Figure 10.31: Annular Pressure Loss of chia in KCl at 20°C

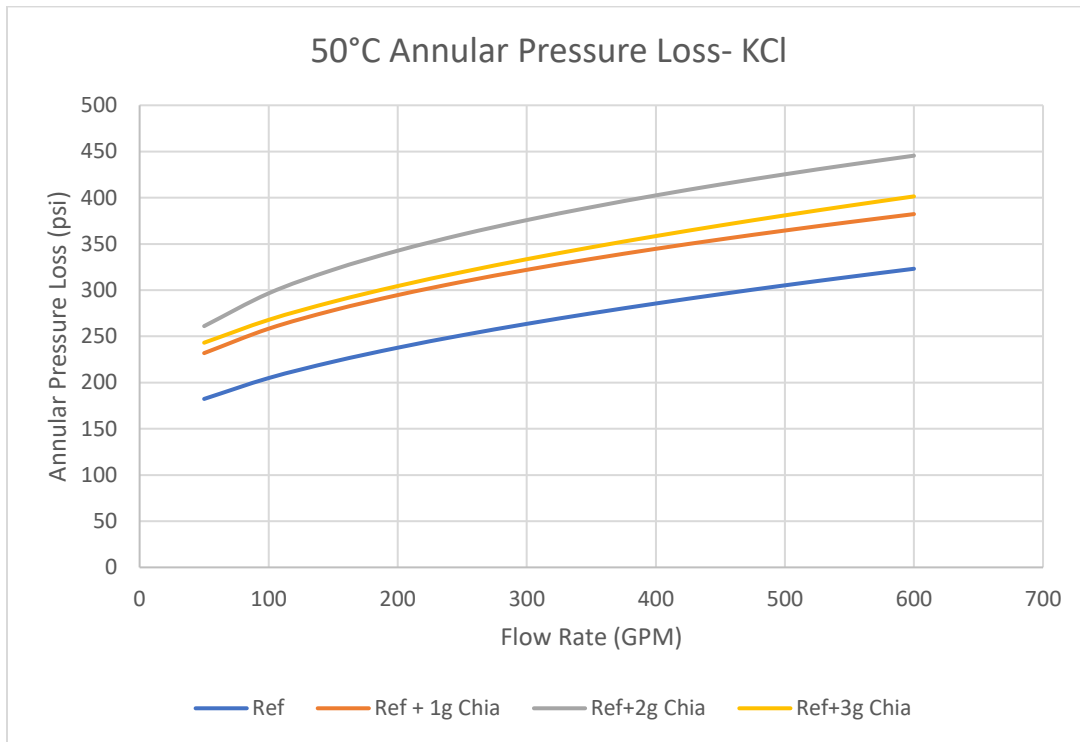


Figure 10.32: Annular Pressure Loss of chia in KCl at 50°C

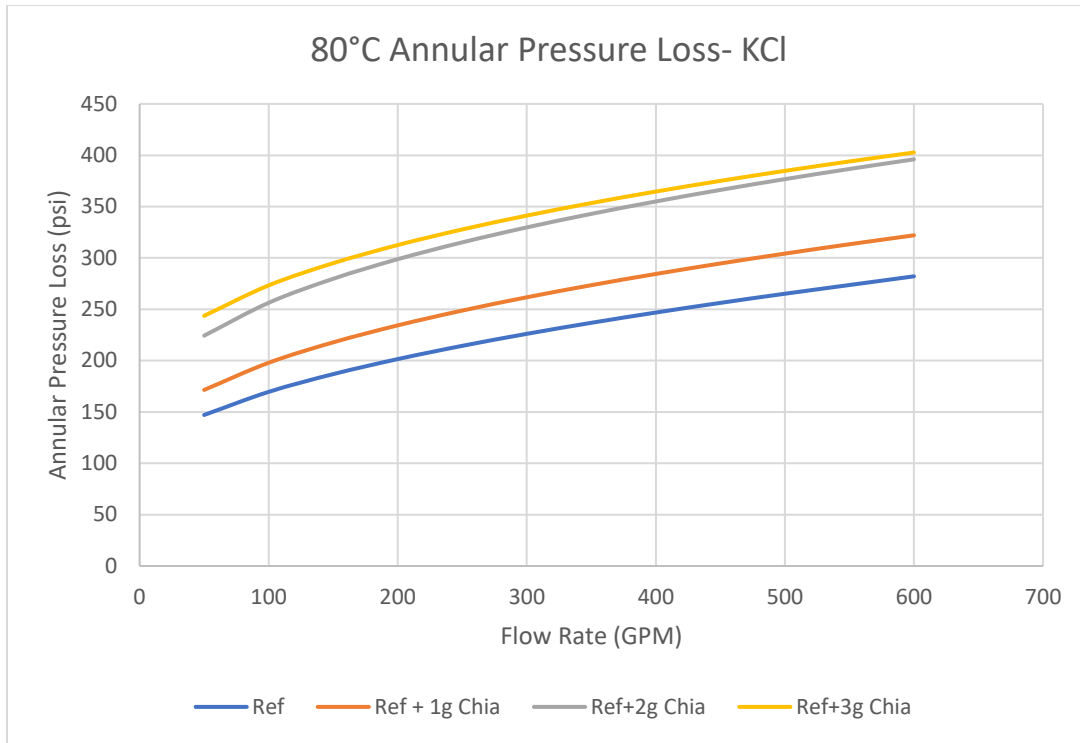


Figure 10.33: Annular Pressure Loss of chia in KCl at 80°C

10.4.2 Pump Pressures

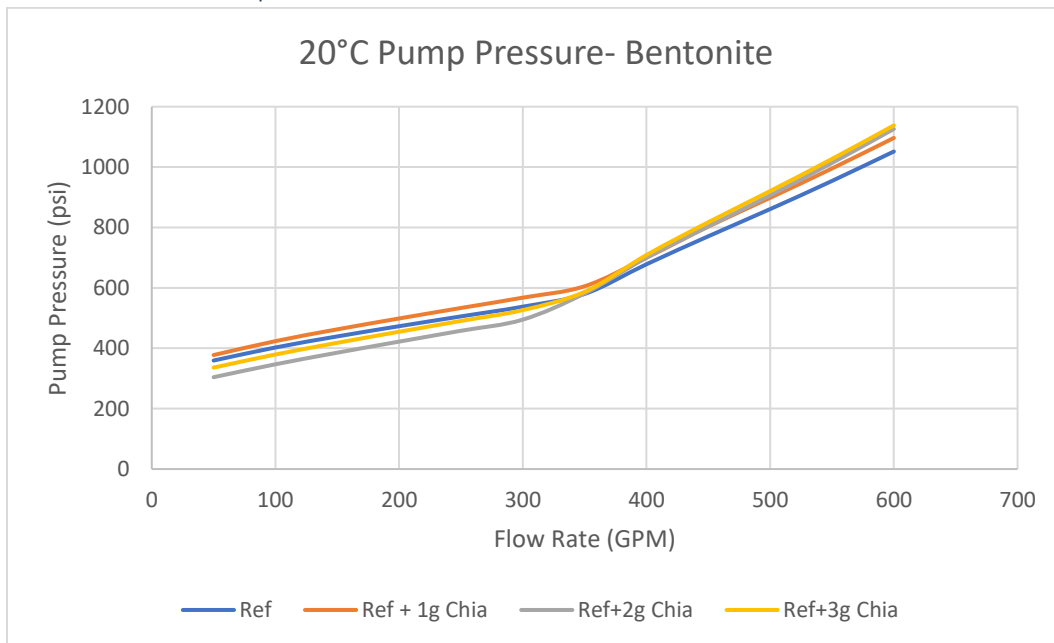


Figure 10.34: Pump Pressure of chia in bentonite at 20°C

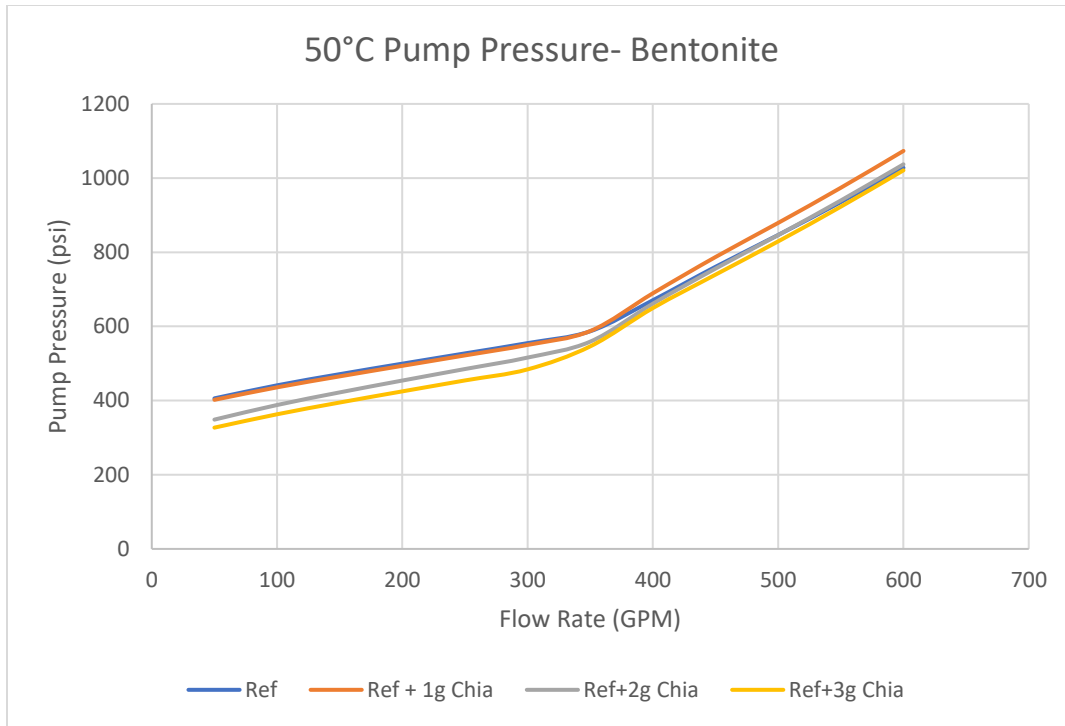


Figure 10.35: Pump Pressure of chia in bentonite at 50°C

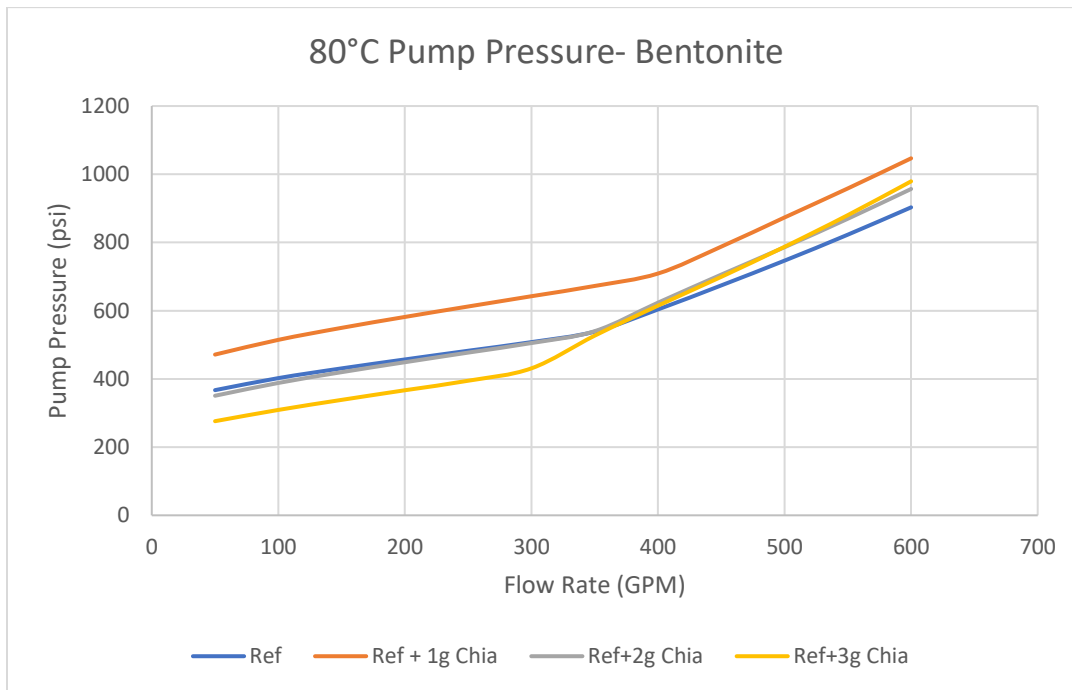


Figure 10.36: Pump Pressure of chia in bentonite at 80°C

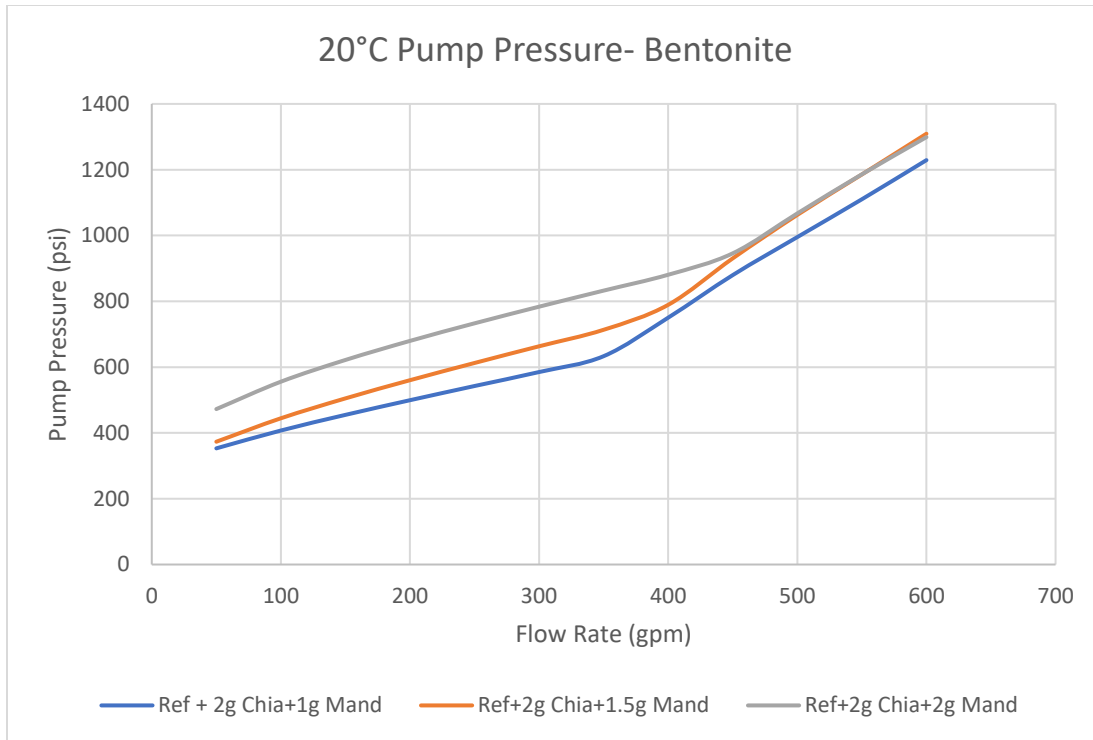


Figure 10.37: Pump Pressure of MPP in Bentonite at 20°C

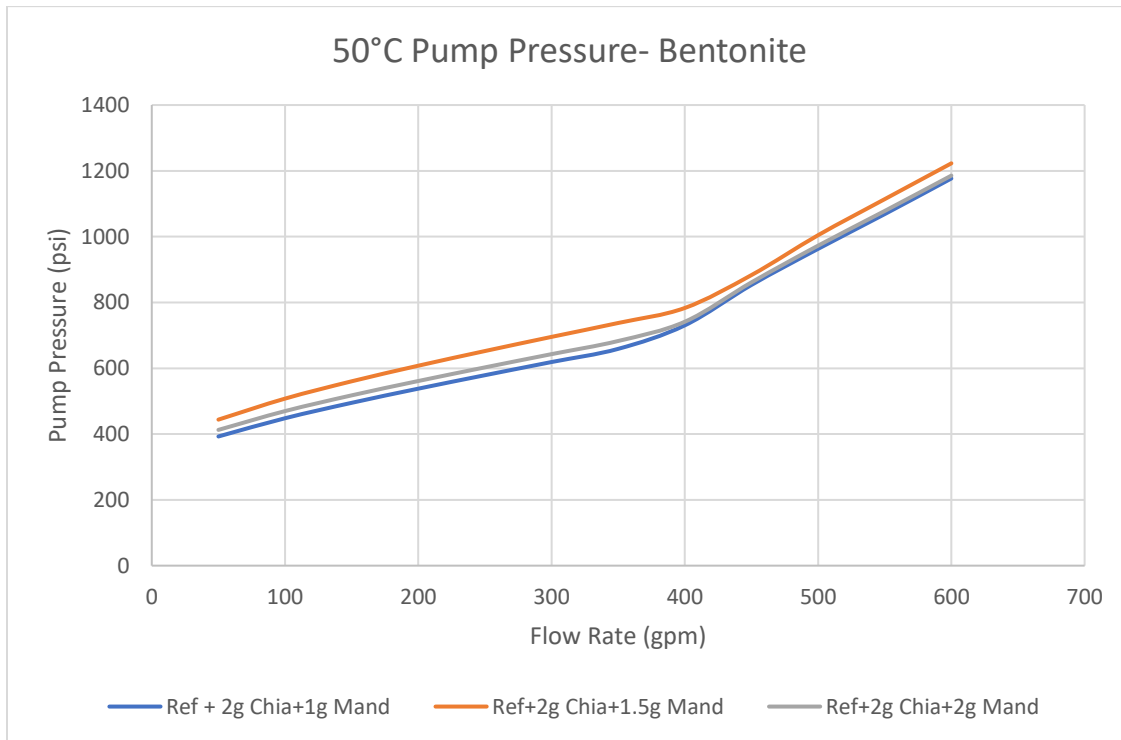


Figure 10.38: Pump Pressure of MPP in Bentonite at 50°C

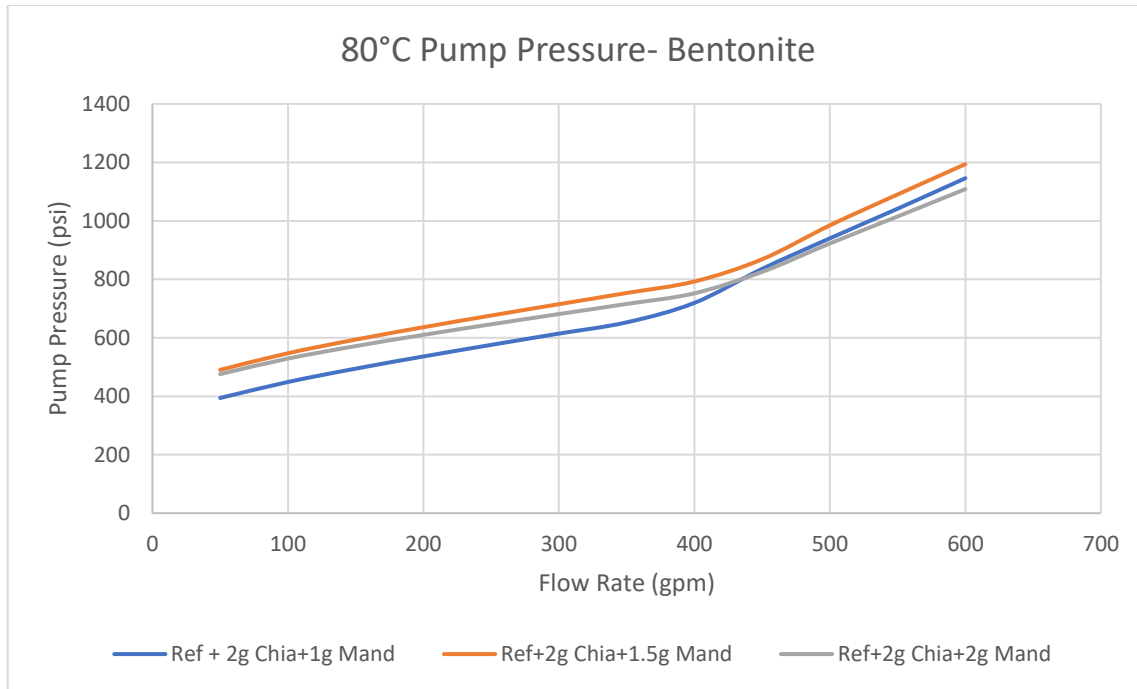


Figure 10.39: Pump Pressure of MPP in Bentonite at 80°C

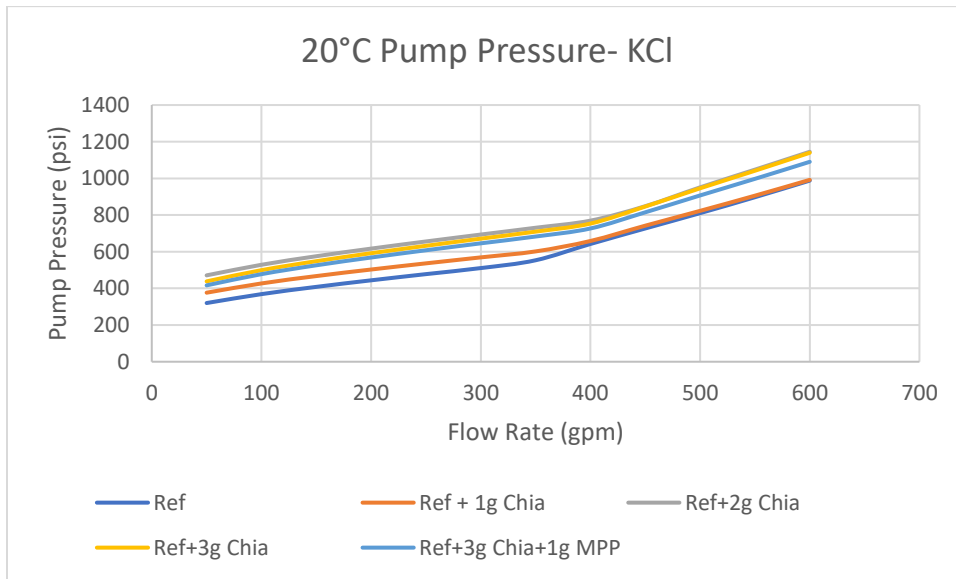


Figure 10.40: Pump Pressure of Chia and MPP in KCl at 20°C

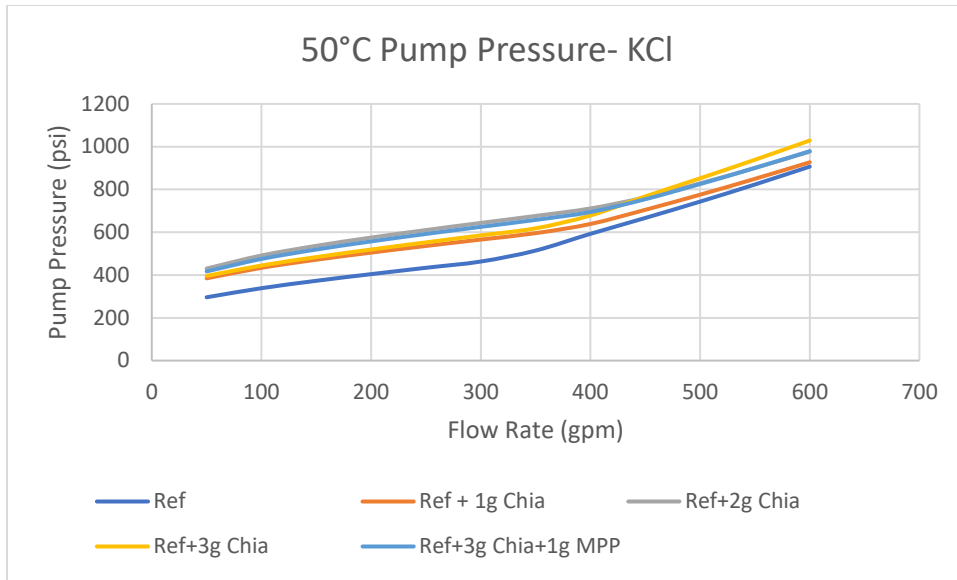


Figure 10.41: Pump Pressure of Chia and MPP in KCl at 50°C

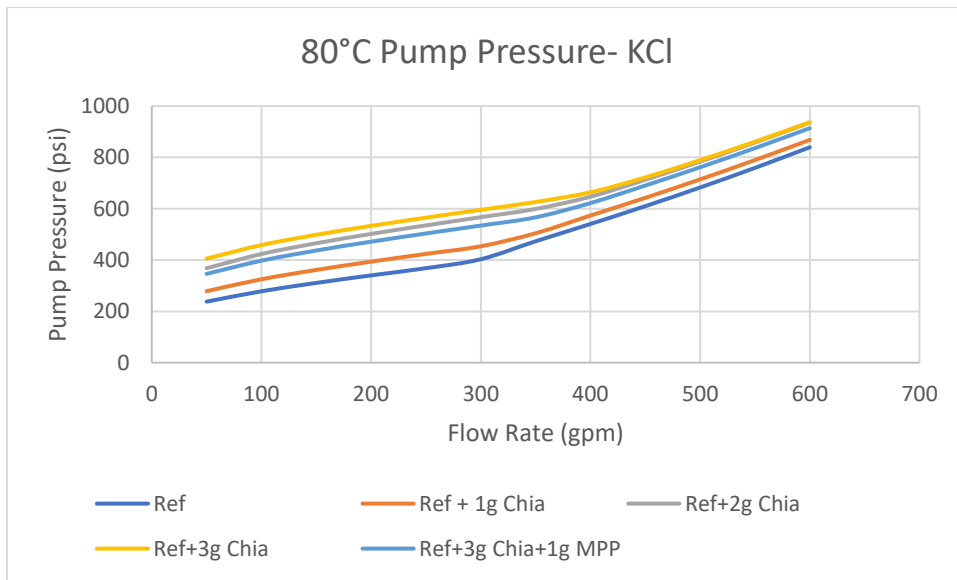


Figure 10.42: Pump Pressure of Chia and MPP in KCl at 80°C

10.4.3 ECD

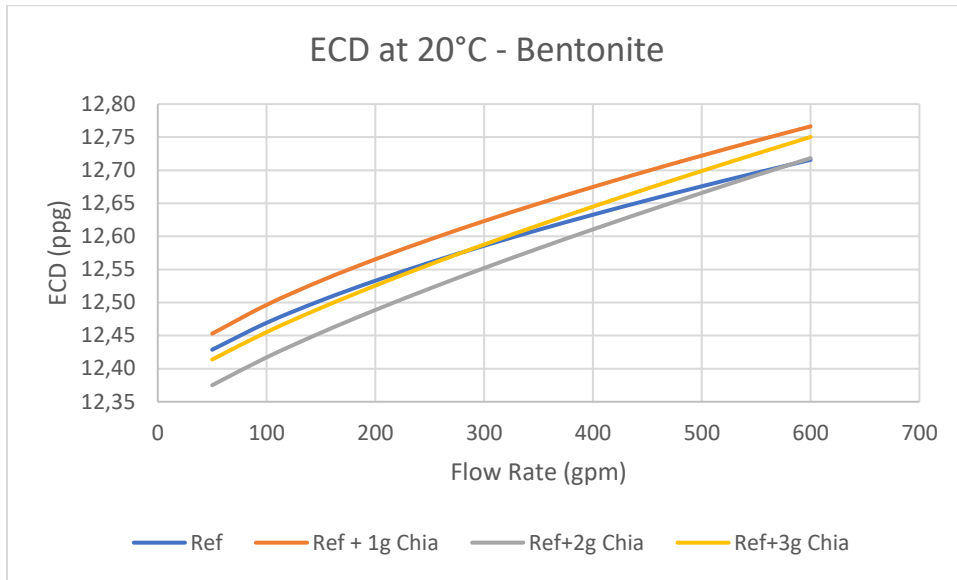


Figure 10.43: ECD of Chia in Bentonite at 20°C

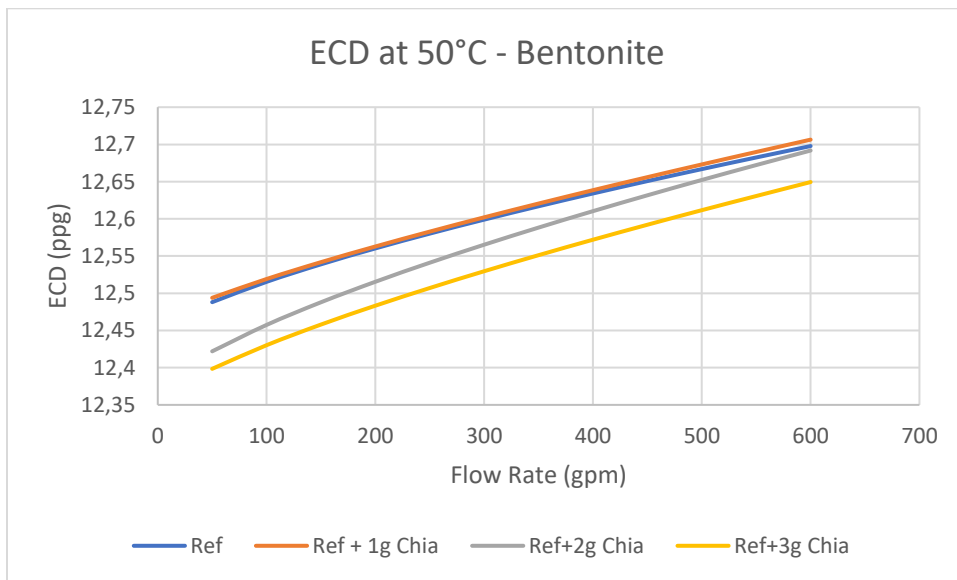


Figure 10.44: ECD of Chia in Bentonite at 50°C

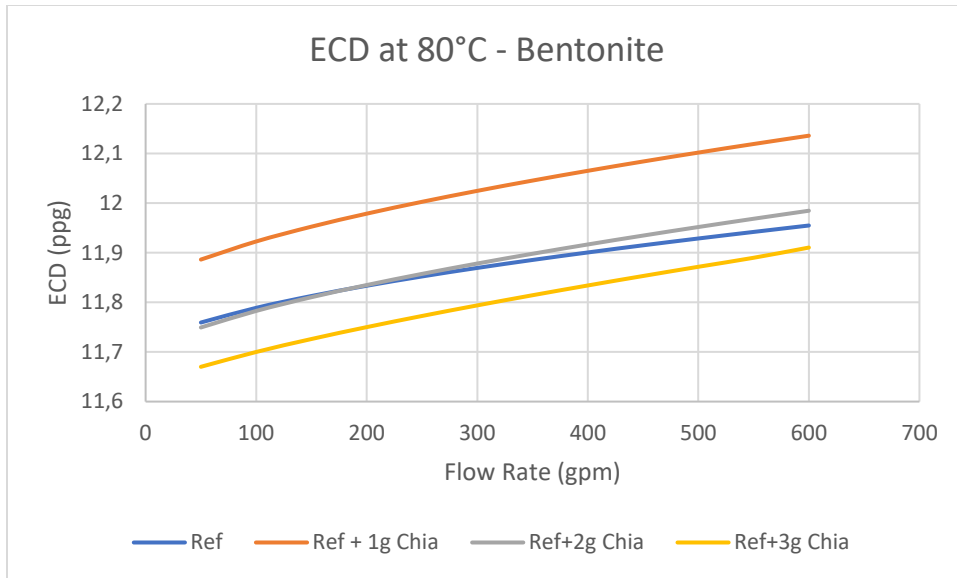


Figure 10.45: ECD of Chia in Bentonite at 80°C

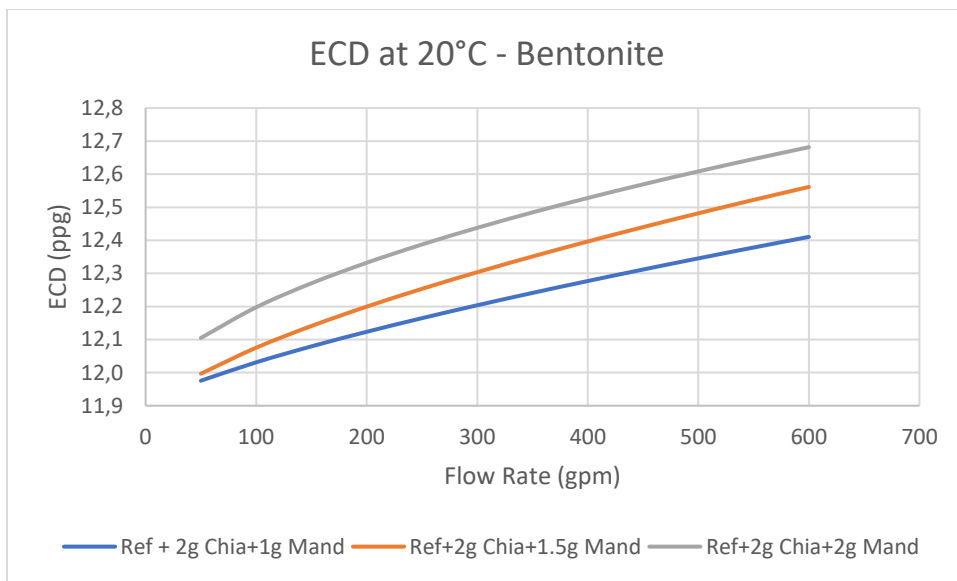


Figure 10.46: ECD of MPP in Bentonite at 20°C

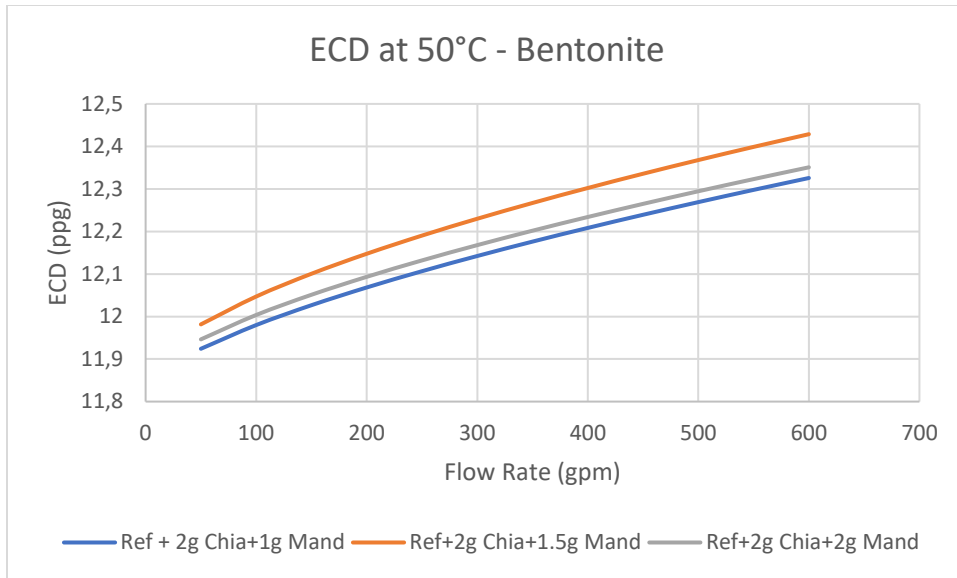


Figure 10.47: ECD of MPP in Bentonite at 50°C

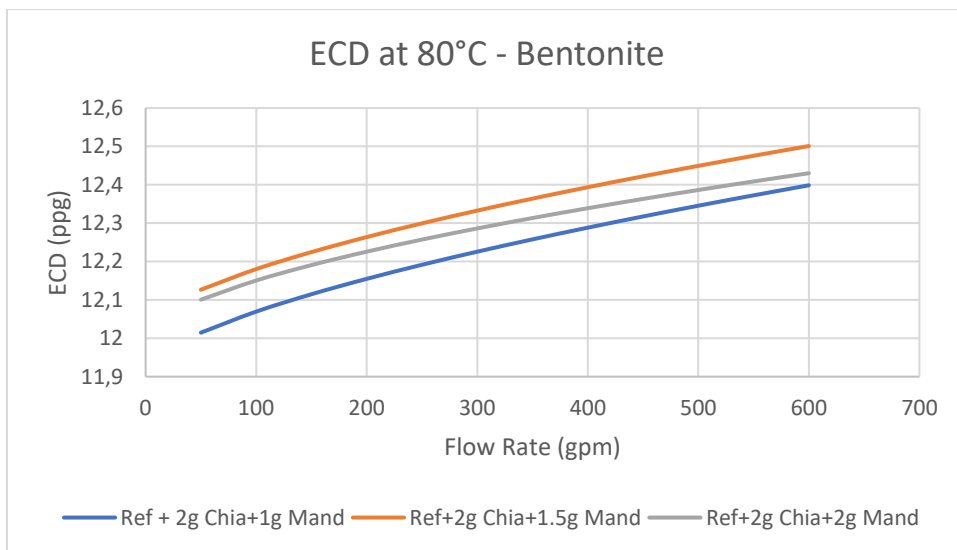


Figure 10.48: ECD of MPP in Bentonite at 80°C

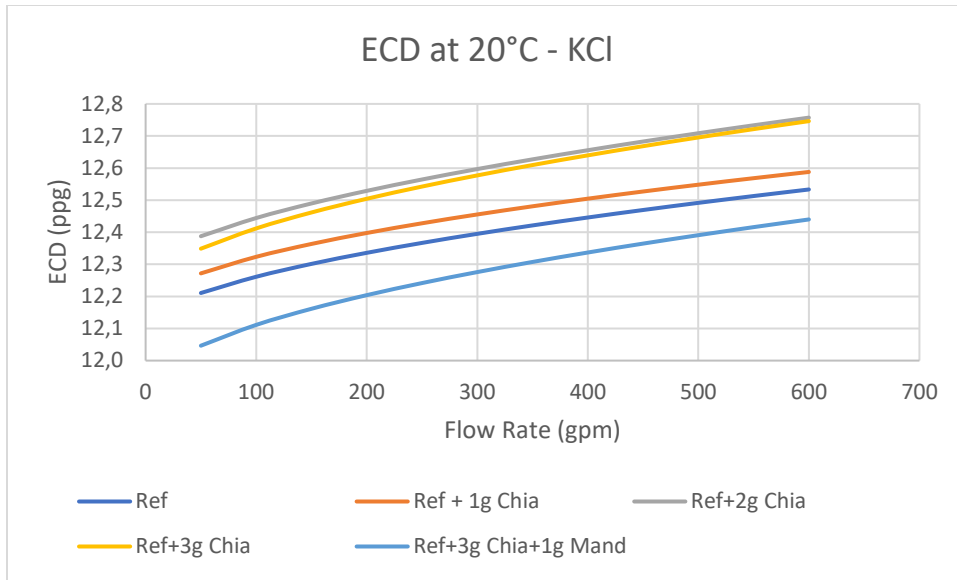


Figure 10.49: ECD of Chia and MPP in KCl at 20°C

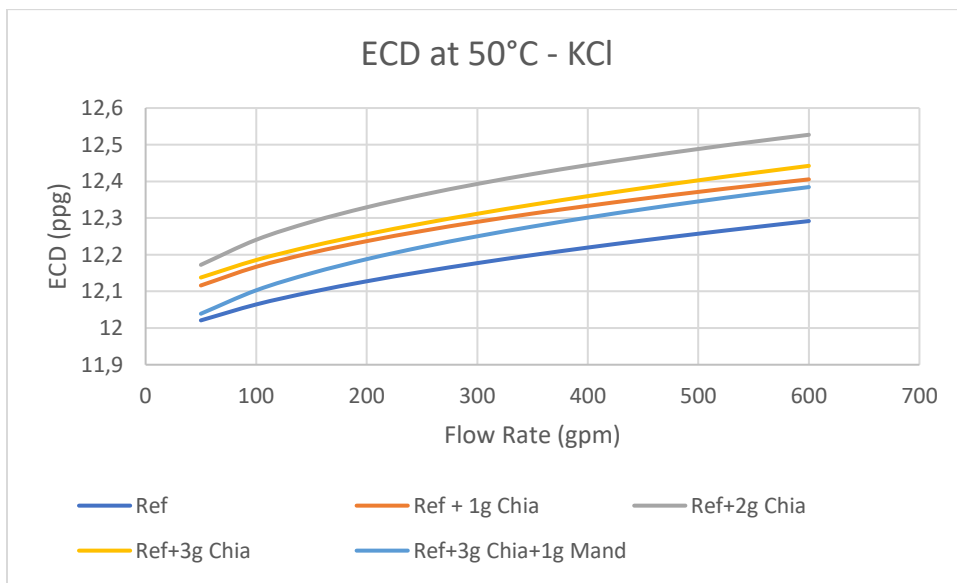


Figure 10.50: ECD of Chia and MPP in KCl at 50°C

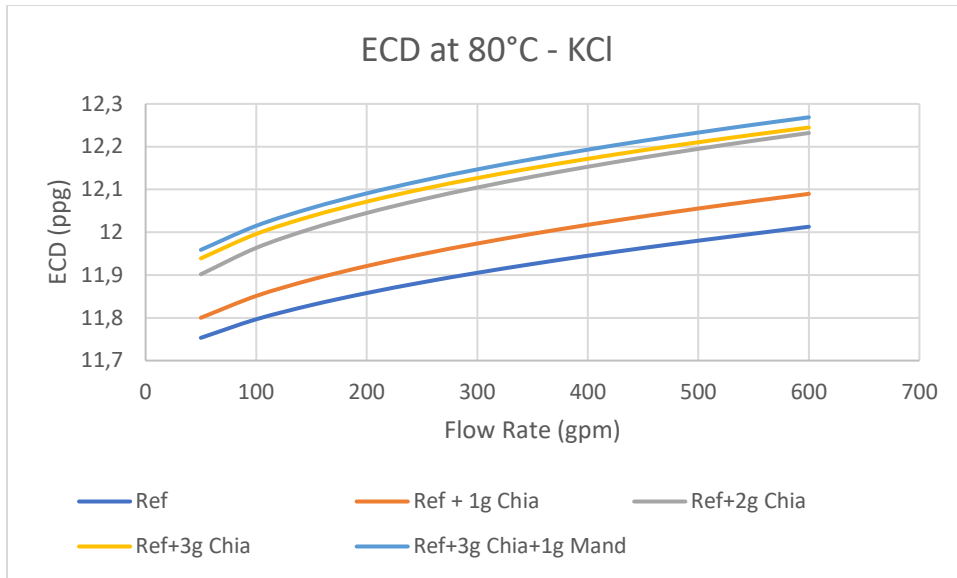


Figure 10.51: ECD of Chia and MPP in KCl at 80°C

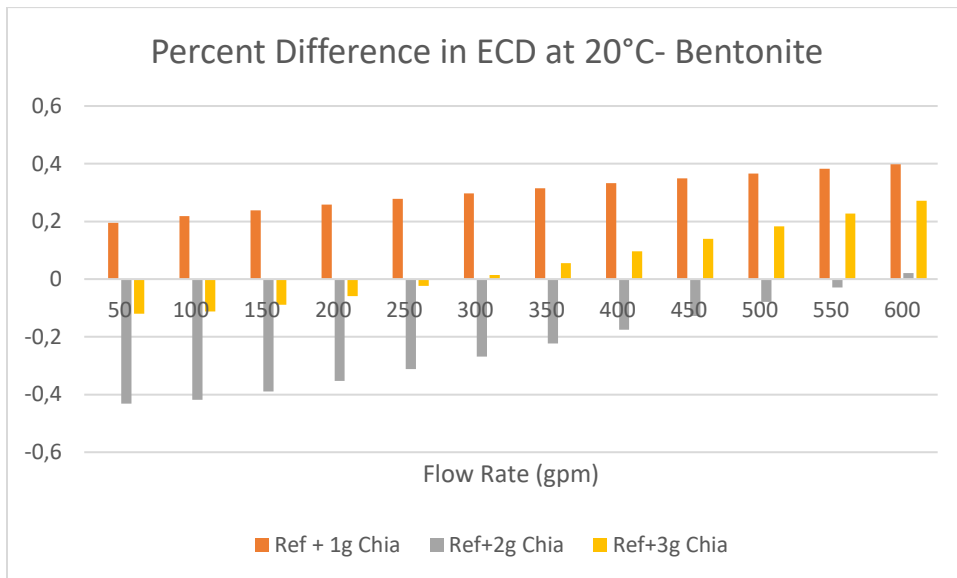


Figure 10.52: Percent Difference in ECD of chia in bentonite at 20°C

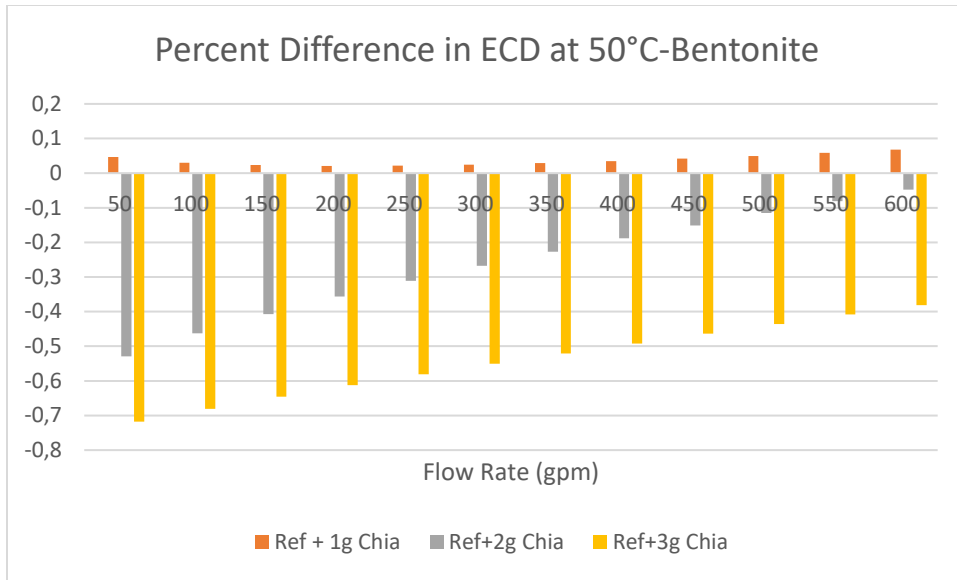


Figure 10.53: Percent Difference in ECD of chia in bentonite at 50°C

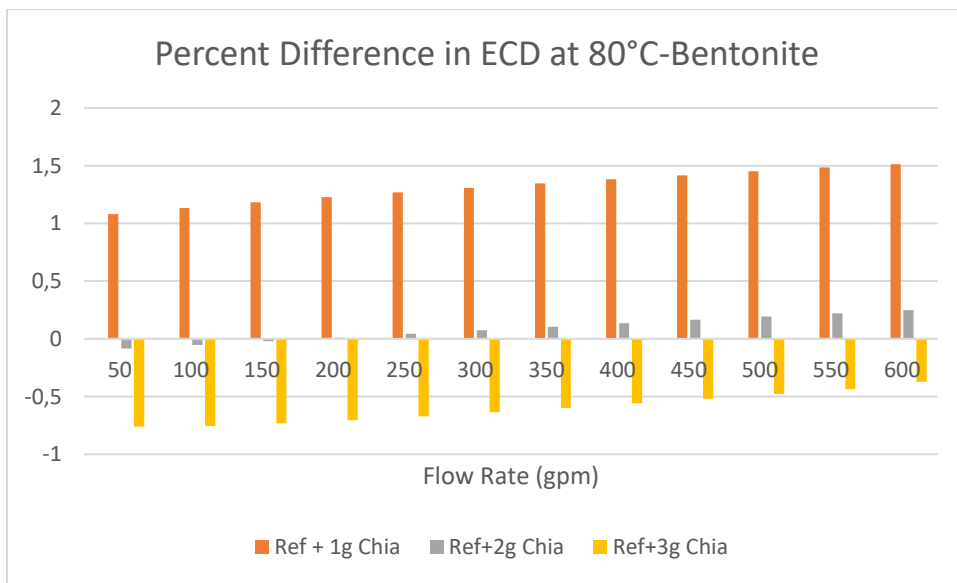


Figure 10.54: Percent Difference in ECD of chia in bentonite at 80°C

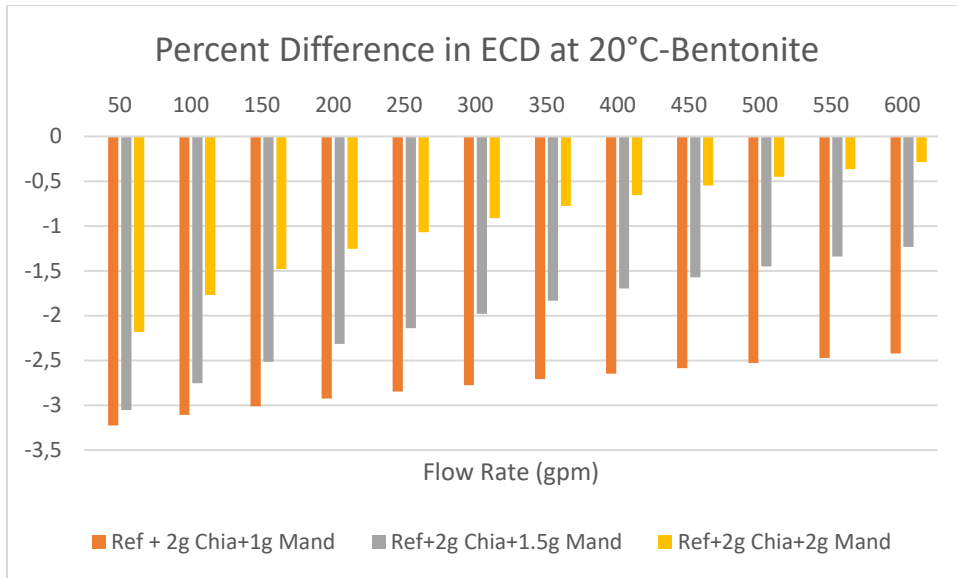


Figure 10.55: Percent Difference in ECD of MPP in bentonite at 20°C

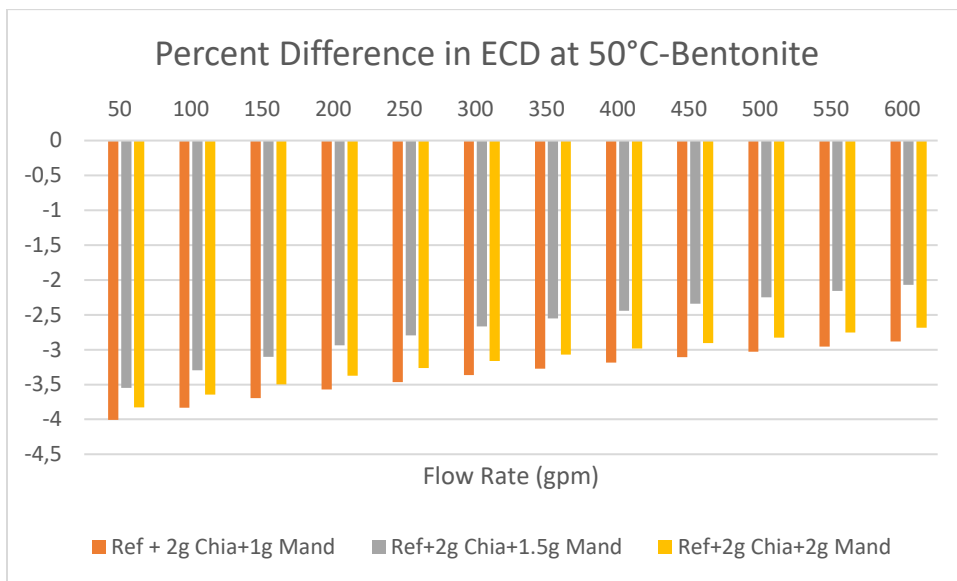


Figure 10.56: Percent Difference in ECD of MPP in bentonite at 50°C

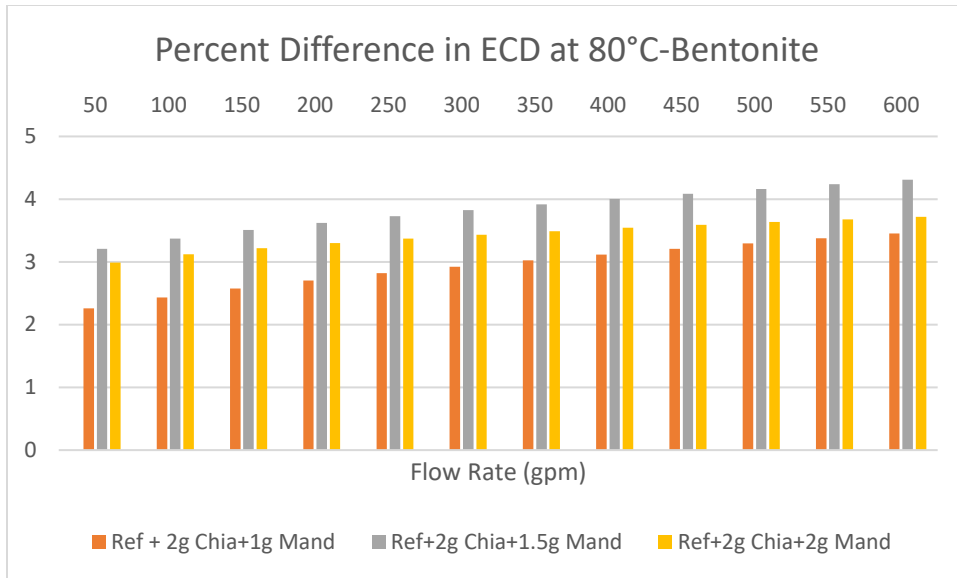


Figure 10.57: Percent Difference in ECD of MPP in bentonite at 80°C

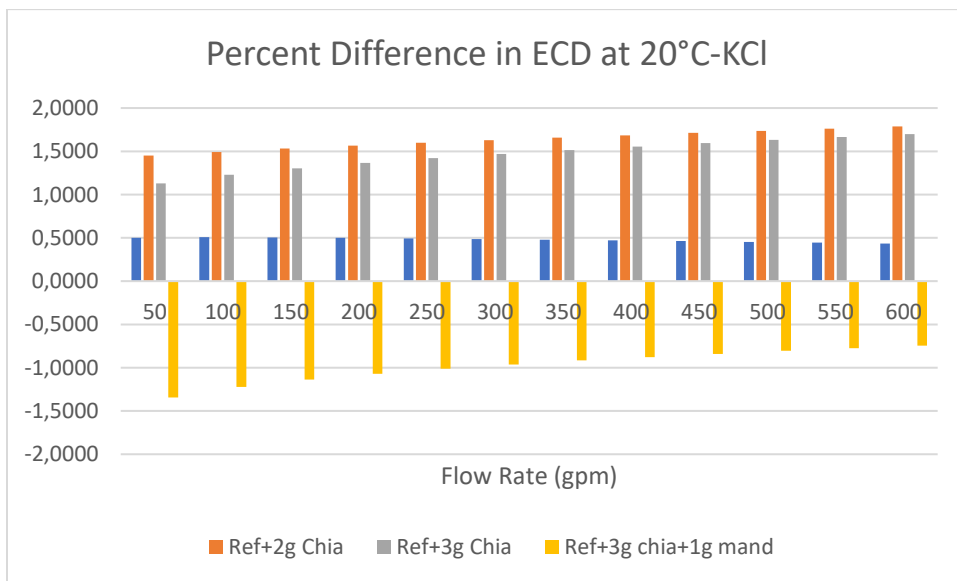


Figure 10.58: Percent Difference in ECD of Chia and MPP in KCl at 20°C

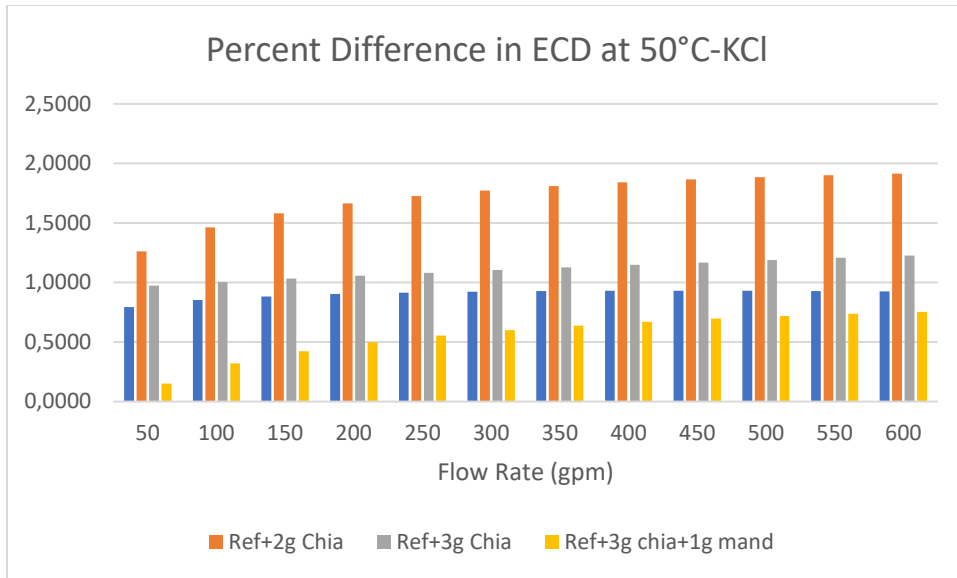


Figure 10.59: Percent Difference in ECD of Chia and MPP in KCl at 50°C

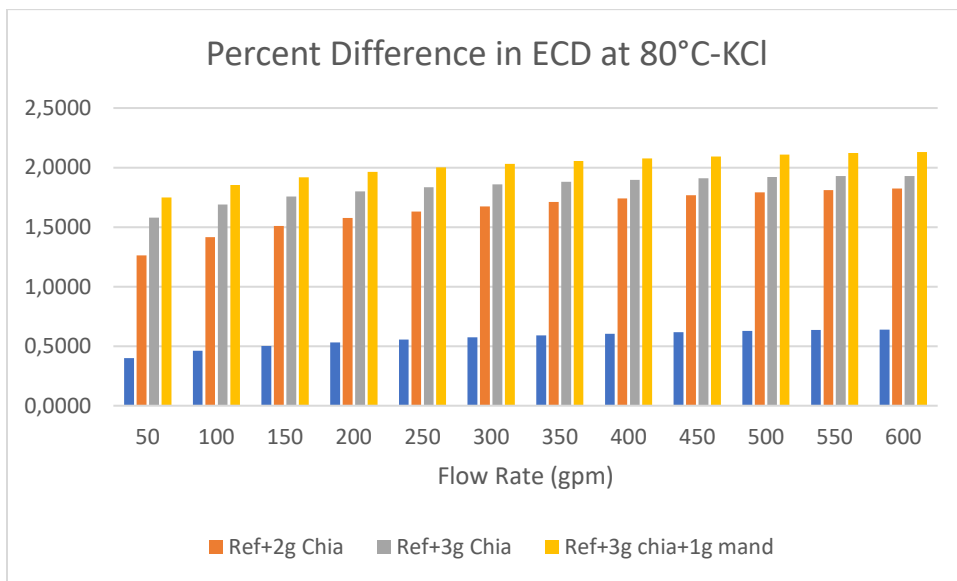


Figure 10.60: Percent Difference in ECD of Chia and MPP in KCl at 80°C